DOCTOR OF SCIENCES

Peripheral O-annulation of porphyrin macrocycles

Biloborodov, Dmytro

Award date:
2018

Awarding institution:
University of Namur

UNIVERSITE DE NAMUR
NAMUR RESEARCH COLLEGE
FACULTE DES SCIENCES
Laboratoire de Chimie Organique
des Matériaux Supramoléculaires

Peripheral O-annulation of porphyrin macrocycles

Thesis presented by
Dmytro Biloborodov

Under the supervision of Prof. Davide Bonifazi
For the degree of Doctor of Philosophy (Ph.D.)

Doctoral Commision
Prof. Stephane Vincent
Prof. Guillaume Berionni
Prof. Luigi Vaccaro
Prof. Angela Sastre-Santos
Prof. Davide Bonifazi

Namur, December 2018

Acknowledgement

I would like to express my deep gratitude to *Prof. Davide Bonifazi* for giving me the opportunity to join interesting and challenging project, for his patient guidance as well as for his encouragement and useful critiques during the course of the whole Ph.D. I will be always grateful for the tools he provided me to enlarge my chemistry knowledge and for the enthusiasm for research that he has transferred to me and has always inspired me to do better.

Many thanks go to *Prof. Stephane Vincent, Prof. Guillaume Berionni, Prof. Luigi Vaccaro* and *Prof. Angela Sastre-Santos* for accepting the co-examination of this thesis.

I give special thanks to *Prof. Alain Krief* for his valuable and constructive suggestions during the development of this research work and for having contributed enlarging my knowledge in chemistry. His willingness to give his time so generously has been very much appreciated.

I am also grateful to *Dr. Irene Georgiou, Dr. Olesia Kulyk* for the proofreading of various parts of this manuscript.

Many thanks go to *Prof. Roberto Lazzaroni* and *Dr. Claudio Quarti* for the calculations performed, the one included in this thesis; Dr. *Luka Đorđević* for NICS calculations; *Dr. Andrea Folli* for the EPR measurements; *Nicolas Biot* for solving the complicated X-ray crystal structures; *Dr. Andrea Fermi* for the introduction in cyclovoltammetry analysis. In addition, I have to thank *Dr. Julien De Winter* for all the mass measurements performed and for his help on the MS/MS investigations. I would like also to thank *Dr. Daphne Stassen* for the scientific collaboration on the oxygen-embedded porphyrin scaffolds. Thanks to all for the fruitful collaboration.

I would like to acknowledge all the members of UCO for the pleasant environment of work and for their fast and accurate assistance with all administrative and technical questions.

Thanks to all the former and present members of Bonifazi's group for the nice working atmosphere and for their friendship. I am particularly grateful for the assistance given by *Dr. Andrey Berezin* in solving difficult synthetic problems**.** In addition, I would like to thank *Dr. Antoine Stopine* and *Dr. Irene Georgiou* for useful advices, constructive recommendations and fruitful discussions. Many thanks go to the all my lab-mates *Dr. Lou Rocard, Dr. Jonathan Tasseroul, Dr. Florent Pineux, Dr. Silvia Forensi, Dr. Dario Mosca, Dr. Riccardo Marega, Dr. Valentina Corvaglia, Dr. Federica De Leo, Dr. Laure-Elie Carloni, Dr. Rosaria Vulcano, Dr. Maria Mercedes Lorenzo Garcia, Dr. Hamid Oubaha, Dr. Tanja Miletić, Dr.*

Andrea Sciutto, Dr. Davide Marinelli, Dr. Francesco Fasano, Cataldo Valentini, Rodolfo Tondo, Stavroula Melina Sakellakou, Deborah Romito, Oliwia Matuszewska, Jacopo Dosso. Thank you all for the help and for the unforgettable time we spent together along those years.

Many thanks go to all my family and friends for their love, patience, understanding and encouragement along this period of my life. I am especially grateful to my parents for the continuous support they have given me throughout my course of Ph.D. Second, I would like to thank my dear wife Olesia for all the love, comfort and guidance she has given me during this time.

Table of contents

List of Abbreviations

Å	Angstrom
Ac	Acetyl
acac	Acetylacetonate
AICD	anisotropy of the induced current density
APCI	atmospheric pressure chemical ionization
Ar	Aryl
aq.	Aqueous
BAHA	*tris*(4-bromophenyl)aminium hexachloroantimonate
BAHAf	*tris*(4-bromophenyl)aminium hexafluoroantimonate
Bu	Butyl
°C	degree centigrade (0 °C = 273.16 K)
ca.	*circa* (latin) - around, about or approximately
calc.	calculated
cod	1,5-cyclooctadiene (ligand)
conc.	concentrated
CV	cyclic voltammetry
Cy	cyclohexyl
δ	chemical shift (NMR)
d	doublet (NMR)
dba	dibenzylideneacetone
DBU	1,8-diazabicyclo[5.4.0]undec-7-ene
DCE	1,2-dichloroethane
DDQ	2,3-dichloro-5,6-dicyano-1,4-benzoquinone
DFT	density functional theory
DSSC	dye-sensitized solar cells
DMF	dimethylformamide
DMSO	dimethylsulfoxide
ε	extinction coefficient
EPR	electron paramagnetic resonance
eq.	equivalent
ES (ESI)	electrospray ionisation

et al.	*et alia* (latin) – and others
Et	ethyl
EWG	electron withdrawing group
exp.	experimental
eV	electronvolt (1eV = 1.602 x 10-19 J)
Fc	ferrocene
Fc^+	ferricinium
GPC	gel permeation chromatography
g	gram
h	hour
HOMO	highest occupied molecular orbital
HPLC	high-performance liquid chromatography
HR	high resolution
Hz	Hertz (s^{-1})
IUPAC	International Union of Pure and Applied Chemistry
i.e.	*Id est* (latin) – that is to say
IR	infra-red (spectroscopy)
J	coupling constant (NMR)
λ	wavelength
L	litre
liq.	liquid
LR	low resolution
LUMO	lowest unoccupied molecular orbital
µ	micro (10^{-6})
M	metal
m	milli (10^{-3}), multiplet (NMR)
MALDI	matrix assisted laser desorption-ionization
Me	methyl
MFA	N-methylformanilide
mg	milligram
min	minute
MO	molecular orbital
m.p.	melting point

MS	mass spectrometry
mV	millivolt
NBS	N-bromosuccinimide
NICS	nucleus-independent chemical shift
NIR	near-IR region
nm	nanometer
NMR	nuclear magnetic resonance
o-DCB	1,2-dichlorobenzene
OLED	organic light emitting diode
ORTEP	oak ridge thermal ellipsoid plot (to present crystal structure)
OTFT	organic thin-film transistor
OTf	triflate
ox	oxidation
PAH	polyaromatic hydrocarbon
Ph	phenyl
PhMe	toluene
$PhNO_2$	nitrobenzene
PivOH	pivalic acid
ppm	parts per million
PXX	*peri*-xanthenoxanthene
Py	pyridine
red	reduction
rt	room temperature
s	second, singlet (NMR)
SiO_2	silica gel
t	triplet
TAnP	tetraanthraporphyrin
TBAF	tetrabutylammonium fluoride
$TBAPF_6$	Tetrabutylammonium hexafluorophosphate
$TBABF_4$	Tetrabutylammonium tetrafluoroborate
TBP	tetrabenzoporphyrin
TNP	tetranaphthoporphyrin

TPP	5,10,15,20-tetraphenylporphyrin
Ts	tosyl (toluenesulfonyl)
TFA	trifluoroacetic acid
THF	tetrahydrofurane
TLC	thin layer chromatography
TMS	trimethylsilyl
UV	ultraviolet
V	Volt

Abstract

Extended π-conjugated systems are the focus of intense research in constructing nanostructured molecular devices as they exhibit peculiar optoelectronic properties directly ensuing from the HOMO-LUMO bandgap energy of the molecule. The unique ability to the precise tuning of these properties through the functionalization of the molecular periphery (*e.g.* chain length, planarity of the conjugated paths, heteroatom insertion *etc.*) enables controllable manipulation of structure-properties relationship. Among a variety of π-conjugated molecules, porphyrins are of particular interest for their application in material science due to their advantageous properties, such as photostability, visible-light absorption, low energy excited states and high molar extinction coefficients.

Hence, the main objective of this thesis was to design novel π-extended O-embedded porphyrins in order to examine and better understand the relationship between their structure and emerged properties. Four generations of O-fused porphyrins with a different number of pyran rings in each case, were studied delving into their synthesis and physicochemical features.

In *Chapter I*, a brief introduction to porphyrin chemistry with an emphasis on the peripheral modification of the porphyrin core, including the synthesis of annulated and heteroatom-modified porphyrins, is given to the reader. *Chapter II* reports the aim of the project and the succinct outline of the present work.

Following up, *Chapter III* describes the first part of the manuscript, in which the synthesis of mono- and di-pyranoporphyrins was investigated. In *section 3.1* of this chapter, a simple and efficient protocol for a CuO-mediated pyran annulation reaction of monohydroxyporphyrin **3-2** was successively developed. In addition, metal and free-base monopyranoporphyrin derivatives were then prepared and examined. *Section 3.2* focuses on the preparation of dipyranoporphyrins **3-16**, **3-27**, **3-35** and **3-36**, in which the successful implementation of the formerly developed protocol was unravelled. Notably, CuO-promoted ring closure reaction of **3-29** led to the inseparable mixture of isomers **3-17** and **3-18**, the separation of which was impossible due to their similar polarity. To circumvent this, the crude material was demetallated to afford *cis*- and *trans*-like dipyranoporphyrins **3-35** and **3-36**, easily separated by SiO_2 column chromatography. Confirmation of the successful synthesis of O-fused porphyrins was obtained by ^{1}H- and ^{13}C-NMR, IR, UV-vis spectroscopy and HRMS measurements. Additionally, the chemical structures of mono- **3-1**, **3-14** and di-

3-16, **3-36** pyranoporphyrins were unambiguously established by X-ray crystallographic analyses.

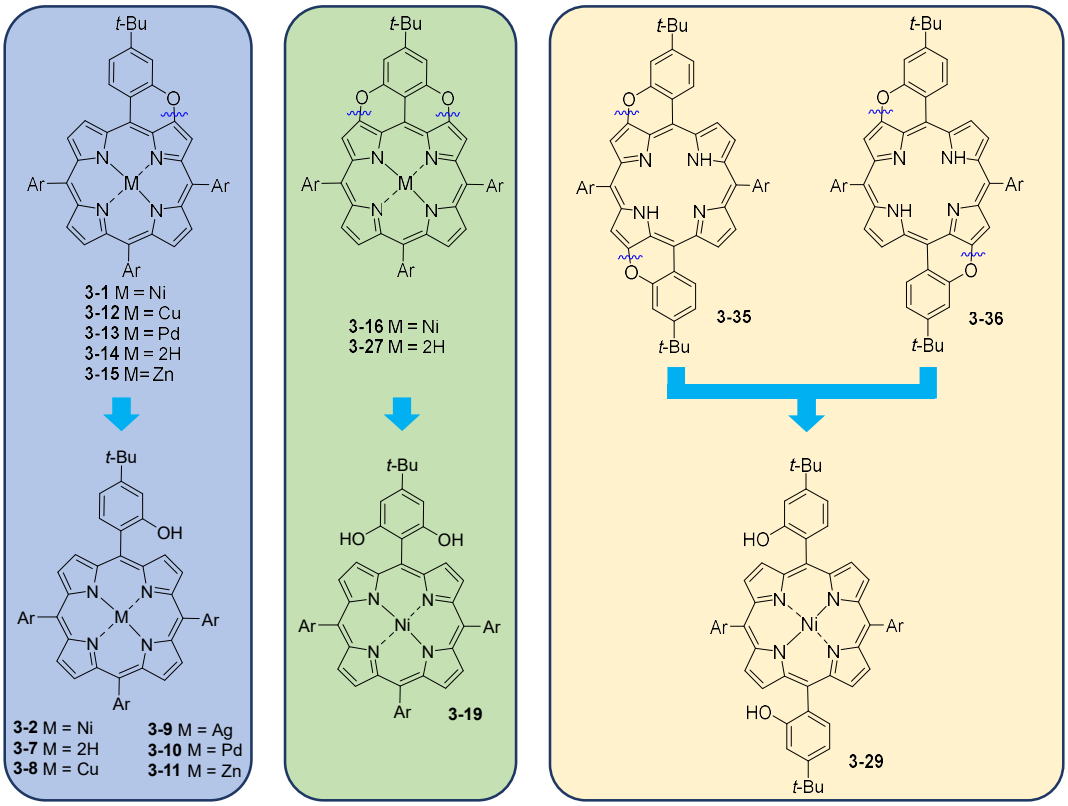

The last section of *Chapter III* is dedicated to the physicochemical investigations of as-prepared O-embedded porphyrins. It was found that the increase in the number of O-bridges led to the slight bathochromic shift of absorption maxima, thus indicating a weak conjugation between the porphyrin core and the co-planarized *meso*-aryl substituents. Consequently, the insignificant changes of the optical bandgap along the series of mono- and di- pyranoporphyrins were detected. On the other hand, the cyclic voltammograms of O-embedded porphyrins showed the pronounced shrinking of the electrochemical HOMO-LUMO bandgap. Moreover, CV investigation revealed the dependence of second oxidation potential upon the number and position of O-bridges.

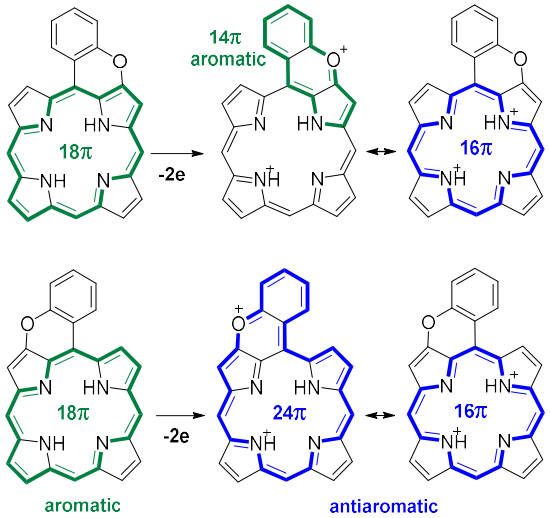

This was attributed to the antiaromaticity of porphyrin dication species, formed upon the

second oxidation process. The major contribution in the global antiaromaticity of all O-fused porphyrin dications was ascribed to the 16π antiaromatic circuit. Meanwhile, O-annulation with pyrrole subunit decreases the antiaromatic character of the dication through the realization of additional aromatic 14π circuit. On the other hand, O-fusion with the azafulvene subunit results in the emerging of an antiaromatic 24π conjugation pathway, which increases the antiaromatic character of porphyrin dications. In contrast to the monopyranoporphyrin dication, the global antiaromaticity of dipyranoporphyrin dication is determined by the superposition of aromatic 14π, antiaromatic 24π and 16π conjugated circuits.

In *Chapter IV*, a detailed description of our extended investigation towards the synthesis of tetra- and octa- pyranoporphyrins is reported. In *section 4.1*, the CuO-mediated pyran annulation reactions of tetrahydroxyporphyrins **4-3** and **4-7** were explored. The successful implementation of the formerly used protocol in case of **4-3** was proved by HRMS-MALDI characterizations, MS/MS MALDI investigation and IR-spectroscopy. However, the ring closure reaction of **4-7** yielded only traces of expected tetrapyranoporphyrin **4-2** as a mixture with the oxygenated products according to LRMS-MALDI. In addition, the isolation of **4-2** was not accomplished due to its low stability.

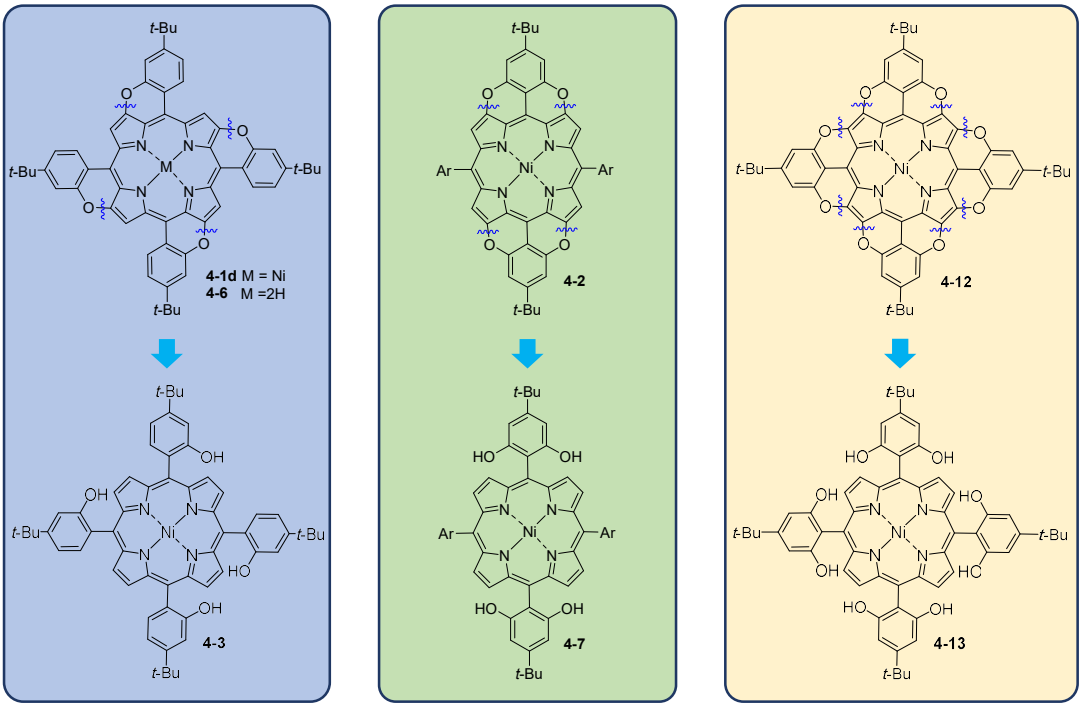

Section 4.2 of this chapter focuses on the synthesis of full-conjugated octapyranoporphyrin **4-12**. Similarly as for the synthesis of tetrapyranoporphyrin **4-2**, CuO-mediated ring closure reaction of octahydroxyporphyrin **4-13** led to a mixture of desired **4-12**

and oxygenated products according to LRMS-MALDI. In both cases, the formation of side products was assigned to the photosensitization of highly reactive singlet molecular oxygen $^1O_2$ and subsequent reaction of $^1O_2$ with pyranoporphyrin molecules. In this way, the porphyrin macrocycles of **4-2** and **4-12** play role of photosensitizers.

The isolation of full-conjugated porphyrin was achieved *via* reductive aromatization of crude **4-12** with $SnCl_2$, followed by GPC purification of reaction mixture. While mono- and di- pyranoporphyrins were successively analysed by NMR spectroscopy, octa- **4-12** and tetra- **4-6** pyranoporphyrins exhibited radical character, as was revealed by EPR investigation. The chemical structure of **4-12** was undoubtedly proved through HRMS-MALDI analysis.

Résumé

Les systèmes π-conjugués étendus sont au centre de la recherche pour la conception d'objets moléculaires nanostructurés car ils possèdent des propriétés optoélectroniques intéressantes liées à la différence d'énergie entre leurs orbitales HOMO et LUMO. La possibilité de faire évoluer ces propriétés via la fonctionnalisation périphérique de la molécule (ex : longueur de chaine, planarité du système conjugué, insertion d'hétéroatomes, *etc.*) permet la manipulation contrôlée de leur relation structure/propriétés. Parmi de nombreux systèmes π-conjugués, les porphyrines sont particulièrement intéressantes pour leur application en science des matériaux grâce à certaines de leurs propriétés telles que leur photostabilité, leur absorption de la lumière visible, le faible niveau d'énergie de leur état excité ainsi que leur fort coefficient d'extinction molaire.

Ainsi, l'objectif premier de cette thèse consiste à concevoir de nouvelles porphyrines O-incorporées π-étendues et d'analyser de manière détaillée leur relation structure/propriétés. A cet égard, quatre générations de porphyrines O-fusionnées avec un nombre différent d'anneaux pyraniques ont été étudiées, allant de la synthèse à la caractérisation physicochimique.

Dans le *Chapitre I*, une brève introduction sur la chimie des porphyrines est donnée au lecteur, avec une intention particulière sur les modifications périphériques de leur corps, incluant la synthèse de porphyrines annulées et héteroatome-modifiées. *Chapitre II* rapporte d'objectif du projet et de manière succincte les lignes directrices du travail présenté.

Chapitre III représente la première partie du manuscrit, dans laquelle la synthèse de mono- and di-pyronoporphyrines est étudiée. Dans la *section 3.1* de ce chapitre, un protocole simple et efficace pour la réaction d'annulation pyranique catalysée au CuO de la monoporphyrine **3-2** a été développé avec succès. De plus, des dérivés monopyranoporphyrine métal et base libre ont été préparés et examinés. *Section 3.2* se concentre sur la préparation de dipyranoporphyrines **3-16**, **3-27**, **3-35** et **3-36**, pour lesquelles le protocole précédemment développé a été modifié. Notablement, la réaction catalysée au CuO permettant la fermeture de cycle de **3-29** a mené à un mélange inséparable des isomères **3-17** et **3-18**, et leur séparation ne s'est pas avérée réalisable due à leur polarité similaire. Ainsi, la réaction de démétallation a été effectuée sur le mélange pour donner les dipyranoporphyrines **3-35** et **3-36**, facilement séparable sur colonne chromatographique de SiO_2. Des preuves du succès des synthèses des porphyrines O-fusionnées ont été obtenues par

^{1}H- et ^{13}C-RMN, spectroscopie IR, UV-vis et des mesures de masse spectrométrique à haute résolution (HRMS). En outre, les structures chimiques des mono- **3-1**, **3-14** et di- **3-16**, **3-36** pyranoporphyrines ont été établies sans ambiguïté par analyses crystallographiques aux rayons X.

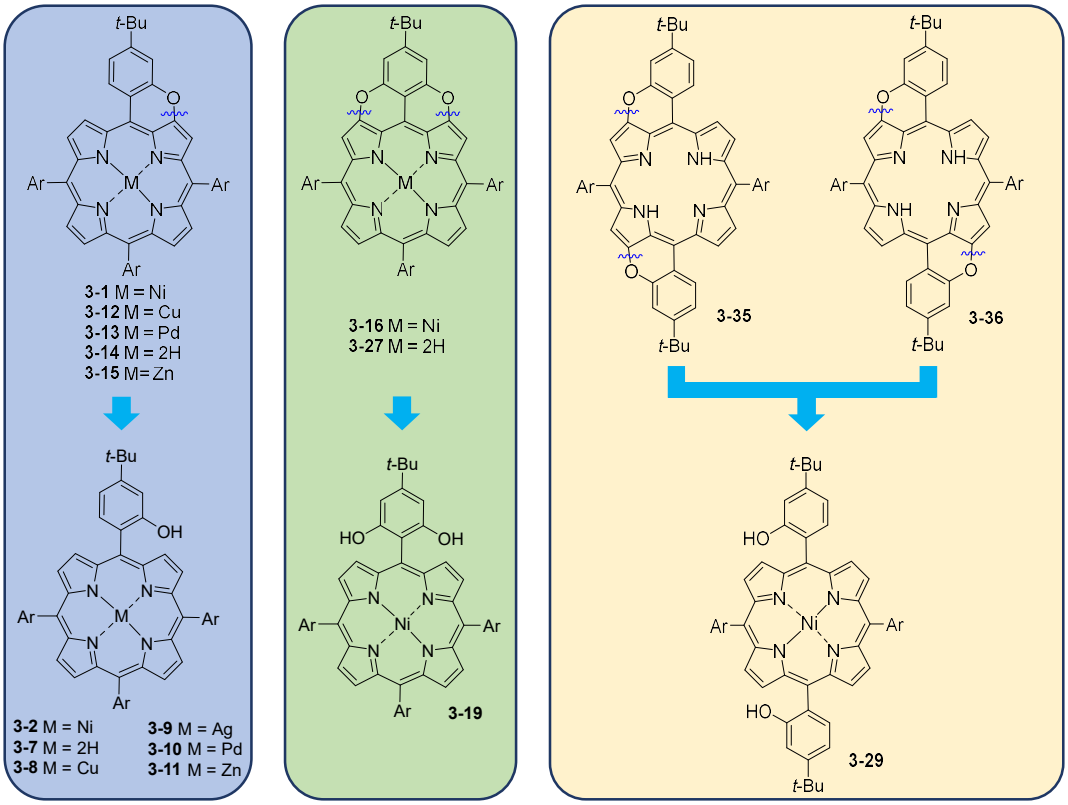

La dernière section du *Chapitre III* est dédiée à l'analyse physicochimique des porphyrines O-fusionnées ainsi préparées. Il a été prouvé que l'augmentation du nombre de ponts O mène à un léger décalage bathochromique du maximum d'absorption, indiquant la faible conjugaison entre le corps de la porphyrine et les substituants coplanaires *meso*-aryles. Par conséquent, des changements insignifiants en terme de différences d'énergies optiques pour les séries de mono- et di-pyranoporphyrines ont été détectés. En revanche, les cyclovoltamogrammes des porphyrines O-fusionnées ont montré un rétrécissement prononcé de la bande HOMO-LUMO électrochimique. De plus,

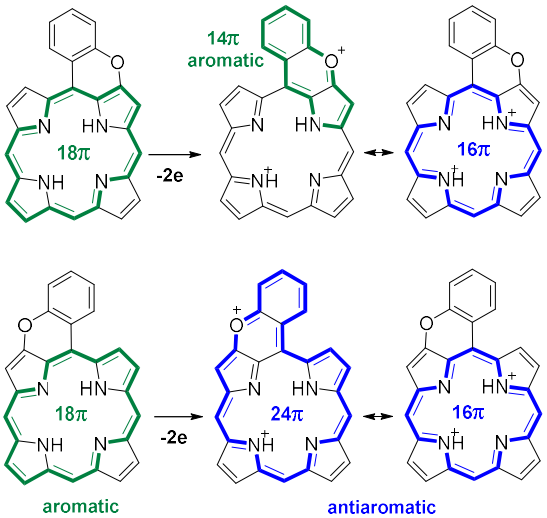

l'investigation CV a révélé la dépendance du second potentiel d'oxydation avec le nombre et la position des ponts O. Cela a été attribué à l'antiaromaticité de l'espèce dicationique porphyrine, formée lors de la seconde oxydation. La contribution majeure dans l'antiaromaticité globale de toutes les porphyrines O-fusionnées est attribuée au circuit antiaromatique 16π. En même temps, l'O-annulation avec la sous-unité pyrrole diminue le caractère antiaromatique du dication au travers l'implémentation d'un circuit additionnel aromatique 14π circuit. D'autre part, l'O-fusion avec l'entité azafulvene résulte en l'apparition d'un chemin antiaromatique 24π, qui augmente le caractère antiaromatique des porphyrines dications. En opposition avec le dication monopyranoporphyrine, l'antiaromaticité globale du dication dipyranoporphyrine est déterminée par la superposition des circuits aromatiques 14π, antiaromatiques 24π et 16π conjugués.

Dans le *Chapitre IV*, une description détaillée de notre investigation vers la synthèse de tetra- et octa- pyranoporphyrines est reportée. Dans la *section 4.1*, la réaction d'annulation au CuO pour les dérivés tetrahydroxyporphyrines **4-3** et **4-7** a été explorée. La modification du protocole premier utilisé dans le cas de **4-3** a été prouvée par caractérisation HRMS-MALDI, MS/MS MALDI and spectroscopie IR. Cependant, la réaction de fermeture de cycle appliquée à **4-7** a seulement donné des traces du produit attendu tetrapyranoporphyrin **4-2** en mélange avec des produits oxygénés selon l'analyse LRMS-MALDI. L'isolation de **4-2** n'a pas été effectuée due à sa faible stabilité.

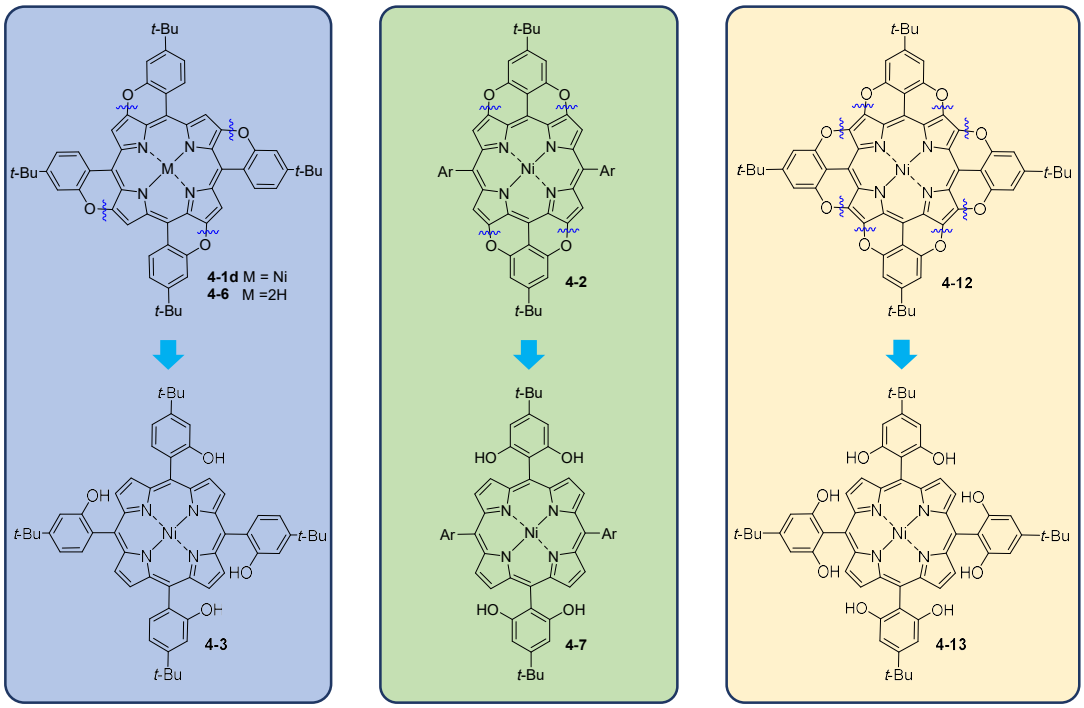

La *section 4.2* de ce chapitre est consacrée à la synthèse du composé complètement conjugué octapyranoporphyrine **4-12**. Similairement à la synthèse de la tetrapyranoporphyrine **4-2**, la réaction de fermeture de cycle catalysée au CuO appliquée à la octahydroxyporphyrin **4-13** a mené à un mélange de produit désiré **4-12** et de produits oxygénés selon l'analyse LRMS-MALDI. Dans les deux cas, la formation de sous-produits a été assignée à la photosensibilisation d'oxygène singulet moléculaire hautement réactif $^1O_2$ et de réactions subséquentes entre $^1O_2$ et les dérivés pyranoporphyrines. Ainsi, les porphyrines **4-2** et **4-12** joue le rôle de photosensibilisants.

L'isolation de la porphyrine conjuguée a été effectuée *via* aromatisation réductive du mélange de **4-12** et des sous-produits en présence de $SnCl_4$, suivie par purification par CPG. Si les mono- et di- pyranoporphyrines ont été analysées par spectroscopie RMN avec succès, l'octa- **4-12** et la tetra- **4-6** pyranoporphyrines possèdent un caractère radical, comme l'ont révélé les analyses par RPE. La structure chimique de **4-12** a été prouvée par analyse HRMS-MALDI.

1. Introduction

In the past decades, π-conjugated molecules have been actively studied for their potential use in a variety of optoelectronic devices such as organic light emitting diodes (OLEDs),[1–3] thin-film transistors (OTFTs),[4] solar cells *etc*.[5–7] To improve stability, efficiency and materials variety, a number of π-extended polycyclic molecules have been developed and employed in various device settings. Among them, particular attention was drawn to porphyrin-based molecules due to their attractive photophysical and optoelectronic properties along with their structural similarity to biologically important heme and chlorophyll.[8–10]

In this context, the present chapter is dedicated to the general overview on the chemistry of porphyrins. In *section 1.1* the structural features, synthesis and key properties of porphyrins are described. The approaches to peripheral modification of the porphyrin core, including the synthesis of annulated and heteroatom-modified porphyrins, are reviewed in *section 1.2*. Finally, the aim of this thesis is outlined *in section 1.3*.

1.1 General account on porphyrins

Porphyrins are a class of heterocyclic compounds comprising of four pyrrole rings interconnected by methine bridges through their α-positions to form a larger ring. The resulting, tetrapyrrolic core provides a highly conjugated planar structure to the porphyrin molecules. These macrocyclic compounds have a rigid internal cavity, which in its deprotonated form has a 1.2-1.4 Å diameter and is suitable for metal incorporation.[11] Thus, different metal ions can be incorporated into the porphyrin cycle, leading to compounds with new electronic and binding properties.

Metalloporphyrin derivatives are widely occurred in nature and play pivotal role in the supporting of life on Earth. As an example, Figure 1.1 shows three well-known natural porphyrin-like molecules, which are important in key biochemical processes. Iron-containing *heme b* was found in mammalian blood, as a prosthetic group of hemoglobin and myoglobin proteins. The ability of this molecule to reversible bind with O_2, makes it responsible for the transportation and storage of O_2 in organisms.[12,13] *Chlorophyll a* is a Mg(II)-metallated porphyrin-like chromophore, playing a significant role in the light-driven

reactions of photosynthesis.[14] Specifically, sunlight is absorbed by light harvesting pigments, including *chlorophyll a*, that is, the antenna moiety, which funnels the excitation energy to the reaction center through a sequence of energy-transfer steps.[15,16] *Coenzyme F430* is a nickel derivative of partially reduced porphyrin core, known also as corphyn. It acts as a prosthetic group in the enzyme methyl coenzyme M reductase of methanogenic *Archaea* and is responsible for the release of methane on the final step of methanogenesis.[17,18]

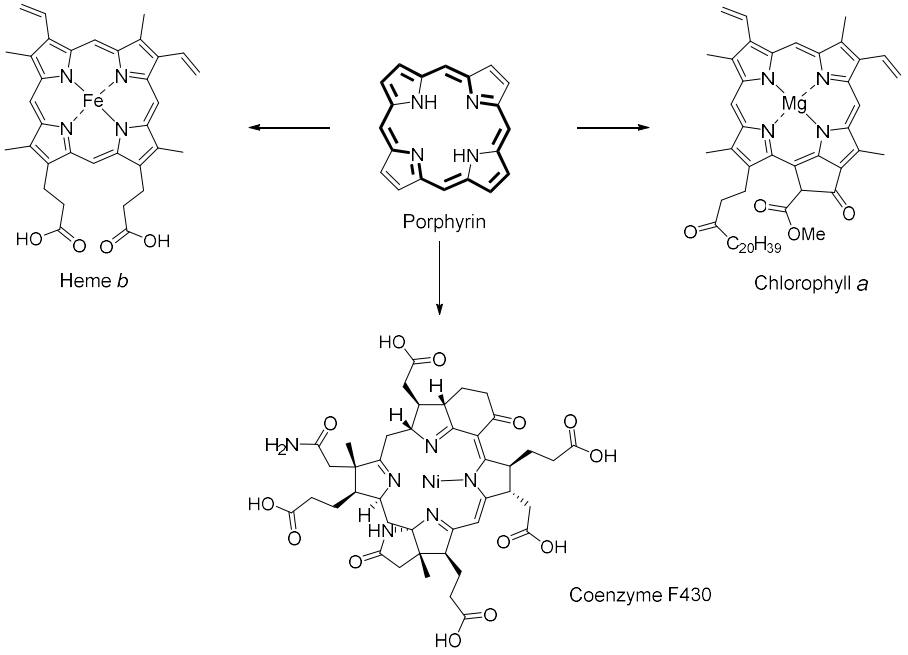

Figure 1.1 Some examples of porphyrin-like derivatives present in nature.

The broad range of porphyrin derivatives present in nature, is the result of their unique optical and electrochemical properties, a consequence of the conjugated π-system of the porphyrin core. Despite the fact, that the porphyrin system has 26π delocalized electrons, including two unpaired electrons of two nitrogen atoms, *Sondheimer* and *Vogel* indentified and reported the 18π electron delocalization pathway, which is responsible for their aromatic characteristics (bold bonds on porphyrin structure, depicted in Figure 1.1).[19–22] Furthermore, porphyrin's aromaticity was evidenced by X-ray crystallography, NMR-spectroscopy, MASS-spectrometry along with studies related to the porphyrin core stability.[11]

1.1.1 Nomenclature of porphyrins

The nomenclature system for porphyrins was first introduced by *Hans Fisher*.[23] According to this system, the eight outer carbon atoms belonging to the pyrrolic subunits are numbered from 1 to 8, while the four methine C atoms are defined as α, β, γ, and δ as outlined in Figure 1.2. Subsequent development of porphyrin science led to the synthesis of new complex derivatives, therefore, a more convenient and systematic nomenclature system was required. As a result, in 1979, IUPAC nomenclature was introduced, in which all the atoms in the macrocycle (including nitrogen atoms) are numbered, as illustrated in Figure 1.2.[24] It should be noted, that owing to the high symmetry of porphyrins there are only two types of carbon atoms along the ring, capable to the substitution reactions. In this context, the bridging methine carbons are defined as *meso*-positions, while pyrrolic carbons are defined as β-positions.

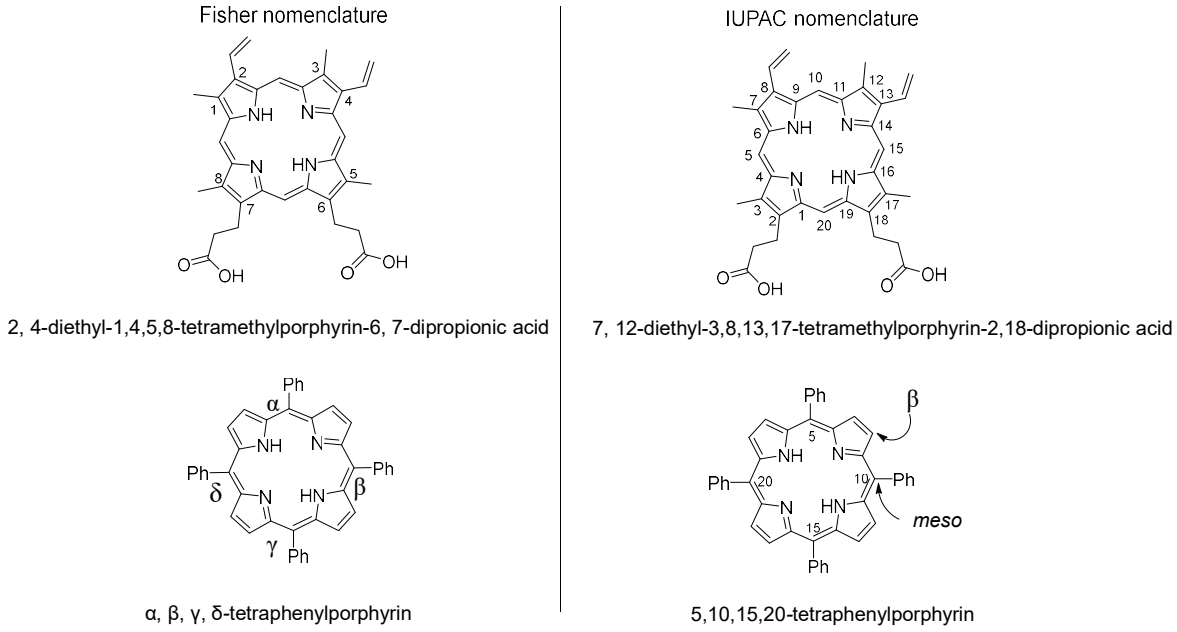

Figure 1.2 Names of porphyrin derivatives using different nomenclature systems.

1.1.2 Synthesis of porphyrins

Initially, nature was the main source of porphyrin-based molecules, such as *heme b* and *chlorophyll a*, from which other derivatives of porphyrins were synthesized. However,

having to follow this "natural route" only β-substituted derivatives were accessible, while the synthesis of *meso*-substituted porphyrins remained unexplored.

The pioneering synthesis of *meso*-substituted porphyrins was accomplished by *Rothemund* in 1935.[25] Heating of acetaldehyde or benzaldehyde and pyrrole in a sealed vessel in MeOH at 90 °C afforded 5,10,15,20-tetramethyl- and 5,10,15,20-tetraphenylporphyrins **1-1** and **1-2**, respectively (Scheme 1.1).[26] Further optimization of the reaction conditions by replacing the MeOH with pyridine as a solvent at an elevating temperature, *i.e.* 220 °C led to the isolation of **1-2** in 10% yield.[27]

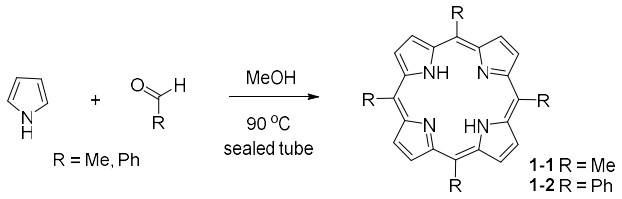

Scheme 1.1 Synthesis of *meso*-substituted porphyrins reported by *Rothemund*.

To avoid the use of harsh conditions and to increase the yield of *meso*-substituted porphyrins, *Adler* and *Longo* refined the *Rothemund* procedure by exploiting acidic conditions. Accordingly, a solution of pyrrole and benzaldehyde in propionic acid was refluxed under open-air conditions for 30 min producing desired porphyrin **1-2** in 20% yield (Scheme 1.2).[28–30]

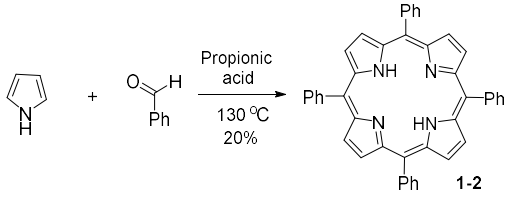

Scheme 1.2 Synthesis of *meso*-substituted porphyrin **1-2** reported by *Adler-Longo*.

Further improvement of *Adler-Longo's* methodology was reported by *Lindsey* and co-workers in the early 1980s. [31,32] In particular, the acid-catalyzed macrocyclization of pyrrole and benzaldehyde in the presence of a Lewis acid such TFA or BF_3, in chlorinated solvent ($CHCl_3$ or CH_2Cl_2) led to porphyrinogen **1-3** (Scheme 1.3). Due to the instability of the latter, its oxidation to form the stable porphyrin macrocycle **1-2** is required. For this purpose, oxidant such as DDQ or *p*-chloranil was added to accomplish the $6e^-/6H^+$ oxidative dehydrogenation of the porphyrinogen and thereby, isolate porphyrin **1-2** in 38% yield.

Notably, the reaction was performed in highly diluted conditions, *i.e.* 0.01 M concentration of each component, to favour the macrocyclization process and to diminish the competitive oligomerization of pyrromethanes.

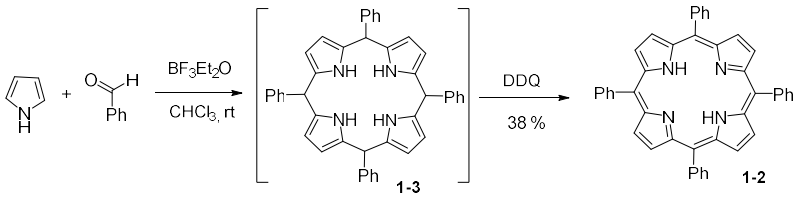

Scheme 1.3 Synthesis of *meso*-substituted porphyrin **1-2** reported by *Lindsey*.

Both *Adler-Longo's* and *Lindsey's* methodologies are appropriate for the synthesis of symmetrical porphyrins, while their applicability to the preparation of unsymmetrical porphyrins is limited. Specifically, the condensation of stoichiometric mixture of appropriate aldehydes and pyrrole results in the formation of complex mixture, from which the desired porphyrin is not always separable. To surpass these limitations, various alternative approaches have been developed, including the use of linear tetrapyrroles, tripyrrans, dipyrromethane derivatives *etc*.[33–35]

1.1.3 Optoelectronic properties of porphyrins

One of the most attractive properties of porphyrins is their intense visible-light absorption. Hence, UV-vis absorption spectroscopy is widely used to analyse the electronic structure of porphyrins.[36] In particular, they exhibit characteristic UV-vis spectra, which consist of two distinct regions or bands. The intense B bands (also known as *Soret* bands) appear around 380 to 450 nm with an extinction coefficient of 10^5 $M^{-1}cm^{-1}$, while the weak Q bands are typically located around 500 to 700 nm with an extinction coefficient of 10^4 $M^{-1}cm^{-1}$ (Figure 1.3). The *Soret* band involves the electronic transition from the ground state to the second singlet excited state ($S_0 \rightarrow S_2$), while the Q band relates to the transition from the ground state to the first singlet excited state ($S_0 \rightarrow S_1$). The location, number and intensity of these bands depend upon the substitution pattern of the macrocycle as well as whether the porphyrin is metallated or not and the kind of central metal. Therefore, free-base porphyrins exhibit four Q bands (Figure 1.3a) with different intensities, depending on the substituents both at the β-pyrrolic and *meso*-positions. Protonation of porphyrins leads to

simplification of the spectrum since the Q bands are reduced from four to two. In addition, the UV-vis spectra of metalloporphyrins display also only two Q bands, defined as α (appearing at lower energy) and β (Figure 1.3b). The relative intensities of these two bands are related to the metal and its coordination mode.

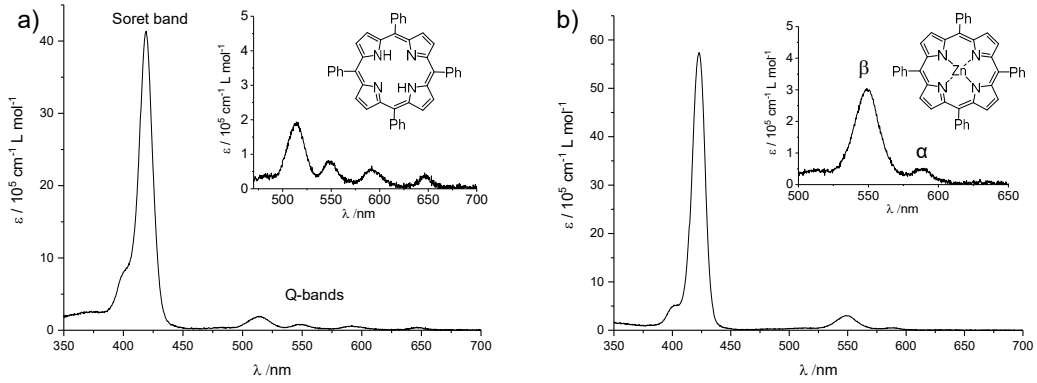

Figure 1.3 Typical UV-vis absorption spectra of a) a free-base 5,10,15,20-tetraphenylporphyrin (TPP) and b) Zn(II) TPP. Insets show zoom of the 700-500 nm area.

Metalloporphyrins are also classified as having either regular or irregular absorbance features, producing normal, hypso or hyper electronic spectra.[37] Regular absorption is determined mainly by the π-electrons of the porphyrin ring and usually is characteristic of metalloporphyrins with closed-shell metal ions (for example, Zn(II)). On the other hand, irregular absorption occurs when there is a strong interaction between the central metal and the ring electrons, which is characteristic of metalloporphyrins with open-shell metal ions (for example, Co(II), Ni(II) *etc.*). It should be noted, that the characteristic absorption spectra of porphyrins undergo perturbations upon the different factors such as the conjugation pathway, symmetry and other chemical variations.[38]

The first theoretical calculations, explaining the main features of the porphyrin absorption bands in the visible region, were reported by *Gouterman* and co-workers.[39,40] They proposed the four-orbital model that uses two HOMOs, namely an a_{1u} and an a_{2u}, and two degenerated LUMOs (e_g^*), responsible for the pattern of the absorption bands. Transitions between these orbitals gave rise to two excited states. Due to orbital mixing these two states are split in energy. This results in a higher energy state with greater oscillator strength, giving rise to the *Soret* band, and a lower energy state with less oscillator strength, giving rise to the Q bands.

Emission from the excited states for porphyrins occurs from the π-π* state of the porphyrin ring. The fluorescence spectra for porphyrins display two Q bands (Figure 1.4) located around 700 nm. The insertion of a heavy metal to form a metalloporphyrin causes a decrease in the fluorescence quantum yield due to increase in the rate of intersystem crossing from the heavy atom effect. The fluorescence bands for metalloporphyrins are typically located around 600 nm (Figure 1.4b), while the phosphorescence bands are found around 700 nm.[39]

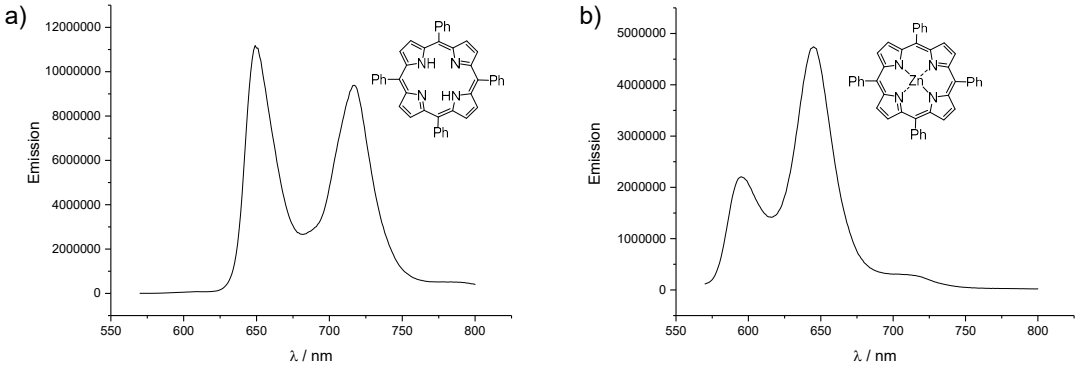

Figure 1.4 Typical fluorescence spectra of a) a free-base TPP and b) Zn(II) TPP.

1.2 Peripheral modification of porphyrin core

The electronic structure of porphyrins can be easily perturbed through conjugative peripheral modifications, resulting in the appearance of appealing optoelectronic properties. Specifically, a simple extension of conjugated length rises the HOMO energy, while lowers the LUMO energy, thus narrowing the HOMO-LUMO gap and realising remarkable red-shift of absorption spectra. The main of this section, is to review the most efficient approaches for tailor-made tuning of the electronic properties of porphyrins. Figure 1.5 depicts two possible pathways towards the modification of the porphyrin macrocycle. The first route includes the peripheral insertion of heteroatom, which strongly affects the π-system of the porphyrin through inductive and mesomeric effects. An additional pathway is based on the extension of the π-conjugation through annulation of the porphyrin core with polyaromatic hydrocarbons (PAHs) or heterocycles. Combination of these two approaches gives a group of so-called "heteroatom-embedded porphyrins", in which heteroatoms are directly incorporated in the

extended conjugated π-system and significantly affect the delocalization pathway of the π-electrons.

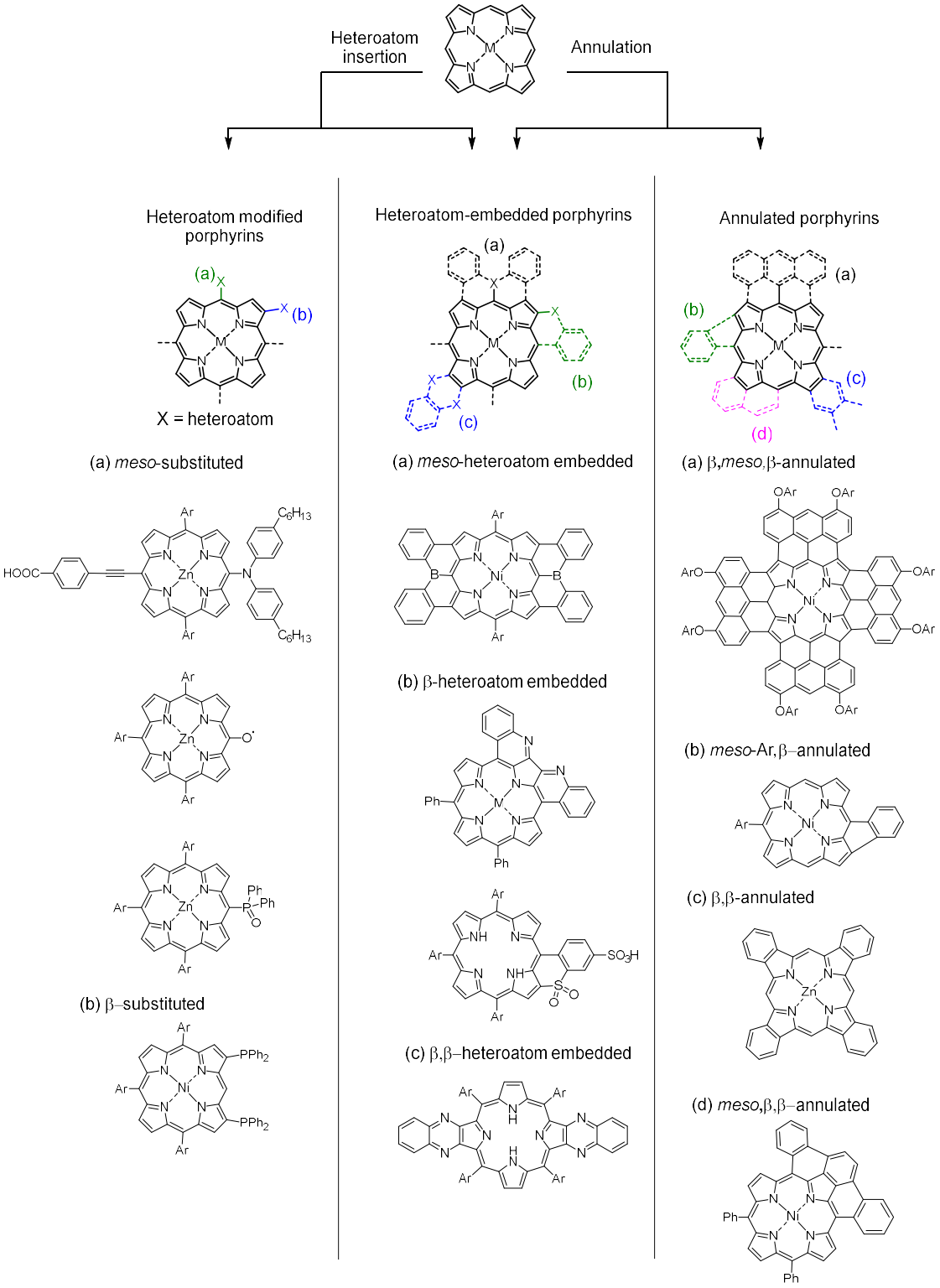

Figure 1.5 Approaches toward modification of porphyrins core.

1.2.1 Heteroatom-modified porphyrins

Peripheral modification of a porphyrin ring by introducing heteroatoms is widely used not only for fine-tuning of the π-electron energy but also for creating structurally well-defined porphyrin arrays.[41–46] Indeed, heteroatom-modified porphyrins exhibit unique coordination behaviour, leading to porphyrin dimers through electrostatic interactions, metal-ligand coordination or hydrogen bonds.[42] Besides, *meso*-hydroxy substituted porphyrins provide a reliable way to remarkably stable *meso*-oxy radicals,[47,48] while *meso*-diarylamino substituted push–pull porphyrins are excellent dyes for dye-sensitized solar cells (DSSC).[49,50] In this context, the main focus will be to reveal the heteroatom-linkage effects on the photophysical and optoelectronic properties of these modified porphyrins. Chemical functionalization of porphyrins with heteroatoms can be achieved through peripheral substitution at the *meso*- or β-positions of the porphyrin core (Figure 1.5). The most convenient route to accomplish this, is based on organometallic methodologies, enabling the synthesis of a wide range of substrates, ready for further modifications.[41,43]

For example, *Matano et al.* reported the synthesis of *meso*-phosphanylporphyrins **1-5**[51] and *meso*-phosphinylporphyrins **1-6**[52] by Pd- or Cu-catalyzed C–P cross-coupling reactions of *meso*-iodoporphyrins **1-4** with Ph_2PH or $R_2P(O)H$ (Scheme 1.4).

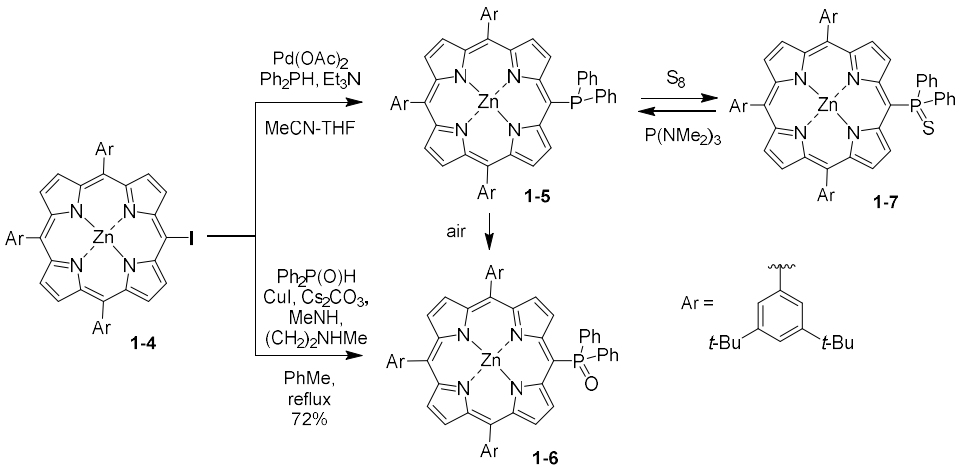

Scheme 1.4 Synthesis of *meso*-phosphanylporphyrins **1-5** and *meso*-phosphinylporphyrins **1-6**.

Due to **1-5** being air-sensitive, the crude material was treated with S_8, producing air-stable *meso*-thiophosphorylporphyrin **1-7**. Subsequent desulfurization of **1-7** was carried out with an excess of $P(NMe_2)_3$ in PhMe, affording **1-5** in 90-95% yields through reprecipitation

under inert conditions.[51] The complexation of **1-5** with Pd(II) or Pt(II) salts through selective cyclometallation at the *β*-position yielded coplanar phosphametallocycle-fused diporphyrins **1-8** and **1-9** respectively (Scheme 1.5).[51,53] The C-M-C linkage (M = Pd, Pt) was achieved by first coordination of the phosphine to the metal cation, followed by regioselective β-C−H activation. Interestingly, treatment of **1-5** with $Pd(OAc)_2$ afforded a mixture of Pd-mononuclear **1-8** and Pd-dinuclear complexes **1-10** in 55% and 23% yield, respectively, while the complexation with $PtCl_2$(cod) (cod-1,5-cyclooctadiene) gave only Pt-mononuclear complex **1-9** in 62% yield.

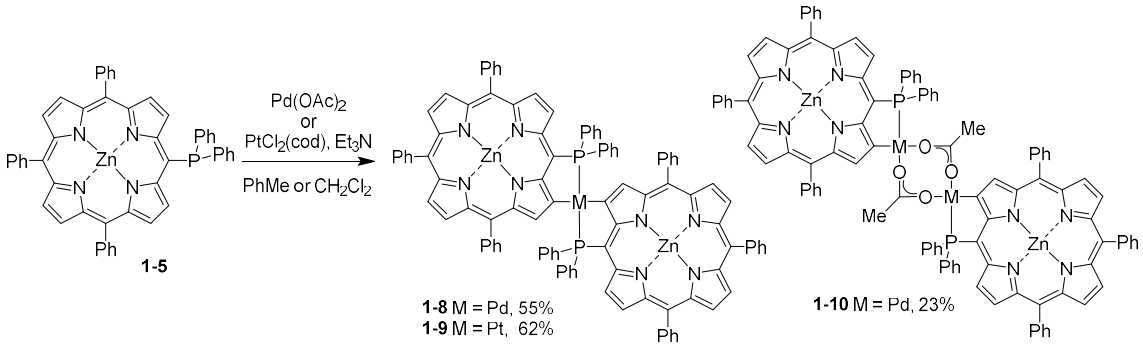

Scheme 1.5 Synthesis of phosphametallacycle-linked diporphyrins **1-8** and **1-9**.

UV-vis spectroscopy revealed the reciprocal electronic communication between the coplanar porphyrin rings of **1-8** and **1-9** by showing split and/or broadened *Soret* bands compared to **1-7**. Moreover, the electrochemical study of phosphaplatinacycle-fused **1-9** showed two-step, one-electron oxidation, indicating the stabilization of radical cation **1-9** by delocalization of the unpaired electron *via* the peripheral Pt–C bonds. These findings suggested the weak but definite impact of dπ-pπ orbital interaction at the C–M–C linkages on the opto-electrochemical properties of the metal-linked porphyrins.[54] Similarly to the synthesis of **1-5** and **1-6**, *meso*-sulfanylporphyrins and *meso*-sulfinylporphyrins were obtained through Cu-catalyzed C–S cross-coupling reaction of *meso*-iodoporphyrin with benzenethiol and *n*-octanethiol.[55]

Later, *Osuka et al.* described the synthesis of porphyrin-based PCP pincer complexes **1-12**–**1-14** through *meso*-C-H metalation of diphosphanylporphyrins **1-11** with Ni(II), Pd(II), and Pt(II) salts respectively (Scheme 1.6).[56] The electronic perturbations caused by the outer metals were displayed by UV-vis absorption spectroscopy. In contrast to **1-13** (*Soret* band: 438 nm; Q bands: 543, 580 nm) and **1-14** (*Soret* band: 444 nm; Q bands: 549, 589 nm), Ni(II)

complex **1-12** exhibits split and broadened *Soret* bands (397 and 458 nm) along with more red-shifted Q bands (558 and 599 nm), suggesting stronger interaction between the outer Ni(II) d orbitals and the π-orbitals of the porphyrin core. Furthermore, it was noted, that the catalytic activity of Pd(II) pincer complex **1-13** in the 1,4-reduction of chalcone is affected by the electronic interplay between the inner and the outer metals.

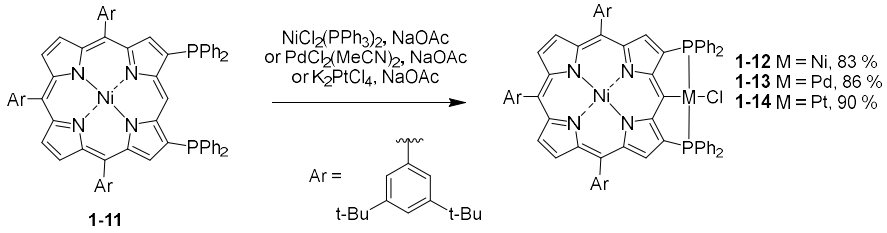

Scheme 1.6 Synthesis of porphyrin-based PCP pincer complexes **1-12**-**1-14**.

A variety of porphyrin derivatives with attractive properties have been prepared by introducing an amino group at the *meso*-position of the macrocycle, and further functionalization through alkylation, nucleophilic substitution, diazotization *etc*.[44] Among them, *meso*-diarylamino substituted push-pull porphyrins have attracted much attention in constructing porphyrin-based sensitizers for DSSC due to their exceptional photostability, visible-light absorption as well as efficient charge-separation capability.[49,57–59] For instance, *Lee et al.* developed a device made of *meso*-diarylaminoporphyrin **1-18**, absorbed on TiO_2, with overall efficiency of power conversion (η-value) reaching to 6.0%.[60] Accordingly, bromination of porphyrin **1-15** with NBS, followed by Pd(II)-catalyzed amination afforded *meso*-diarylamino porphyrin **1-17**. Subsequent deprotection of **1-17** with TBAF followed by *Sonogashira* coupling with 4-iodobenzoic acid yielded **1-18** (Scheme 1.7).

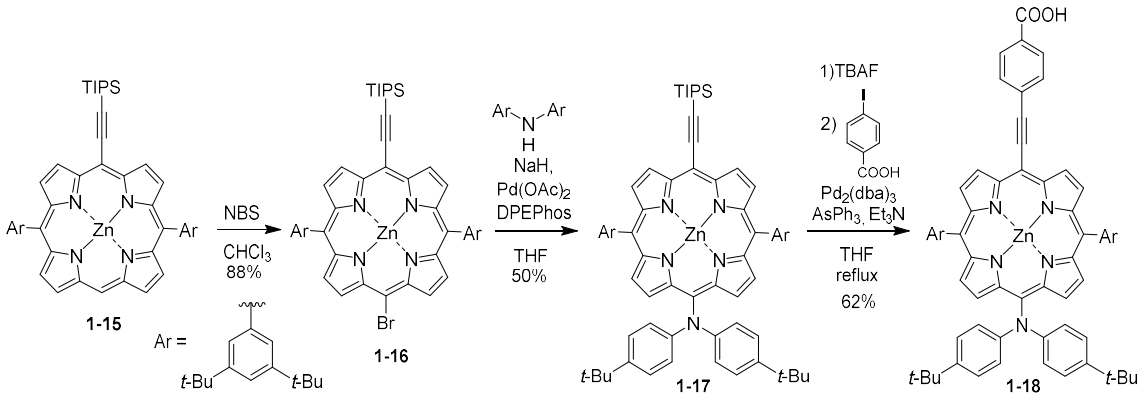

Scheme 1.7 Synthesis of *meso*-diarylaminoporphyrin **1-18**.

Later on, *Grätzel* and co-workers enhanced the η-value of DSSC-device to *ca.* 11% by using porphyrin **1-19** equipped with long aliphatic chains which prevent the stacking of molecules and diminish intermolecular charge recombination (Figure 1.6).[61,62] Further incorporation of 2,3,1-benzothiadiazole moiety in **1-20** resulted in the increase of the η-value to 12.7%. Moreover, the use of bulky *meso*-diarylamino substituent such as in the case of **1-21** enabled to develop a device with η-value of 13%, which is the best result for porphyrin-based DSSCs.[63,64] Therefore, the introduction of a push–pull system and the elongation of π-conjugation within the porphyrin macrocycle are effective means to improve the light-harvesting properties.

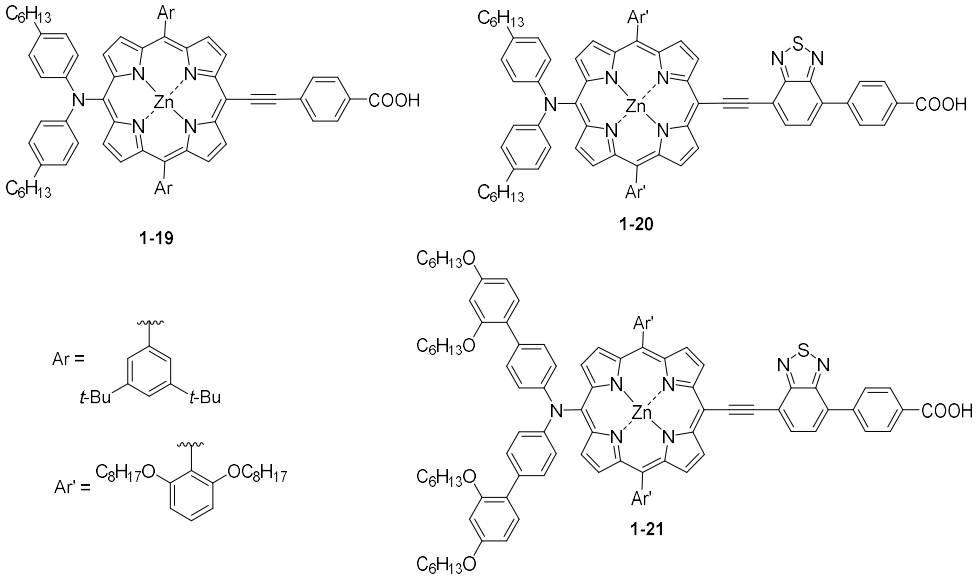

Figure 1.6 Chemical structures of *meso*-diarylaminoporphyrins **1-19–1-21**.

Recently, *Osuka et al.* reported the generation of remarkably stable 10,15,20-triarylporphyrin *meso*-oxy radicals **1-26**–**1-28** by oxidation of *meso*-hydroxyporphyrins **1-23–1-25** with PbO_2 (Scheme 1.8).[47,48] Ni(II) porphyrin **1-23** was first prepared in 82% yield by Pd-catalyzed hydroxylation of *meso*-bromoporphyrin **1-22**. Subsequent demetallation of **1-23** with H_2SO_4/CF_3CO_2H gave free-base porphyrin **1-24** in 97% yield. Zn(II) porphyrin **1-25** was obtained by treating **1-24** with $Zn(OAc)_2$ in 83% yield. Finally, upon oxidation of **1-23–1-25** with PbO_2, *meso*-oxy radicals **1-26, 1-27** and **1-28** were isolated in 91, 86 and 89% yields, respectively.

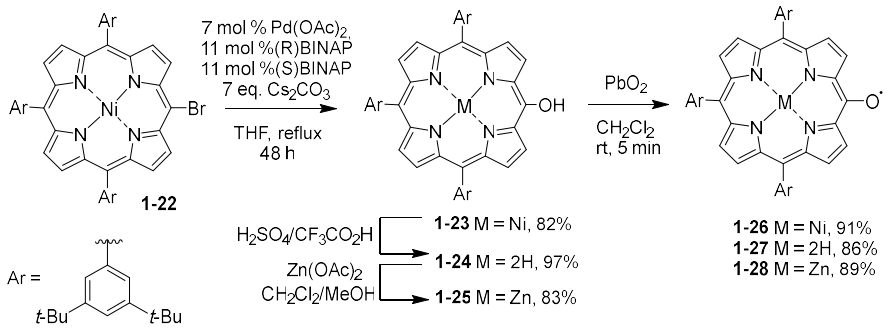

Scheme 1.8 Synthesis of 10,15,20-triarylporphyrin *meso*-oxy radicals **1-26–1-28**.

Curiously, while radicals **1-26** and **1-27** were observed as monoradicals in solution, Zn(II) porphyrin *meso*-oxy radical **1-28** was found as a face-to-face dimer **1-29** both in solution and in the solid state (Scheme 1.9). Addition of pyridine caused the quantitative dissociation of **1-29** into pyridine-coordinated monoradical **1-30**. The dimer **1-29** displayed a broad absorption band at around 1000–2000 nm, suggesting the symmetry-breaking charge transfer band.

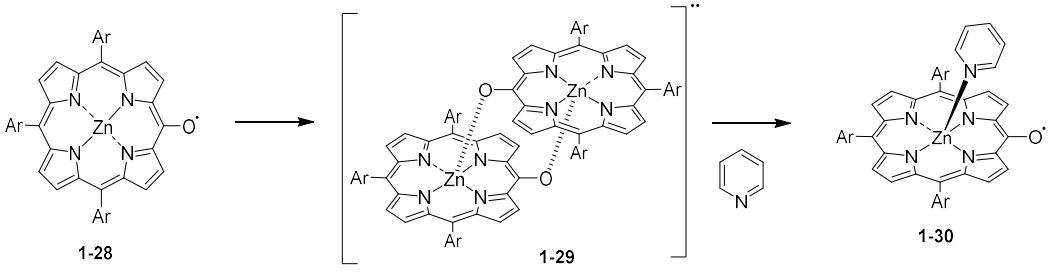

Scheme 1.9 Synthesis of face-to-face dimer **1-30**.

The UV-vis absorption spectra of hydroxyporphyrins **1-23**–**1-25** in THF display *Soret* bands around 420 nm and Q bands around 550 nm (Figure 1.7a). On the contrary, the absorption spectra of monoradicals **1-26**, **1-27** and **1-30** in CH_2Cl_2 show *Soret* bands around 420–440 nm and Q bands around 480-860 nm, along with weak and broad bands around 1100-1600 nm, that are characteristic of porphyrinoid radicals as shown in Figure 1.7b. In addition, all *meso*-oxy radicals exhibited narrow HOMO-LUMO gaps of around 0.7 V according to cyclic voltammetry.

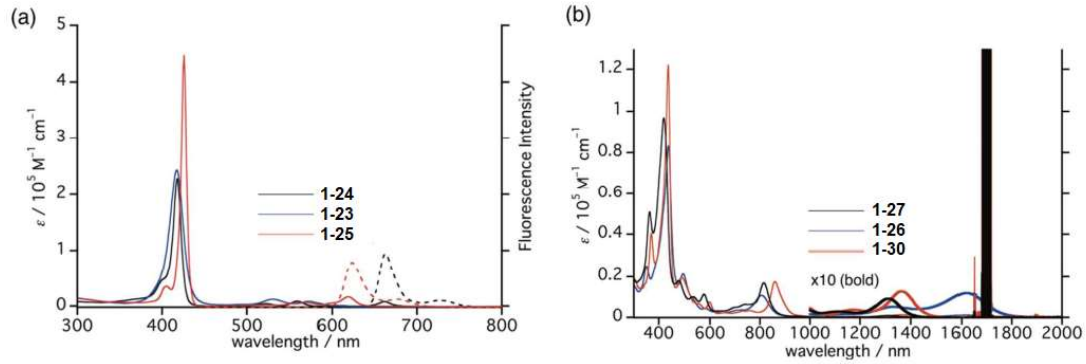

Figure 1.7 a) UV-vis absorption (solid line) and emission (dashed line) spectra of **1-24**, **1-23** and **1-25** in THF; b) UV-vis absorption spectra of **1-27**, **1-26** and **1-30** in CH_2Cl_2.[47]

1.2.2 Annulated porphyrins

The elongation of the porphyrin π-system can be achieved by the fusion of aromatic fragments on β-pyrrolic positions or by the introduction of *meso*-aryl substituents with their further connection to the β-pyrrolic moieties (Figure 1.5). Since the porphyrin system exhibits the electron rich character, the most efficient way to accomplish this type of functionalization, is based on inter- or intra- molecular oxidative aromatic coupling reactions (*e.g.* Scholl reaction).[65,66] The emerged electronic perturbation in the annulated porphyrins depends not only on the fusion type, but also on the entity and number of fused aromatic rings. [66–72]

1.2.2.1 β,β-Arene-annulated porphyrins

The first approach to annulated porphyrins involves the addition of fused aromatic rings to the adjacent β-pyrrolic positions. The simplest example of β,β-arene-annulated porphyrins is *meso*-unsubstituted tetrabenzoporphyrin (TBP) **1-32**, initially prepared by Zn(II)-templated condensation of isoindolinone-3-acetic acid at 350 °C (Scheme 1.10).[73]

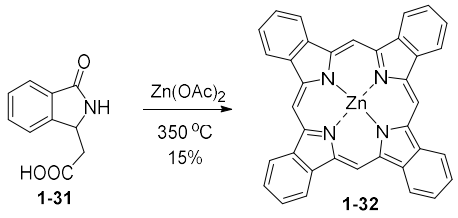

Scheme 1.10 Synthesis of tetrabenzoporphyrin **1-32**.

Independently, *Lash*[74,75] and *Ono*[76,77] groups have developed more convenient synthetic route towards the conjugated porphyrins using arene-fused pyrroles. The latter were preliminary prepared by *Barton-Zard* reaction of aromatic nitro compounds with ethyl isocyanoacetate.[78,79] For instance, tetraaryltetraacenaphthoporphyrins **1-35** was synthesized starting from the reaction of 1-nitroacenaphthylene **1-33** with ethyl isocyanoacetate in the presence of DBU, followed by the cleavage of the ester moiety with KOH in ethylene glycol at 180 °C (Scheme 1.11).[80] Subsequently, tetracycle **1-34** was condensed with benzaldehyde in the presence of $BF_3{\cdot}Et_2O$, followed by the oxidation with DDQ to produce desired TPP **1-35** in 56% yield.

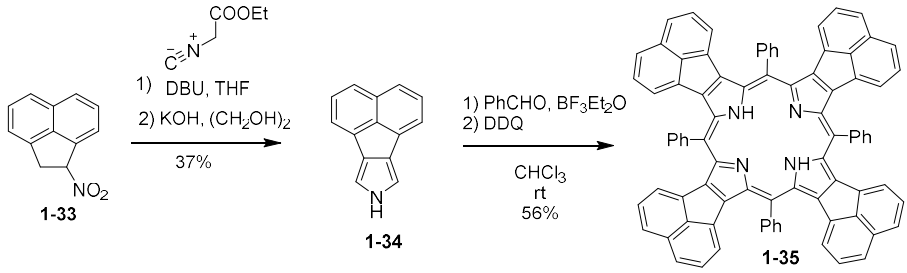

Scheme 1.11 Synthetic route toward tetraaryltetraacenaphthoporphyrin **1-35**.

Vinogradov et al. reported an alternative approach to the synthesis of β,β-arene-fused porphyrins, involving the oxidative aromatization of cyclohexane-annelated porphyrins on the final step.[81–84] As a typical example, the preparation of tetranaphthoporphyrins (TNP) **1-40** is shown in Scheme 1.12.[83] Initially, sulfone **1-36** was subjected to the *Barton-Zard* reaction, yielding pyrrole ester **1-37**, which was then converted to pyrrole **1-38**. The latter was introduced into a *Lindsey*-type condensation, followed by oxidation with DDQ. Interestingly, instead of expected porphyrin **1-39** the target TNP **1-40** was obtained directly as the only product. Similarly to the synthesis of **1-40**, tetraanthraporphyrin (TAnP) **1-41** was also prepared in 36% yield (Scheme 1.12).[85,86]

Remarkably, *meso*-unsubstituted TBPs and TNPs along with their metal complexes display powerful absorption bands in the near-IR (λ_{max} = 610–710 nm, ε = 100,000–300,000 $M^{-1}cm^{-1}$) and strong luminescence ($\Phi \sim 50\%$). Notably, the phosphorescence quantum yields of Pd(II) and Pt(II) TBPs were found to reach as high as 20–50%.[87]

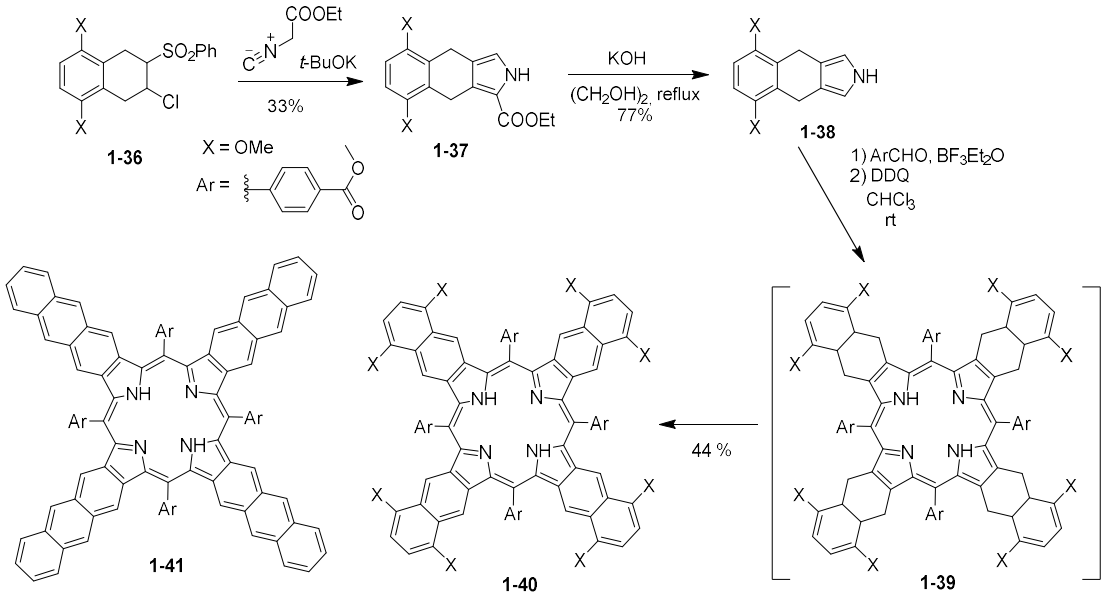

Scheme 1.12 Synthetic route towards tetraaryltetranaphthoporphyrin **1-40**.

Another appealing approach to β,β-arene-fused porphyrins was proposed by *Ono* and co-workers and it is based on a retro-*Diels-Alder* reaction[88] of bicyclo[2.2.2]octadiene-fused precursors.[89] Following this route, soluble porphyrins fused with bicyclo[2.2.2]octadiene were quantitatively converted into insoluble TBPs, TNPs[90] or TAnPs[91] upon heating at 200-290 °C. For instance, the preparation of *meso*-free **1-47** and *meso*-substituted TAnPs **1-48** is outlined in Scheme 1.13.

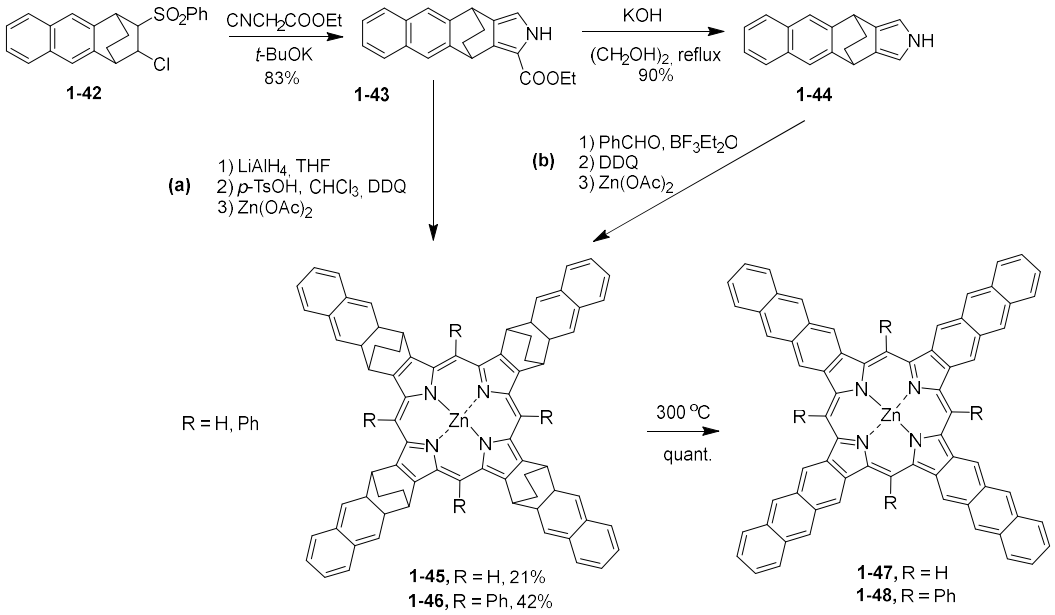

Scheme 1.13 Synthetic routes towards *meso*-free and *meso*-substituted TAnPs.

The *Barton-Zard* reaction of sulfone **1-42** with ethyl isocyanoacetate was followed by the treatment of **1-43** with KOH affording pyrrole **1-44** in 90% yield. The bicyclo[2.2.2]octadiene-fused precursors **1-45** and **1-46** were obtained in two different ways: (a) reduction of **1-43** with $LiAlH_4$, followed by acid-catalyzed condensation in the presence of TsOH and further treatment by DDQ and (b) *Lindsey*-type condensation of **1-44** with aldehyde, followed by oxidation with DDQ. Metallation of the free-base macrocycle in both cases afforded Zn(II) porphyrins **1-45** and **1-46**. Upon heating at 300 °C, metalloporphyrins **1-45** and **1-46** were converted in pure Zn(II) TAnPs **1-47** and **1-48**, respectively, with quantitative yield. The main advantage of this approach is the fact, that precursors **1-45** and **1-46** are well soluble in common organic solvents and can be easily purified by silica gel column chromatography, thus yielding pure insoluble TAnPs **1-47** and **1-48**.

Along the series TBPs-TNPs-TAnPs each additional benzene moiety fused onto the pyrrolic subunits causes unprecedented bathochromic shifts of about 20 and 70 nm to both the *Soret* and the Q band absorptions, respectively.[92] Thus, the UV-vis spectroscopy revealed a red shift of λ_{max} from 553 nm for **1-46** to 802 nm for **1-48,** indicating a reduced HOMO-LUMO gap upon the linear enlargement of π-conjugation.[91]

1.2.2.2 β,Meso,β-arene-annulated porphyrins

In 2004, *Scott et al.* for the first time reported the synthesis of *meso,*β,β triply fused porphyrins **1-49** and **1-50**.[93] They were obtained through initial oxidative rearrangement of dispiro-porphodimethane in the presence of DDQ to form *cis*- and *trans*- doubly linked porphyrins, followed by oxidation with $FeCl_3$/DDQ (Scheme 1.14).

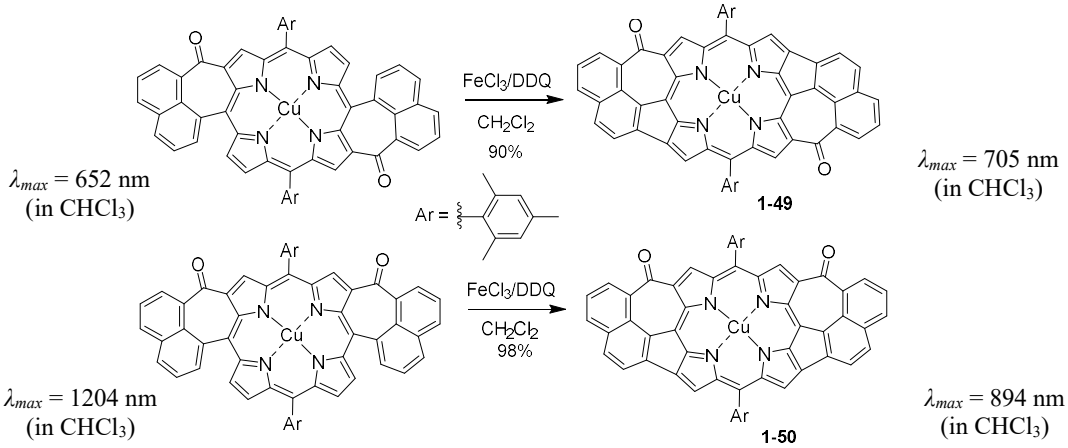

Scheme 1.14 Synthesis of *bis*(naphthoazulen-8-one)-fused Cu(II) porphyrins **1-49** and **1-50**.

Wu et al. developed the stepwise synthesis of mono- and *bis*-BODIPY-fused porphyrins **1-51** and **1-52**, respectively (Figure 1.8).[94] These compounds exhibit significant bathochromic shift with an absorption maximum at 890 nm and 1040 nm for **1-51** and **1-52**, respectively. Moreover, *bis*-BODIPY-fused porphyrin **1-52** has a larger value of near-IR absorption maximum compare to that of the corresponding *bis*-azulene-fused porphyrin **1-54** (λ_{max} = 1014 nm)[95] and *bis*-anthracene-fused porphyrins **1-57** (λ_{max} = 973 nm).[96]

Along with mono- and *bis*-azulene-fused porphyrins **1-53** and **1-54**, *Osuka et al.* have extended the synthetic strategy, involving the oxidation of *meso*-(4-azulenyl)-porphyrins with $FeCl_3$, to quardruply azulene-fused porphyrin **1-55** (Figure 1.8).[95] The latter displays a red-shifted absorption with *Soret* band at 684 and Q band at 1136 nm, thus covering the whole visible and near-IR regions up to ~1200 nm.

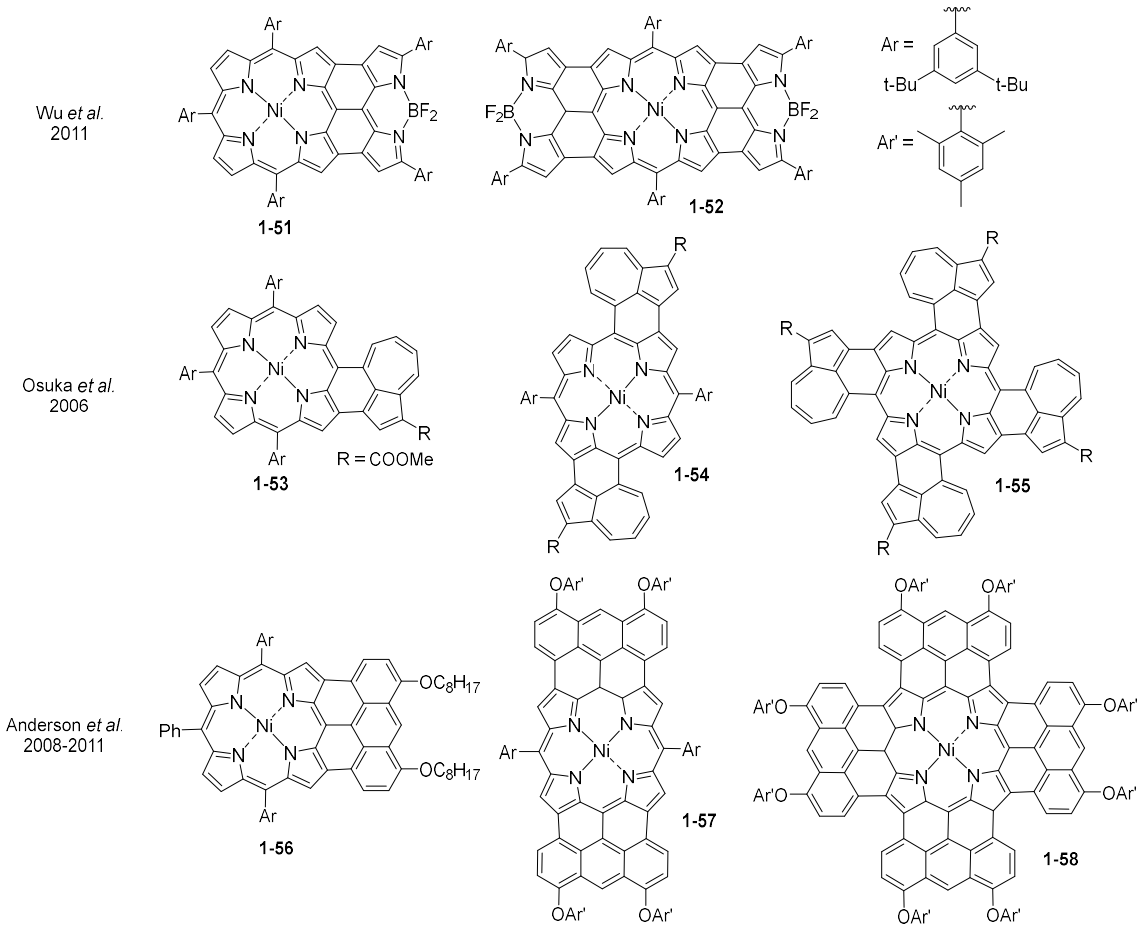

Figure 1.8 Chemical structures of BODIPY-, azulene- and anthracene-fused porphyrins.

On the other hand, *Anderson et al.* expanded the porphyrin core with one, two and even four fused anthracenes to produce **1-56**, **1-57** and **1-58**, respectively (Figure 1.8).[96–98] As an example, the synthesis of tetraanthracenylporphyrin **1-58** is shown in Scheme 1.15. Anthrone **1-59** was reacted with PBr_3. The resulted bromoanthracene **1-60** was treated with *n*-BuLi and sequentialy with pyrrole-2-carboxaldehyde to afford alcohol **1-61** which was not isolated. Subsequent tetramerization of **1-61** with propionic acid led to **1-62** in 10% yield. Treatment of metallated **1-63** with $FeCl_3$ in CH_2Cl_2 resulted in eightfold ring closure, producing fully fused **1-58** in 49% yield.

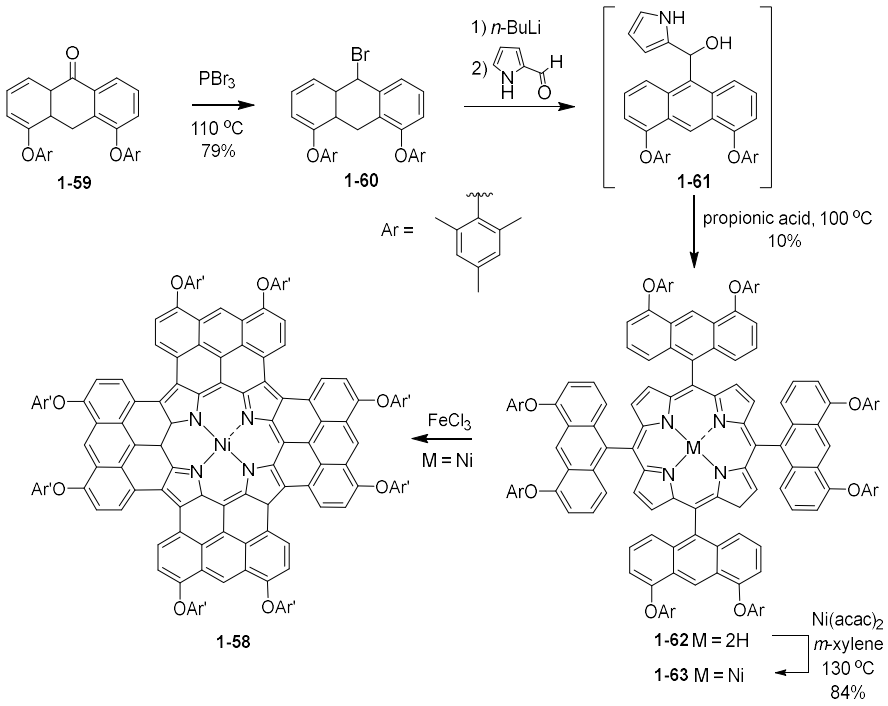

Scheme 1.15 Synthesis of tetraanthracenylporphyrin **1-58**.

In contrast to unfused derivative **1-63**, tetraanthracenylporphyrin **1-58** shows sharper and more profound Q band at 1417 nm due to the high symmetry of the macrocycle and exceptionally small electrochemical HOMO-LUMO gap (0.61 eV) (Figure 1.9). Interestingly, the *Soret* band of **1-58**, located at 850 nm, is the longest detected wavelength for *Soret* bands of porphyrin monomers.[97] It should be noted, that **1-58** (λ_{max} = 1417 nm) displays more profound changes in the absorption spectra compared to TAnP **1-48** (λ_{max} = 802 nm), where the anthracene units are fused to the β-pyrrolic positions.

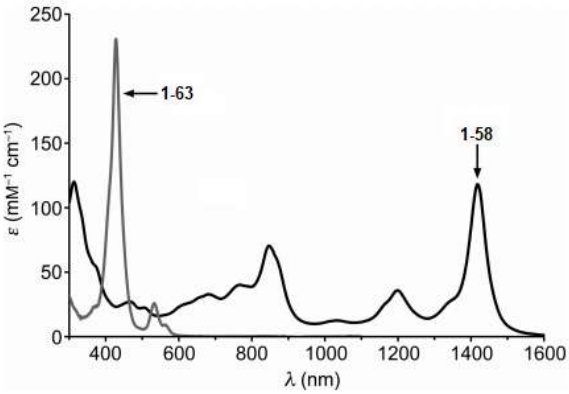

Figure 1.9 UV-vis/NIR absorption spectra of unfused tetraanthracenylporphyrin **1-63** (grey line) and fused tetraanthracenylporphyrin **1-58** (black line) in PhMe.[97]

Other representative examples of β,meso,β-arene-annulated porphyrins are oligoporphyrins, connected by multiple covalent bonds. Porphyrin oligomers have attracted special attention due to their coplanar structure, extended π-electron conjugation, extremely small HOMO–LUMO gaps and red-shifted absorption. Among them various directly fused porphyrin oligomers are of particular interest. The pioneering work by *Sakata*, describing the synthesis of *meso*-β-fused diporphyrin **1-64** in the presence of $TeCl_4$ (Scheme 1.16), was published in 1999.[99]

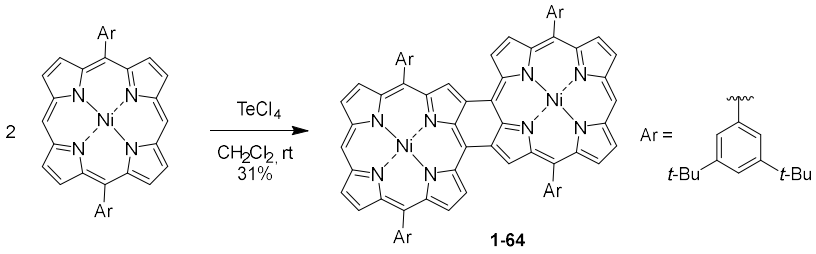

Scheme 1.16 Synthesis of *meso*-β-fused diporphyrin **1-64**.

This strategy was further modified and extended by *Osuka* and co-workers.[100–104] In particular, the oxidative fusion of *meso–meso* linked porphyrin oligomers in the presence of *tris*(4-bromophenyl)aminium hexachloroantimonate (BAHA) was carried out to produce *meso-meso*, β-β, β-β triply linked di- and triporphyrins **1-65** and **1-66**, respectively (Scheme 1.17).[100] To suppress the concurrent chlorination at the porphyrin periphery and to increase the yield of the triply linked porphyrin oligomers, $Sc(OTf)_3$ was used in addition to DDQ.[101] Interestingly, triply linked dimer **1-65** (λ_{max} = 996 nm) exhibits a different red-shift compared to *Sakata's* doubly fused diporphyrin **1-64** (λ_{max} = 743 nm), indicating the

dependence of the electronic properties on the type of annulation. The linear porphyrin tapes were extended up to dodecamer **1-67**[101] and later, up to the 24-mer with the aid of bulky substituents to avoid the undesired aggregation.[105] It was found, that the increase in the number of porphyrins causes progressive bathochromic shift reaching 2400 nm for a 12-mer **1-67**. Despite the poor solubility, aggregation and facile oxidative degradation of longer arrays, their remarkable properties (*e.g.* low HOMO-LUMO gaps, absorption in NIR regions, low one-electron oxidation potentials *etc*.) make them promising materials for nonlinear optics, molecular wires, NIR sensors and for molecular-scale electronic devices.[101,106,107]

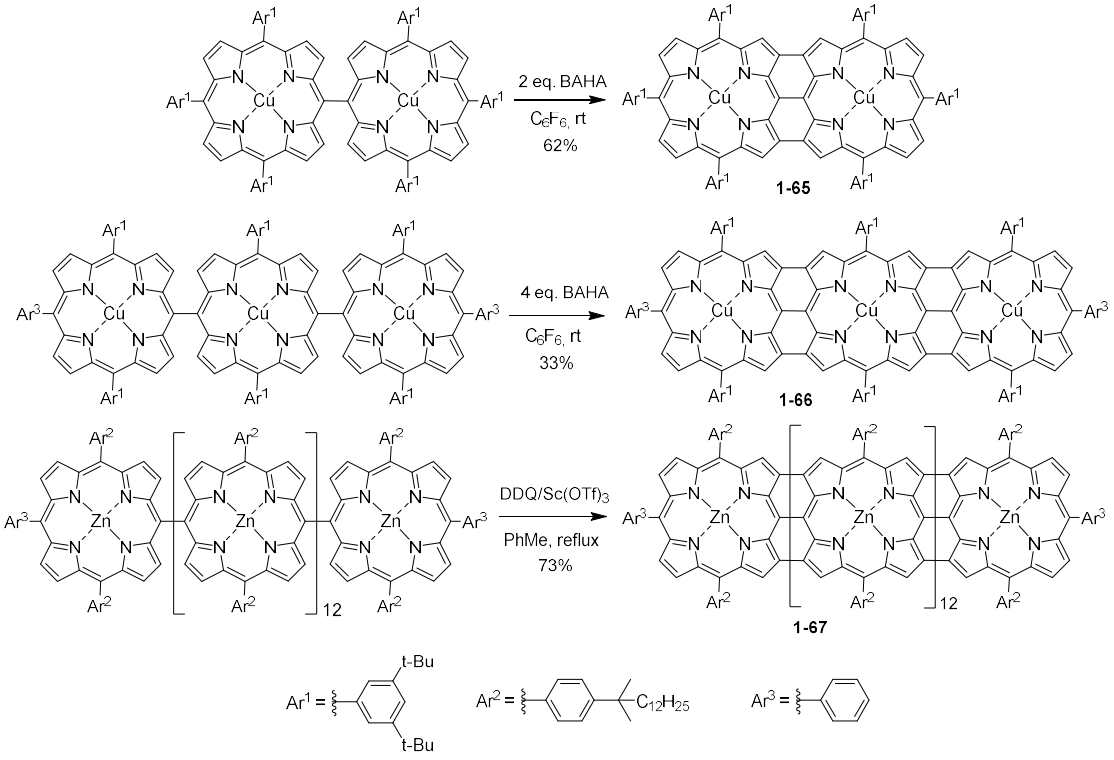

Scheme 1.17 Synthesis of *meso-meso*, β-β, β-β triply linked porphyrin oligomers **1-65**–**1-67**.

1.2.2.3 Meso,β-arene-annulated porphyrins

The synthesis of π-extended porphyrins can be also achieved by the fusion of the *meso*-aryl group to the β-pyrrolic position with the formation of an additional five-membered ring.[68] In this context, *Boyle et al.* reported the Pd(0)-catalysed intramolecular cyclisation of *meso*-(2-iodophenyl)porphyrin **1-68**, leading to fused product **1-69** in 44% yield (Scheme 1.18).[108]

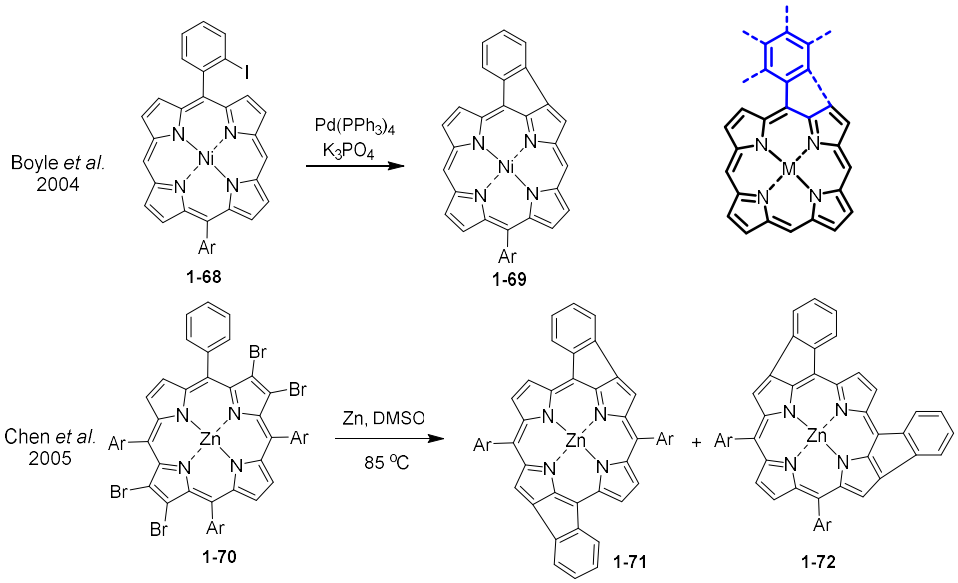

Scheme 1.18 Synthesis of mono and doubly fused products **1-69**, **1-71** and **1-72**.

A further extension of this strategy was reported by *Chen et al.*[109,110] Upon the heating of 2,3,12,13-tetrabromoporphyrin **1-70** in the presence of Zn (50 eq.) in DMSO at 85 °C, doubly fused products **1-71** and **1-72** were obtained in moderate yields as an inseparable mixture (Scheme 1.18). The UV-vis spectra of isomers **1-71** and **1-72** displayed a large bathochromic shift along with the broadening of the *Soret* and Q bands.

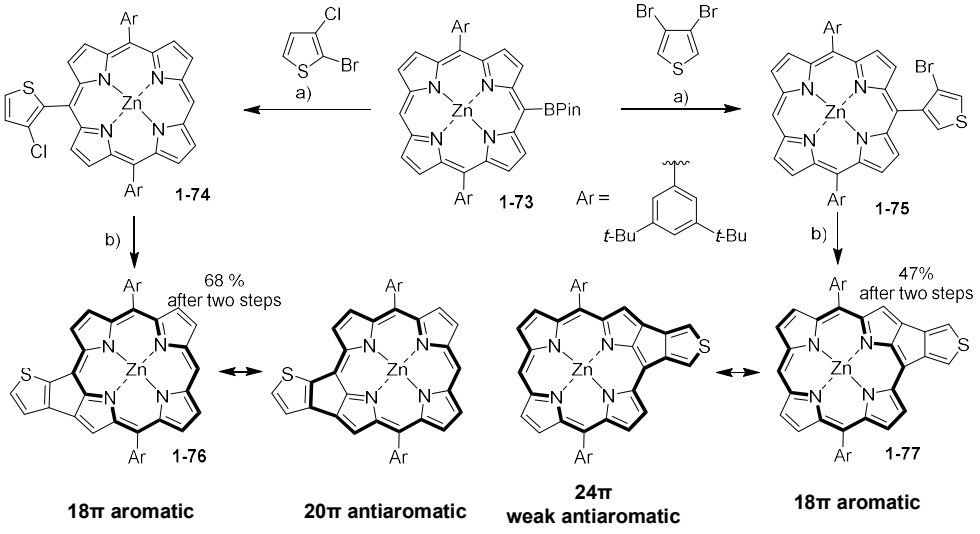

Scheme 1.19 Synthesis of thienoporphyrins **1-76** and **1-77**. Reagents and conditions: a) Pd_2dba_3, PPh_3, Cs_2CO_3, PhMe/DMF, 100 °C; b) $Pd(OAc)_2$, $PCy_3 \cdot HBF_4$, K_2CO_3, DMF, 155 °C.

In 2012, *Matsuo* and co-workers have developed the synthesis of thienoporphyrins **1-76** and **1-77** by the fusion of the *meso*-thiophene ring to the β-pyrrolic position with different directions of the thiophene unit (Scheme 1.19).[111] To achieve this, *Suzuki-Miyaura* coupling of mesoborylporphyrin **1-73** with 2-chloro-3-bromothiophene or 3,4-dibromo-thiophene, followed by intramolecular *Heck* reaction was carried out. The desired thienoporphyrins **1-76** and **1-77** were obtained in 68 and 47% yields, respectively, over two steps. In contrast to **1-77**, where the disruption of the possible 24π antiaromatic circuit by the sulfur atom is observed, porphyrin **1-76** showed a larger antiaromatic contribution due to its 20π conjugated circuit.

1.2.2.4 Meso,β,β-arene-annulated porphyrins

The *Bergman* cyclization[112] was exploited by *Smith* and co-workers in order to achieve the cyclisation of β,β-diethynylporphyrin **1-78** into a highly extended picenoporphyrin **1-79**.[113] Upon heating of **1-78** with 5% of 1,4-cyclohexadiene in chlorobenzene at 190 °C, an unexpected radical cyclization with the adjacent *meso*-phenyl groups occurred, leading to the isolation of **1-79** in 89% yield (Scheme 1.20). To circumvent the initial harsh reaction conditions and to accelerate the desired cyclization, the addition of DDQ was used by *Nath et al*.[114] In this report, the photoinduced cyclization as well as the role of the alkyne terminal group in the cyclization process were thoroughly studied.[115,116]

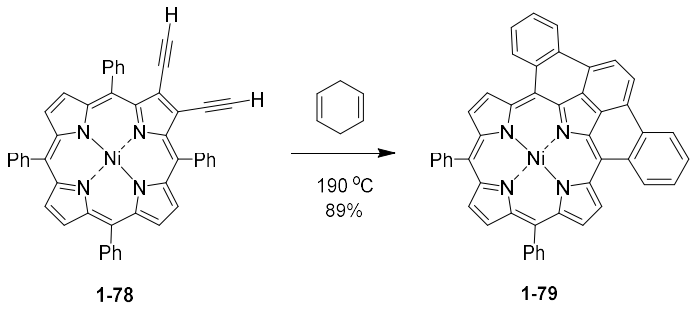

Scheme 1.20 Synthesis of picenoporphyrin **1-79** through *Bergman* cyclization.

1.2.3 Heteroatom-embedded porphyrins

Taking into consideration what has been reported so far, the annulation of porphyrins with PAHs is an effective approach to extend the conjugated length, enabling the fine-tuning

of optoelectronic properties. On the other hand, the peripheral insertion of heteroatoms strongly perturbates the electronic system of porphyrins, resulting in the formation of stable radicals with exceptional coordination behaviour. Combining these two approaches opens the perspective to the synthesis of highly conjugated radicals and other appealing porphyrin derivatives Herein, the term "heteroatom-embedded porphyrin" is defined as an heterocycle annulated porphyrin having heteroatoms directly attached to the *meso*- or β-positions.[117] In this regard, the main message of this section is to reveal the impact of *meso*- and β-embedded heteroatoms on the electronic perturbations within the porphyrin core.

1.2.3.1 Meso-heteroatom embedded porphyrins

Coplanar *meso*-heteroatom-embedded porphyrins are implied as porphyrins, where the *meso*-heteroatom is anchored by one or two β-substituents. Selected examples of *meso*-heteroatom-embedded porphyrins are shown in Figure 1.10.[118–121]

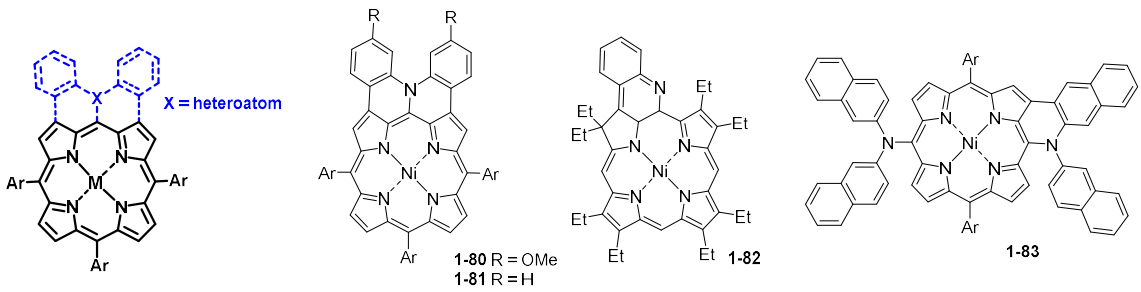

Figure 1.10 Chemical structures of *meso*-heteroatom-embedded porphyrins.

In 2013, *Osuka et al.* reported the oxidative fusion of a *meso*-(diarylamino)porphyrin **1-84** using 20 eq. of $FeCl_3$ and DDQ to afford doubly *meso*-N-fused porphyrin **1-80** (Scheme 1.21).[119] However, the double cyclization was accompanied by undesired β-chlorination, leading to **1-85** in 25% yield. Dechlorination of the latter was achieved by Pd(II)-catalyzed reduction in 81% yield. Notably, using 10 eq. of $FeCl_3$ and DDQ only singly N-fused singly N-fused porphyrin **1-85** was formed in 69% yield. Later, the same group reported an alternative approach to the synthesis of doubly diphenylamine-fused porphyrin **1-81** in 81% yield, involving S_NAr reaction of *meso*-chloro-β,β-diiodoporphyrin **1-86** with diphenylamine in the presence of NaO*t*Bu (Scheme 1.21).[122]

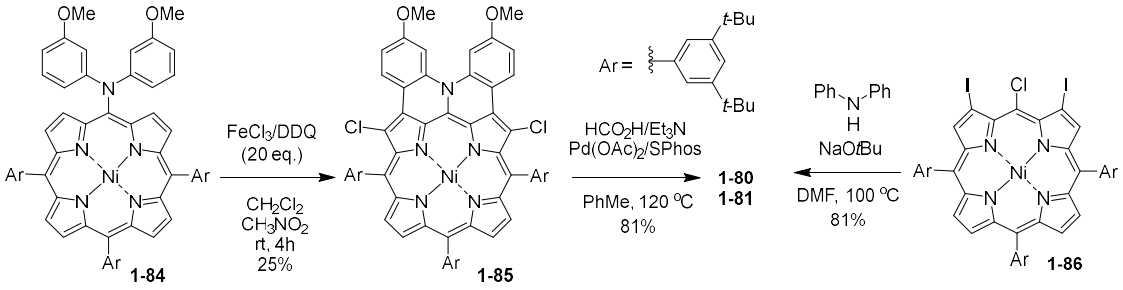

Scheme 1.21 Synthesis of *meso*-diarylamino-fused porphyrins **1-80**.

The cyclic voltammograms of *meso*-diarylaminoporphyrin **1-84** and doubly fused product **1-80** are depicted in Figure 1.11. The first oxidation potential of **1-80** was negatively shifted by 0.21 V compared to that of **1-84**, while the first reduction potential of **1-80** remained almost unchanged. These findings suggested the enhanced electron-donating ability of **1-80** after the planarization of the nitrogen atom. Moreover, the electrochemically generated radical cation was effectively stabilized by delocalization within the porphyrinic system according to the significant difference between the first and second oxidation waves ($E_{ox1} - E_{ox2} = 0.56$ V).

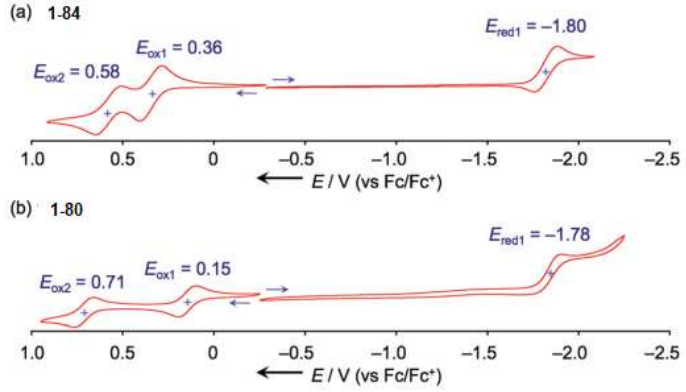

Figure 1.11 Cyclic voltammograms of *meso*-diarylaminoporphyrin **1-84** and doubly fused product **1-80**. Solvent: CH_2Cl_2, supporting electrolyte: *n*-Bu_4NPF_6, and reference electrode: $Ag/AgClO_4$.[117]

The isolation and thorough characterization of the relevant radical cation was accomplished for the first time by *Osuka et al.*[123] For this purpose, **1-86** was protected by chlorination with 2-chloro-1,3-b*is*(methoxycarbonyl)guanidine (Palau'Chlor) to give **1-87**, and then reacted with tris(4-bromophenyl)aminium hexachloroantimonate (Magic Blue) to generate radical cation **1-88** in 91% yield (Scheme 1.22). In a similar way, phenoxazine-fused

porphyrinium radical cation **1-91** was prepared in 79% yield. Interestingly, in both cases the generated radicals were isolated using silica gel column chromatography under open-air conditions. Moreover, the obtained species can be stored for over 6 months without any sign of decomposition, and they exhibited no degradation even after washing with water the solutions of **1-88** and **1-91** in CH_2Cl_2. The remarkable stability of **1-88** and **1-91** was explained by the effective spin-delocalization over the whole molecule and appropriate steric protection at the *meso*- and β-positions. In contrast to the neutral species **1-87** (λ_{max} = 615 nm) and **1-90** (λ_{max} = 628 nm), the absorption bands of radical cations **1-88** (λ_{max} = 903 nm) and **1-91** (λ_{max} = 1583 nm) were found to reach near-IR region, which is typical for radical porphyrinoid species.

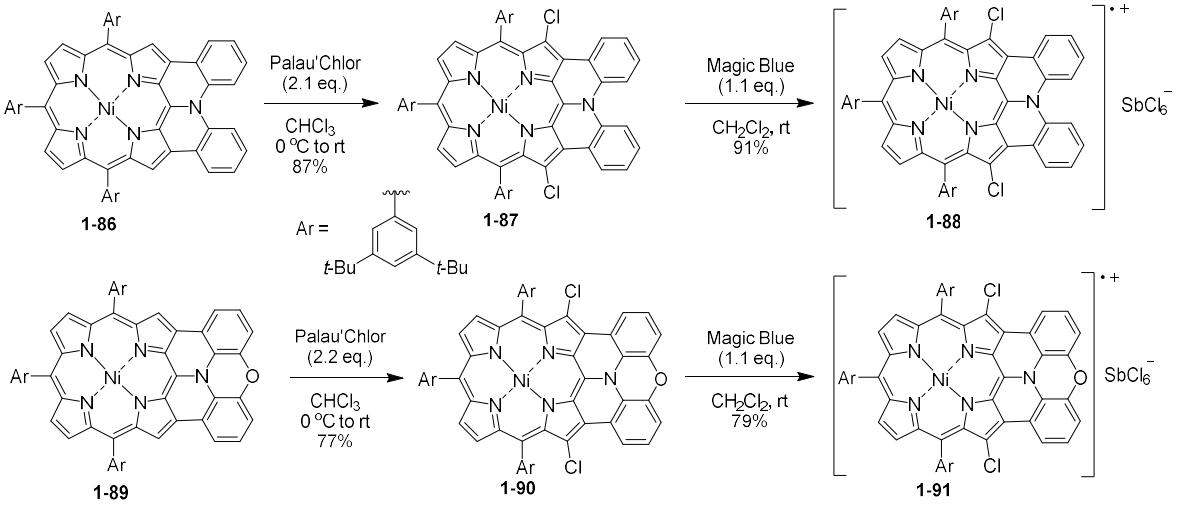

Scheme 1.22 Synthesis of β,β′-dichloro diphenylamine-fused **1-88** and phenoxazine-fused **1-91** porphyrinium radical cations.

Insertion of a phosphorus atom into a fused π-system was described by *Osuka et al.*[124,125] In particular, desired diarylphosphine-fused porphyrin **1-95** with a planarized phosphorus centre was obtained in a stepwise manner starting from 3,5,7-trichloroporphyrin **1-92**, as shown in Scheme 1.23. The S_NAr reaction of **1-92** with lithium diphenylphosphide and the subsequent oxidation with H_2O_2 afforded **1-93** in 56% yield. The latter was subjected to Pd-catalyzed intramolecular C–H arylation producing diphenylphosphineoxide-fused porphyrin **1-94** in 46% yield. Subsequent reduction with $HSiCl_3$ gave **1-95** in 65% yield.

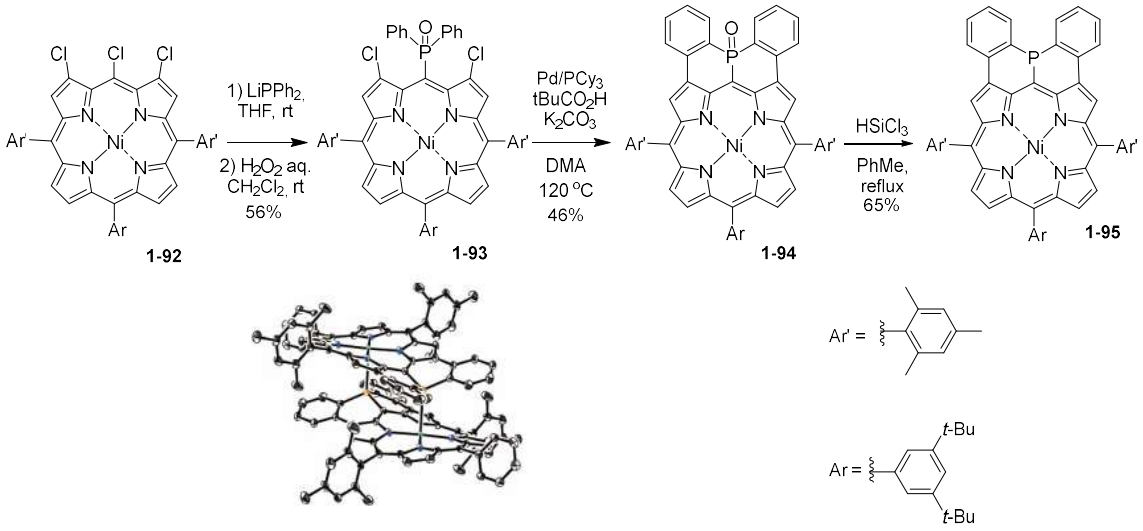

Scheme 1.23 Synthesis of *meso*-diarylphosphine-fused porphyrins **1-95**. Inset: X-ray crystal structure of face-to-face dimer **1-95**.

Interestingly, **1-95** was found in the solid state as a covalently linked face-to-face dimer, in which the embedded atom of phosphorous was coordinated to Ni(II), thus demonstrating the high coordinating ability of phosphorous (Scheme 1.23).

The same group reported the synthesis of triphenylsilane-fused porphyrin **1-99** by exploiting an intramolecular sila-*Friedel-Crafts* reaction.[126] Key intermediate **1-97** was obtained by *Negishi* coupling of 2-chloro-18-iodoporphyrin **1-96** with Zn reagent in 48% yield (Scheme 1.24). Then, **1-97** was subjected to intramolecular sila-*Friedel-Crafts* reaction in the presence of trityl cations to afford *meso*-silylated product **1-98** in 55% yield. This was followed by the Pd-catalyzed intramolecular C–H arylation of **1-98** to furnish **1-99** in 23% yield. The emerged electronic perturbations over **1-99**, where Si atom takes a distorted planarized structure with an almost perpendicular Si–Ph group, are attributed to the effective σ*-π* interaction between the porphyrin π-system and the Si–Ph σ-bond.

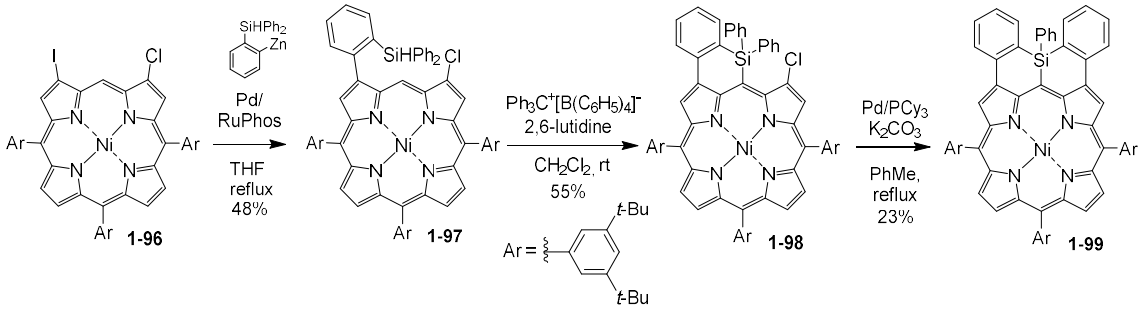

Scheme 1.24 Synthesis of triphenylsilane-fused porphyrin **1-99**.

Organoboron compounds are known to be difficult in handling because of their easy degradation upon exposure to air. However, the "structurally constrained" triarylborones, where the boron atom is embedded in a planar π-system, display high chemical stability.[127–129] In this context, *Osuka* and co-workers developed the synthesis of diphenylborane-fused porphyrin **1-99**, involving the sequential formation of three C–B bonds: *i*) conversion of the TMS-group into BBr_2 through Si–B exchange reaction; *ii*) intramolecular bora-*Friedel-Crafts* reaction at the *meso*-carbon atom; *iii*) ring-closing Si–B exchange reaction.[130] To accomplish this in a one-pot manner, porphyrin **1-100** was treated with BBr_3 in 1,2-dichlorobenzene (*o*-DCB) at 80 °C to give **1-101** in 32% yield (Scheme 1.25). Similarly, *bis*(diphenylborane)-fused porphyrin **1-103** from the corresponding precursor **1-102** was prepared in 3.3% yield.

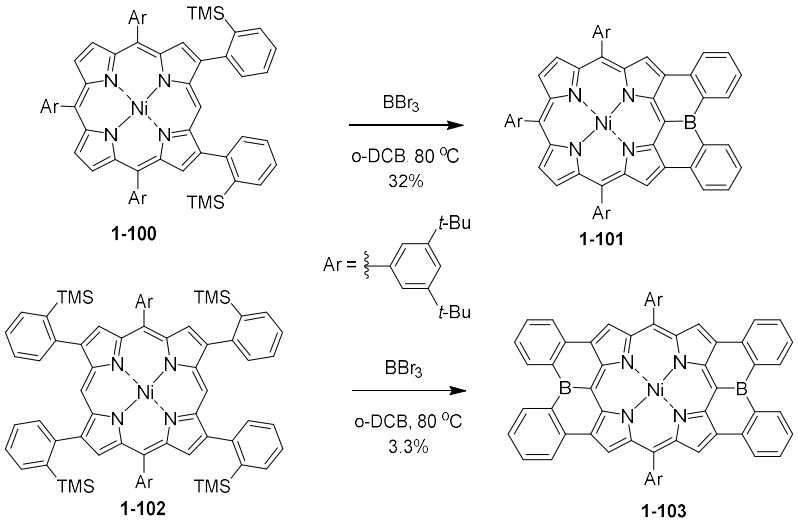

Scheme 1.25 Synthesis of diphenylborane-fused porphyrins **1-101** and **1-103**.

In contrast to the reference porphyrin **1-104** (λ_{max} = 410 nm), *meso*-β-embedded porphyrins **1-101** (λ_{max} = 755 nm) and **1-103** (λ_{max} = 956 nm) exhibit significantly red-shifted absorption bands and enhanced electron-accepting abilities because of the effective electronic conjugation between the boron and porphyrin π-system. Curiously, upon the addition of pyridine to a solution of **1-101** in CH_2Cl_2 a distinct blue shift with the absorption maximum at 596 nm was observed, suggesting the formation of pyridine complex **1-101·Py** and hence, the interruption of the mentioned conjugation.

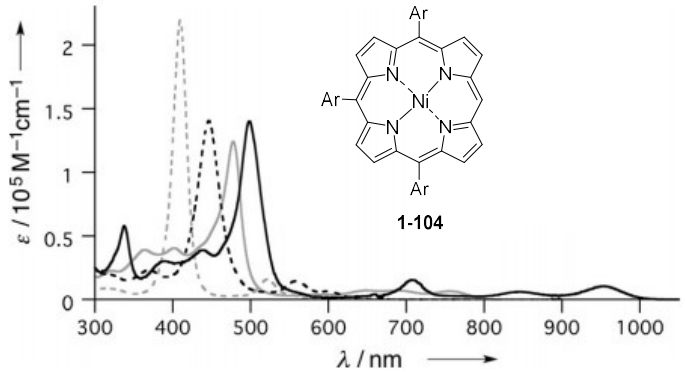

Figure 1.12 UV-vis absorption spectra of **1-104** (grey, dashed line), **1-101** (grey, solid line), **1-101·Py** (**1-101**: 5.0 μM, Py: 0.15 mM, black, dashed line), and **1-103** (black, solid line) in CH_2Cl_2.

1.2.3.2 β-Heteroatom embedded porphyrins

By the term "β-heteroatom-embedded porphyrins" is implied the porphyrins, where β-attached heteroatom is anchored by the β-substituent. Representative examples of such porphyrins are depicted in Figure 1.13.

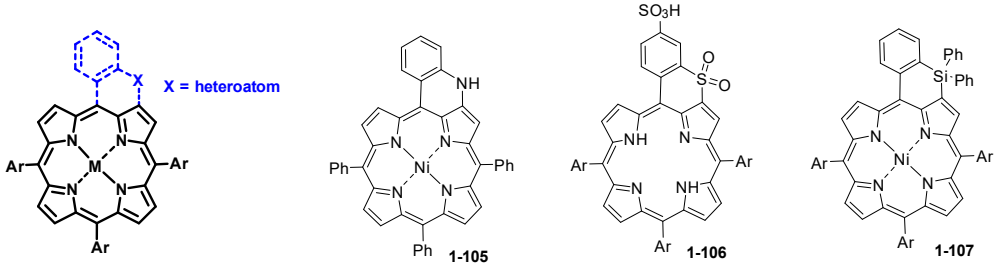

Figure 1.13 Chemical structures of β-heteroatom-embedded porphyrins.

Callot and co-workers reported the synthesis of enaminoporphyrin **1-105** in 75% yield by the initial nitration of **1-108** with $LiNO_3$, followed by the treatment of **1-109** with excess of $P(OEt)_3$ at 155 °C in *o*-DCB (Scheme 1.26).[131] Formylation of **1-105** by *Vilsmeier–Haack* reaction led to enaminoaldehyde **1-110** in 90% yield. The subsequent complexation with $Pd(OAc)_2$ produced two isomeric Pd(II)-connected dimers *cis*-**1-111** and *trans*-**1-111** as the thermodynamic and kinetic products, respectively.

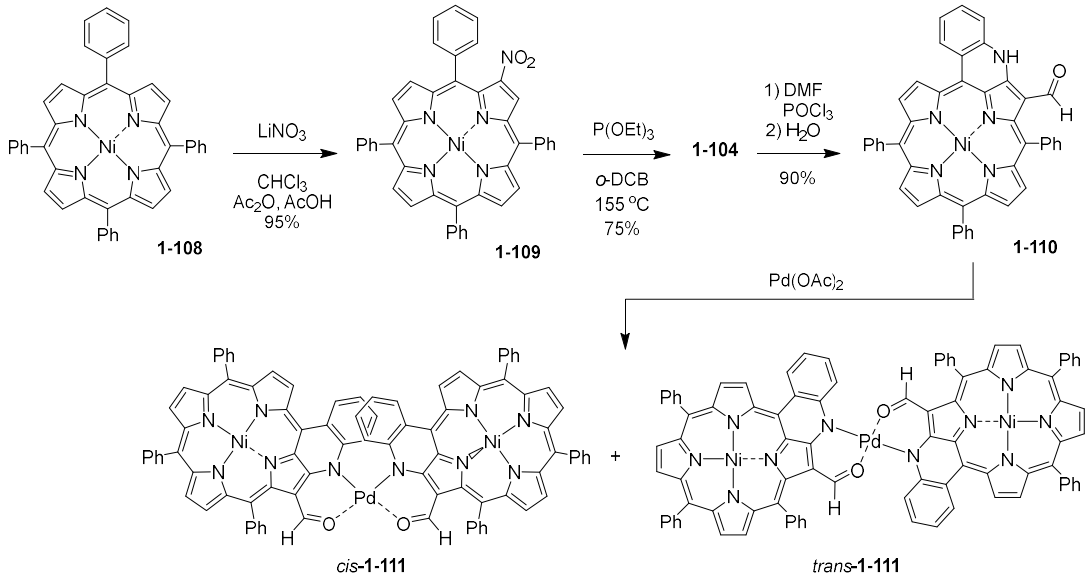

Scheme 1.26 Synthesis of enaminoporphyrin **1-105** and Pd(II)-bridged dimers *cis*-**1-111** and *trans*-**1-111**.

Chenet et al. proposed an alternative approach to the synthesis of **1-105** based on the intramolecular cyclization of β-porphyrinylazide **1-111** in refluxing PhMe (Scheme 1.27).[132] Later, *Cavaleiro et al.* described the synthesis of β-arylamino-substituted porphyrins **1-113** through intermolecular oxidative cyclization of **1-112** in nitrobenzene.[133] Further transformations of **1-105**, including N-arylation,[134] N-alkylation[135] and oxidation,[136] were thoroughly studied.

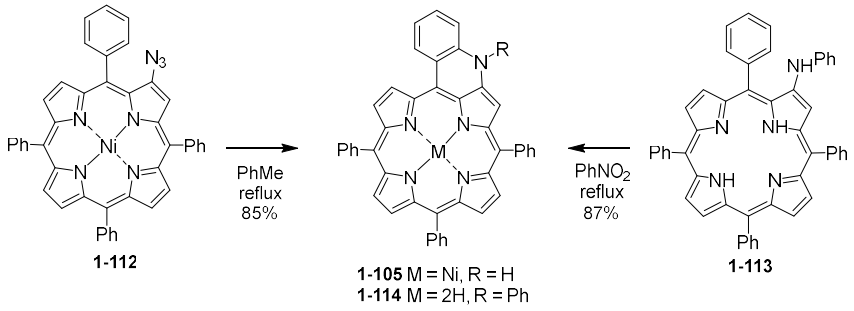

Scheme 1.27 Alternative approaches to the synthesis of enaminoporphyrins **1-105** and **1-114**.

In 2009, *Ruppert* and co-workers described the synthesis of doubly fused Ni(II) porphyrin **1-115** through intramolecular *Friedel–Crafts* reaction of enaminoaldehyde **1-110** with 10 eq. of TsOH in refluxing chlorobenzene (Scheme 1.28).[137]

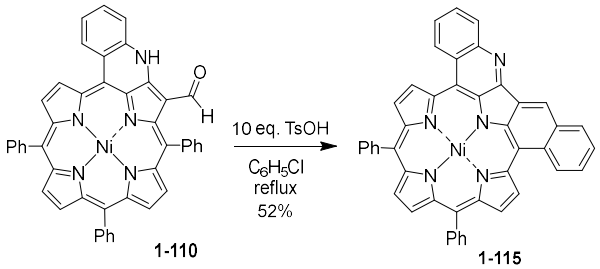

Scheme 1.28 Synthesis of doubly fused Ni(II) porphyrin **1-115**.

Later, the same group reported the synthesis of *bis*-quinoline-annulated porphyrin **1-118** in 80% yield through firstly the N-protection of **1-105**, followed by nitration of **1-116** and further intramolecular cyclization of **1-117** in refluxing *o*-DCB (Scheme 1.29).[138] Independently, free-base *bis*-quinoline-annulated porphyrin **1-119** was also prepared by *Brückner et al.* following the strategy, shown in Scheme 1.29.[139,140] Firstly, monooxime **1-120**, was obtained by the reaction of the relevant dione with excess $NH_2OH{\cdot}HCl$. Then it was treated with TsOH in refluxing PhMe to afford N-embedded porphyrin **1-121**. Subsequent reaction of the latter with $NH_2OH{\cdot}HCl$ and the intramolecular cyclization of the formed oxime afforded **1-119** in 64% yield. Ni(II) **1-118** (λ_{max} = 765 nm) and free-base **1-119** (λ_{max} = 775 nm) *bis*-quinoline-annulated porphyrins exhibited red-shifted UV-vis absorption spectra compared to porphyrin **1-115** (λ_{max} = 730 nm) fused with one naphthalene and one quinoline units.

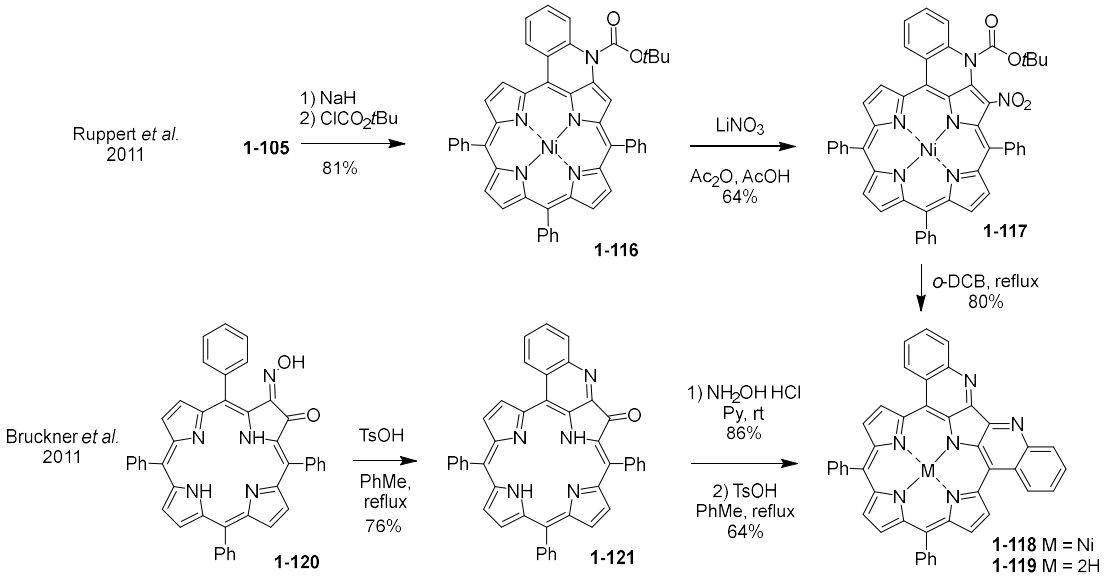

Scheme 1.29 Two approaches towards Ni(II) **1-118** and free-base **1-119** *bis*-quinoline-annulated porphyrins.

β-Sulfone-embedded porphyrin **1-106** was synthesized by the treatment of 5,10,15,20-tetrakis(4-sulfonatophenyl)porphyrin **1-122** with fuming H_2SO_4 (Scheme 1.30).[141] Notably, the *Soret* band of **1-106** is red-shifted by about 32 nm compared to that of **1-122**, due to the co-planarization of the *meso*-aryl group and electronic perturbation by the inserted sulfonyl group.

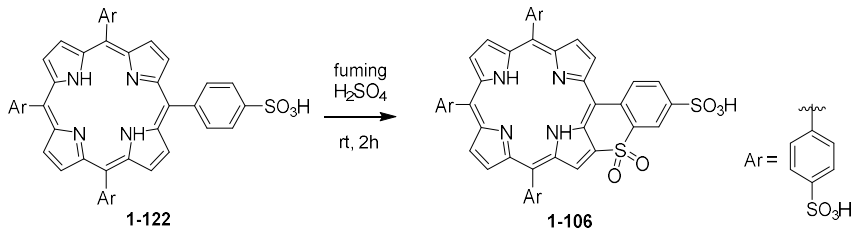

Scheme 1.30 Synthesis of β-sulfone-embedded porphyrin **1-106**.

Furthermore, incorporation of silicon was accomplished by *Osuka et al.*[126] For this purpose, *meso*-[2-(diphenylsilyl)phenyl]porphyrin **1-123** was subjected to the intramolecular sila-*Friedel–Crafts* reaction affording β-Si-embedded porphyrin **1-107** in 90% yield (Scheme 1.31). Curiously, the absorption maximum of β-Si-embedded porphyrin **1-107** (λ_{max} = 605 nm) is red-shifted compared to that of *meso*-Si-embedded porphyrin **1-124** (λ_{max} = 522 nm), thus indicating more effective conjugation of *meso*-aryl substituent with the porphyrin core.

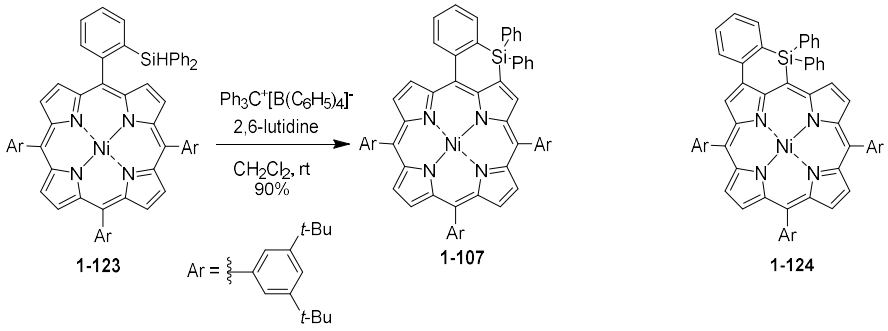

Scheme 1.31 Synthesis of β-Si-embedded porphyrin **1-107**.

As we can see, nitrogen, silicon, boron, sulphur and phosphorous were successfully incorporated and the properties of the corresponding porphyrin derivatives were thoroughly investigated. Meanwhile, the embedding of oxygen into the porphyrin cycle is not well explored. Only few O-embedded porphyrinoids were reported up to date. Specifically, *Osuka* and co-workers described the incorporation of a planarized oxygen atom in the

[28]hexaphyrin cycle of **1-125** by simple heating it in acetic acid, affording benzopyran-fused [28]hexaphyrin **1-126** in 27% yield (Scheme 1.32).[142]

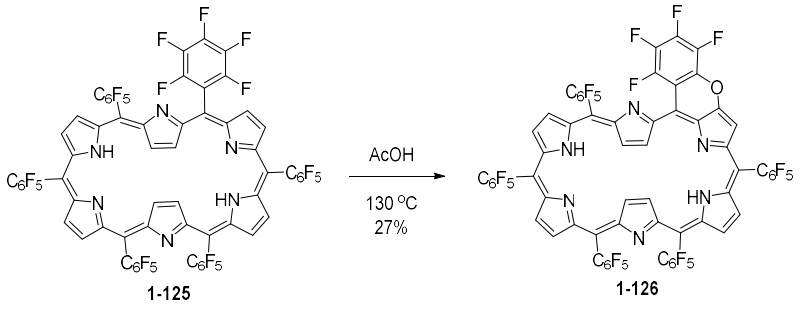

Scheme 1.32 Synthesis of benzopyran-fused [28]hexaphyrin **1-126**.

Besides, *Brückner* and co-workers reported the synthesis of mono- and *bis*-chromene-annulated *meso*(pentafluorophenyl)chlorins through intramolecular S_NAr reaction.[143] For instance, mono-O-embedded chlorine **1-129** was prepared by OsO_4-mediated dihydroxylation of *meso*(pentafluorophenyl)porphyrin **1-127**, followed by intramolecular ring closure of dihydroxychlorin **1-128** (Scheme 1.33).

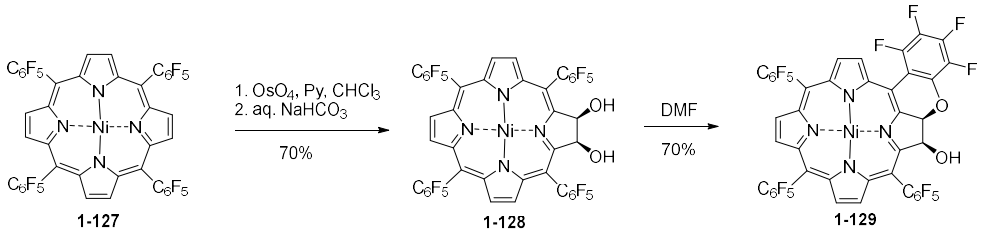

Scheme 1.33 Synthesis of mono-chromene-annulated *meso*(pentafluorophenyl)chlorine **1-129**.

Similarly to the synthesis of mono-chromene-annulated chlorin **1-129**, various isomers of *bis*- and *tetrakis*-chromene-annulated bacteriochlorins were successfully obtained.[144] However, all attempts to oxidize bacteriochlorin derivatives in order to get fully conjugated π-system turned to failure, and only different rearrangements were observed.[145]

1.2.3.3 β,β-Heteroatoms embedded porphyrins

The term "β,β-heteroatoms embedded porphyrin" is defined as an annulated porphyrin, in which heteroatoms are directly attached to the β-positions of the same pyrrole unit as a part of a fused heterocyclic ring. A variety of heterocycles such as quinoxaline, imidazole, tetrathiafulvalene, 1,4-dithiine *etc.* have been successfully annulated to the β-

positions of porphyrin macrocycle.[117] For instance , *Crossley et al.* reported for the first time the synthesis of β-β pyrazinoquinoxaline-bridged diporphyrin **1-131** (λ_{max} = 705 nm) in 71% yield by condensation of porphyrin-2,3-dione **1-130** with 1,2,4,5-tetraaminobenzene tetrahydrochloride (Scheme 1.34).[146,147] Cyclic voltammetry of **1-131** revealed four reversible one-electron reductions (-1.11, -1.28, -1.53, -1.73 V), suggesting the effective conjugation between two porphyrin ring.

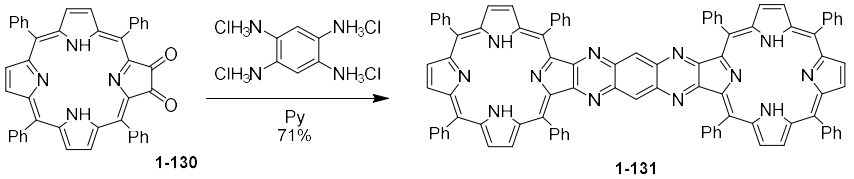

Scheme 1.34 Synthesis of β-β pyrazinoquinoxaline-fused diporphyrin **1-131**.

This strategy was further expanded to the corresponding trimer **1-33** and tetramer **1-34** with the molecular length of the latter reaching 65 Å (Figure 1.14).[148] Following the same synthetic route, L-shaped trimer **1-32** was also obtained in 93% yield.[148] Thanks to the efficient conjugation of the porphyrin units through the fused pyrazinoquinoxaline linker, the red-shifted absorption bands and split first reduction potentials were observed. These findings allow authors to consider the obtained oligoporphyrins as potential candidates of a molecular wire.

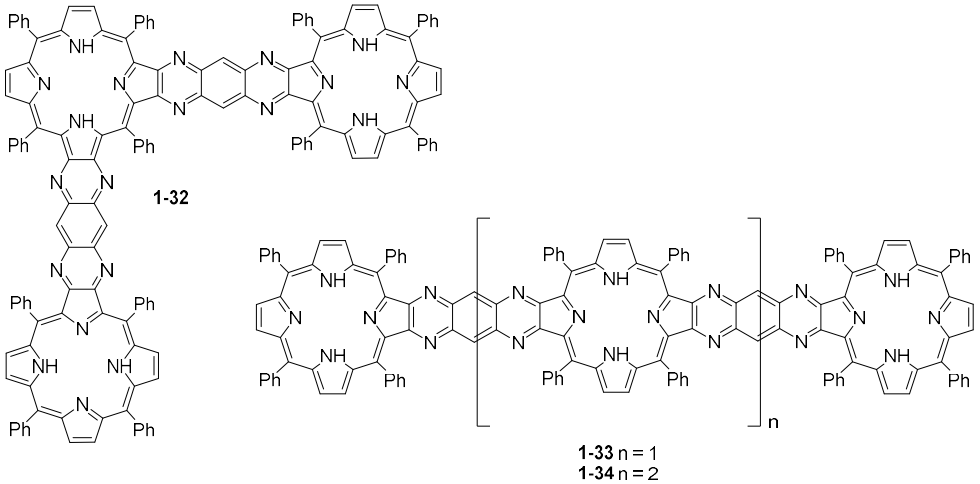

Figure 1.14 Chemical structures of β-β fused porphyrin oligomers.

2. Aim of the work

2.1 Aim and objectives

The aim of the project proposed here is inspired by the intriguing properties of porphyrins together with the unique ability to tune these properties by controlling the π-conjugated length along with a precise heteroatom insertion. While introduction of N, P, Si and S heteroatoms on the direct periphery of porphyrins was thoroughly described, there are no reports up to now on O-fused porphyrins. Hence, the ambition of this thesis is to design novel π-extended O-embedded porphyrins, where the *ortho*-position of the *meso*-aryl substituent is interconnected with the β-pyrrolic position through an O-bridge, forming a pyran ring. In this respect, a detailed understanding on the relationship between the properties and the structure of O-fused porphyrins is required. Indeed, the embedding of an oxygen atom is believed to emerge the appealing electronic perturbation within the macrocycle due to the co-planarization of the aromatic subunits with the macrocyclic plane (Figure 2.1). Therefore, the extension of the conjugation length will lead to the narrowing of the energy gap between the HOMO and LUMO of the porphyrin, inducing the bathochromic shift of the absorption bands. Furthermore, it is envisaged that the insertion of oxygen atoms in a controlled manner *via* pyran formation should produce an electron saturated family of O-fused porphyrins exhibiting increasing electron donating character with respect to the original macrocycle. All these attractive features allow considering the O-embedded porphyrins as promising candidates for the creation of novel NLO dyads, photosensitizers, molecular electronic devices *etc*.[149]

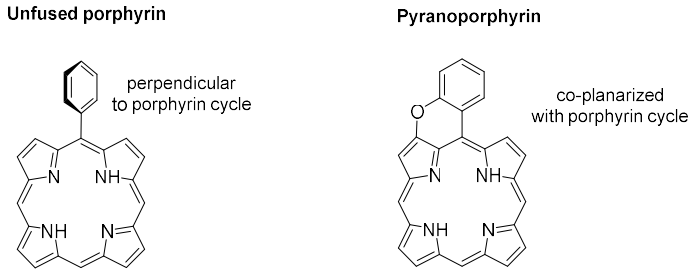

Figure 2.1 Conjugation pathways of unfused porphyrin and pyranoporphyrin.

In our study, we plan to extend the tetrapyrrolic core by functionalizing the periphery with a series of fused pyran rings. Specifically, the peripheral *meso*-aryl substituent should undergo oxidative intramolecular cyclization reaction with β-pyrrolic position through diaryl-ether bond formation. Since the intention of this thesis is to investigate the effect of oxygen embedding on the chemo-physical properties of porphyrins, four generations of O-fused porphyrins, possessing different number of O-bridges, will be studied (Figure 2.2).

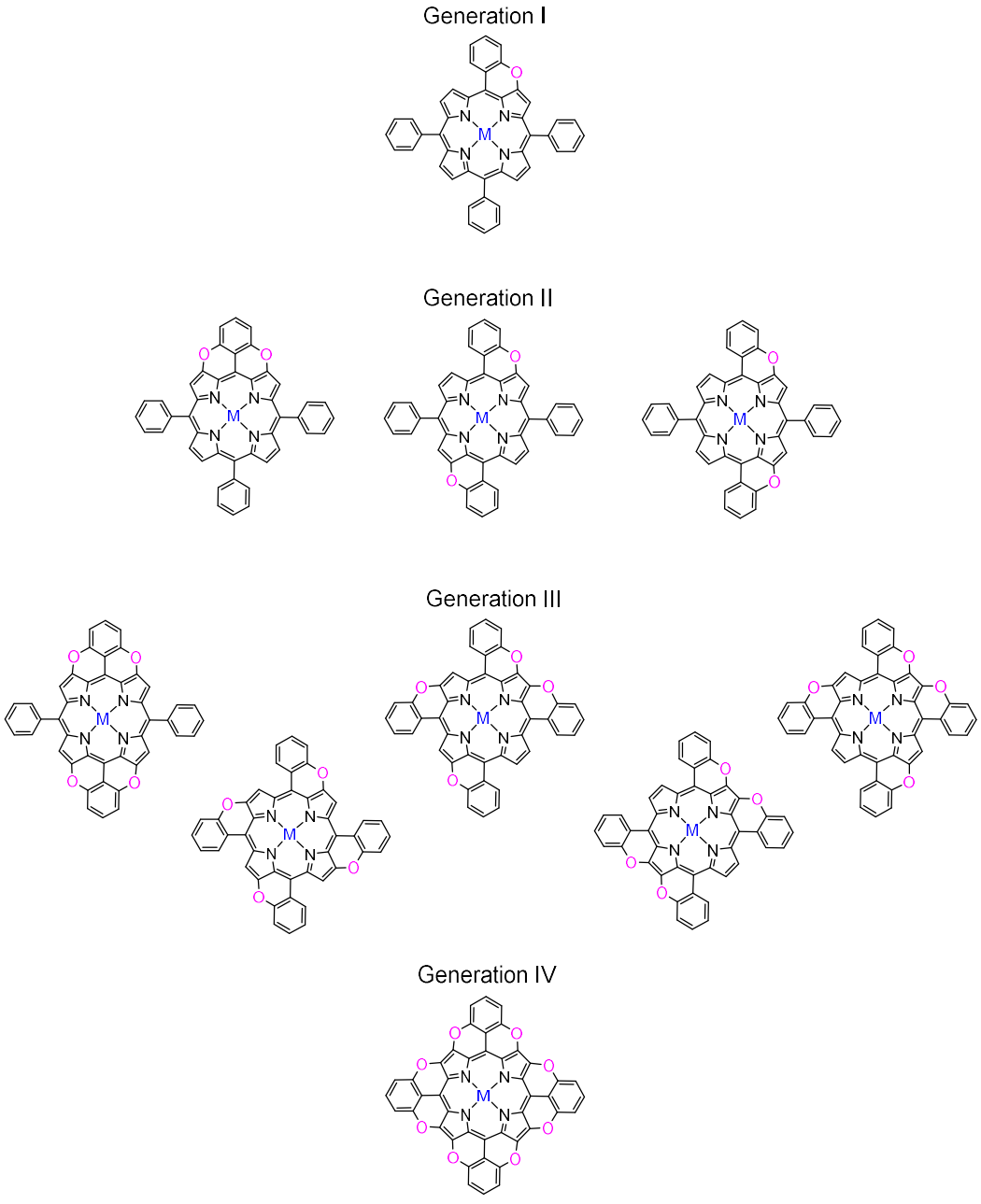

Figure 2.2 Generations of targeted pyranoporphyrins.

Monopyranoporphyrin (Generation I), which includes only one oxygen atom, have been chosen as the first target compound for developing and optimizing a protocol for a pyran annulation reaction. By increasing the number of oxygen bridges along with the changing of their peripheral location, we intend to reveal the specific patterns of electronic perturbation within the generations of targeted pyranoporphyrins. For this purpose, the sets of di- and tetrapyranoporphyrin isomers (Generations II and III, respectively) have been proposed as the next objectives of investigation. Further extension of this thesis involves the preparation of full-conjugated octapyranoporphyrin (Generation IV), which is believed to present more electron-saturated character of π-system and narrower HOMO-LUMO gap than mono-, di- and tetrapyranoporphyrin derivatives.

2.2 Outline of the dissertation

In this thesis, our research activities were focused on the design of novel O-fused porphyrin-based π-extended molecules. For the reasons discussed above, O-embedded porphyrins are expected to possess intrinsic optoelectronic properties that make them exploitable as functional materials for a wide range of applications. Therefore, in-depth knowledge and understanding of the relationships between the structure and the properties of targeted porphyrins need to be achieved. The work presented here is divided into two main chapters. Figure 2.3 schematically illustrates the outline of this dissertation.

Chapter III addresses the synthesis of mono- and di-pyranoporphyrins, comprising one or two oxygen bridges, respectively. After the successive development of efficient synthetic methodology to prepare monopyranoporphyrin *via* pyran annulation reaction, the implementation of the developed protocol to synthesize dipyranoporphyrins is then discussed. The last section is focused mainly on the physicochemical properties of O-annulated porphyrins. In order to reveal the emerged electronic perturbations within the macrocycle, cyclic voltammetry, UV-vis spectroscopy and DFT calculations were used.

Chapter IV is dedicated to the extended investigation towards pyranoporphyrins with an increased number of oxygen bridges in the porphyrin core. The formerly developed protocol for diaryl ether bond formation was successively implemented for the preparation of tetra- and octa- pyranoporphyrins. The unexpected properties of obtained compounds prompt us to explore their behavior through EPR technique, tandem MS/MS analysis and DFT calculations.

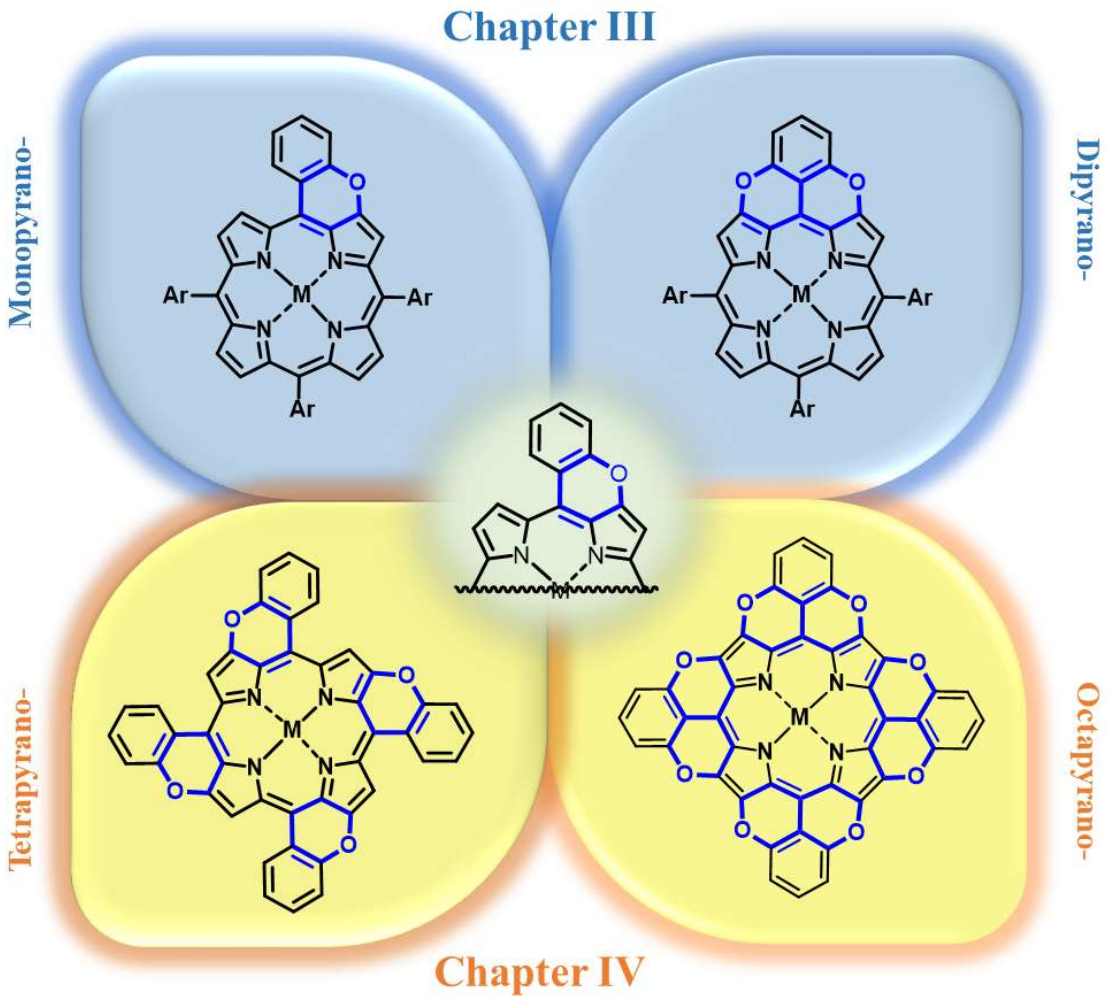

Figure 2.3 Schematic representation of the outline of this doctoral dissertation.

3. Mono- and di- pyranoporphyrins

The focus of this chapter is the synthesis and thorough investigation of the optoelectronic and electrochemical properties of mono- and di- pyranoporphyrins (generation I and II, respectively, Figure 2.2). In this context, the chapter is divided in four sections: *i) section 3.1* focuses on the development of an efficient synthetic pathway towards the synthesis of monopyranoporphyrins (generation I); *ii) section 3.2* includes the initial synthesis of dipyranoporphyrin (generation II) macrocycles, previously accomplished in our laboratory by *Dr. Daphne Stassen*, and the consecutive optimization of the reaction conditions along with the synthesis of new scaffolds as an extension of her work; *iii) section 3.3* in which the results of the photophysical, electrochemical and computational studies of the O-embedded porphyrins are reported; and *iv) section 3.4* concludes the obtained results.

DFT geometry optimization and NICS calculations presented in this chapter were performed by *Dr. Luka Đorđević* (University of Trieste, Italy); X-ray resolution was done by *Nicolas Biot* (Cardiff University, UK).

3.1 Synthesis and characterization of monopyranoporphyrins

Monopyranoporphyrin **3-1** was selected as the first target compound in order to develop a convenient synthetic strategy towards O-embedded porphyrins (Figure 3.1).

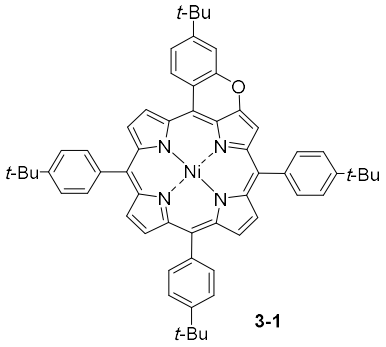

Figure 3.1 Structure of monopyranoporphyrin **3-1**.

In order to avoid potential problems due to poor solubility, *tert*-butyl groups in the *para*-position of *meso*-phenyl substituents were incorporated. Besides, phenyl substituents,

attached to the *meso*-positions of the porphyrin core were introduced, in an attempt to protect it from possible dimerization. Moreover, Ni(II) was chosen as a central metal due to its stable oxidation state +2 and ability to activate β-position of porphyrin cycle.

3.1.1 Retrosynthetic analysis

The key step towards the synthesis of pyranoporphyrins involves the formation of the pyranocycle through an intramolecular C-O coupling reaction. Accordingly, two disconnections of C-O bonds, such as *i*) *ortho*-C-O bond disconnection (route A) and *ii*) β-C-O bond disconnection (route B), were envisaged (Scheme 3.1). A key factor in deciding on the preferred disconnection was the synthetic accessibility of the involved intermediates in order to arrive at simple and easily available starting materials. In this regard, route A appears limited by the accessibility of β-hydroxy substituted porphyrin precursors, which are known to be unstable and can easily undergo oxidative degradation. On the other hand, route B seems to be more promising, because *meso*-(*ortho*-hydroxy)aryl substituted porphyrins are stable and can be easily accessed from the corresponding aldehydes and pyrrole.

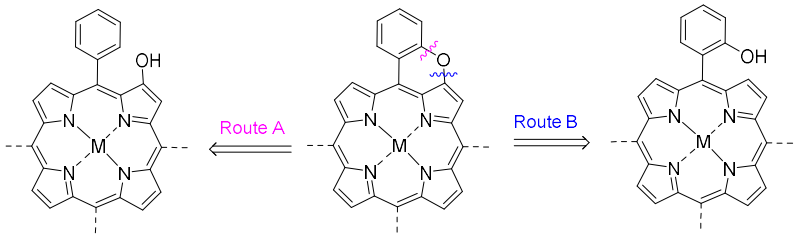

Scheme 3.1 Possible disconnection routes of the C-O bond of pyranoporphyrins.

In the scope of our study, the development of an efficient protocol displaying selective diaryl-ether bond formation is essential for the preparation of O-embedded porphyrins. Among a variety of the ring closure reactions, the metal catalysed diaryl-ether coupling (*e.g.* Pd-catalyzed *Buchwald–Hartwig*[150] and Cu-catalysed *Ullmann* reactions[151–153]) and nucleophilic aromatic substitution [154] are the most investigated approaches. However, the metal catalysed coupling between an aryl halide and a phenol involves the use of preactivated substrate, thus requiring the preliminar functionalization with halide of the porphyrin macrocycle in our case. Hence, our attention was drawn to the alternative approach to form diaryl-ether bond, involving the direct C-H functionalization, which avoids the

preactivation of the substrate.[155] In this context, the synthesis of *peri*-xanthenoxanthene (PXX) from binaphtol is the most representative example of intramolecular C-O coupling formation of six-membered pyran cycle. Among the reported synthetic methodologies to accomplish this, two approaches are of particular interest for us (Scheme 3.2). The first one was reported by *Pummerer et al.* in 1926 and based on the synthesis of PXX through CuO or $Cu(OAc)_2$-promoted oxidative C-O coupling reaction.[156] The second approach includes the more recent C-H activation methodologies using CuI in the presence of PivOH developed by *Bonifazi* group.[157] In both cases, the desired PXX was obtained in satisfactory yield using inexpensive copper derivatives. These results became a starting point in our searching of optimized conditions for the synthesis of O-embedded porphyrins.

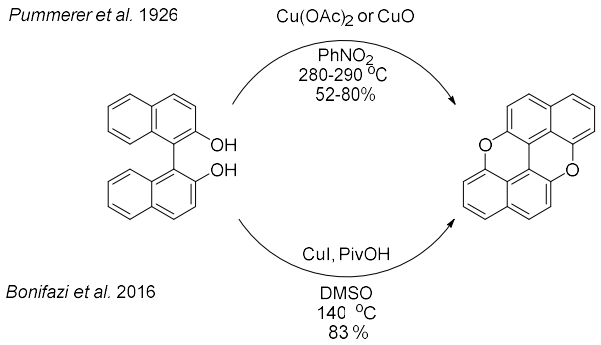

Scheme 3.2 Synthesis of PXX through Cu-promoted intramolecular C-O coupling reaction.

Taking into consideration what has been reported so far, based on route B the retrosynthetic pathway outlined in Scheme 3.3 toward porphyrin **3-1** was proposed. The planned synthesis includes initially the synthesis of methoxyporphyrin **3-3** by condensation of pyrrole with the appropriate aldehydes and formation of the macrocycle. Further demethylation followed by metallation of **3-3** should provide key precursor **3-2** for the final pyran annulation reaction.

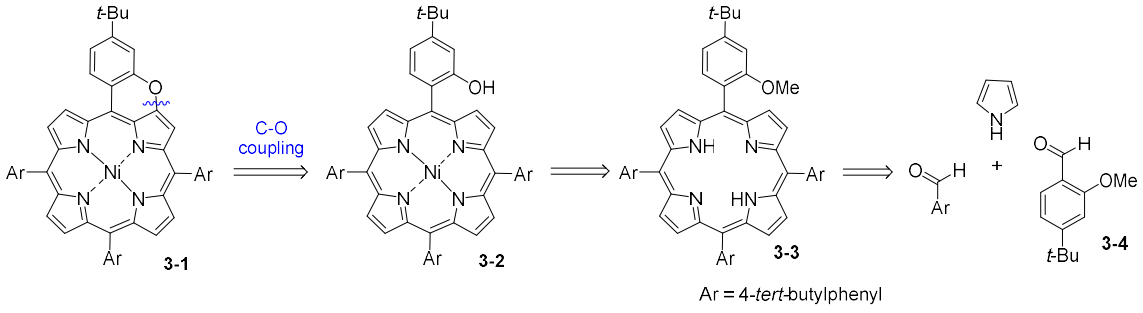

Scheme 3.3 Retrosynthesis of monopyranoporphyrin **3-1**.

3.1.2 Synthesis of monopyranoporphyrins

The preparation of methoxybenzaldehyde **3-4**, described in Scheme 3.4, commenced with the methylation of commercially available 3-(*tert*-butyl)phenol **3-5** using NaH and MeI in THF.[158] The resulting methoxyphenol **3-6** undergone selective *Vilsmeier-Haack* formylation at position 6 in the presence of MFA in $POCl_3$ affording desired aldehyde **3-4** in good yield.[159]

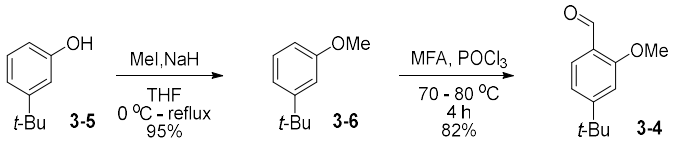

Scheme 3.4 Synthesis of methoxybenzaldehyde **3-4**.

The monomethoxyporphyrin **3-3** was synthesized from a stoichiometric mixture of methoxybenzaldehyde **3-4**, 4-(*tert*-butyl)benzaldehyde and pyrrole under the classical conditions developed by *Lindsey* using a diluted solution in $CHCl_3$ in the presence of $BF_3{\cdot}Et_2O$ as a catalyst (Scheme 3.5). The obtained porphyrinogen is not stable and oxidation to form the stable porphyrin macrocycle is required. Thus, 2,3-dichloro-5,6-dicyano-1,4-benzoquinone (DDQ) was added to carry out the $6e^-/6H^+$ oxidative dehydrogenation of the porphyrinogen. The desired porphyrin **3-3** was separated from a mixture of side porphyrins by SiO_2 column chromatography eluting with 1:1 mixture of CH_2Cl_2/cyclohexane. Subsequently, BBr_3-promoted demethylation of the methoxy group yielded **3-7**. This was followed by metallation with $Ni(acac)_2$ of free-hydroxyl porphyrin **3-7** affording monohydroxyporphyrin **3-2** in 92% yield through precipitation from cold methanol. All intermediates and porphyrin **3-2** were fully characterized by HRMS-MALDI-spectrometry, ^1H and ^{13}C NMR-, IR- and UV-spectroscopy as described in Chapter VI.

Inspired by recent publications,[157,160,161] where copper catalyzed reaction conditions were used to promote the cycloetherification, we decided to extend these results to our work. In particular, the conditions reported by *Bonifazi* group,[157] *i.e.* CuI in the presence of PivOH, where applied to our substrate. Accordingly, a solution of monohydroxyporphyrin **3-2** in DMSO was treated with 2 eq. of CuI and 1 eq. of PivOH at 140 °C for 4 h under open-air conditions (Scheme 3.5). The reaction was monitored by TLC and upon completion it was

concentrated under reduced pressure and the residue was purified several times by silica gel column chromatography giving target porphyrin **3-1** in 32% yield.

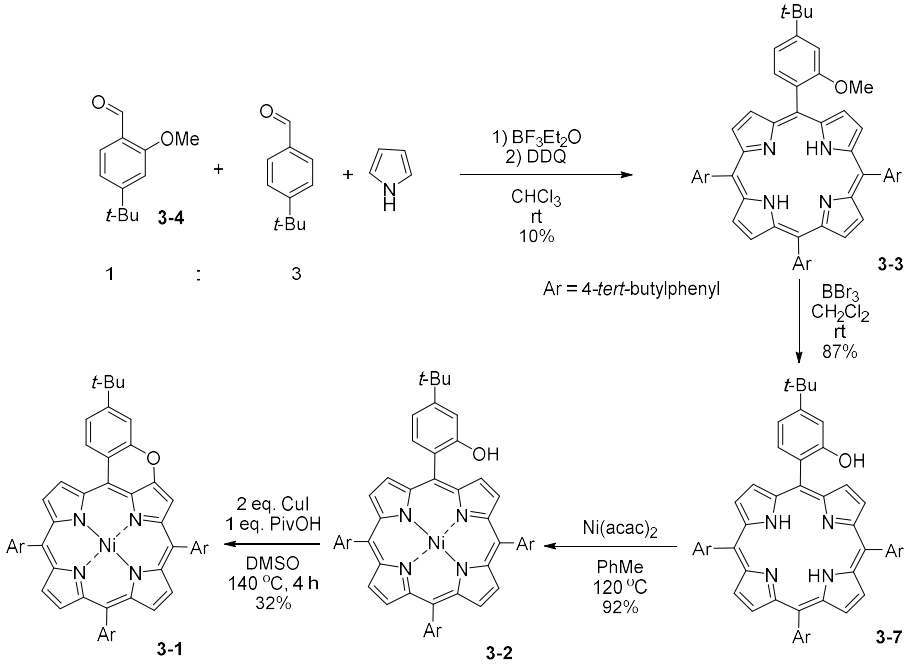

Scheme 3.5 Synthesis of monopyranoporphyrin **3-1**.

Despite the low yield of monopyranoporphyrin **3-1**, the formation of O-embedded porphyrins encouraged us to further optimize the reaction. Subsequently, various reaction conditions for the formation of pyranoporphyrin **3-1** have been screened. Specifically as summarized in Table 3.1, different copper additives in various solvents were used to evaluate their effect in the preparation of **3-1**.

In order to clarify the necessity of PivOH, CuI was used in the absence of PivOH (Table 3.1, entry 1). Surprisingly, the yield of the reaction remained the same as in the presence of PivOH (Scheme 3.5), thus suggesting that C-O coupling reaction is proceeded through the one electron oxidation mechanism. Furthermore, it was found that the use of CuI (5 eq.) in $PhNO_2$ afforded desired monopyranoporphyrin **3-1** in an increased 54% yield (Table 3.1, entry 2). This can be attributed to the possible exclusion of side reactions occurring when a higher boiling solvent such as $PhNO_2$ is used instead of DMSO. In order to further optimize the reaction conditions, other copper salts were examined. In particular, when 5 eq. of $CuCl_2$ in $PhNO_2$ were used, the formation of only chlorinated products was detected by LRMS-MALDI analysis (Table 3.1, entry 3). In addition, a complete decomposition of **3-2** when $CuNO_3$ and $Cu(OTf)_3$ were exploited (Table 3.1, entry 4, 5).

Subsequently, $CuSO_4$, CuOAc and $Cu(OAc)_2$ were also examined to our system (Table 3.1, entry 6-8). However, a significant difference was not observed when compared to CuI. In all cases, the moderate yields of **3-1** can be associated with the oxidation of porphyrins to radical-cations, followed by their interaction with nucleophiles, thus causing the formation of side products.

Table 3.1 Optimization of the reaction conditions for the pyran annulation reaction.

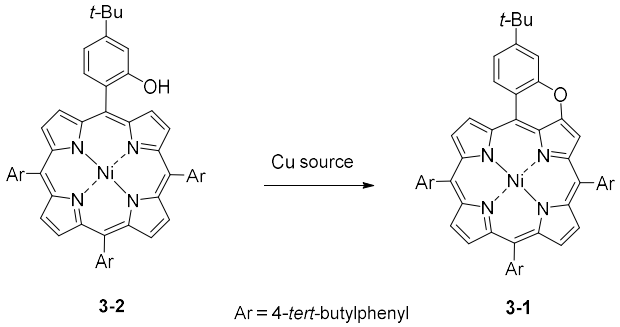

Entry	Cu source	Solvent	Conditions	Yield (%)	Conversion(%)
1	CuI	DMSO	140 °C, 4h	32	100
2	CuI	$PhNO_2$	210 °C, 7h	54	100
3	$CuCl_2$	$PhNO_2$	210 °C, 7h	-[a]	100
4	$CuNO_3$	$PhNO_2$	210 °C, 7h	-[a]	100
5	$Cu(OTf)_2$	$PhNO_2$	210 °C, 7h	-[a]	100
6	$CuSO_4$	$PhNO_2$	210 °C, 7h	55	100
7	CuOAc	$PhNO_2$	210 °C, 7h	51	100
8	$Cu(OAc)_2$	$PhNO_2$	210 °C, 7h	53	100
9	CuO	$PhNO_2$	210 °C,12h	92	100
10	CuO	PhMe	110 °C, 36h	-[b]	0
11	CuO	$PhNO_2$	110 °C, 36h	-[b]	0
12	$Cu(ClO_4)_2$	MeCN	60 °C, 12h	-[b]	0

[a] decomposition; [b] no reaction

Inspired by the successful use of CuO for the preparation of PXX (Scheme 3.2),[162] we decided to use CuO as a promoter of intramolecular oxidative C-O coupling on porphyrin derivatives. The best result was obtained by refluxing monohydroxyporphyrin **3-2** with 5 eq. of CuO in $PhNO_2$ at 210 °C (Table 3.1, entry 9). The desired product was easily isolated by

SiO_2 flash chromatography in 92% yield. Importantly it was noted that temperature plays a crucial role in the formation of **3-1**. Indeed, when the reaction was performed at 110 °C, the starting porphyrin **3-2** was fully recovered (Table 3.1, entry 10, 11). Besides, the use of $Cu(ClO_4)_2$ in MeCN at 60 ºC, as a strong one-electron oxidizer,[163] also led to full recovery of starting material **3-2** (Table 3.1, entry 12).

Having in hands monopyranoporphyrin **3-1**, we confirmed its structure by HRMS-MALDI spectrometry, ^1H and ^{13}C NMR-. IR- and UV-spectroscopy, as described in Chapter VI. HRMS-MALDI of **3-1** showed the peak corresponding to the molecular ion at m/z 908.3987 (M^+, $[C_{60}H_{58}N_4NiO^+]$, calc.: 908.3964). Further comparison of the ^1H NMR-spectra of monohydroxyporphyrin **3-2** and O-embedded porphyrin **3-1** revealed the crucial difference in the character of hydrogen resonances corresponding to the pyrrolic protons. In contrast to the ^1H NMR-spectrum of **3-2**, where a multiplet of the pyrollic protons around 8.9-8.75 ppm is observed (Figure 3.2a), the ^1H NMR-spectrum of **3-1** displays four well split signals (Figure 3.2b) as a consequence of the ring closure on the β-position of the pyrrole. Specifically, two doublets of H_e (9.55 ppm) and H_d (8.95 ppm), one singlet of H_c at 8.29 ppm and the multiplet of the rest pyrrolic protons around 8.74-8.67 ppm, were observed. Comparing the signals of H_a, H_b and H_c, the shifting from 7.73 (H_a), 7.28 (H_b) and 7.32 ppm (H_c) for **3-2** to around 8.72 (H_a), 7.70 (H_b) and 7.93 ppm (H_c) for **3-1** was revealed (Figure 3.2). This deshielding can be explained by the increasing aromaticity of O-fused porphyrin **3-1** and the reducing electron donating effect of the oxygen atom.

To provide additional proofs for the assignment of the observed peaks to the appropriate aromatic protons of the benzopyran moiety, 2D Homonuclear Correlation spectroscopy (COSY) was also carried out (Figure 3.3). By changing the deuterated solvent from $CDCl_3$ to C_6D_6, the overlapping of H_a, H_b and H_c signals with other aromatic protons was not any more observed and hence, the spin-spin coupling between them could be revealed. Therefore, the COSY spectrum of **3-1** presents that the doublet of H_a at 8.64 ppm correlates with the doublet of H_b at 7.37 ppm on the benzopyran moiety (Figure 3.3, dashed lines), while the doublet of H_e at 9.49 ppm correlates with the doublet of H_d at 9.03 ppm, both belonging to the same pyrrole unit.

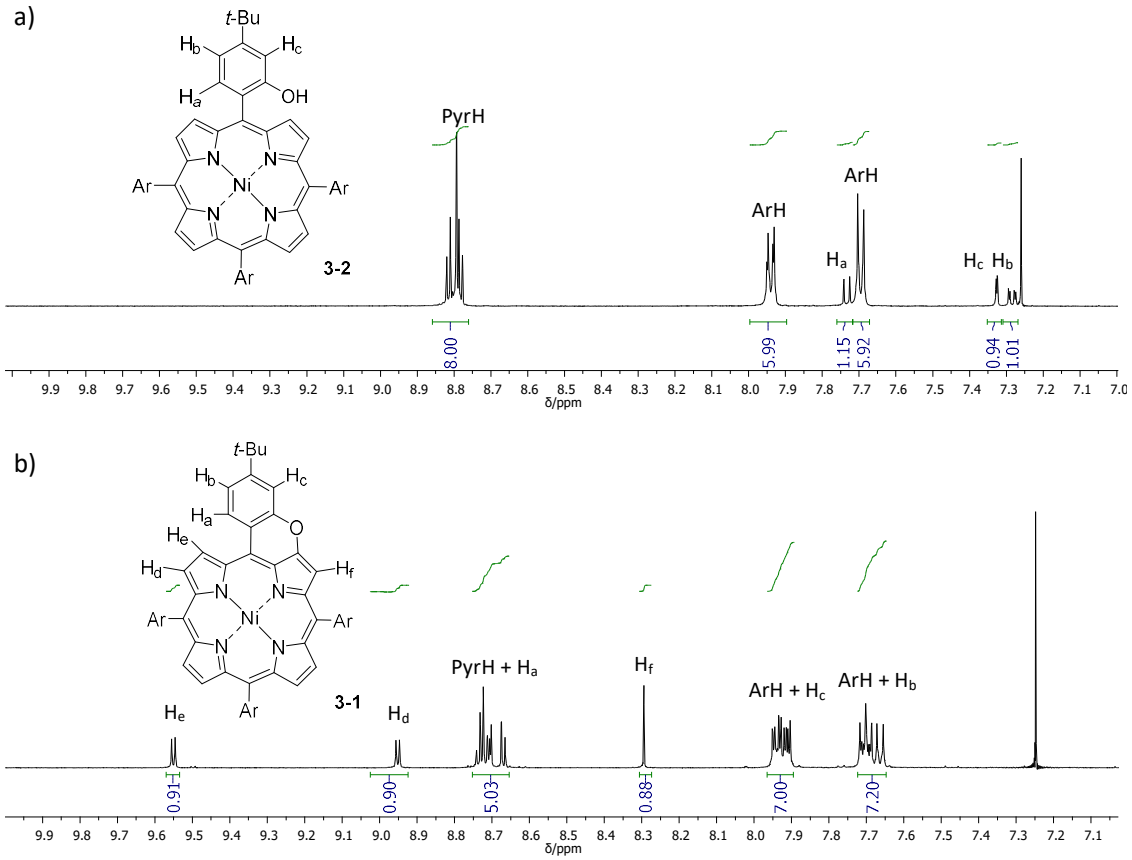

Figure 3.2 ^{1}H NMR-spectra of a) monohydroxyporphyrin **3-2** and b) monopyranoporphyrin **3-1** (400 MHz, $CDCl_3$, zoom of the 10.00-7.00 ppm area), Ar = 4-*tert*-butylphenyl.

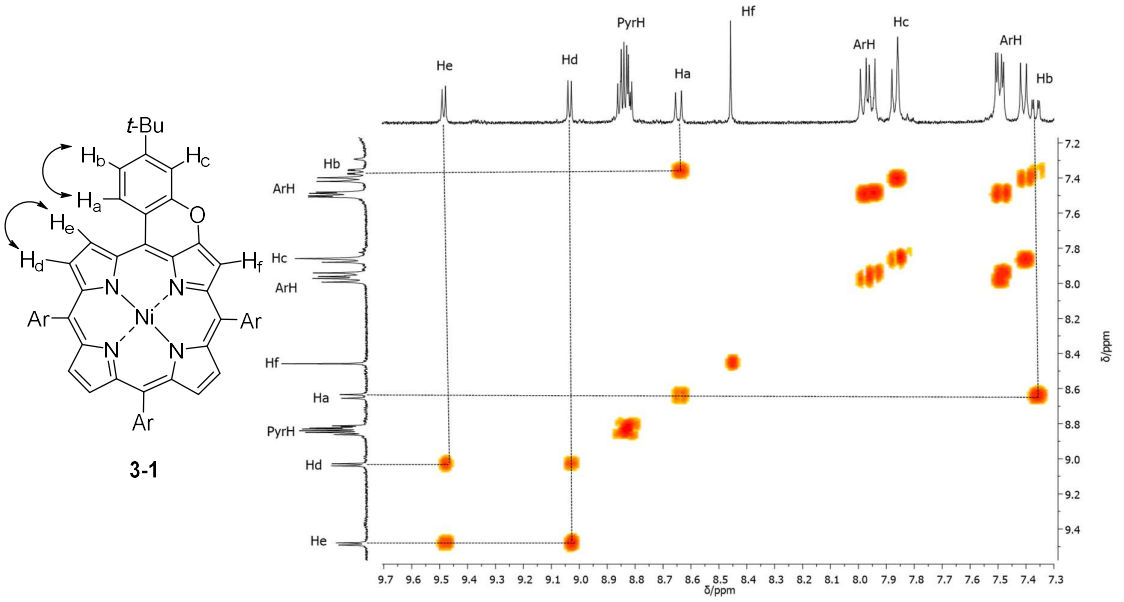

Figure 3.3 2D COSY-NMR spectrum of monopyranoporphyrin **3-1** (400 MHz, C_6D_6, zoom of the 9.75-7.30 ppm area), Ar = 4-*tert*-butylphenyl.

Meanwhile, the effect of the central metal atom on the reactivity of the porphyrin core under the CuO-mediated oxidative ring closure reaction was also examined. For this purpose, free-base monohydroxyporphyrin **3-7** was subjected to metallation using various metal acetates. The resulting analogues were subjected to the pyran annulation reaction affording the corresponding O-embedded porphyrins (Scheme 3.6). Metallation of porphyrin **3-7** proceeded smoothly yielding desired metallated porphyrins **3-8**–**3-11** in good yields *via* precipitation from MeOH. Specifically, treatment of **3-7** with $Zn(OAc)_2$ in $MeOH/CH_2Cl_2$ (1:9) led to Zn(II) porphyrin **3-11** in 78% yield. The closed-shell Zn(II) atom induces the negative charge onto the porphyrin periphery, thus conferring the decreasing of oxidation potential and potentially favouring the pyran annulation reaction. On the other hand, the insertion of open-shell Cu(II), Ag(II) or Pd(II) atoms using the same conditions afforded porphyrins **3-8**, **3-9** and **3-10** with 94%, 90% and 92% yields, respectively. Since these metals are capable of π-back-bonding, the electron density on the porphyrin macrocycle is decreased, while the oxidation potential is increased.

Subsequent CuO-mediated ring closure reaction led to fused systems **3-12** and **3-13** only when Cu(II) **3-8** and Pd(II) **3-10** porphyrins were introduced. However, when Ag(II) **3-9** and Zn(II) **3-11** porphyrins were exploited, metal exchange with Cu occurred and only Cu(II) porphyrin **3-12** was isolated in both cases.

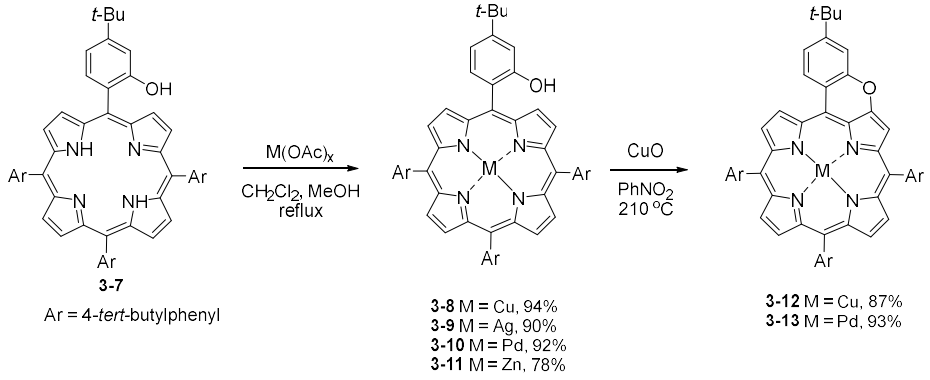

Scheme 3.6 Synthesis of metalloporphyrins **3-8**–**3-11**, followed by CuO-mediated oxidative ring closure reaction affording monopyranoporphyrins **3-12** and **3-13**.

Following the conditions described by *Ruppert* and co-workers,[137] we successfully obtained free-base O-embedded porphyrin **3-14** in 85% yield upon treatment of Ni(II) porphyrin **3-1** with a mixture of TFA and H_2SO_4 at 0 °C (Scheme 3.7). Notably, the demetallation of **3-1** at rt led to partial decomposition of the starting material affording

desired porphyrin **3-14** in only 25% yield. Subsequent Zn-metallation of **3-14** afforded Zn(II) monopyranoporphyrin **3-15** in 98% yield (Scheme 3.7). These findings extend the synthetic capacity of the CuO-mediated pyran annulation reaction, demonstrating two different approaches to prepare O-fused porphyrins with different central metal atom. As already described, the first method includes the initial synthesis of a metal hydroxyporphyrin and the subsequent O-fusion reaction, while the second approach is based on the preliminary synthesis of Ni(II) pyranoporphyrin followed by a two step metal exchange process. In this manner, the synthesis of metal monopyranoporphyrins which cannot be achieved using the first method, mainly due to the metal exchange with Cu during the ring closure reaction, could be achieved with the second alternative approach.

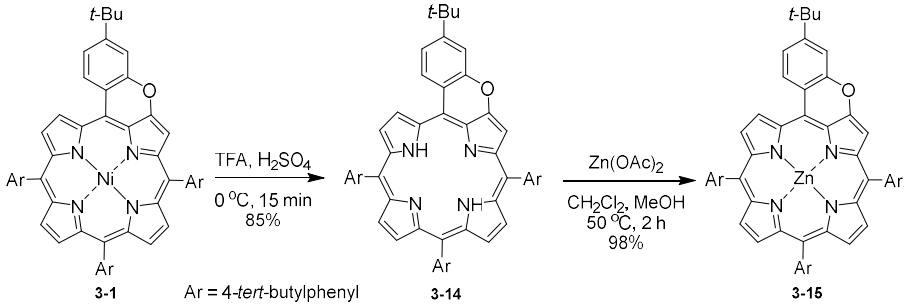

Scheme 3.7 Synthesis of Zn(II) monopyranoporphyrin **3-15**.

The chemical structures of metal and free-base O-embedded porphyrins **3-12**–**3-15** were confirmed by HRMS-MALDI spectrometry, ^{1}H and ^{13}C NMR-. IR- and UV-spectroscopy (see details in Chapter VI). Noteworthy, the NMR-spectra of Cu(II) porphyrins **3-8** and **3-12** could not be recorded, due to the paramagnetic nature of Cu(II). Instead, the chemical structures of **3-8** and **3-12** were proved by HRMS-MALDI analysis. For instance, the molecular mass of **3-12** was unambiguously established by HRMS-MALDI, which displayed the peak corresponding to the molecular ion at m/z 913.3927 (M^+, $[C_{60}H_{58}N_4OCu]^+$, calc.: 913.3907) (Figure 3.4).

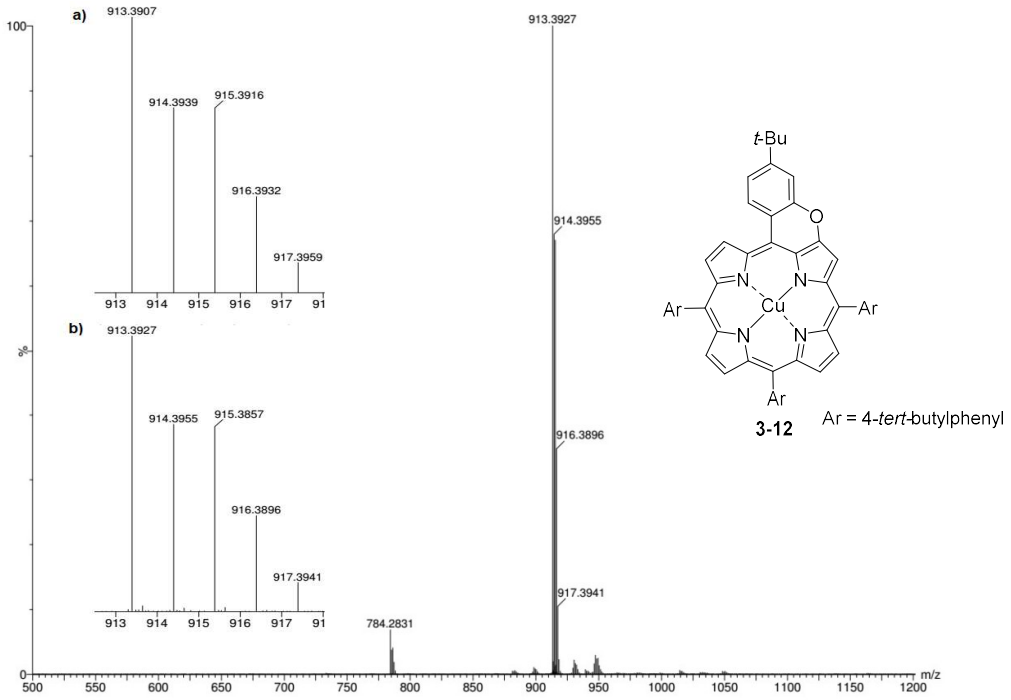

Figure 3.4 HRMS-MALDI spectrum of Cu(II) O-embedded porphyrin **3-12**. The inset shows a) calculated and b) found data.

In contrast to the ^{1}H NMR-spectra of metal pyranoporphyrins (see Appendix), the ^{1}H NMR-spectrum of free-base porphyrin **3-14** shows the presence of the inner NH-protons at -1.37 ppm, thus confirming successful demetallation (Figure 3.5). The ^{1}H NMR analysis of the aromatic and aliphatic protons of **3-14** presented an analogous pattern as described above for Ni(II) porphyrin **3-1** (Figure 3.2b). In particular, it involves one doublet of H_e (9.65 ppm), one singlet of H_f (8.81 ppm) and the multiplet around 9.07-8.96 ppm for the pyrrole rings; two doublets of H_a (9.24 ppm) and H_c (8.11 ppm) and one doublet of doublets of H_b (7.57 ppm) corresponding to the benzopyran ring. In addition, the chemical structure of **3-14** was undoubtedly identified by HRMS-MALDI through detection of the peak corresponding to the molecular ion at m/z 853.4843 (M^+, $[C_{60}H_{61}N_4O]^+$, calc.: 853.4845).

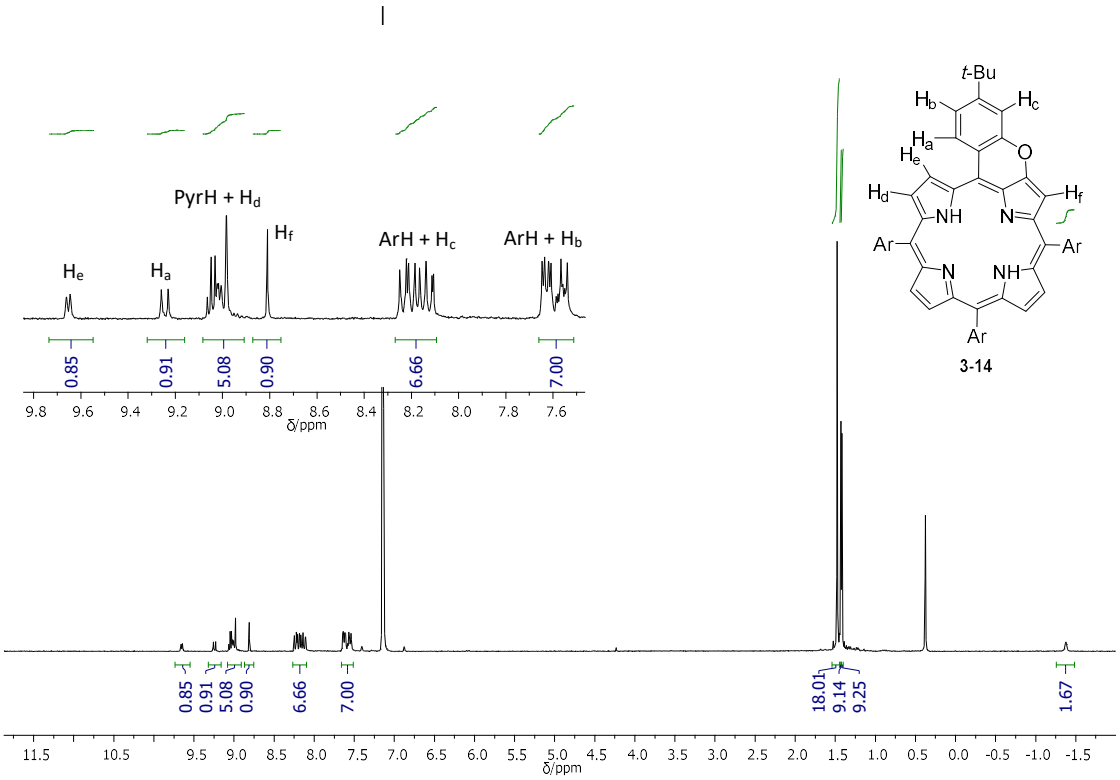

Figure 3.5 ^{1}H NMR-spectrum of free-base O-embedded porphyrin **3-14** (400 MHz, $CDCl_3$), Ar = 4-*tert*-butylphenyl. The inset shows zoom of the 9.8-7.7 ppm area.

The purple needle like crystals of Ni(II) and free-base monopyranoporphyrins **3-1** and **3-14,** respectively, were suitable for single-crystal X-ray analysis, and were grown by vapour diffusion of MeOH in CH_2Cl_2 at rt in the dark (Figure 3.6). In both cases, the appropriate crystal structures were determined at 150 K and found to belong to the monoclinic space group I 2/a. Further details related to the crystal structures are described in the Appendix. X-ray analyses of **3-1** and **3-14** showed the disordering of position of the oxygen atom due to the coexisting and overlapping of two packing modes. Nevertheless, we were able to compare the geometry of the porphyrin cores. It was found, that free-base porhyrin **3-14** displays almost a planar structure. Meanwhile, Ni(II) porphyrin **3-1** shows ruffled conformation due to the stronger complexing of the porphyrin macrocycle by the Ni(II) (Figures 3.6c,d). Obviously, the non-planar confirmation is explained by the gain in energy owing to the complexation, which overcomes the stabilizing energy, contributed by the delocalization of the π-bonding for the planar conformation. Interestingly, the lengths of the C-O bonds for **3-1** (C(5)-O(1), 1.32 Å) and **3-14** (C(2)-O(1), 1.29 Å) are close to the length of a double C-O bond (1.23 Å), suggesting the conjugation between the oxygen lone pair and the porphyrin

core. Moreover, the lengths of C-C bonds for **3-1** (C(7)-C(21), 1.47 Å) and **3-14** (C(10)-C(11), 1.50 Å) correspond to the characteristic length of C_{sp2}-C_{sp2} bond (1.47 Å), indicating the weak conjugation between the porphyrin core and the co-planarized phenyl substituents.

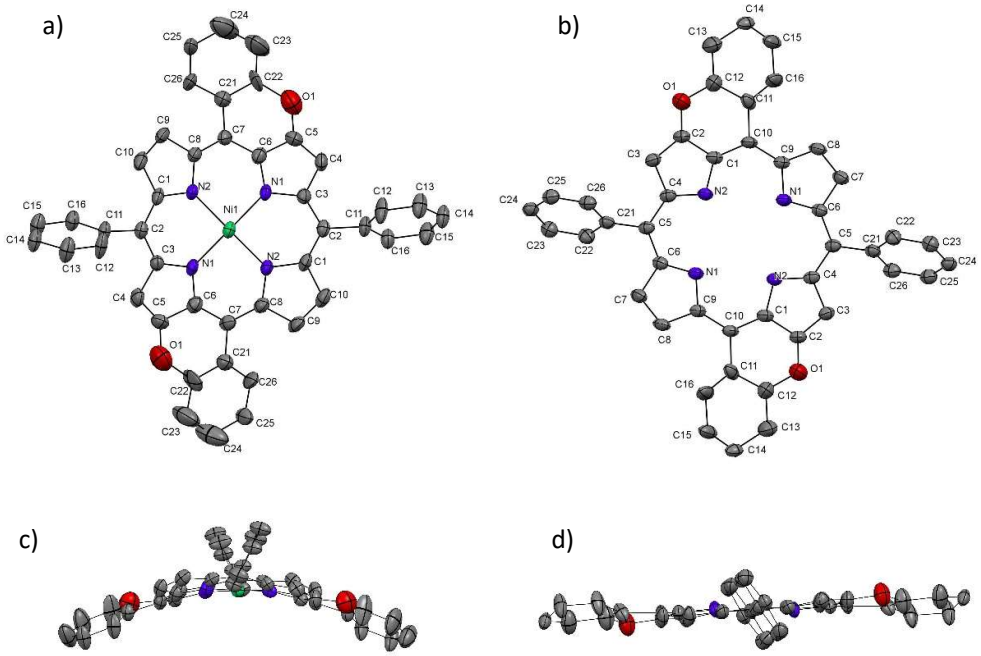

Figure 3.6 ORTEP representation of monopyranoporphyrins: a) **3-1**, top view; b) **3-14**, top view; c) **3-1**, side view; d) **3-14**, side view (the *tert*-butyl substituents have been omitted). For practical reasons, the atom numbering does not follow the IUPAC recommendations. Atomic displacement parameters obtained at 150 K are drawn at the 30% probability level. Atom colours: blue N, red O, white C, green Ni.

3.2 Synthesis and characterization of dipyranoporphyrins

In the following section, a detailed description of our extended investigation towards pyranoporphyrins with an increased number of oxygen bridges in the porphyrin core is reported. In this context, we selected three different dipyranoporphyrin isomers **3-16–3-18** on which the diaryl-ether bond formation through CuO-mediated pyran annulation reaction will be studied (Figure 3.7).

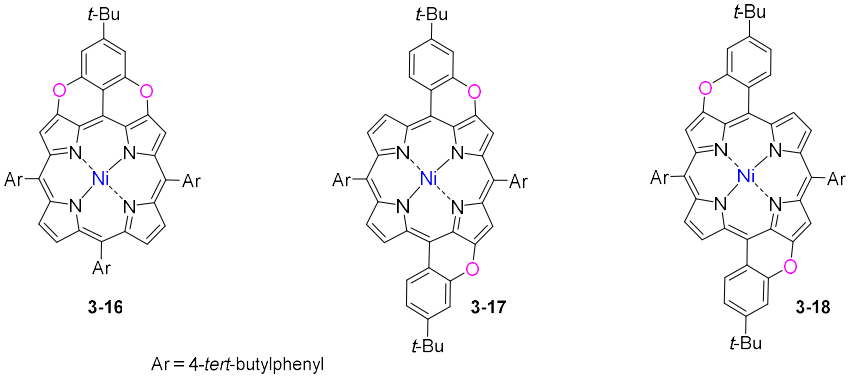

Figure 3.7 Chemical structures of dipyranoporphyrin isomers **3-16**–**3-18**.

3.2.1 Synthesis of dipyranoporphyrin 3-16

Similarly, as for the monopyranoporphyrins, the retrosynthesis of dipyranoporphyrin derivative **3-16**, involves the simultaneous formation of two pyranocycles upon intramolecular ring fusion reaction (Scheme 3.8). Dimethoxyporphyrin **3-20** can be obtained by condensation of the corresponding aldehydes and pyrrole under classical *Lindsey* conditions.

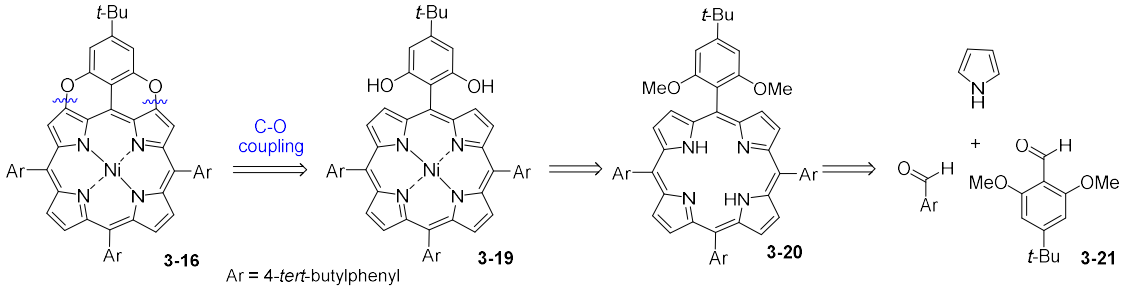

Scheme 3.8 Retrosynthesis of dipyranoporphyrin **3-16**.

In order to obtain desired fused porphyrin **3-16**, precursor **3-20** was prepared. Thus, 4-*tert*-butyl-2,6-dimethoxybenzaldehyde **3-21** was chosen as a suitable aldehyde to react with pyrrole. Its synthesis was commenced from alkylation of commercially available 2,6-dimethoxyphenol **3-22** under *Friedel-Crafts* conditions (Scheme 3.9). Treatment with *tert*-BuOH in the presence of CH_3SO_3H led to 4-*tert*-butyl-2,6-dimethoxyphenol **3-23** in 78% yield.[158] Crude **3-23** was directly reacted with $HOP(OEt)_2$ in the presence of Et_3N to afford phosphate **3-24** in 56% overall yield. Subsequent *Birch*-type reduction of **3-24** using Li in NH_3(liq.) yielded compound **3-25** as a white solid. Reaction of the latter with *n*-BuLi and

further treatment of the formed anion with DMF gave desired aldehyde **3-21** as a yellow solid in 57% yield.

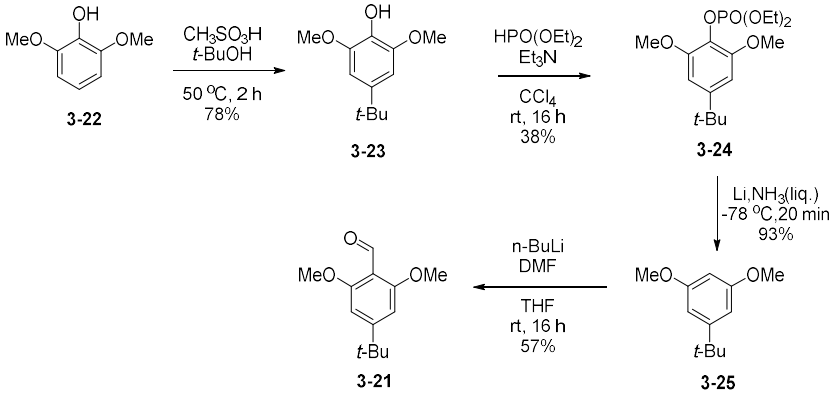

Scheme 3.9 Synthesis of starting 4-*tert*-butyl-2,6-dimethoxybenzaldehyde **3-21**.

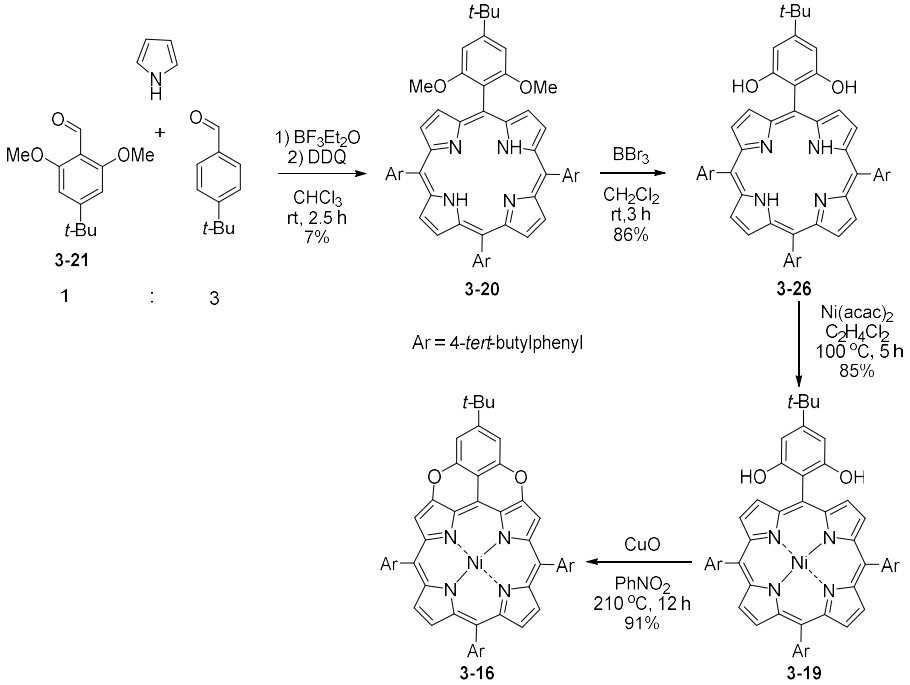

Scheme 3.10 Synthetic pathway towards the preparation of dipyranoporphyrin **3-16**.

Furthermore, dihydroxyporphyrin **3-19** was synthesized in the same manner as monohydroxyporphyrin **3-2**, but using dimethoxybenzaldehyde **3-21** instead of monomethoxybenzaldehyde **3-4** (Scheme 3.10). Accordingly, the macrocyclization reaction of **3-21** and 4-(*tert*-butyl)benzaldehyde with pyrrole in $CHCl_3$ in the presence of $BF_3{\cdot}Et_2O$, followed by oxidation of porphyrinogen with DDQ afforded a mixture of porphyrins. Crude

material was purified by silica gel column chromatography yielding free-base porphyrin **3-20** in 7% yield. The latter was then reacted with an excess of BBr_3 in CH_2Cl_2 to give free-hydroxyl porphyrin **3-26**, directly followed by Ni-metallation affording product **3-19** in 85% yield.

Similarly to the synthesis of **3-1**, dihydroxyporphyrin **3-19** was subjected to the CuO-mediated pyran annulation reaction in $PhNO_2$ at 210 °C affording target dipyranoporphyrin **3-16** in 91% yield (Scheme 3.10). It should be noted, that for the first time O-fused porphyrin **3-16** was prepared by *Dr. Daphne Stassen* using CuI in the presence of PivOH in DMSO at 120 °C in 35% yield. Hence, an increased yield is noted (35% *vs* 91%) using the optimized reaction conditions in the presence of CuO, initially developed for the formation of the monopyranoporphyrins as described in *section* 3.1.2. Further demetallation of **3-16** using strong acidic conditions, followed by Zn-metallation with $Zn(OAc)_2$ led to the replacement of the central metal atom giving Zn(II) porphyrin **3-28** (Scheme 3.11).

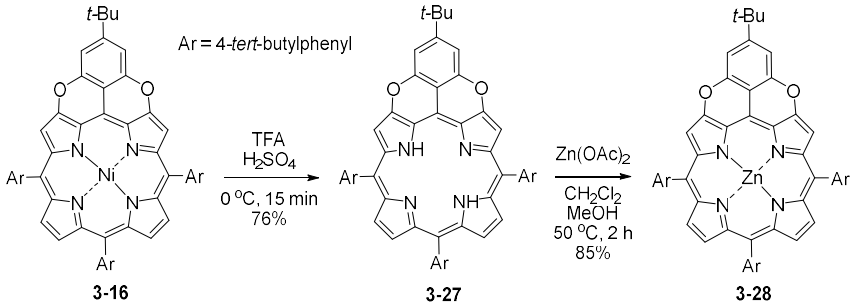

Scheme 3.11 Synthetic pathway towards the preparation of free-base **3-27** and Zn(II) **3-28** dipyranoporphyrins.

As-obtained metal and free-base dipyranoporphyrins were thoroughly characterized by HRMS-MALDI spectrometry, ^1H and ^{13}C NMR-. IR- and UV-spectroscopy, as reported in Chapter VI. For instance, ^1H NMR-spectrum of free-base dipyranoporphyrin **3-27** is depicted in Figure 3.8. In contrast to free-base monopyranoporphyrin **3-14**, which is non-symmetrical, porphyrin **3-27** has C_{2v} point group of symmetry. This feature simplifies the ^1H NMR-spectrum, providing well-defined splitting of all signals. Specifically, the pyrrole ring is retrieved in one singlet of H_b (8.65 ppm) and two doublets of H_c (9.07 ppm) and H_d (8.97 ppm), while the benzopyran ring exhibited only one singlet of H_a (7.72 ppm), integrating for 2H. Additionally, HRMS-MALDI measurement of **3-27** displayed the presence of the desired peak at m/z 867.4647 (M^+, $[C_{60}H_{58}N_4O_2^+]$, calc.: 867.4638), thus confirming that a double pyranocycle formation has occurred.

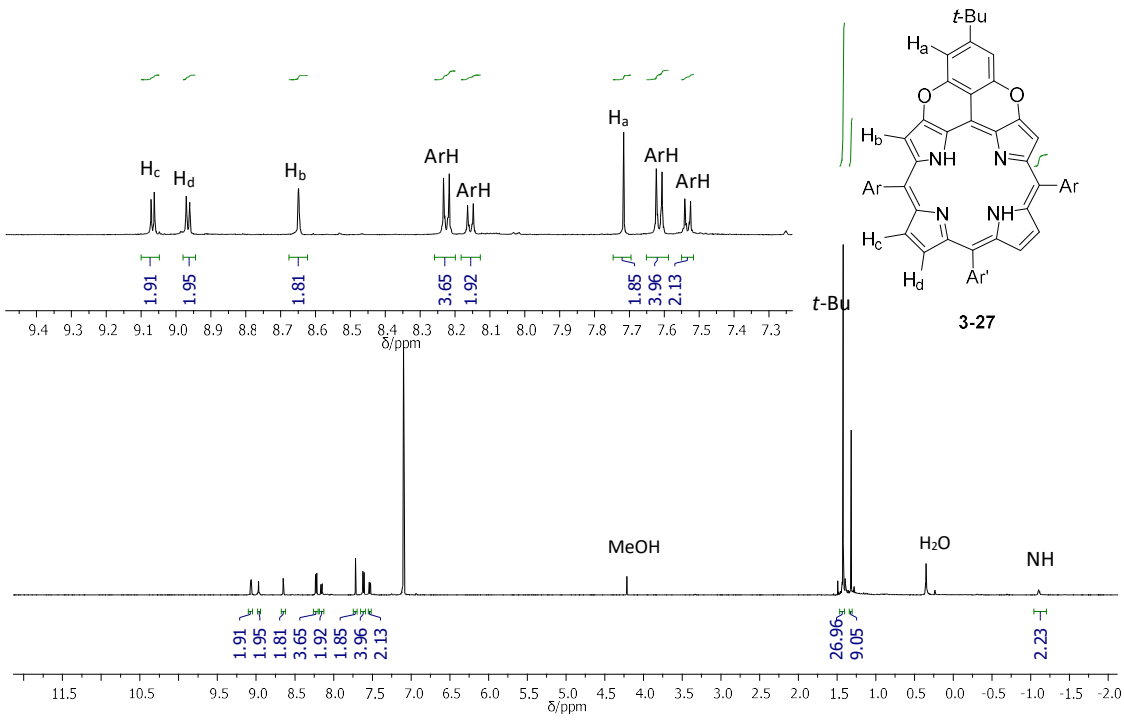

Figure 3.8 ^{1}H NMR-spectrum of free-base dipyranoporphyrin **3-27** (400 MHz, $CDCl_3$). The inset shows zoom of the 9.5-7.25 ppm area.

X-ray radiocrystallographic analysis confirmed the structure of Ni(II) dipyranoporphyrin **3-16**. Dark-purple needle-like crystals of **3-16** were grown by slow vapour diffusion of MeOH in CH_2Cl_2 at rt. The crystal structure, depicted in Figure 3.9, was determined at 150 K and found to belong to the monoclinic space group P 21/c. Further details on the crystal structure are provided in the Appendix. Dipyranoporphyrin **3-16**, as was expected, is almost planar, except the fused *meso*-aryl substituent, slightly deviating from the mean plane of the porphyrin core. The angle between the N4-plane (mean plane of the four pyrrolic nitrogens) and fused *meso*-aryl substituent is 14.1°. Interestingly, the lengths of the C(34)-O(2) (1.45 Å) and C(22)-O(1) (1.42 Å) bonds, where the oxygen atom is fused to the porphyrin core, as well as the lengths of the C(47)-O(2) (1.49 Å) and C(60)-O(1) (1.63 Å) bonds, in which the oxygen atom is fused to the *orto*-positions of the *meso*-aryl group, correspond to the length of a single C-O bond, demonstrating no conjugation of the oxygen atoms with porphyrin core.

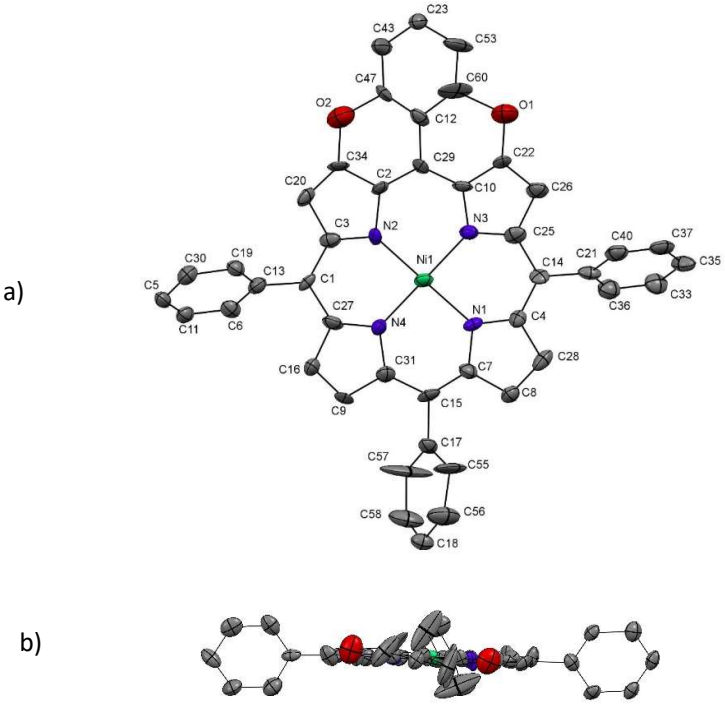

Figure 3.9 ORTEP representation of Ni(II) dipyranoporphyrin **3-16**: a) top and b) side views (the *tert*-butyl substituents have been omitted). For practical reasons, the atom numbering does not follow the IUPAC recommendations. Atomic displacement parameters obtained at 150 K are drawn at the 30% probability level. Atom colours: blue N, red O, white C, green Ni.

3.2.2 Synthesis of dipyranoporphyrins 3-17 and 3-18

Retrosynthetic analysis of **3-17** and **3-18** shows that the disconnection of the C-O bonds in both cases lead to the same starting dihydroxyporphyrin **3-29** and both products can be synthesized simultaneously using the pyran annulation reaction (Scheme 3.12).

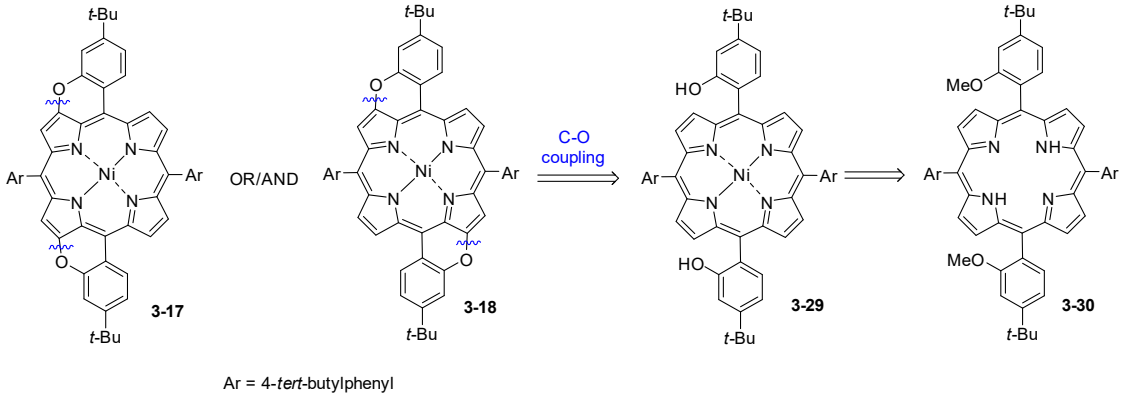

Scheme 3.12 Retrosynthesis of dipyranoporphyrins **3-17** and **3-18**.

Similarly to the preparation of mono- and di- hydroxyporphyrins **3-2** and **3-19**, respectively, the synthesis of target dihydroxyporphyrin **3-29** was started from obtaining free-base dimethoxyporphyrin **3-30** (Scheme 3.13). Accordingly, a stoichiometric mixture of methoxybenzaldehyde **3-4**, 4-(*tert*-butyl)benzaldehyde and pyrrole were subjected to the classical condensation type reaction, producing a complex mixture of porphyrins. Unfortunately, all our attempts to separate desired porphyrin **3-30** by silica gel column chromatography were unsuccessful. We attributed this failure to the formation of "*trans*-" and "*cis*-" isomers **3-30** and **3-31**, respectively, the separation of which was complicated due to the similar polarity. Moreover, MeO-groups attached to the *orto*-positions led to the hindered rotation of the *meso*-aryl substituents, thus causing the arising of different atropisomers.

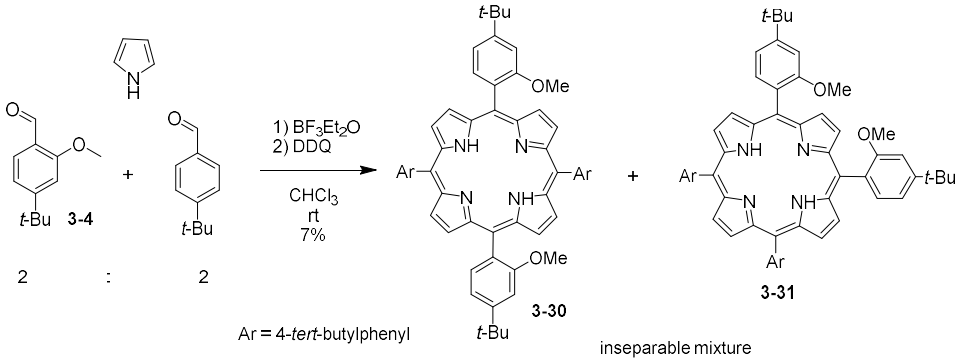

Scheme 3.13 Direct synthesis of dimethoxyporphyrin, resulting in formation of "*trans*-" and "*cis*-" isomers **3-30** and **3-31**, respectively.

In light of these results, an alternative approach was proposed that allows the preparation of desired **3-30** by circumventing the formation of an inseparable mixture. Hence, the use of the so-called *MacDonald* [2+2] porphyrin macrocyclization reaction was proposed (Scheme 3.14).

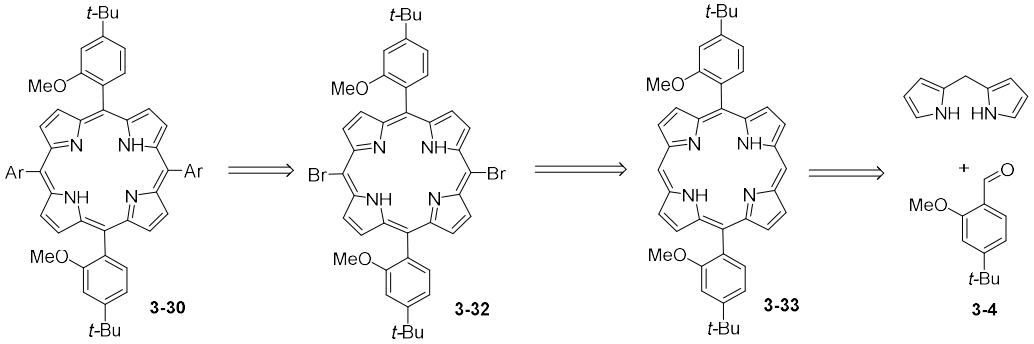

Scheme 3.14 Retrosynthesis of dimethoxyporphyrin **3-30**.

This approach involves the preliminary formation of porphyrin precursor **3-33** by condensation of as-prepared dipyrromethane with methoxybenzaldehyde **3-4** according to the typical *Lindsey's* procedure (Scheme 3.15). Subsequent treatment of **3-33** with NBS in CH_2Cl_2 for 15 min at rt afforded dibromoporphyrin **3-32** in 95% yield. This was followed by *Suzuki* coupling reaction of **3-32** with an excess of 4-*tert*-butylphenylboronic acid in the presence of $Pd(PPh_3)_4$ yielding free-base dimethoxyporphyrin **3-30** in 49% yield. Further removal of the methyl protecting groups of **3-30** with BBr_3 in CH_2Cl_2, followed by metallation with $Ni(acac)_2$ led to desired dihydroxyporphyrin **3-29** after precipitation from MeOH.

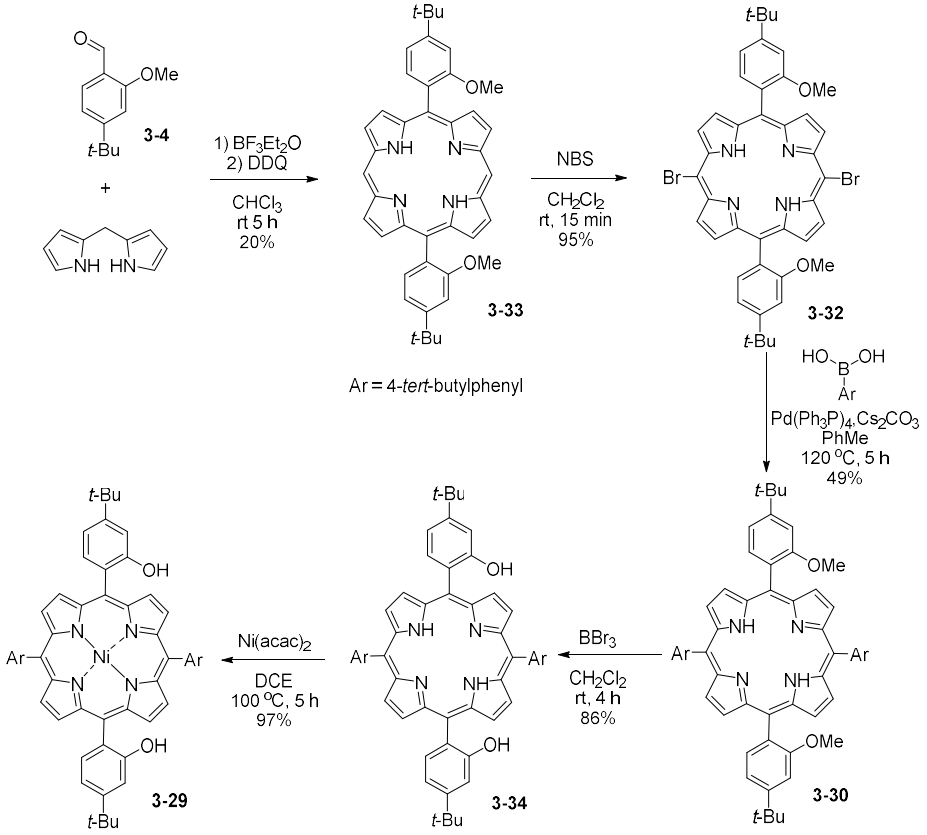

Scheme 3.15 Rational synthesis of dihydroxyporphyrin **3-29**.

Herein, the pyran annulation reaction follows the same reaction conditions described for the precedent mono- and di- pyranoporphyrins, using dihydroxyporphyrin **3-29**. CuO-promoted oxidative cycloetherification of **3-29** yielded a mixture of two isomers **3-17** and **3-18** (Scheme 3.16). Due to the similar polarity of those isomers the separation of them neither by silica gel column chromatography using various mixtures of solvents nor by HPLC was fruitful. Therefore, we assumed that the removal of the central metal could favour the

interactions between free-base porphyrin and SiO_2, facilitating the separation process. For this purpose, the demetallation reaction was carried out, yielding a mixture of two products, clearly detected by TLC. Fortunately, the obtained isomers were easily separated by SiO_2 column chromatography eluting with 1:1 mixture of CH_2Cl_2/cyclohexane. Both structural isomers, namely *cis*- and *trans*-like dipyranoporphyrins **3-35** and **3-36**, were isolated in 29% and 32% overall yield, respectively.

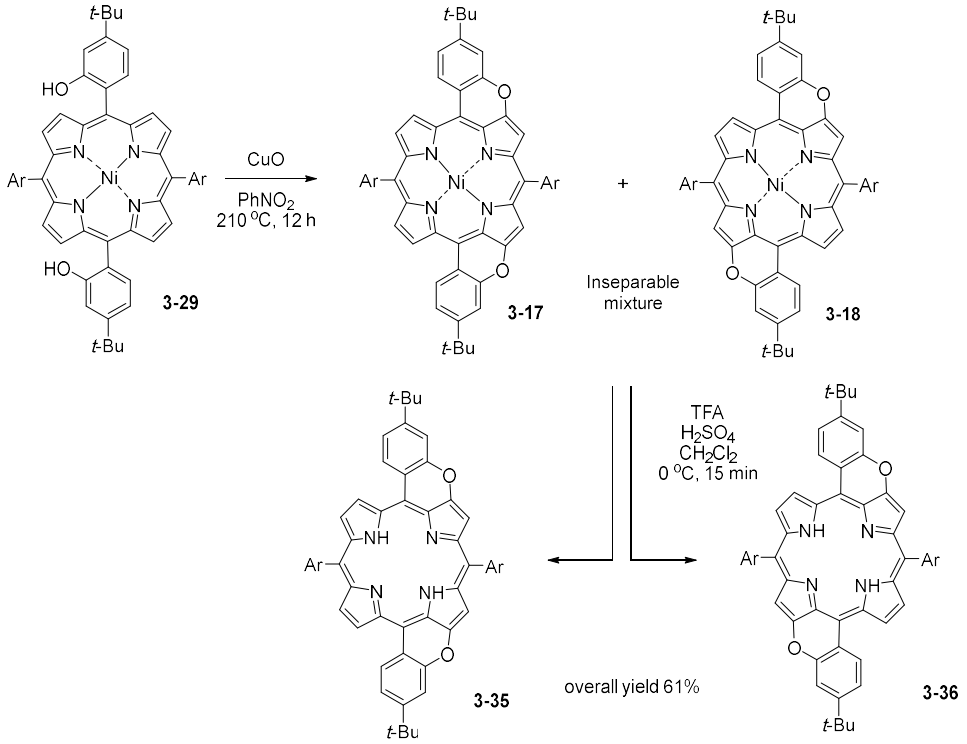

Scheme 3.16 Synthetic pathway towards the synthesis and separation of dipyranoporphyrins **3-35** and **3-36**.

The thorough NMR analysis of each fraction proved the chemical structures of **3-35** and **3-36**. Similarly as for free-base dipyranoporphyrin **3-27** (Figure 3.8), ^{1}H NMR-spectra of **3-35** and **3-36** presented identical pattern for the pyrrolic protons (Figures 3.10a, 3.11a). Both show three signals, two doublets of H_d (**3-35**: 9.51 ppm; **3-36**: 9.85 ppm) and H_e (**3-35**: 8.80 ppm; **3-36**: 9.05 ppm) and one singlet of H_h (**3-35**: 8.37 ppm; **3-36**: 8.49 ppm) that refers to the 6H of the pyrrole rings. In addition, both porphyrin isomers present analogous pattern of signals assigned to the 6H of the benzopyran ring: one singlet of H_a (**3-35**: 8.02 ppm; **3-36**: 8.10 ppm), one doublet of H_c (**3-35**: 9.10 ppm; **3-36**: 9.21 ppm) and the multiplet of H_b, overlapped with other aromatic protons.

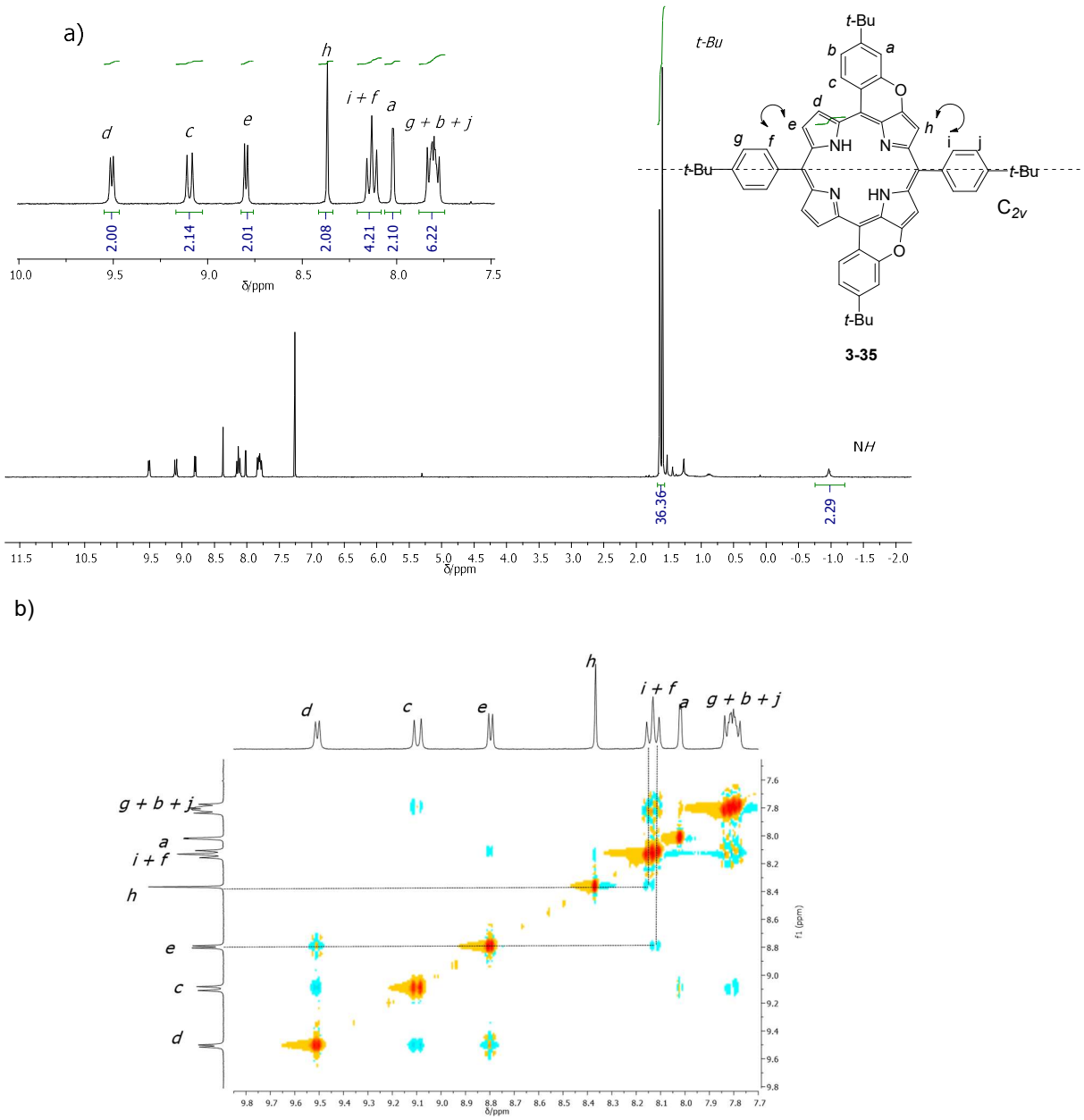

Figure 3.10 NMR analysis of *cis*-like dipyranoporphyrin **3-35**: a) 1D ^{1}H NMR-spectrum (300 MHz, $CDCl_3$), the inset shows zoom of the 10.00-7.50 ppm area; b) 2D NOESY NMR-spectrum (300 MHz, $CDCl_3$, zoom of the 10.00–7.50 ppm area).

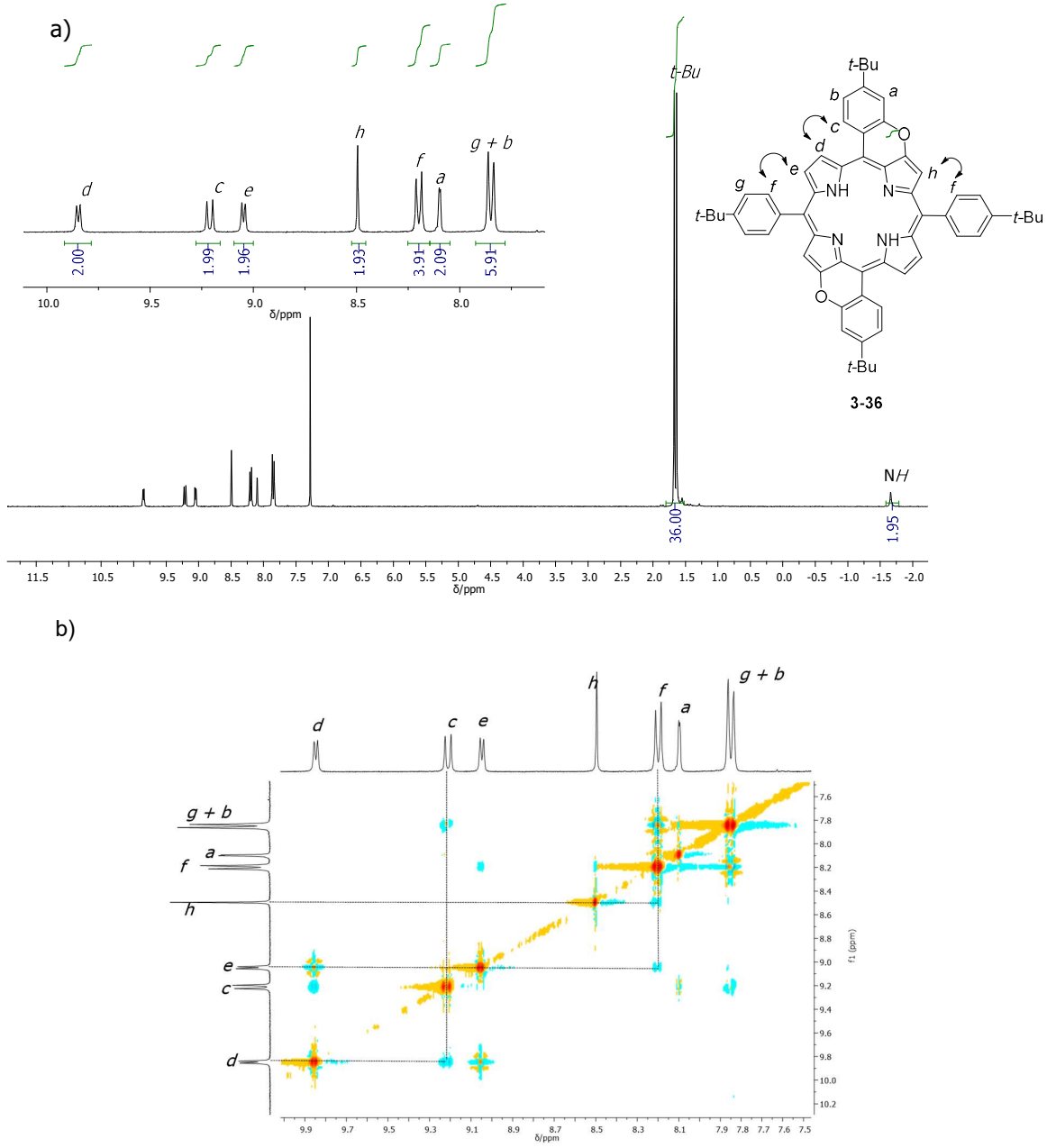

Figure 3.11 NMR analysis of *trans*-like dipyranoporphyrin **3-36**: a) 1D ^{1}H NMR-spectrum (300 MHz, $CDCl_3$), the inset shows zoom of the 10.00-7.50 ppm area; b) 2D NOESY NMR-spectrum (300 MHz, $CDCl_3$, zoom of the 10.00–7.50 ppm area).

The full-assignment of other peaks to the appropriate aromatic protons was provided by 2D Nuclear Overhauser effect spectroscopy (NOESY). This analysis allows establishing correlations between nuclei, which are spatially close to each other (within about 5 Å). The

most representative space correlations between protons of pyrrolic rings and the *meso*-aryl substituents are depicted in Figures 3.10b, 3.11b. Specifically, the NOESY spectrum presents the correlations between pyrrolic $H_{e,h}$ with H_f of 4-(*tert*-butyl)phenyl groups, suggesting the C_2 group of symmetry for *trans*-like isomer **3-36**, aroused after O-annulation (Figure 3.11b, dashed lines). Meanwhile, since *cis*-like isomer **3-35** is a C_{2v}-symmetrical molecule, 4-(*tert*-butyl)phenyl substituents are not equal anymore, and hence, two different correlation are observed (Figure 3.10b, dashed lines). In particular, the singlet of pyrrolic H_h (8.37 ppm) correlates with the doublet of H_i (8.14 ppm), belonging to the *meso*-aryl substituent, while the doublet of H_e (8.80 ppm) correlates with the doublet of H_f (8.12 ppm).

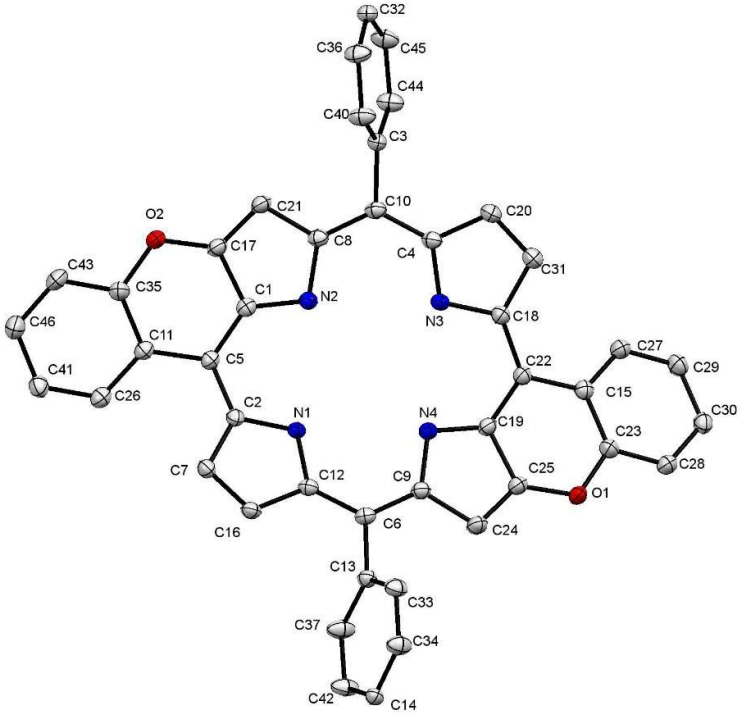

Figure 3.12 ORTEP representation of porphyrin **3-36** (the *tert*-butyl substituents have been omitted). For practical reasons, the atom numbering does not follow the IUPAC recommendations. Atomic displacement parameters obtained at 150 K are drawn at the 30% probability level. Atom colours: blue N, red O, white C.

The structure of **3-36** was confirmed by X-ray radiocrystallographic analysis (Figure 3.12). Purple needle like crystals were obtained by slow vapour diffusion of MeOH into a solution of porphyrin **3-36** in CH_2Cl_2 at rt at dark. The crystal structure was determined at 150 K and found to belong to the triclinic space group P-1. Further details on the crystal structure are described in the Appendix. Dipyranoporphyrin **3-36** exhibits a ruffled

conformation which is not typical for free-base porphyrins. The mean deviation of the tetrapyrrolic macrocycle from the plane of the four nitrogen atoms is 0.65 Å. The lengths of the C-O bonds (C(25)-O(1), C(23)-O(1), C(35)-O(2), C(17)-O(2)) are found to be 1.35-1.36 Å, which is slightly less than the length of a usual C-O single bond (1.38-1.42 Å). In addition, the length of the C-C bonds (C(22)-C(15), C(5)-C(11)) is determined as 1.47 Å, which corresponds to the characteristic length of C_{sp2}-C_{sp2} bond. These findings suggested a weak conjugation between the porphyrin core and the co-planarized phenyl substituents. Similarly to other planar or moderately distorted porphyrin derivatives,[164] molecule **3-36** forms π-stacked layers in a parallel-displaced fashion with an interplanar separation of *ca.* 3.1 Å and a lateral shift of the porphyrin ring centers of *ca*. 6.83 Å (Figure 3.13).

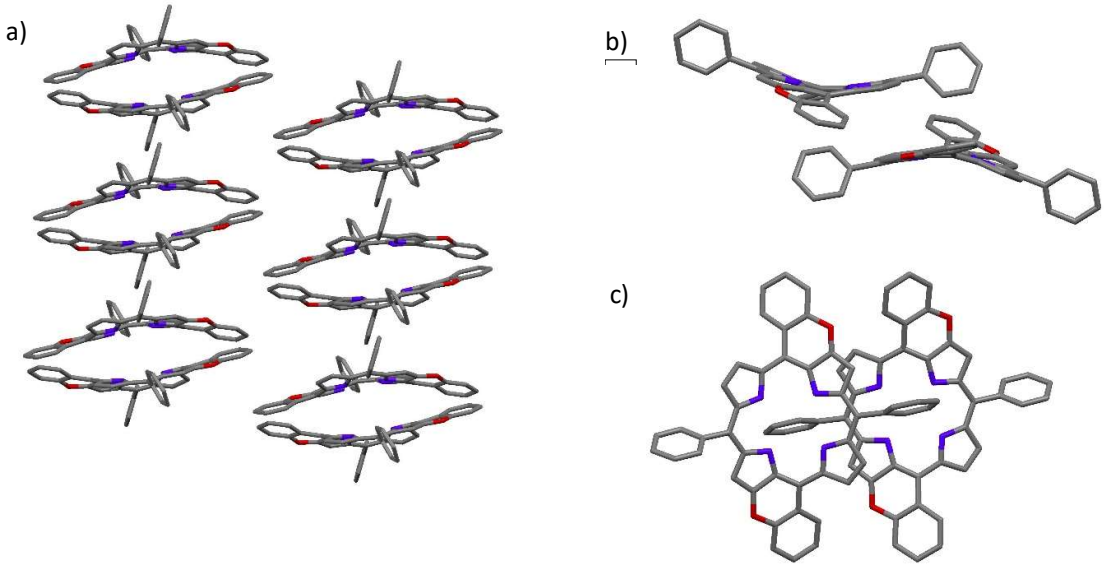

Figure 3.13 a) Packing diagram of **3-36** along the *c* axe; b) View of a dimeric aggregate in the crystal. c) Top view of the porphyrin pairs showing their relative orientation and offset (*ca.* 6.83 Å). The *tert*-butyl substituents have been omitted. Atom colours: blue N, red O, gray C.

3.3 Investigation of physicochemical properties

3.3.1 Adsorption and emission spectroscopic measurements

Since the extension of the π-conjugation through the structure leads to very attractive photophysical behaviour, we were interested to study the photophysical properties of the O-annulated porphyrins. The absorption spectra of all investigated compounds have been recorded in CH_2Cl_2 at rt. UV-vis spectra of methoxyporphyrin **3-3** and O-fused porphyrins

3-14 and **3-27** reveal a slight bathochromic shift of the absorption maxima from 647 nm for **3-3** to 655 and 663 nm for **3-14** and **3-27**, respectively (Figure 3.14). These changes of absorption maxima can be attributed to the weak conjugation between the porphyrin core and the *meso*-aryl substituent. This finding is in full accordance with the X-ray data.

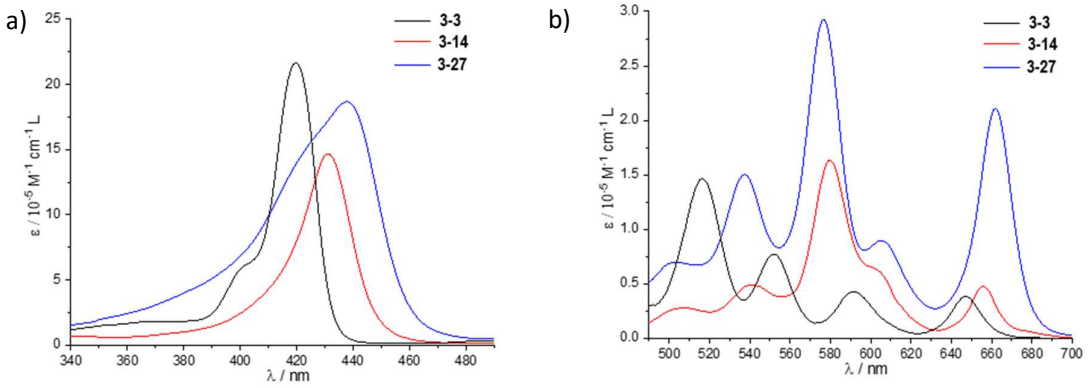

Figure 3.14 UV-vis absorption spectra of monomethoxyporphyrin **3-3** (black line), free-base mono- and di-pyranoporphyrins **3-14** (red line) and **3-27** (blue line), respectively, recorded in CH_2Cl_2 at rt: a) *Soret* bands; b) Q-bands.

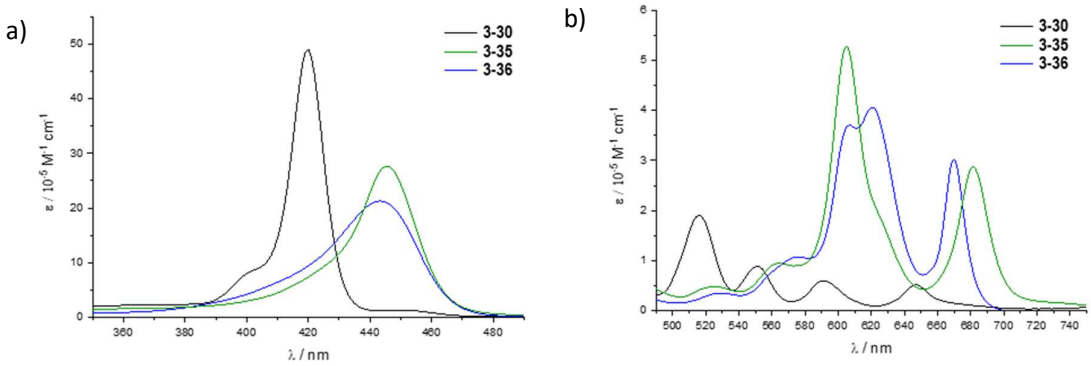

Figure 3.15 UV-vis spectra of free-base dimethoxyporphyrin **3-30**, free-base *cis*- and *trans*-like dipyranoporphyrins **3-35** and **3-36**, respectively, recorded in CH_2Cl_2 at rt: a) *Soret* bands; b) Q-bands.

In contrast to O-fused porphyrins **3-14** and **3-27**, the UV-vis absorption spectra of free-base *cis*- and *trans*-like dipyranoporphyrins **3-35** and **3-36**, respectively, display more profound red shift of the absorption maxima compare to reference porphyrin **3-3** (Figure 3.15). Interestingly, the optoelectronic properties of structural isomers **3-35** and **3-36** are not the same. Depending on the position of the O-annulation, the wavelengths of absorbance maximum for *trans*- and *cis*-like isomers **3-36** (670 nm) and **3-35** (681 nm), respectively, are different. It could be hypothesized that the *cis*-isomer **3-35** displays a larger conjugated system compared to the *trans*-isomer **3-36**, leading to shrinking of the HOMO-LUMO gap.

In contrast to free-base monopyranoporphyrin **3-14**, the UV-vis absorption spectra of metal O-fused porphyrins **3-1**, **3-12**, **3-13** and **3-15**, incorporating Ni, Cu, Pd and Zn, respectively, show a reduced number of Q bands from 5 to 2 along with bathochromic shifts of absorbance maxima. Moreover, the data, presented in Figure 3.16a, demonstrate slight red shifts along the series Pd(II) < Ni(II) < Cu(II) < Zn(II), which fully correspond to a behaviour already reported in the literature.[165] Metalloporphyrins **3-1**, **3-12** and **3-13**, in which the open-shell Ni, Cu and Pd cause significant metal *d* π to porphyrin π* orbital interaction (metal to ligand π-backbonding), display an increased porphyrin π to π* energy separation leading to hypsochromic (blue) shifts. Zn(II) porphyrin **3-15** includes closed-shell Zn(II), in which the *d* π (d_{xz}, d_{yz}) metal-based orbitals are relatively low in energy, causing very little effect on the porphyrin π to π* energy gap in the porphyrin electronic spectra.

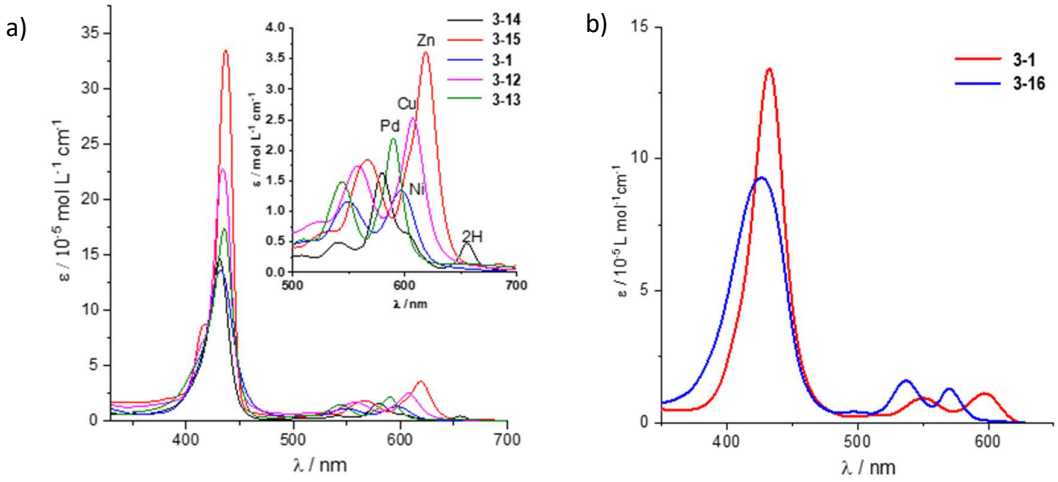

Figure 3.16 UV-vis absorption spectra of: a) free-base monopyranoporphyrin **3-14** (black line); Ni(II) **3-1** (blue line), Cu(II) **3-12** (magenta line), Pd(II) **3-13** (green line) and Zn(II) **3-15** (red line) monopyranoporphyrins in CH_2Cl_2 at rt; b) Ni(II) mono- and di- pyranoporphyrins **3-1** (red line) and **3-16** (blue line), respectively.

When porphyrins **3-14** and **3-27** were coordinated with Ni(II), the simplification of the Q bands pattern and specifically the formation of only two Q bands was observed (Figures 3.14, 3.16b). Besides, the insertion of Ni(II), led to a hypsochromic (blue) shift of the electronic absorption in the case of mono- and di- pyranoporphyrins **3-1** and **3-16**, respectively, compared to free-base porphyrins. These observations fully coincide with the literature data,[165] indicating the interaction of occupied d_{xz} and d_{yz} orbitals of Ni(II) with π^* orbital of the porphyrin ligand. It should be also noted that the wavelength of absorbance maximum for **3-1** (595 nm) is red-shifted compared to that of **3-16** (570 nm), as shown in

Figure 3.16b. This phenomenon can be explained by the out-of-planarity distortion of **3-1** (Figure 3.6), inducing the destabilization of the HOMO energy and decreasing the HOMO-LUMO gap. Meanwhile, since the structure of **3-16** is assumed to be planar, the shrinking of the HOMO-LUMO gap is not observed.

Fluorescence spectra of free-base mono- and di- pyranoporphyrins were recorded in CH_2Cl_2 at rt. We selected as excitation wavelength the maxima of the peaks detected around 420 nm. In all cases, the excitation at selected wavelengths resulted in emission around 650-690 nm and 720-760 nm (Figure 3.17).

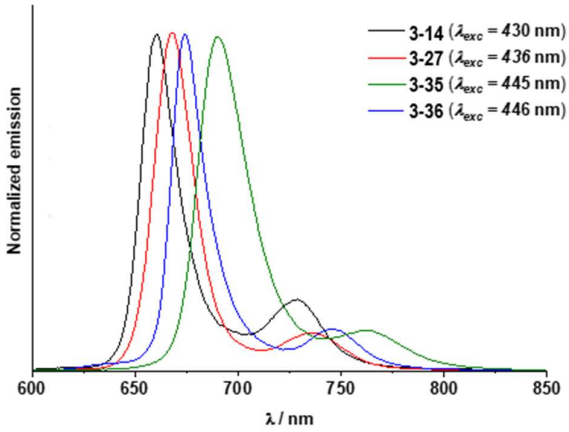

Figure 3.17 Fluorescence spectra of free-base mono- and di- pyranoporphyrins **3-14** (black line) and **3-27** (red line), **3-35** (green line), **3-36** (blue line), respectively, in CH_2Cl_2 at rt.

An enhancement of the quantum yields was expected as a result of the increased rigidity of the O-fused porphyrins. However, O-annulation led to the negligible increasing of quantum yields compared to that of the reference non-fused porphyrin **3-3** (Table 3.2).

Table 3.2 Emission properties of reference monomethoxyporphyrin **3-3** and free-base O-embedded porphyrins

Compound	λ_{max}/nm *Soret band*	λ_{max}/nm *Q bands*	λ_{em}/nm	Φ %
3-3	419	486, 516, 552, 593, 647	653, 720	2.4
3-14	431	506, 541, 580, 602, 655	660, 729	2.6
3-27	438	502, 538, 577, 605, 662	667, 736	4.2
3-36	445	563, 576, 607, 620, 670	675, 746	3.7
3-35	443	524, 564, 605, 625, 681	691, 762	5.8

3.3.2 Electrochemical investigation

An in-depth examination of the influence the O-annulation has on the electronic system of porphyrins was also studied, by measuring the half-wave potentials of O-embedded porphyrins using cyclic voltammetry. The measurement of redox potentials was performed in dry O_2-free *o*-DCB solutions using 0.1 M *n*-Bu_4NPF_6 as supporting electrolyte and ferrocene as an internal reference. The redox properties of Ni(II) and Zn (II) O-fused porphyrins are reported in Figure 3.18. Non-fused Ni(II) dimethoxyporphyrins **3-37** was chosen as a reference compound.

The electrochemical properties of the studied porphyrins, as expected, are fully coincide with those of well-known TPPs by showing two reversible oxidations ($E^{1/2}_{ox1}$, $E^{1/2}_{ox2}$) and two reductions ($E^{1/2}_{red1}$, $E^{1/2}_{red2}$).[166] It should be noted that Ni(II) porphyrins possess a third oxidation potential ($E^{1/2}_{ox3}$) above 1 eV, which is assigned to the oxidation of Ni(II) to Ni(III).[166,167] Taking into consideration that the first oxidation ($E^{1/2}_{ox1}$) and the first reduction ($E^{1/2}_{red1}$) potentials relate to HOMO and LUMO energies, respectively, the electrochemical HOMO-LUMO gap is determined as $E^{1/2}_{ox1}$-$E^{1/2}_{red1}$. Consequently, electrochemical HOMO-LUMO gap for **3-37** is found to be 2.33 V. Comparing the cyclic voltammograms of Ni(II) O-fused derivatives **3-1** and **3-16** with that of **3-37**, a shrinking of the electrochemical HOMO-LUMO gap (*ca.* 100-130 mV) was observed. In contrast to monopyranoporphyrin **3-1**, the second reduction potential of dipyranoporphyrin **3-16** is anodically shifted by 170 mV indicating the formation of a more electron saturated system in case of **3-16** after the first reduction. Meanwhile, the first reduction potential remained almost unchanged both for **3-1** and **3-16**. Additionally, incorporation of the second oxygen atom led to negligible changes of the electrochemical HOMO-LUMO gap, while its impact to the difference in potentials between the first and second oxidations ($E^{1/2}_{ox2}$-$E^{1/2}_{ox1}$) as well as between the first and second reductions ($E^{1/2}_{red2}$-$E^{1/2}_{red1}$) were found to be more pronounced. For instance, in the case of Ni(II) porphyrins $E^{1/2}_{ox2}$-$E^{1/2}_{ox1}$ was increased from 0.43 V for **3-1** to 0.53 V for **3-16**, while $E^{1/2}_{red2}$-$E^{1/2}_{red1}$ was increased from 0.37 V for **3-1** to 0.6 V for **3-16**. It should be noted, that cyclic voltammograms of Zn(II) porphyrins **3-15** and **3-28** revealed the same patterns as those of **3-1** and **3-16**.

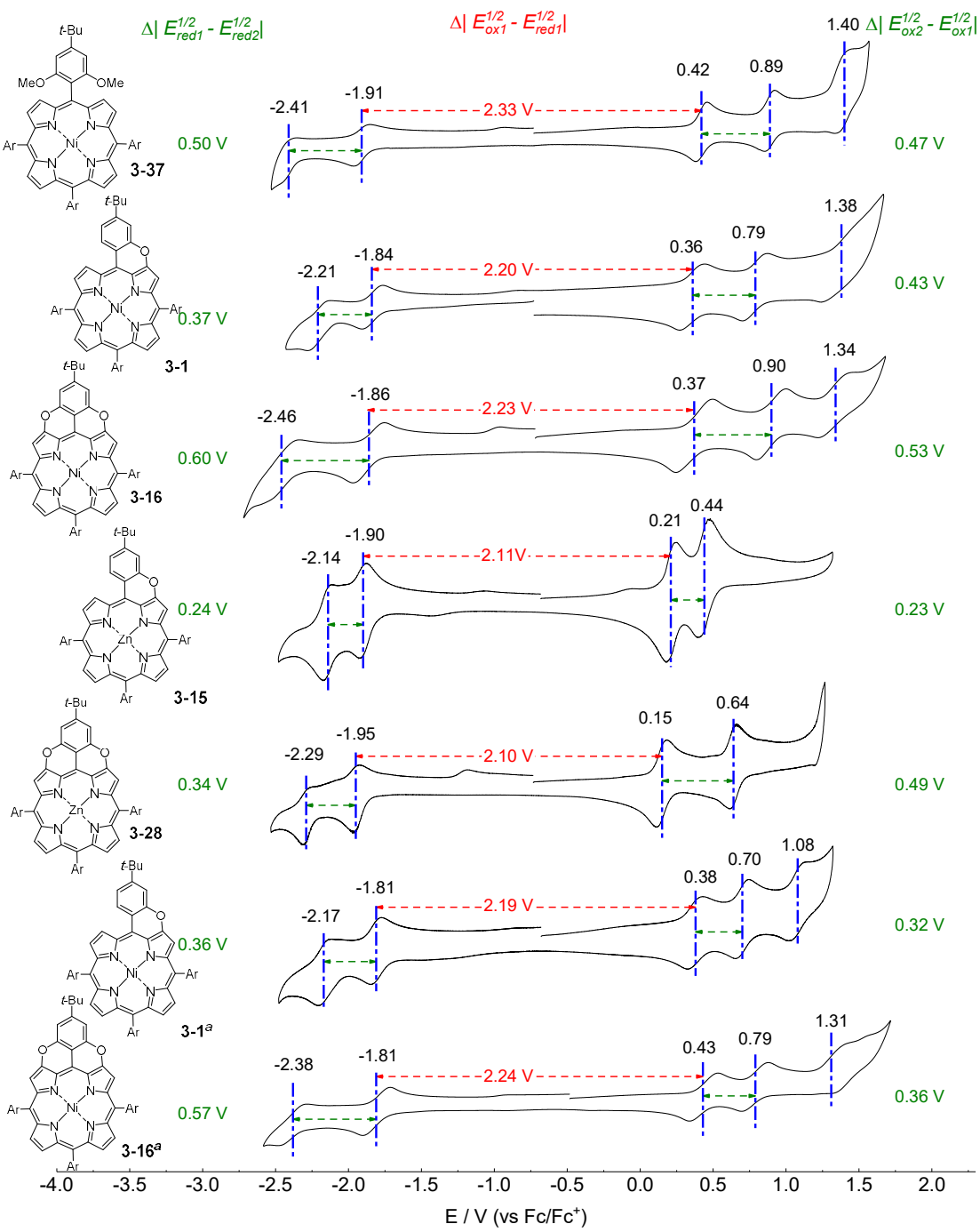

Figure 3.18 Cyclic voltammetry of Ni(II) dimethoxyporphyrin **3-37**, metal mono- and di- pyranoporphyrins at scan rate100 mV/s in *o*-DCB with 0.1 M of $TBAPF_6$; [a] 0.1 M of $TBABF_4$ as a supporting electrolyte.

Interestingly, by changing the supporting electrolyte from $TBAPF_6$ to $TBABF_4$, the difference in value of $E^{1/2}_{ox2}$-$E^{1/2}_{ox1}$ between Ni(II) mono- and di- pyranoporphyrins **3-1** and **3-16**, respectively, was smoothed. Similar behaviour was observed by *Kadish*, who has noted

that $E^{1/2}_{ox2}$-$E^{1/2}_{ox1}$ of metal TPPs depends on the solvent and electrolyte, while $E^{1/2}_{ox1}$-$E^{1/2}_{red1}$ is relatively insensitive to the experimental parameters.[166,168] This is attributed to the ion pairing interaction of doubly-oxidized porphyrin species with the electrolyte anion, resulting in stabilization of the porphyrin dication along with a decrease of the second oxidation potential.[169,170] In our case, the replacement of PF_6^- for the more nucleophilic BF_4^- led to the anodic shift of the second oxidation potential for **3-1** (90 mV) as well as for **3-16** (110 mV) indicating a stronger ion pairing of BF_4^- with dipyranoporphyrin dication, rather than with doubly-oxidized monopyranoporphyrin specie. To diminish the impact of supporting electrolyte on redox processes, hereinafter we only used $TBAPF_6$.

In order to exclude the influence of the central metal and to gain further insight in redox properties of as-obtained O-fused porphyrins, free-base derivatives were also investigated. Non-fused free-base mono- and di- methoxyporphyrins **3-3** and **3-20** were chosen as reference compounds. Cyclic voltammograms of free-base mono- and di-methoxyporphyrins **3-3** and **3-20**, respectively, along with their O-fused derivatives are shown in Figure 3.19. Comparing the electrochemical properties of O-fused porphyrins **3-14** and **3-27** with those of non-fused **3-3** and **3-20**, a narrowing of the electrochemical band gap (*ca.* 170-190 mV) was revealed. In contrast to monopyranoporphyrin **3-14**, the first and second reduction potentials of dipyranoporphyrin **3-27** are anodically shifted by 30 and 90 mV, respectively, indicating the formation of a more electron saturated system in case of **3-27**. Interestingly, $E^{1/2}_{ox2}$ of **3-14** is cathodically shifted by 190 mV compared to that of **3-27**, while $E^{1/2}_{ox1}$ remained unchanged for both porphyrins. Similarly to what observed for metal mono- and dipyranoporphyrins (Figure 3.18), insertion of a second oxygen atom in case of free-base analogue **3-27** strongly affects the second oxidation potential, while its impact to electrochemical HOMO-LUMO gap is insignificant.

Cis- and *trans*-like isomers **3-35** and **3-36**, respectively, demonstrate the narrowing of the electrochemical band gap compared to dipyranoporphyrin **3-27**. Besides, CV investigation of **3-35** and **3-36** revealed a significant influence of the position of the oxygen bridges on the redox potentials. Since $E^{1/2}_{red1}$ and $E^{1/2}_{red2}$ of **3-36** are cathodically shifted by 100 mV relative to those of **3-35**, the $E^{1/2}_{ox1}$-$E^{1/2}_{red1}$ gap of *trans*-isomer **3-36** was calculated to be 1.87 V, which is smaller than that of **3-35** (1.94 V). Comparing the first oxidation potential of **3-36** with that of **3-35**, a cathodic shift of only 30 mV was observed while the second oxidation potential of **3-36** was anodically shifted by 290 mV. Apparently, the first oxidation potential depends on the alignment of the *meso*-aryl substituent with the porphyrin core, and each

subsequent co-planarization causes the decrease of $E^{1/2}_{ox1}$ by *ca.* 100 mV. Meanwhile, the number and position of the oxygen bridges has a dramatic impact on $E^{1/2}_{ox2}$.

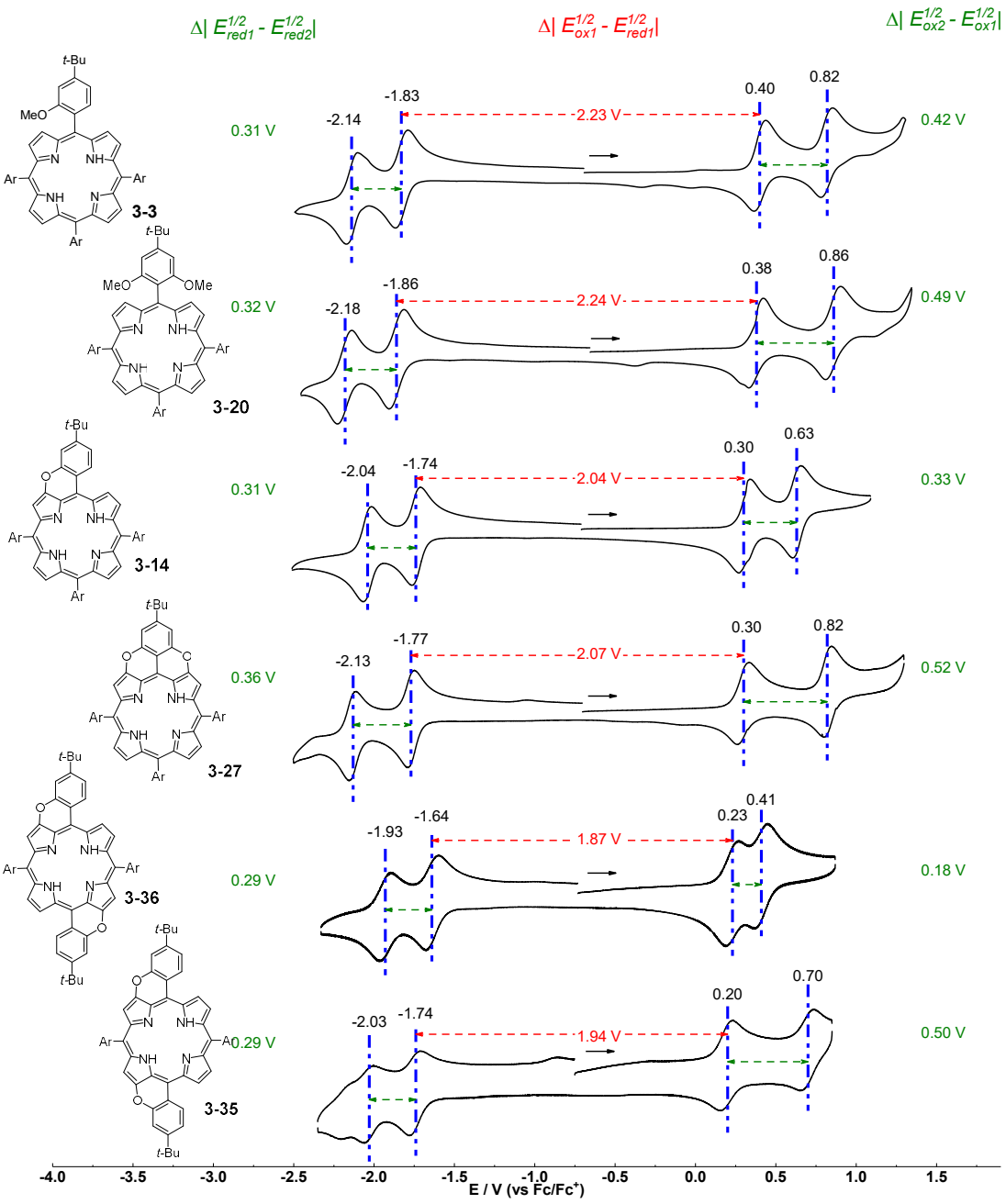

Figure 3.19 Cyclic voltammetry of free-base mono- and di- methoxyporphyrins **3-3** and **3-20**, respectively; mono- and di- pyranoporphyrins **3-14** and **3-27**, **3-35**, **3-36**, respectively, at scan rate100 mV/s in *o*-DCB with 0.1 M of $TBAPF_6$.

3.3.3 DFT calculations

3.3.3.1 Calculations of HOMO-LUMO gap

With the aim of having a deeper understanding of the foregoing experimental data, quantum-based simulations have been carried out. Geometry optimization with further frontier orbital energy calculations of free-base O-embedded porphyrins and reference compound **3-3** have been performed at the B3LYP/6-31* level of theory (Figure 3.20). [171] It should be noted, that due to the presence of NH-tautomerism in the case of mono- and di-pyranoporphyrins **3-14** and **3-36**, respectively, all possible tautomers with the oxygen atom fused at the pyrrole or the azafulvene rings, were accounted.

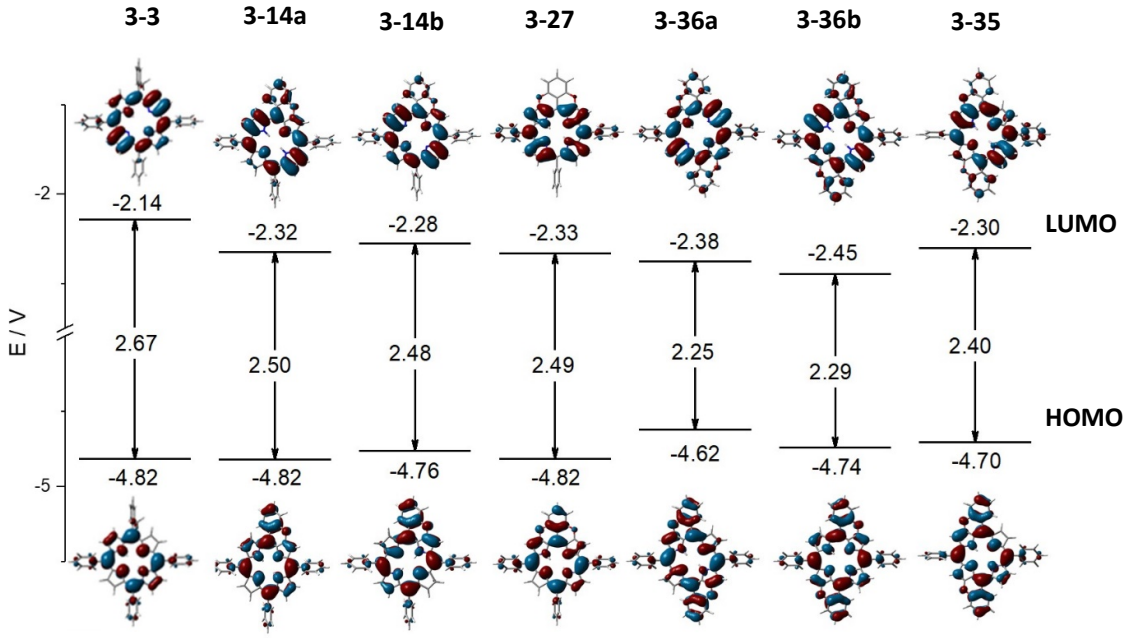

Figure 3.20 Energy diagram and *Kohn-Sham* orbital representation of methoxy- and pyrano- porphyrins, calculated at the B3LYP/6-31* level of theory.

Kohn-Sham representation of the frontier orbitals for all O-fused porphyrins displays the extension of HOMO on the annulated benzopyran rings, while the LUMO density is primarily localized on the porphyrin macrocycle (Figure 3.20). Interestingly, in the case of dipyranoporphyrin **3-27** the introduction of a double O-bridging allows for an extension of the orbitals, but the effect for the LUMO is minimal and the benzopyran rings are not involved in the delocalization of the orbital.

The calculated HOMO-LUMO gap was defined as the difference between the energies of the HOMO and LUMO orbitals in vacuum. It was found, that the calculated values of the HOMO-LUMO gap for all porphyrins are overestimated in the region of 0.4-0.6 V compared to the experimental data. However, the ratio between the values of the HOMO-LUMO gaps of non-fused and O-fused porphyrins is in agreement with as-obtained electrochemical data. Specifically, the HOMO-LUMO gaps of O-annulated porphyrins are narrowed compared to those of non-fused porphyrin. Among studied porphyrins, *trans*-like dipyranoporphyrin **3-36** showed the lowest value of bandgap for both tautomers **3-36a** (2.25 V) and **3-36b** (2.29 V), which is fully coincide with experimental data. It should be also noted that the calculated values of the LUMO energies demonstrate the similar pattern as experimentally obtained $E^{1/2}_{red1}$. Indeed, the LUMO energies of O-fused porphyrins **3-14a,b** (-2.32 V, -2.28 V), **3-27** (-2.33 V) and **3-35** (-2.30 V) are found to be lower than that of non-fused porphyrin **3-3** (-2.14 V) and higher than that of **3-36a,b** (-2.38 V, -2.45 V).On the other hand, the slight HOMO rising effect of O-annulation for **3-35**, **3-14b** and **3-36a,b** was revealed, while the HOMO energies of **3-14a** and **3-27** remained the same as in case of non-fused **3-3**. This was explained by the weak conjugation between the porphyrin macrocycle and the annulated benzopyran ring.

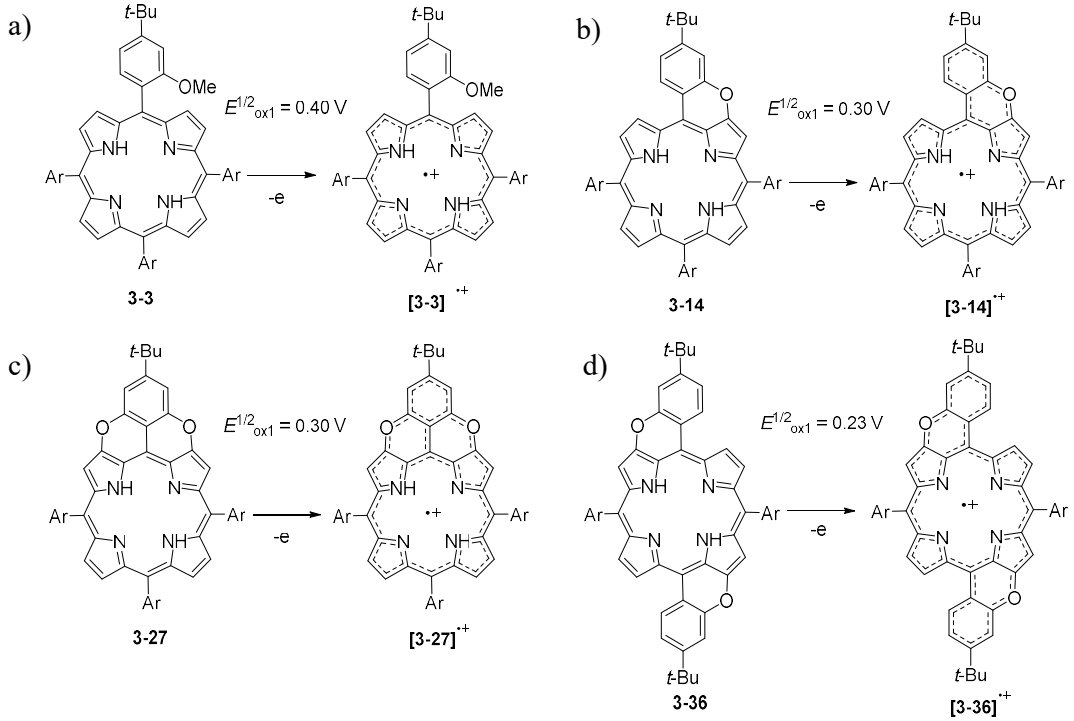

Figure 3.21 Schematic representation of porphyrin radical cation species formed as a result of the first oxidation process of: a) **3-3**; b) **3-14**; c) **3-27**; d) **3-36**.

In contrast to DFT calculations, CV investigations of O-annulated porphyrins revealed the decrease of $E^{1/2}_{ox1}$ compared to non-fused **3-3** by *ca.*100 mV and *ca.* 200 mV in case of **3-14**, **3-27** and **3-35**, **3-36**, respectively. This discrepancy was explained by the inverse correlation of the first oxidation potential with the stability of the oxidized porphyrin species. Furthermore, the stability of radical cation species was found to be dependent on the delocalization of positive charge on the porphyrin macrocycle. Thus, in case of **[3-3]**$^{\bullet+}$ the positive charge is delocalized only on the porphyrin core, while in case of O-annulated **[3-14]**$^{\bullet+}$ the benzopyran ring is also involved in delocalization pathway (Figure 3.21a,b). This leads to the stabilization of positive charge and increasing the stability of **[3-14]**$^{\bullet+}$. In contrast to **[3-14]**$^{\bullet+}$, the delocalization pathway of **[3-27]**$^{\bullet+}$ was extended by the involving of the second oxygen atom. However, $E^{1/2}_{ox1}$ of **3-27** remained the same, indicating that the delocalization of positive charge on *meso*-aryl substituent makes the major contribution to the stability of radical cation species (Figure 3.21c). In case of *trans*-like **[3-36]**$^{\bullet+}$ the delocalization of positive charge was further extended over two benzopyran cycles, resulting in significant decrease of $E^{1/2}_{ox1}$ (Figure 3.21d). Notably, the same behaviour was revealed in case of *cis*-like **[3-35]**$^{\bullet+}$.

In summary, the obtained values of the HOMO-LUMO gap for free-base pyranoporpyrins, determined by the different methods, are reported in Table 3.3. Comparing the values of the optical bandgap for O-fused porphyrins with that for non-fused **3-3**, the insignificant narrowing of optical bandgap was observed, suggesting the limited conjugation effect of O-annulation. On the other hand, the values of electrochemical bandgap for O-fused porphyrins, relating to the stability of the formed charged species, exhibit more pronounced shrinking of the $E^{1/2}_{ox1}$-$E^{1/2}_{red1}$ gap.

Table 3.3 HOMO-LUMO gap values determined by different methods.

Compound	*Optical bandgap (V)*[a]	*Electrochemical bandgap (V)*	*Calculated ΔHOMO-LUMO (V)*
3-3	1.92	2.23	2.67
3-14	1.88	2.04	2.49
3-27	1.86	2.07	2.49
3-36	1.85	1.87	2.27
3-35	1.81	1.94	2.4

[a] Optical bandgap energy was defined as an energy of wavelengths at the crossing point of absorption and emission spectra.

3.3.3.2 NICS and AICD calculations

In light of the obtained electrochemical data, our next step was to elucidate the revealed dependence of $E^{1/2}_{ox2}$ upon the number and position of oxygen bridges. We assumed that the value of second oxidation potentials inversely correlates with the aromaticity of the doubly-oxidized porphyrin species. Specifically, the decrease of aromaticity results in the destabilization of the dication species, leading to an increase of $E^{1/2}_{ox2}$. We proceeded by taking into consideration that macrocyclic aromaticity can be given as a sum of the contributions from all macrocyclic conjugation pathways.[113,172,173] According to *Vogel's* [18]annulene model, the major contribution to macrocyclic aromaticity of porphyrin species comes from the 18π macrocyclic conjugation pathway.[174] At the same time, ring fusion leads to the extension of the π-conjugated framework with the formation of various aromatic and antiaromatic circuits on the fused porphyrins. In order to reveal the additional conjugation pathways arose from O-fusion, the nucleus-independent chemical shift (NICS) computational method was exploited. This method is based on MO calculation of the absolute magnetic shielding at the centre or other points of the aromatic ring and provide NICS values as quantitative criteria of local aromaticity.[175–177] Negative NICS values denote the presence of induced diatropic ring currents and correspond to aromaticity, while positive NICS values indicate paratropic ring currents and match to antiaromaticity. The NICS values depend upon the distance from the plane of the aromatic ring. The calculation of NICS(1) value, which is an average of the point 1 Å above and 1 Å below the center of the aromatic ring, is commonly used in literature. However, due to the non-planar structure of some pyranoporphyrin derivatives, the use of NICS(1) values is limited. Thus, we decided to use NICS(0) computed in plane of rings at characteristic points (namely, at the centres of porphyrin macrocycle, pyrrole, pyran and phenyl rings) as more representative values. All calculations were performed at GIAO-RHF/6-31+G*.

Calculated NICS(0) values for reference monomethoxyporphyrin **3-3** are depicted on Figure 3.22. Accordingly, NICS(0) values at the centres of the neutral porphyrin macrocycle (-12.57 ppm, point 4) and the pyrrole rings (-10.38 ppm, point 3; -10.57 ppm, point 5) are clearly more negative than those at the centres of the azafulvene rings (-1.17 ppm, point 2; -1.63 ppm, point 6), thus suggesting a 18π main macrocyclic conjugation pathway of **3-3**, which is in agreement with the [18]annulene model. Meanwhile, NICS(0) calculations for the doubly oxidized specie exhibit an antiaromatic porphyrin macrocycle (+16.84 ppm, point 4) and non-aromatic pyrrole subunits (+0.75 ppm, point 3; +0.95 ppm, point 5), indicating the

formation of an "internal cross" of an 16π antiaromatic circuit with localization of the positive charges on the nitrogen atoms.

Point	NICS (ppm)	
	0	+2
1	-6.83	-4.09
2	-1.17	-6.17
3	-10.38	+.075
4	-12.57	+16.84
5	-10.53	+0.95
6	-1.63	-4.38

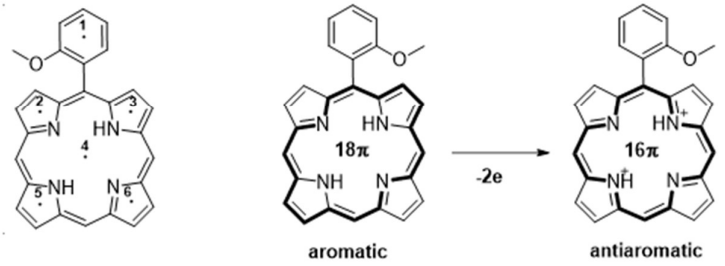

Figure 3.22 Calculated NICS(0) values for the neutral and doubly oxidized monomethoxyporphyrin **3-3** with appropriate aromatic and antiaromatic circuits. *tert*-Butyl groups and *meso*-(4-*tert*-butyl)phenyl substituents are omitted.

To estimate the aromaticity of the O-fused porphyrins, firstly NICS calculations for monopyranoporphyrin **3-14** were performed (Figure 3.23). Since the oxygen atom can be attached either to the pyrrole or the azafulvene rings, two structural isomers of **3-14** were considered. Similarly to reference compound **3-3**, the aromaticity of neutral porphyrin macrocycle both for **3-14a** (structure I) and **3-14b** (structure V) comes from an 18π electron circuit. Indeed, NICS(0) values computed at the centers of pyran rings for **3-14a** (+2.21 ppm, point 7) and **3-14b** (-0.07 ppm, point 7) are more positive than those calculated for the porphyrin cycle, suggesting insignificant contribution of **3-14a** to the global aromaticity. Comparing NICS(0) values at the point 2 for structures **3-14a** (-3.85 ppm) and **3-14b** (-10.13 ppm), the azafulvene ring of the latter is more aromatic than that of the former owing to the donation of electron lone pair by the oxygen atom in case of **3-14b**. Accordingly, resonance structure IV with a local 14π aromatic circuit can be considered. Computations for doubly oxidized species of **3-14a** and **3-14b** revealed a paratropic ring current, highlighting a significant contribution of 16π antiaromatic circuits (structures III and VII). However, NICS(0) value at the point 4 for **3-14a** (+14.87 ppm) is lower than that for reference dication specie **3-3** (+16.84 ppm), while NICS(0) computed for **3-14b** (+19.96 ppm, point 4) is higher than in the case of the latter, demonstrating the contribution of additional conjugation circuits. Meanwhile, negative NICS(0) values at the pyran rings of **3-14a** (-6.66 ppm, point 7) and **3-14b** (-3.00 ppm, point 7) suggest the localization of positive charge on the oxygen atom with the formation of an aromatic pyrylium cation. Thus, resonance structures II and VII for **3-14a** and **3-14b**, respectively, with additional O-involving circuits can be drawn

(Figure 3.23c,d). Hence, the emerged aromatic 14π pathway decreased the antiaromaticity of doubly-oxidized **3-14a**, while antiaromatic 24π circuit increased the antiaromaticity of dication **3-14b**. In this way, the global aromaticity of the dications is perturbed in a different manner depending on the position of the O-fusion.

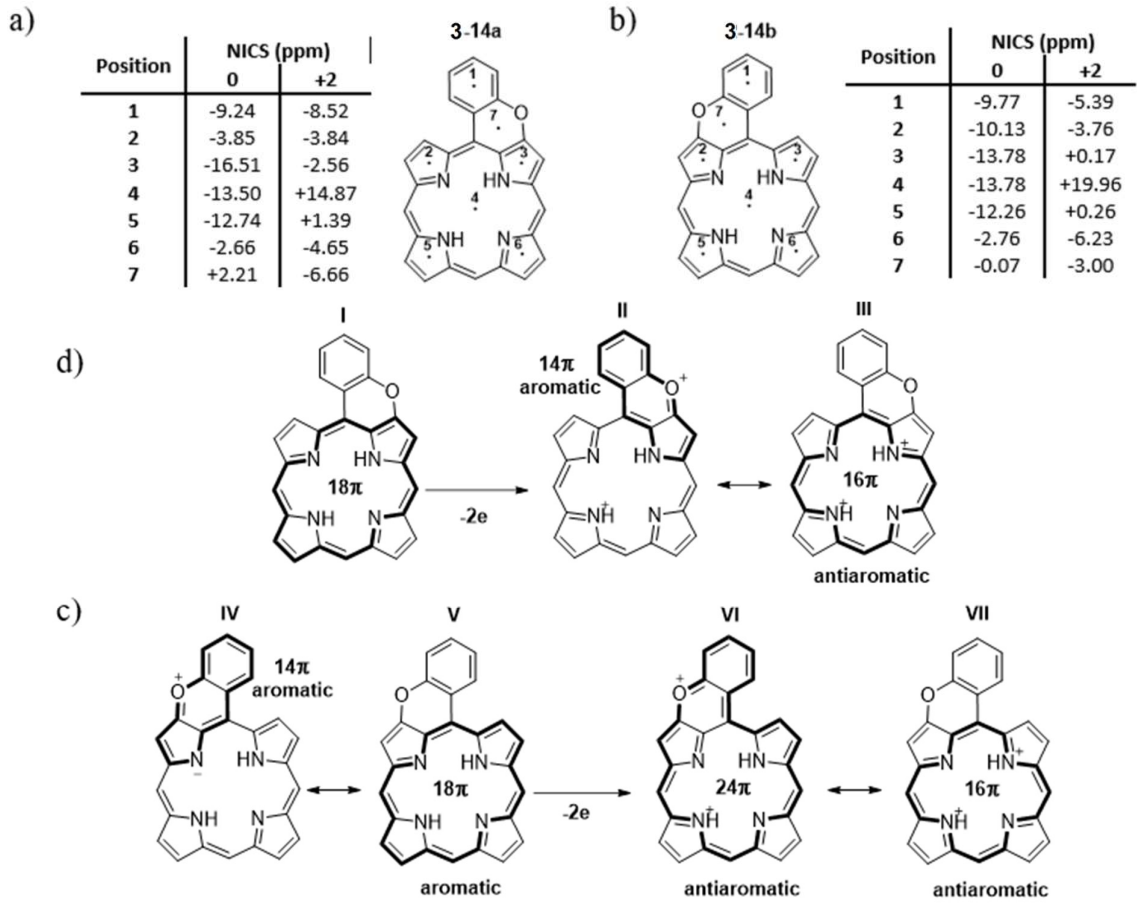

Figure 3.23 Calculated NICS(0) values for the neutral and doubly oxidized: a) monopyranoporphyrin **3-14a**; b) monopyranoporphyrin **3-14b**. Resonance structures with aromatic and antiaromatic circuits for: c) monopyranoporphyrin **3-14a**; d) monopyranoporphyrin **3-14b**. *tert*-Butyl groups and *meso*-(4-*tert*-butyl)phenyl substituents are omitted.

In contrast to monopyranoporphyrin **3-14,** dipyranoporphyrins **3-27** and **3-35** bear two oxygen bridges attached both to the azafulvene and the pyrrole subunit. Thus, the global aromaticity of the porphyrin dication species should be determined by the superposition of aromatic 14π, antiaromatic 24π and 16π conjugated circuits (Figure 3.24). According to the calculations, the NICS(0) value at the center of the porphyrin macrocycle for doubly oxidized **3-27** (+22.48 ppm, point 4) is more positive than that for dication **3-35**

(+16.88 ppm, point 4). In order to understand this tendency, we decided to compare the DFT optimized geometry of the dipyranoporphyrin dications (Figure 3.25). In contrast to the distorted geometry of *cis*- and *trans*-like dications **3-35** and **3-36**, respectively, dication **3-27** exhibits planar structure, favouring the delocalization of the positive charge and the contribution of an antiaromatic 24π circuit (structure II) to the global aromaticity of **3-27**. On the other hand, the distorted geometry of **3-35** diminishes the contribution of antiaromatic 24π circuit (structure VIII), and so the aromaticity of **3-35** is determined mainly by antiaromatic16π circuit (structure VI).

a)

Position	NICS (ppm) 0	+2
1	-11.13	-3.30
2	-9.45	-0.95
3	-16.13	+0.49
4	-13.99	+22.48
5	-12.55	+0.97
6	-3.13	-5.68
7	+4.27	-7.48
8	+1.38	+0.74

b)

Position	NICS (ppm) 0	+2
1	-9.29	-8.05
2	-3.77	-7.47
3	-15.60	-1.79
4	-12.38	+16.88
5	-13.66	-2.96
6	-9.67	-2.04
7	-9.85	-4.76
8	+1.79	-5.52
9	-0.59	-0.56

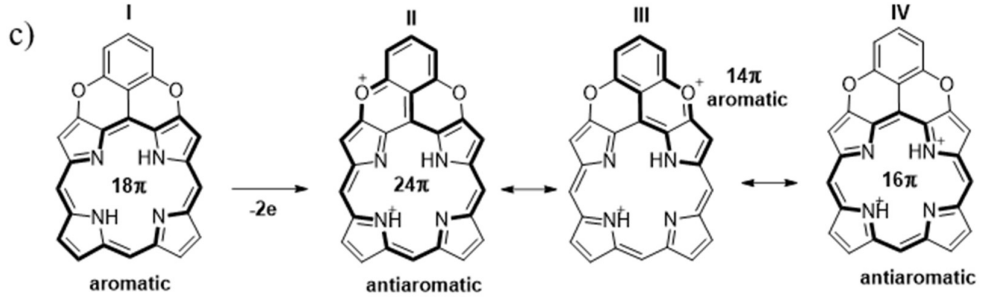

Figure 3.24 Calculated NICS(0) values for the neutral and doubly oxidized: a) dipyranoporphyrin **3-27**; b) *cis*-like dipyranoporphyrin **3-35**. Resonance structures with aromatic and antiaromatic circuits for: c) dipyranoporphyrin **3-27**; d) *cis*-like dipyranoporphyrin **3-35**. *tert*-Butyl groups and *meso*-(4-*tert*-butyl)phenyl substituents are omitted.

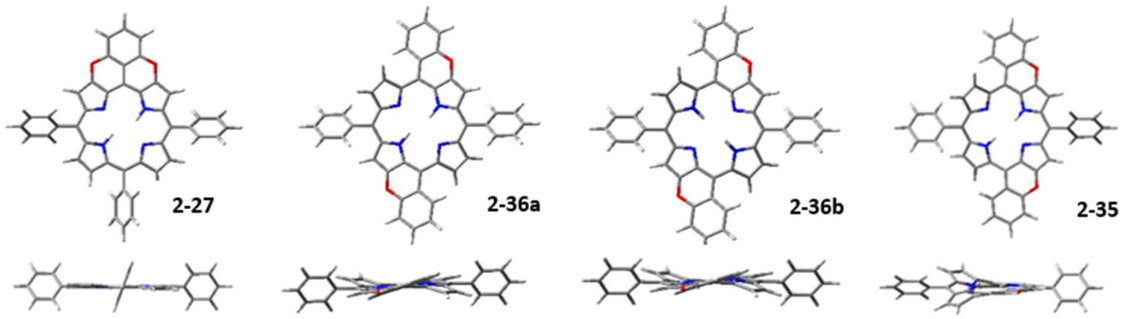

Figure 3.25 DFT geometry optimization of free-base dipyranoporphyrin dications (top view and side view).

Similarly to monopyranoporphyrin **3-14**, two structural isomers of *trans*-like dipyranoporphyrin **3-36** were considered (Figure 3.26). In both cases, two oxygen atoms are attached either to the pyrrole or the azafulvene rings. NICS(0) calculations for dication **3-36a** (+10.60 ppm, point 4; -6.42 ppm, points 8 and 9) revealed the large contribution of two aromatic 14π circuits (structure II). Meanwhile, NICS(0) values computed for dication **3-36b** (+16.43 ppm, point 4; -3.59 ppm, points 8 and 9) indicated the formation of an antiaromatic 32π circuit (structure V). However, the distorted geometry of **3-36b** weakened the contribution of the latter to the overall electronic structure.

a)

Position	NICS (ppm) 0	+2
1	-9.10	-9.17
2	-3.59	-3.65
3	-16.51	-5.42
4	-13.24	+10.60
5	-16.50	-5.42
6	-3.59	-3.65
7	-9.10	-9.17
8	+2.59	-6.42
9	+2.59	-6.42

b)

Position	NICS (ppm) 0	+2
1	-9.62	-6.48
2	-9.95	-4.87
3	-13.42	-1.80
4	-13.78	+16.43
5	-13.42	-1.80
6	-9.95	-4.87
7	-9.62	-6.48
8	+0.22	-3.59
9	+0.22	-3.59

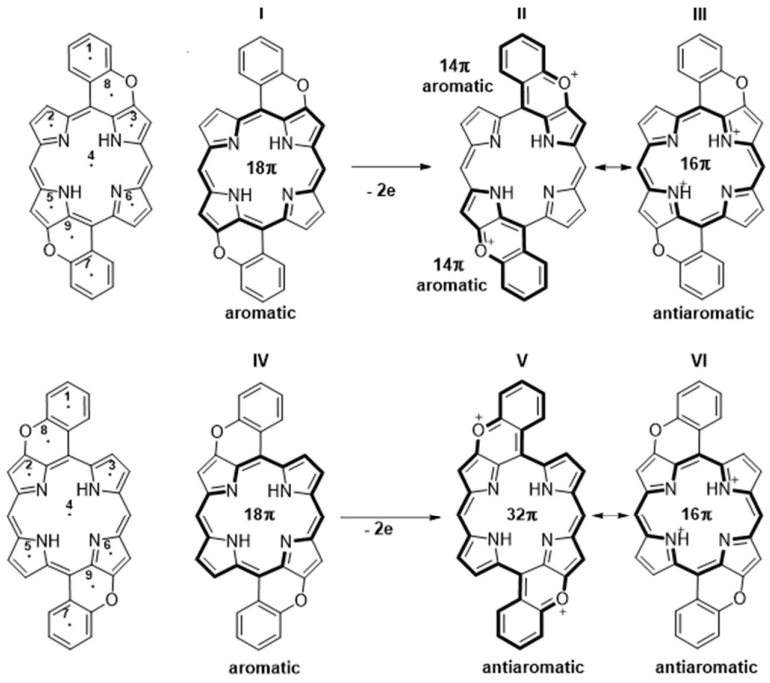

Figure 3.26 Calculated NICS(0) values for the neutral and doubly oxidized *trans*-like dipyranoporphyrin tautomers with appropriate aromatic and antiaromatic circuits: a) **3-36a**; b) **3-36b**. *tert*-Butyl groups and *meso*-(4-*tert*-butyl)phenyl substituents are omitted.

To visualize the induced delocalization of π electrons, we calculated the anisotropy of the induced current density (AICD), which represents the three-dimensional delocalized electron density with a scalar field and illustrates the paramagnetic term of the induced current density.[178,179] Aromatic molecules show clockwise current density, while antiaromatic species display counterclockwise current density.

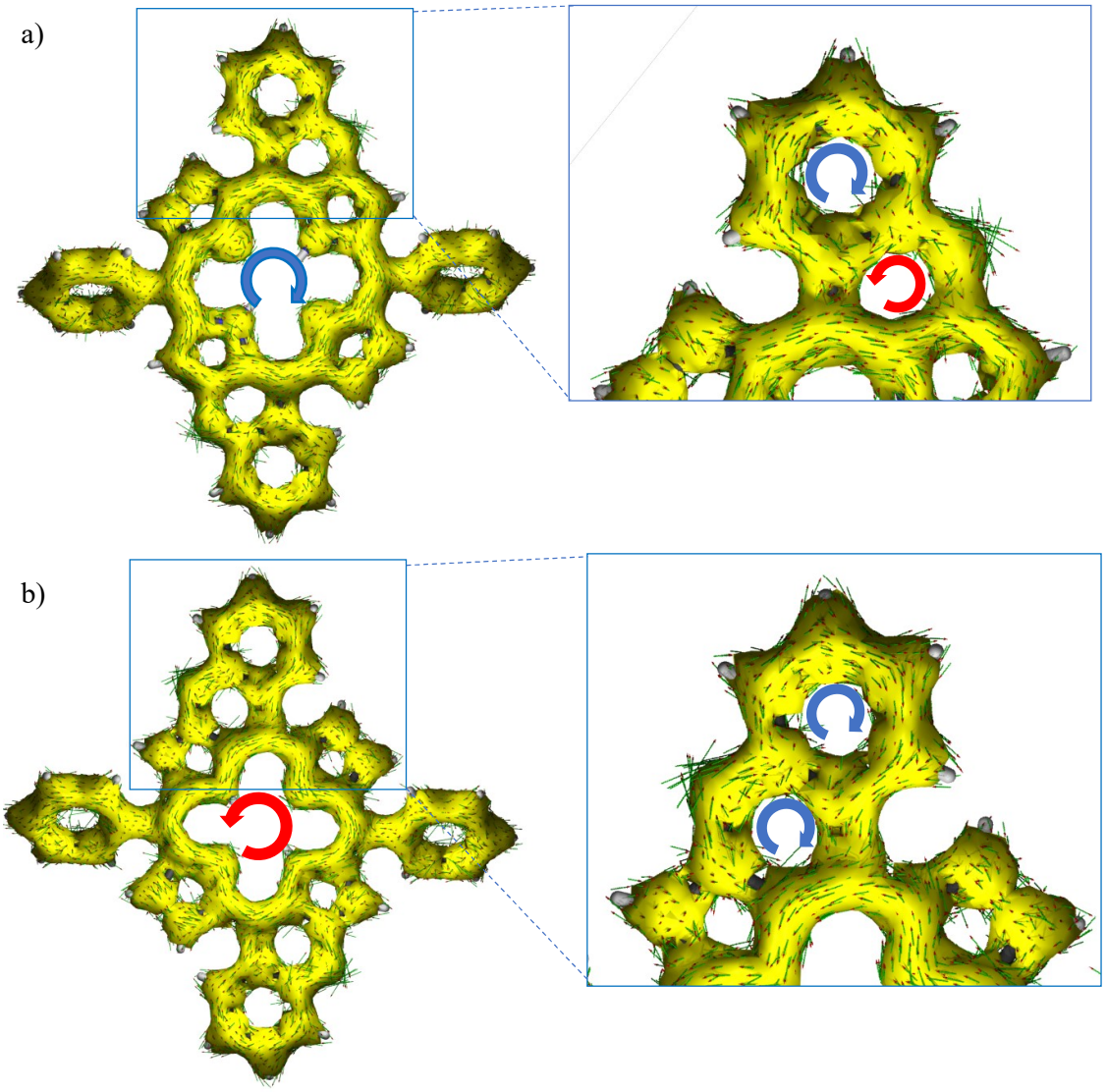

Figure 3.27 AICD plots of dipyranoporphyrin **3-36a**: a) neutral specie; b) dication specie. Aromatic clockwise current density – blue arrow, antiaromatic counterclockwise current density – red arrow.

In our study, AICD plots computed for free-base O-fused porphyrins are fully coincide with NICS(0) calculations (all examples are reported in Appendix), by showing the major contribution of 18π aromatic circuit (for neutral species) or 16π antiaromatic circuit

(for dication species) in global aromaticity. For instance, AICD plot of neutral **3-36a** presents strong aromatic clockwise current density along porphyrin macrocycle, indicating the 18π main macrocyclic conjugation pathway (Figure 3.27a). In addition, calculations of local currents reveal the aromatic character of fused *meso*-aryl substituents and antiaromatic behaviour of fused pyran rings. Meanwhile, in the case of dication **3-36a** strong antiaromatic counterclockwise current density along the porphyrin macrocycle was observed, suggesting a significant contribution of an "internal cross" of a 16π antiaromatic circuit (Figure 3.27b). On the contrary to the neutral specie, dication **3-36a** displays a local aromatic 14π circuit along the benzopyran ring.

3.3.4 Titration with BAHAf

Since O-annulation led to the electron saturation of the porphyrin heterocycle, we decided to examine the ability of as-prepared free-base pyranoporphyrins to form radical cation and dication species. To achieve this, monitoring of the UV-vis spectral changes upon the oxidative titration in CH_2Cl_2 was carried out. As an oxidant, *tris*(4-bromophenyl)aminium hexafluoroantimonate (BAHAf) **3-40** was chosen due to its appropriate oxidation potential (E_{ox} = 0.7 V).

Oxidant **3-40** was synthesized by the addition of 1 eq. *tris*(4-bromophenyl)amine **3-38**, dissolved in CH_2Cl_2, to a solution of nitrosonium hexafluoroantimonate **3-39** in MeCN at rt (Scheme 3.17). The reaction mixture immediately turned to deep blue and was poured into cold diethyl ether. Subsequent filtration of the mixture afforded BAHAf in 52% yield. The freshly prepared oxidant was dissolved in dry CH_2Cl_2, giving a solution with definite concentration, immediately used for titration.

Scheme 3.17 Synthesis of oxidant BAHAf **3-40**.

Hence, oxidation of free-base monopyranoporphyrin **3-14** with BAHAf was carried out (Figure 3.28). Upon addition of the oxidant (1 eq.), the intensity of *Soret* band at 435 nm was decreased, while Q bands were replaced by a structured band system with a maximum at around 658 nm. This was attributed to the formation of radical cation specie **[3-14]$^{\bullet+}$.** Upon addition of a second equivalent, a broad absorption spectrum with ill-define Q band at 700 nm and slight bathochromic shift of *Soret* band from 435 nm to 452 nm was observed. In both cases, isosbestic points were ill-defined, indicating that porphyrin cation radicals undergo proton transfer reaction to yield deprotonated porphyrin dications.

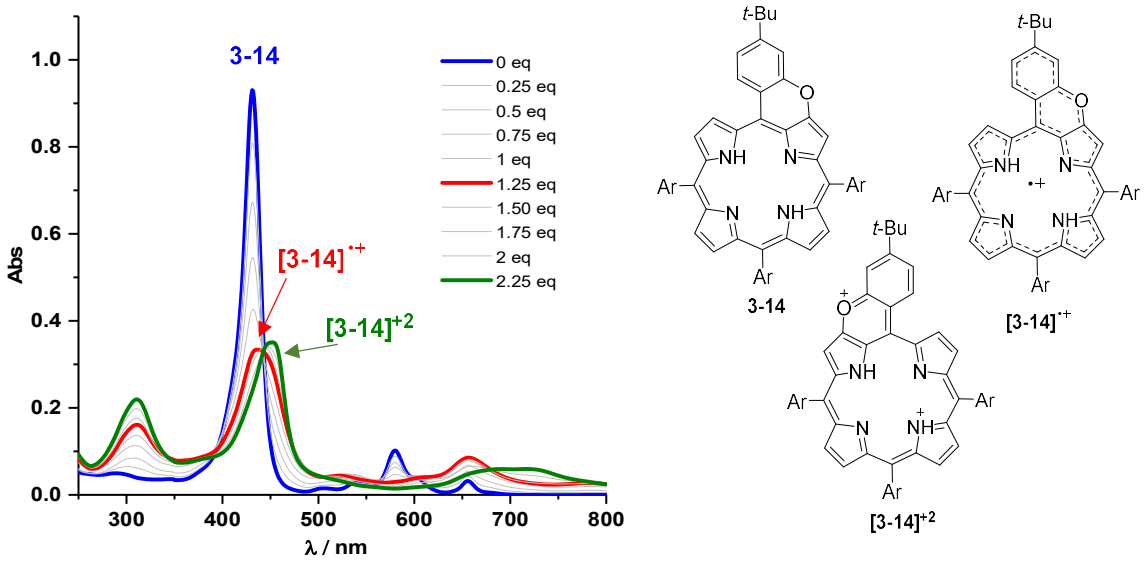

Figure 3.28 Oxidative titration of monopyranoporphyrin **3-14** with BAHAf in CH_2Cl_2 at rt. Chemical structures represent neutral **3-14**, radical cation **[3-14]$^{\bullet+}$** and dication **[3-14]$^{+2}$** porphyrin species.

Regarding the oxidative titration of *trans*-like dipyranoporphyrin **3-36** with BAHAf, UV-vis spectra display well defined two-step oxidation process (Figure 3.29). The first oxidation resulted in splitting of *Soret* band and reaching of Q band system with maximum at 900 nm, thus suggesting the formation of radical cation **[3-36]$^{\bullet+}$** stabilized by delocalization of spin density throughout the whole conjugation system. After the addition of a second equivalent, the absorption spectrum changed significantly by pronounced blue-shifting of maximum absorption from 900 to 600 nm. This observation was assigned to the formation of porphyrin dication specie **[3-36]$^{+2}$**.

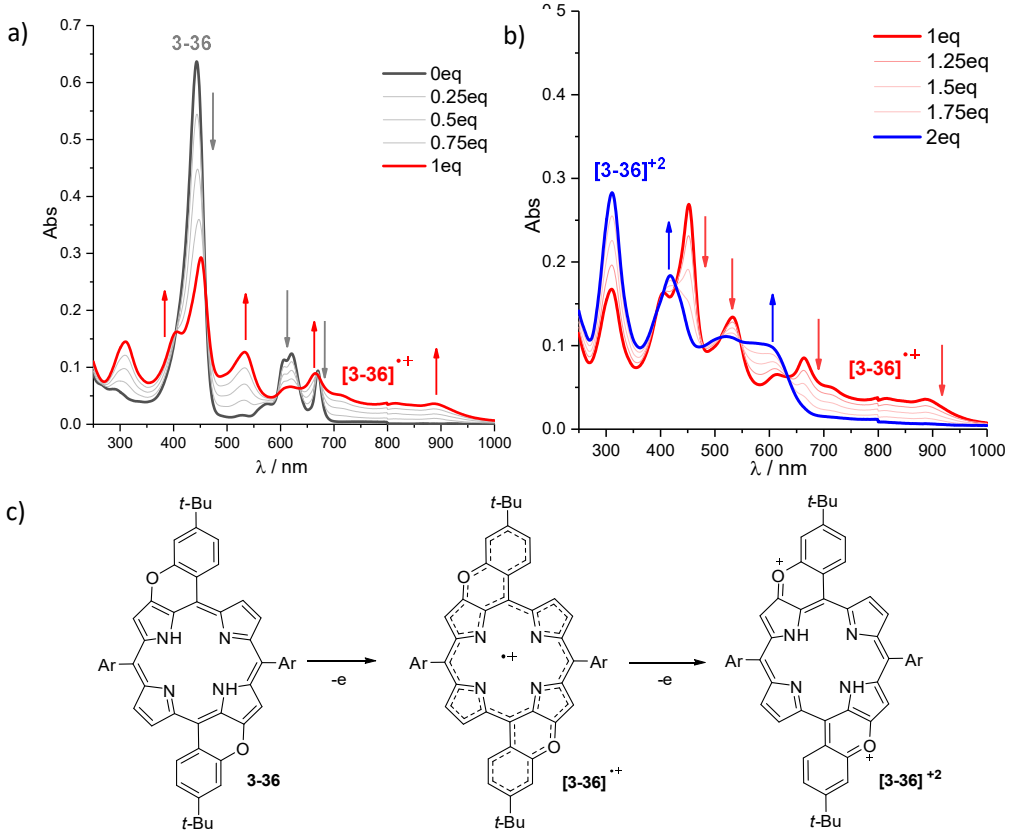

Figure 3.29 Oxidative titration of dipyranoporphyrin **3-36** with BAHAf in CH_2Cl_2 at rt: a) upon addition of 1eq. of BAHAf; b) upon addition of 2 eq. of BAHAf. c) Schematic representation of **3-36** oxidation processes.

The titration of dipyranoporphyrins **3-27** and **3-35** with BAHAf is shown in Figure 3.30. Upon addition of 1 eq. of BAHAf, the bathochromic shift of maximum absorption from 660 to 780 nm and from 680 to 800 nm for **3-27** and **3-35**, respectively, was observed. This phenomenon was associated with the formation of highly conjugated radical cations **[3-27]**$^{\bullet+}$ and **[3-35]**$^{\bullet+}$, similarly to the case of porphyrin **3-36**. Interestingly, in contrast to **3-35** UV-vis spectrum of dipyranoporphyrin **3-27** displays the splitting of *Soret* band after oxidation. As was expected, the addition of a second equivalent of BAHAf did not change the absorption profile. Indeed, the oxidation potential of BAHAf (0.7 V) is lower than the second oxidation potentials of **3-27** (0.82 V) and **3-35** (0.7 V), suggesting that BAHAf is not a strong enough oxidant to carry out the second oxidation process.

To conclude, upon addition of BAHAf (1 eq.) the formation of radical cation species for all O-annulated porphyrins was revealed, while after the addition of 2 eq. of BAHAf the dication species only in case of **3-14** and **3-27** were formed. These findings fully coincide with the obtained electrochemical data.

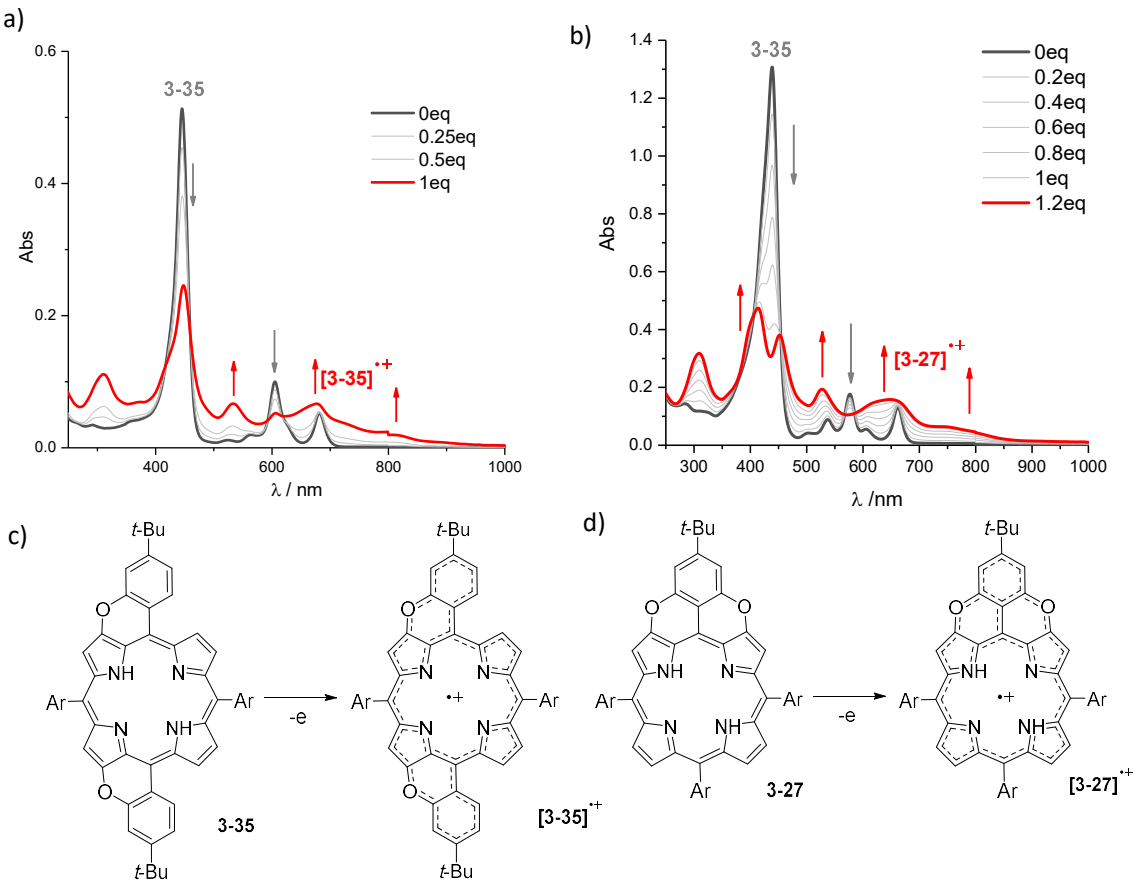

Figure 3.30 Oxidative titration of dipyranoporphyrins: a) **3-35**: b) **3-27**. Schematic illustrations of oxidation processes for: c) **3-35**; d) **3-27**.

3.4 Conclusions

This chapter mainly addressed the design and synthesis of novel π-extended porphyrin-based systems. The chosen strategy is based on an intramolecular oxidative C-O coupling reaction to yield oxygen-embedded porphyrin macrocycles. In the first section, a simple and efficient protocol for CuO-mediated diaryl-ether bond formation was successively developed. Furthermore, various metal and free-base monopyranoporphyrins were synthesized and thoroughly investigated. Subsequently, the synthesis of dipyranoporphyrins was carried out, confirming the successful implementation of the formerly developed protocol. It should be noted that pyran annulation of dihydroxyporphyrin **3-29** yielded the inseparable mixture of pyranoporphyrin isomers possessing the similar polarity. The successive separation was accomplished after the demetallation of obtained isomers, thus

affording free-base *cis*- and *trans*-like dipyranoporphyrins **3-35** and **3-36**. The formation of O-fused porphyrins was proved by ^{1}H- and ^{13}C-NMR, IR, UV-vis spectroscopy and HRMS measurements. In addition, the chemical structures of mono- **3-1**, **3-14** and di- **3-16**, **3-36** pyranoporphyrins undoubtedly confirmed by X-ray analysis.

The last section of this chapter was focused on the physicochemical investigation of as-prepared mono- and di- pyranoporphyrins. UV-vis spectroscopy revealed a slight bathochromic shift of absorption maxima for all O-fused porphyrins compared to non-fused analogues, suggesting a weak conjugation between the porphyrin core and the co-planarized *meso*-aryl groups. Hence, by varying the number and the position of O-bridges along the series of mono- and di- pyranoporphyrins the negligible changes of the optical bandgap were observed. On the other hand, the cyclic voltammograms of O-embedded porphyrins showed the pronounced narrowing of the electrochemical HOMO-LUMO bandgap ($E^{1/2}_{ox1}$-$E^{1/2}_{red1}$). This was explained by the inverse correlation of $E^{1/2}_{ox1}$ with the stability of radical cation species, formed upon the first oxidation process. Specifically, the extension of the positive charge delocalization on the *meso*-aryl substituents and the oxygen atoms of O-fused porphyrins leads to the stabilization of radical cations and the decrease of $E^{1/2}_{ox1}$. Moreover, CV investigation revealed the relationship between the second oxidation potential ($E^{1/2}_{ox2}$) and the number and the position of O-bridges. In particular, $E^{1/2}_{ox2}$ inversely correlates with the antiaromaticity of porphyrin dication species, formed upon the second oxidation process. It was found that the major contribution in the global antiaromaticity of all O-fused porphyrin dications is given by 16π antiaromatic circuit. Meanwhile, the additional aromatic and antiaromatic circuits were also considered. Thus, O-annulation with the pyrrole subunit decreases the antiaromatic character of the dication through the realization of additional aromatic 14π circuit. On the other hand, O-fusion with the azafulvene subunit results in the emerging of antiaromatic 24π conjugation pathway, which increases the antiaromatic character of porphyrin dications. In contrast to monopyranoporphyrin dication, the global antiaromaticity of dipyranoporphyrin dication is determined by the superposition of aromatic 14π, antiaromatic 24π and 16π conjugated circuits.

4. Tetra- and octa- pyranoporphyrins

As an extension of our work and in order to validate and examine the potential of the developed CuO-mediated pyran annulation protocol, our investigation was then focused on the synthesis of tetra- and octa- pyranoporphyrins. In this regard, the present chapter is divided in three sections: *i) section 4.1* deals with the synthesis and characterization of tetrapyranoporphyrins, where the *ortho*-positions of the *meso*-aryl substituents are interconnected with the β-pyrrolic positions through four O-bridges*; ii) section 4.2* focuses on the synthesis and investigation of full-conjugated octapyranoporphyrins with embedded eight oxygen atoms; and *iii) section 4.3* includes the conclusions based on received results.

DFT geometry optimization and IR simulations presented in this chapter were performed by *Dr. Claudio Quarti* (Université de Mons, Belgium); MASS-MALDI investigation was done by *Dr. Julien De Winter* (Université de Mons, Belgium); EPR analyses were done by *Dr. Andrea Folli* (Cardiff University, UK).

4.1 Synthesis and characterization of tetrapyranoporphyrins

In this section, our main goal is to increase the number of pyran rings fused to the porphyrin core to four, leading to two possible types of tetrapyranoporphyrin isomers as outlined in Figure 4.1. The first type of isomers, in which the *meso*-aryl substituents are connected to the porphyrin core through only one O-bridge, can be represented by four different regioisomers **4-1a-d**. On the other hand, when the *meso*-aryl substituents in positions 5 and 15 are interconnected with the porphyrin core through two O-bridges, regioisomer **4-2** can be drawn. In the case of **4-1a-d**, where all the *meso*-aryl substituents are co-planarized with the porphyrin core, a more pronounced extension of the π-conjugation is expected than for **4-2**, where only two *meso*-aryl groups are fused to the porphyrin. Meanwhile, isomer **4-2** is believed to have a more electron saturated structure compared to **4-1a-d** due to the delocalization of the lone pair of electrons of the four oxygen atoms within the porphyrin core and two *meso*-aryl groups.

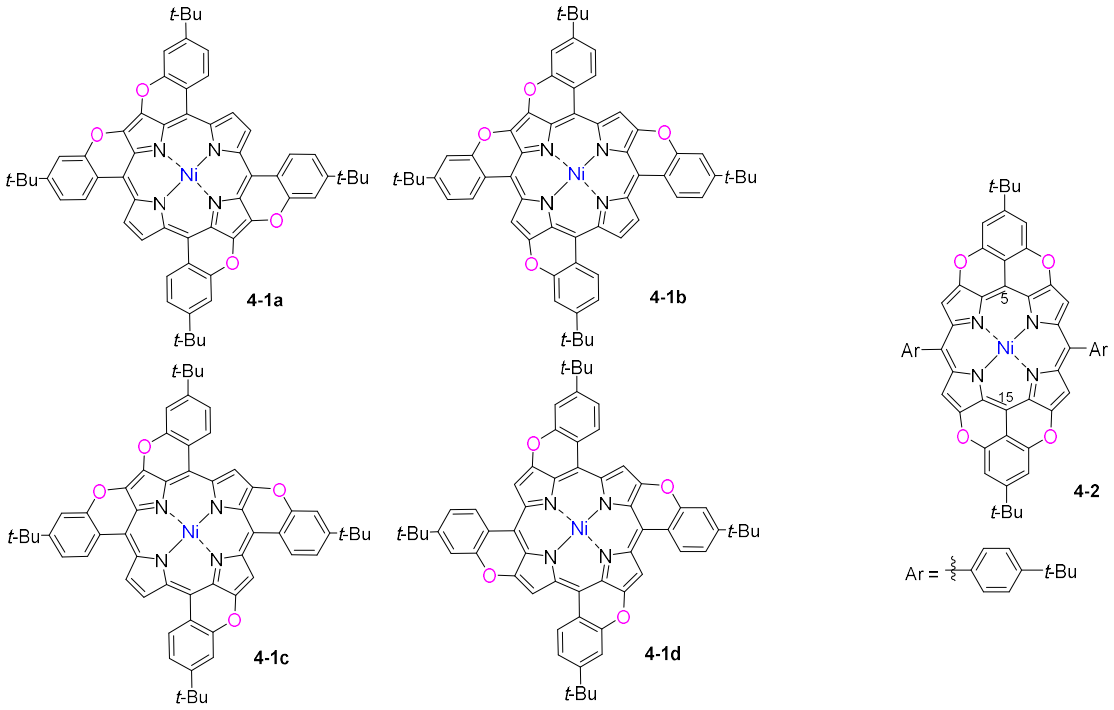

Figure 4.1 Chemical structures of tetrapyranoporphyrin regioisomers **4-1a-d** and **4-2**.

4.1.1 Tetrapyranoporphyrins 4-1a-d

The retrosynthetic analysis of **4-1a-d** shows that the disconnection of the C-O bonds in all cases leads to the same starting compound, namely Ni(II) tetrahydroxyporphyrin **4-3** (Scheme 4.1). Further retrosynthesis for the preparation of **4-3** follows the same strategy, which has been successfully applied in Chapter III. In particular, this would involve the reaction of pyrrole with methoxybenzaldehyde under classical *Lindsey's* condition to form tetramethoxyporphyrin **4-4**, which after demethylation and metallation should provide the corresponding porphyrin **4-3**. Finally, pyran annulation of **4-3** promoted by CuO, should afford a mixture of desired isomers **4-1a-d**.

In order to predict the ratio of formation between the four possible regioisomers **4-1a-d**, we postulated that the formation of the first O-bridge between the *meso*-aryl group and the β-pyrrolic position of the porphyrin core determines the direction of the next O-fusion reaction. In particular, the presence of the O-bridge disfavours the subsequent O-annulation to the adjacent β´-pyrrolic position, thus promoting the fusion of the pyran ring to an alternative pyrrole unit. Apparently, upon the CuO-mediated oxidation of porphyrin **I**, radical cation specie **II**, stabilized by resonance structure **III** with 10π aromatic circuit, is formed (Scheme 4.2). In this way, the localization of the positive charge on the benzopyrylium

fragment (structure **III**) should decrease the electrophilicity of the adjacent β´-pyrrolic position, thus favouring the formation of structure **IV**. Therefore, isomer **4-1d** is expected to be the major product during the pyran annulation reaction.

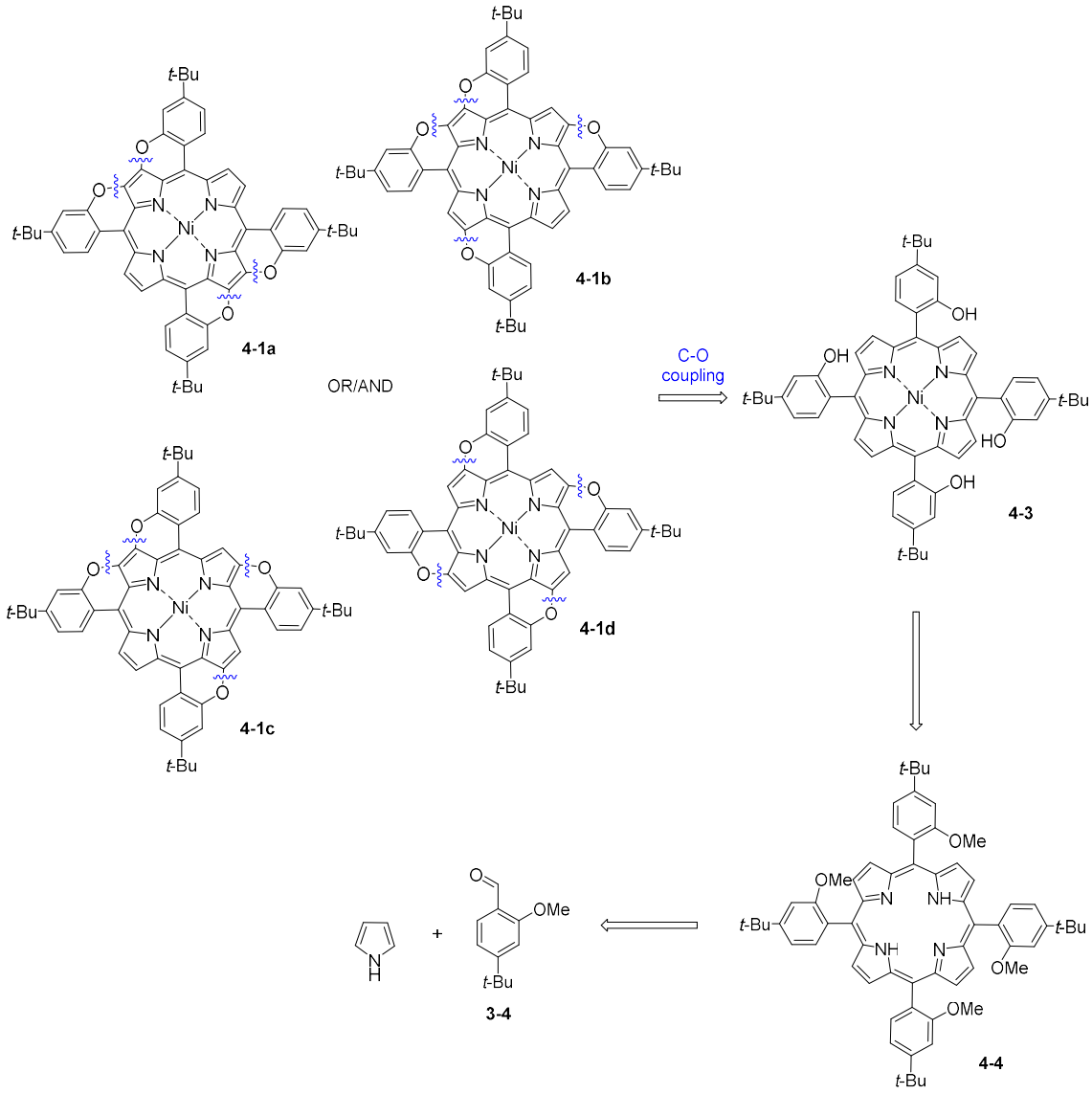

Scheme 4.1 Retrosynthesis of tetrapyranoporphyrins **4-1a-d**.

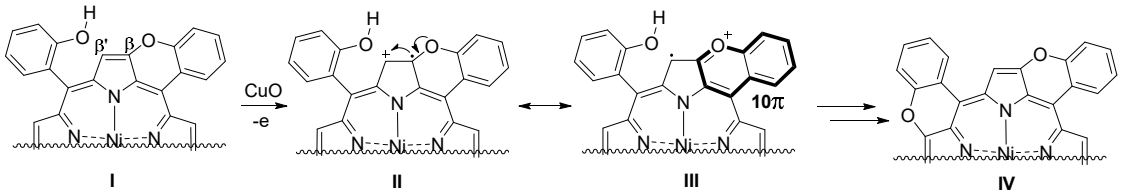

Scheme 4.2 Schematic illustration of the relationship between the structure and the direction of O-fusion.

In order to determine the thermodynamically stable isomer among **4-1a-d**, DFT geometry optimization and calculation of the relative energies were performed at the B3LYP/6-31G* level of theory. DFT optimized structures of **4-1a-d** are presented by ruffled conformation, as shown in Figure 4.2. This finding coincides well with literature, thus indicating that Ni(II) favours a nonplanar conformation of the porphyrin core, enabling shorter metal-nitrogen distances and better overlapping of the Ni *d*-orbitals with the π-system of the porphyrin. In addition, the presence of doubly O-fused pyrrole fragments (Figure 4.2, in blue circle) with nearly planar conformation as in the case of **4-1a-c** causes an increase in relative energies by *ca.* 6 kcal/mol per each dipyranopyrrole unit. However, this phenomenon is not observed for isomer **4-1d**, where only singly O-fused pyrrole units are presented. The lower relative energy of **4-1d** compared to the relative energies of other isomers suggests the thermodynamic stability of **4-1d**, thus favouring its formation upon CuO-promoted pyran annulation reaction.

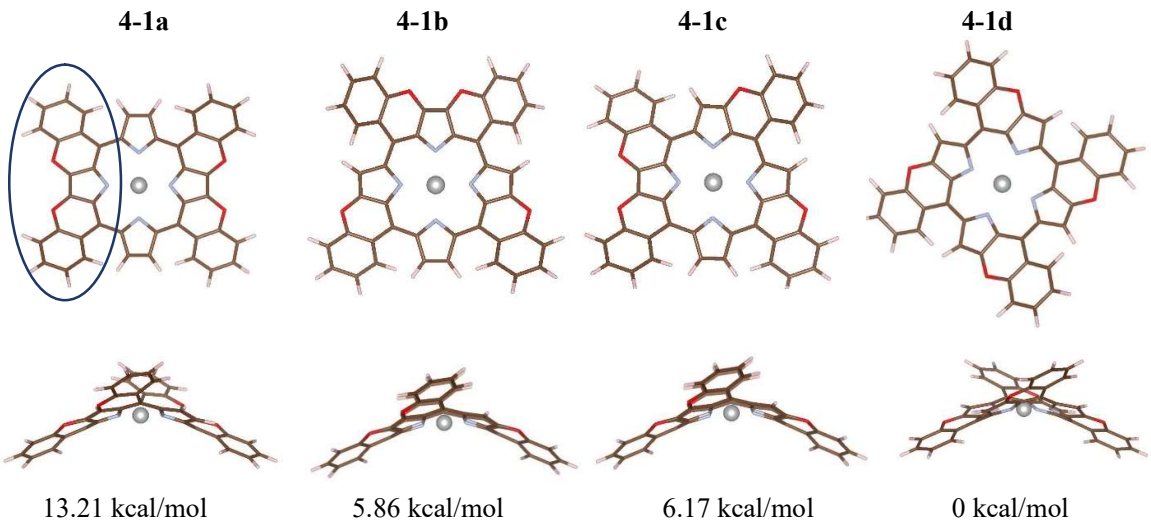

Figure 4.2 DFT optimized structures of isomers **4-1a-d** (top and side views) and its relative energies (kcal/mol), using **4-1d** as a benchmark.

*4.1.1.1 Synthesis of tetrapyranoporphyrin **4-1d***

On the way to tetrahydroxyporphyrin **4-3** (Scheme 4.3), the as-prepared methoxy-benzaldehyde **3-4** (Chapter III) was reacted with pyrrole in the presence of $BF_3{\cdot}Et_2O$ according to the typical *Lindsey's* procedure, giving tetramethoxyporphyrin **4-4** in 13% yield. A successive cleavage of the methoxy substituents by BBr_3 afforded **4-5** as a purple powder

in 96% yield. Subsequent metallation of **4-5** with $Ni(acac)_2$ led to desired Ni(II) tetrahydroxyporphyrin **4-3** in 95% yield.

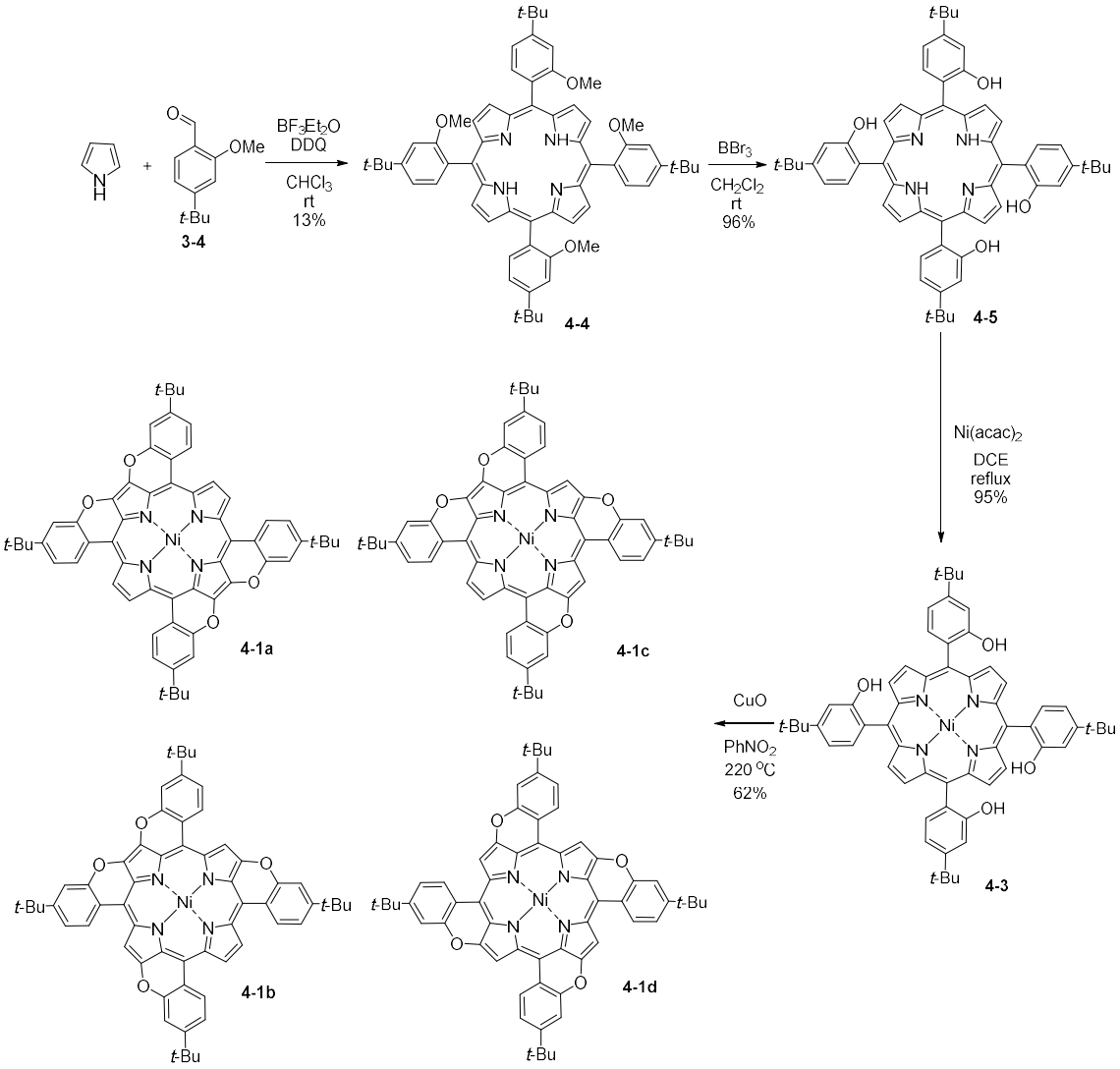

Scheme 4.3 Synthesis of Ni(II) tetrapyranoporphyrins **4-1a-d**.

The chemical structures of all intermediates were proved by ESI-HRMS, ^{1}H and ^{13}C NMR, UV-vis and IR spectroscopy (Chapter VI). To give an example, the ^{1}H NMR-spectrum of **4-3** is characterized by a singlet (8.84 ppm) relating to the 8H of the pyrrole rings (H_a), two multiplets between 7.79-7.58 ppm and 7.27-7.34 ppm given by the 12H of the *meso*-hydroxyaryl groups ($H_{b,c,d}$) and two singlets at 4.86 and 1.54 ppm for the hydrogen atoms on the OH- and *t*-Bu-groups, respectively (Figure 4.3). The chemical structure of **4-3**

was unambiguously confirmed by ESI-HRMS through detection of the peak corresponding to the molecular ion at m/z 959.4059 (M^+, $[C_{60}H_{61}N_4NiO_4^+]$, calc.: 959.4046).

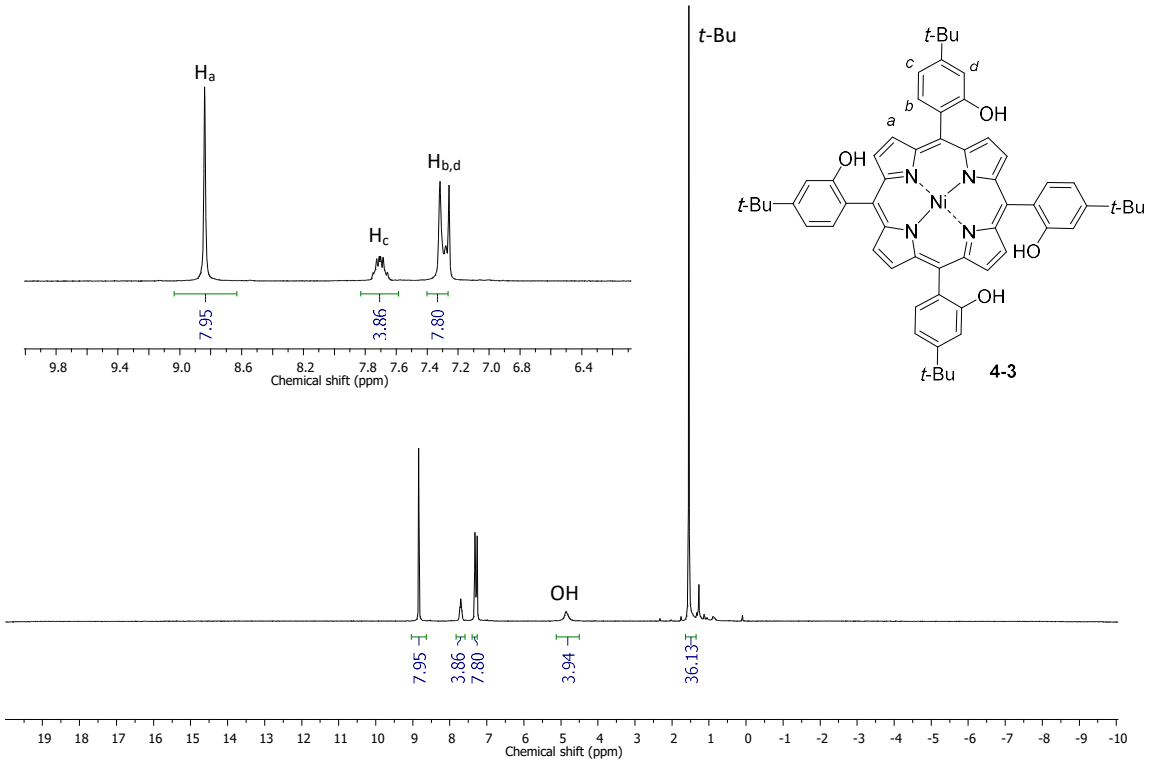

Figure 4.3 ^{1}H NMR-spectrum of tetrahydroxyporphyrin **4-3** (300 MHz, $CDCl_3$).

Subsequently, **4-3** was refluxed with 20 eq. of CuO in $PhNO_2$ at 220 ºC until the complete consumption of starting material was noted by TLC (Scheme 4.3). The crude material was purified by silica gel flash-chromatography (eluent: CH_2Cl_2/Py 9:1) affording a green solid. Unfortunately, the recorded NMR spectra presented broad peaks in the aromatic area around 6.5-7.75 ppm with no conceivable analysis (Figure 4.4).

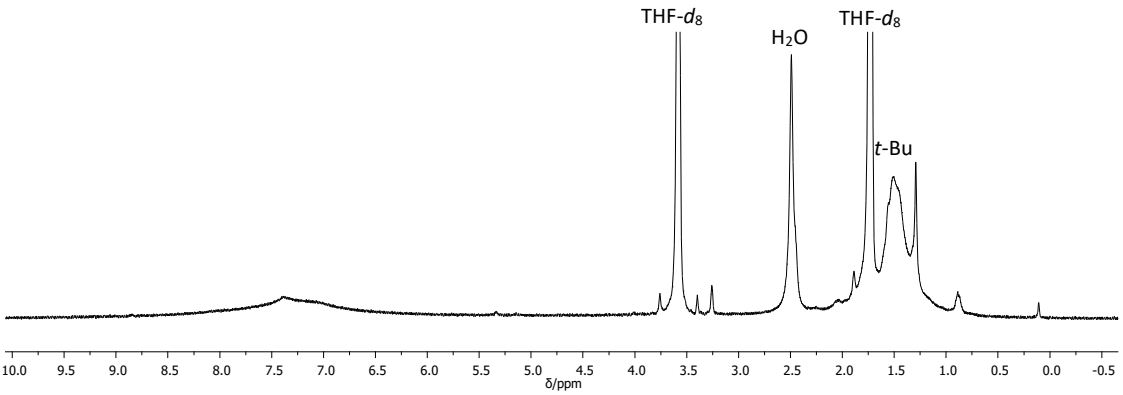

Figure 4.4 ^{1}H NMR-spectrum of **4-1** (300 MHz, THF-d_8).

On the other hand, the molecular mass of **4-1** was established by HRMS-MALDI through detection of the peak corresponding to the molecular ion at m/z 950.3337 (M^+, [$C_{60}H_{52}N_4O_4Ni^+$], calc.: 950.3342). In addition to the peak of molecular ion (m/z 950), LRMS-MALDI analysis of **4-1** revealed the peaks corresponding to porphyrin dimer (m/z 1902) and trimer (m/z 2856) (Figure 4.5).

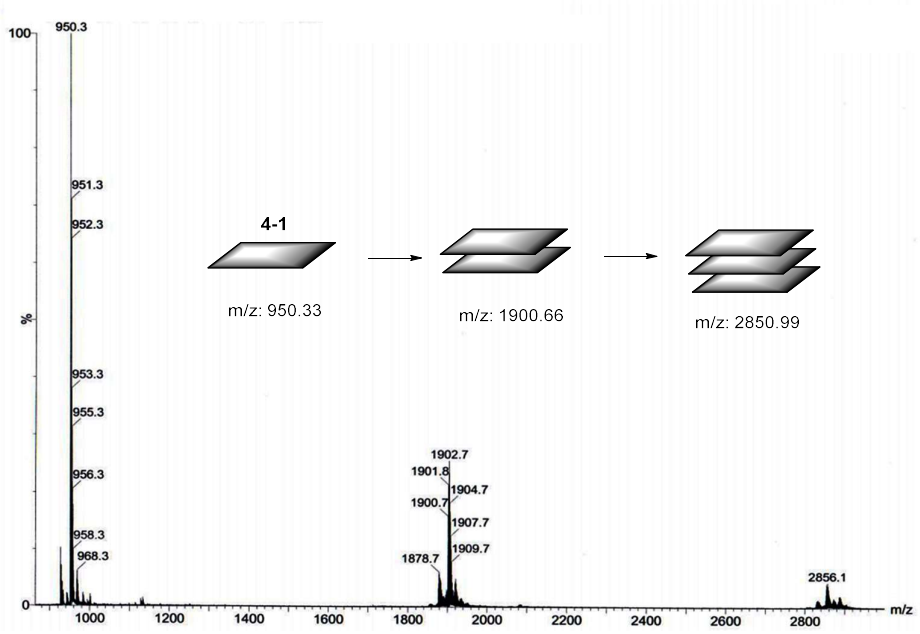

Figure 4.5 LRMS-MALDI spectrum of **4-1**. Inset shows the schematic representation of dimer and trimer formation.

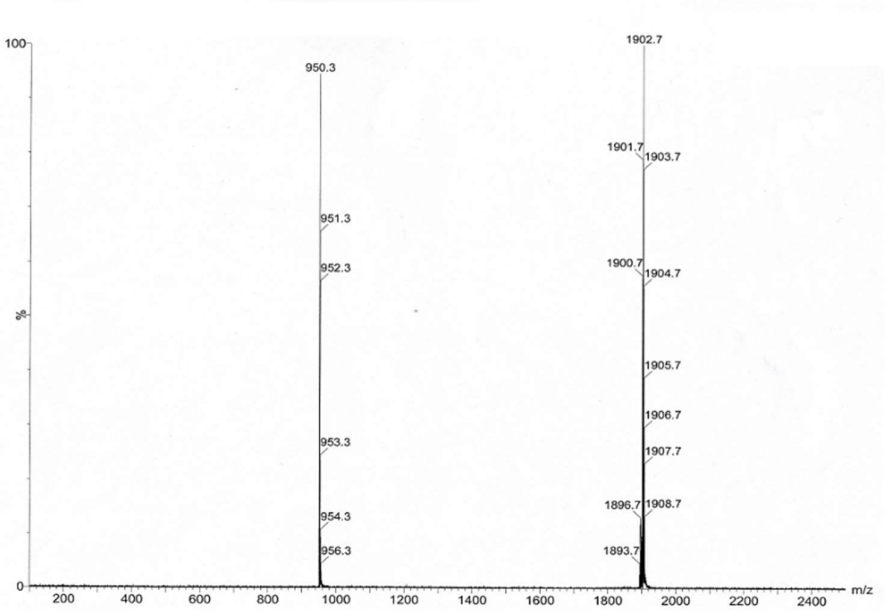

Figure 4.6 MS/MS spectrum at m/z 1902 of **4-1**.

Tandem mass spectrometry, also known as MS/MS, was used to further examine **4-1** and gain information about the nature of bonding in the dimers. Specifically, a precise mass (m/z 1902), characteristic of a dimer, was selected and further fragmented through electron capture dissociation. Figure 4.6 displays the MS/MS spectrum of the dimer in which the dissociation into the monomer at m/z 950 is clearly spotted, thus indicating the non-covalent character of porphyrin dimers.

In order to assign the structure of as-obtained tetrapyranoporphyrin among all possible isomers **4-1a-d**, DFT simulations of IR spectra for **4-1a-d** were performed. When comparing predicted data with that of the experimentally obtained, it was noted that the calculated IR spectrum for **4-1d** better reproduces the IR spectrum of as-prepared **4-1** at 1600-1700 cm^{-1} region (Figure 4.7a). In the case of isomers **4-1a-c** the sharp band at 1650 cm^{-1} was observed, which is assigned to the stretching vibration of the (β-)C-C(-β) bond of a doubly O-fused pyrrole moiety (Figure 4.7b).

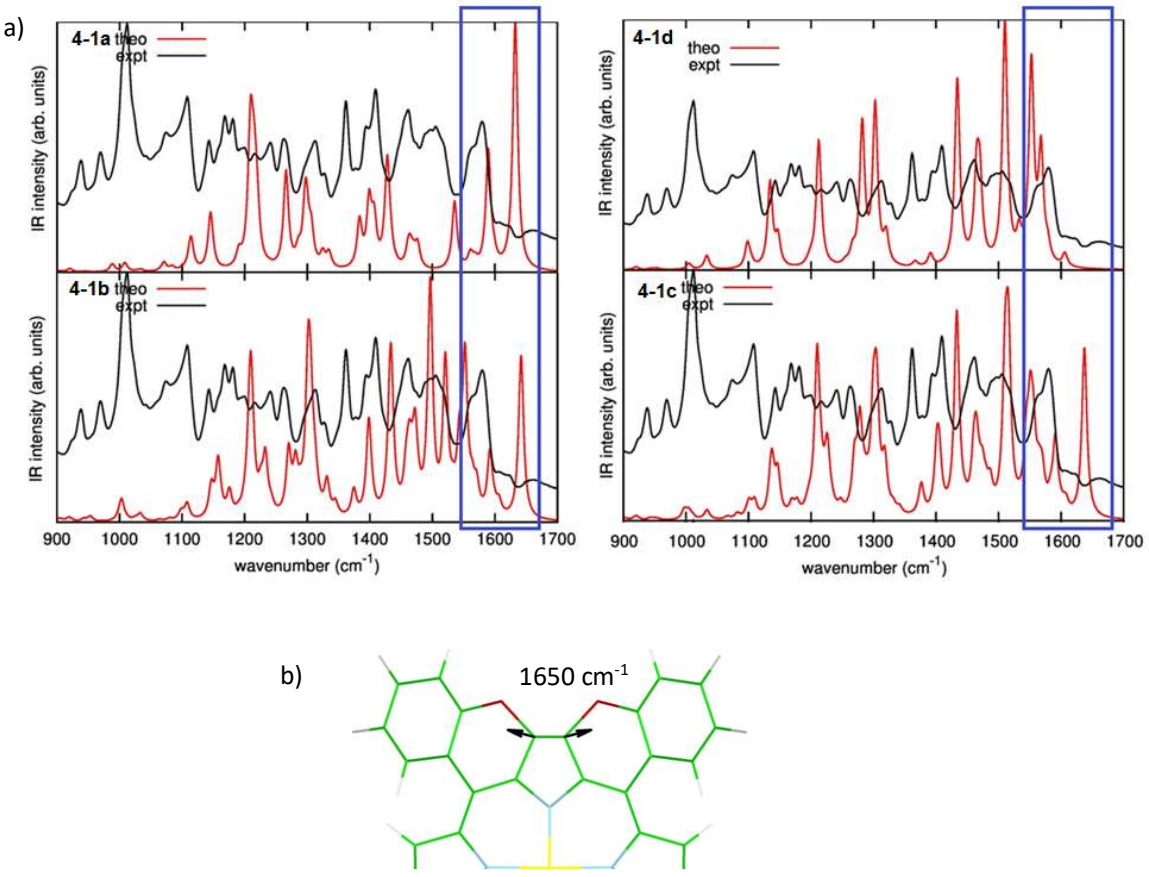

Figure 4.7 a) Comparison of obtained IR spectrum (in black) of **4-1** with calculated IR data (in red) for all possible isomers **4-1a-d**; b) Schematic representation of stretching vibration (β-)C-C(-β) bond of a doubly O-fused pyrrole moiety (green C, red O, blue N, yellow Ni).

Taking into consideration what has been revealed so far, we have postulated that isomer **4-1d** is the major product of pyran annulation reaction of tetrahydroxyporphyrin **4-3** (Scheme 4.3).

*4.1.1.2 Demetallation of tetrapyranoporphyrin **4-1d***

Owing to the fact that it was impossible to record the NMR spectrum of **4-1d**, ICP-OES (inductively coupled plasma optical emission spectrometry) was performed. The sample was dissolved in a mixture of H_2SO_4 and H_2O, and then driven through a nebulizer to produce an aerosol. When plasma energy was given to the sample, the release of energy from the excited atoms was detected by observing the emission wavelength, characteristic for each element. By comparing the wavelengths with standard data and by determining the intensities of the spectra, around 30% of Cu(II) along with expected Ni(II) was found. This was associated with metal exchange processes occurring during the CuO-mediated pyran annulation reaction, resulting in the contamination of the product with the Cu-metallated derivative.

To exclude the influence of central metal, we decided to demetallate **4-1d** using strong acidic conditions (Scheme 4.4). For this purpose, the solution of **4-1d** in CH_2Cl_2 was treated with a mixture of TFA and H_2SO_4 at 0 ^oC for 1 h. The completion of the reaction was monitored by LRMS-MALDI and the reaction stopped when full conversion was reached. The crude material was purified by silica gel flash-chromatography affording free-base tetrapyranoporphyrin **4-6** in 30% yield as a green solid. The low yield of the reaction was attributed to the partial decomposition of **4-1d** under harsh acidic conditions. Unfortunately, similarly to metal tetrapyranoporphyrin **4-1d**, all our attempts to record the NMR spectrum of **4-6** were unsuccessful. On the other hand, LRMS-MALDI of **4-6** revealed the peak corresponding to the molecular ion at m/z 894 (Figure 4.8a). The spectrum also reports peaks at m/z 880.53 and m/z 866.68 referred to the fragments of the molecule obtained after the loss of one CH_3 ($[(MH-CH_3)]^+$) and two CH_3 ($[(MH-2CH_3)]^+$), respectively. In addition photophysical measurements were obtained in order to further proof the formation of **4-6**. Specifically, the longest wavelength absorption maximum of **4-6** is bathochromically shifted by 125 nm with respect to free-base tetrahydroxyporphyrin **4-5**. The origin of this shift was ascribed to the extension of the π-conjugation along with the alignment of the four *meso*-aryl substituents with the plane of the porphyrin core. Upon the excitation of **4-6** at 453 nm, the emission at 740 and 810 nm was observed (Figure 4.8b).

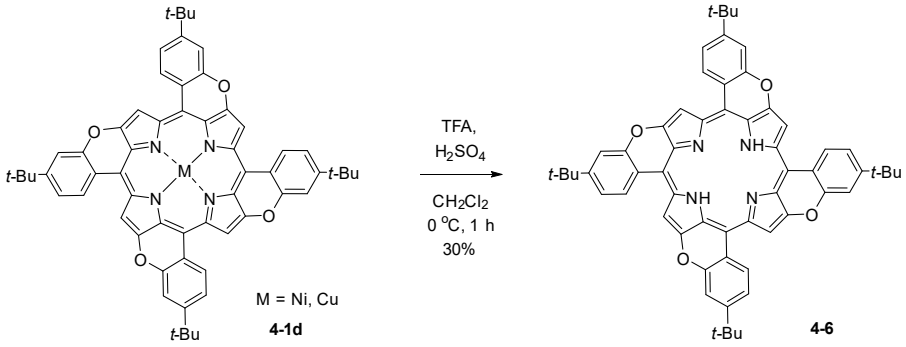

Scheme 4.4 Synthesis of free-base tetrapyranoporphyrin **4-6**.

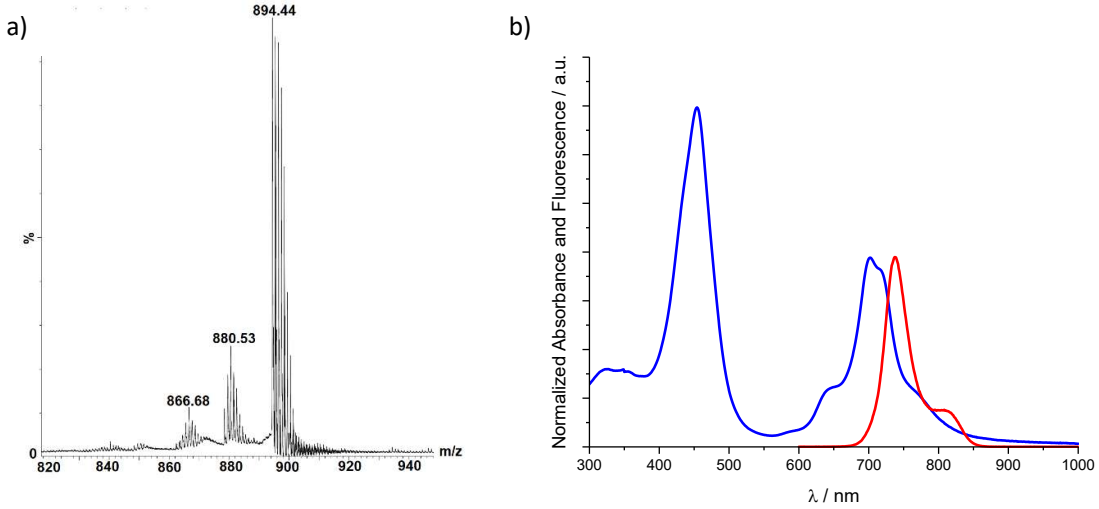

Figure 4.8 a) LRMS-MALDI spectrum of free-base tetrapyranoporphyrin **4-6**; b) Normalized UV-vis absorption (blue line) and emission (red line) spectra of **4-6** (λ_{exc} = 453 nm) in CH_2Cl_2 at rt.

The non-conclusive NMR analyses of **4-6** steered us to assume the presence of paramagnetic radical cation species. In order to confirm the presence radical cations, the use of electron paramagnetic resonance (EPR) spectroscopy was envisaged. Accordingly, EPR investigations at rt in O_2-free CH_2Cl_2 confirmed the presence of organic radical species by showing a sharp signal (g = 1.99) (Figure 4.9). It was hypothesised that the radical species were generated upon a mono electronic oxidation occurring during the pyran annulation reaction.

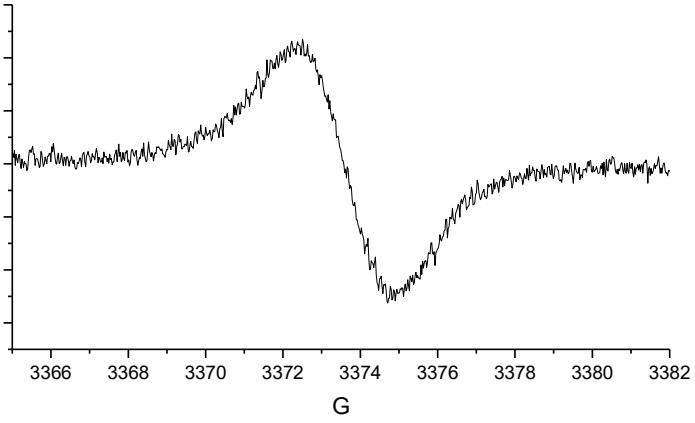

Figure 4.9 EPR spectrum of free-base tetrapyranoporphyrin **4-6**.

*4.1.1.3 Electrochemical studies of free-base tetrapyranoporphyrin **4-6***

To gain further insight on the character of free-base tetrapyranoporphyrin **4-6**, its redox properties were investigated. The redox potentials were measured by cyclic voltammetry in anhydrous CH_2Cl_2 and *o*-DCB solutions using 0.1 M *n*-Bu_4NPF_6 as a supporting electrolyte (Figure 4.10). O-embedded porphyrin **4-6** showed reversible second oxidation wave at 0.85 V and two reversible reduction waves at -1.45 and -1.17 V (Figure 4.10a). Notably, the first oxidation wave seems to be split into two waves at 0.31 and 0.54 V. This behaviour is similar to electrochemical responses of the other porphyrin complexes[180–182] and phthalocyanines,[183] capable of forming π-dimers, and can be explained by a two-step first oxidation process. In particular, the first step includes the generation of π-radical cation $\mathbf{[4\text{-}6]^{\bullet+}}$ followed by its interaction with neutral specie **4-6** affording mixed-valence specie $\mathbf{[4\text{-}6]_2^{\bullet+}}$(Figure 4.10b). Following, the second step involves a one electron oxidation of $\mathbf{[4\text{-}6]_2^{\bullet+}}$ yielding two $\mathbf{[4\text{-}6]^{\bullet+}}$ monomers. Interestingly, using more polar *o*-DCB than CH_2Cl_2 the splitting of the first oxidation wave was not observed (Figure 4.10c). This was attributed to the formation of a solvation shell of porphyrin radical cation $\mathbf{[4\text{-}6]^{\bullet+}}$, preventing the formation of $\mathbf{[4\text{-}6]^{2\bullet+}}$

Although EPR investigation showed the presence of organic radical cation specie, CV investigation did not reveal any evidence confirming this fact. Indeed, CV of **4-6** exhibited two reversible oxidation and two reversible reduction processes, characteristic of neutral porphyrin. Taking into consideration that CV is a less sensitive method of analysis compared to EPR, potentially the amount of radical cation porphyrin species present is negligible in order to be detected by CV.

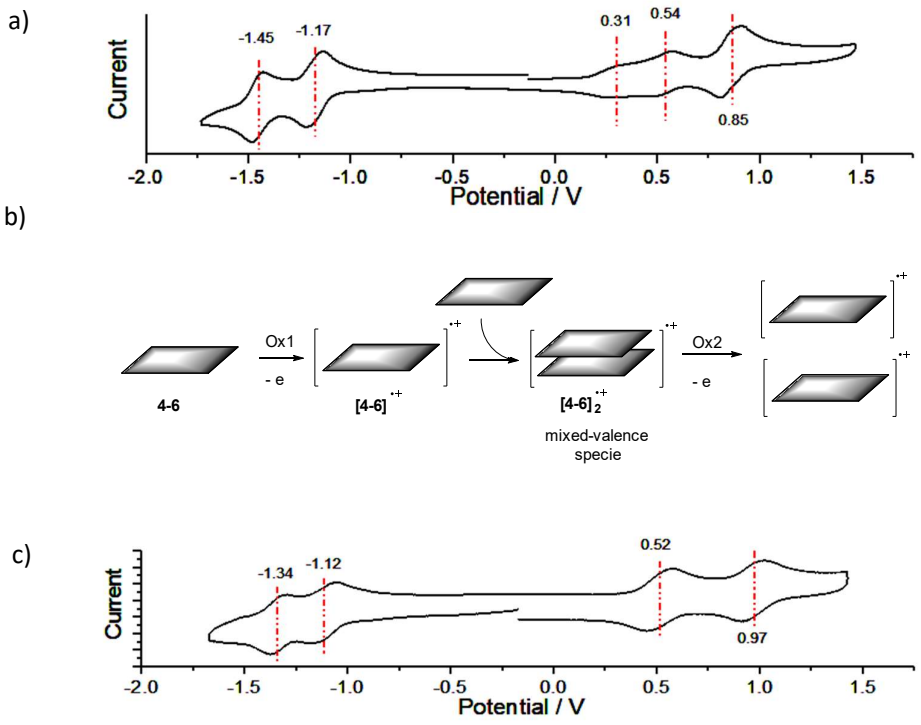

Figure 4.10 Cyclic voltammograms of **4-6** in a) CH_2Cl_2 and c) *o*-DCB. $Ag/AgClO_4$ was used as a reference electrode. The decamethylferrocene/decamethylferrocenium ion couple was used as an internal reference. Scan rate: 0.1 V s^{-1}; b) Schematic representation of two-step first oxidation process of **4-6** in CH_2Cl_2.

Table 4.1 Half-wave potentials for free-base mono- **3-14**, di- **3-27** and tetra- **4-6** pyranoporphyrins in *o*-DCB, with 0.1 M of $TBAPF_6$ (scan rate 0.1 V/s). The decamethylferrocene/decamethylferrocenium ion couple was used as an internal reference.

	$E^{1/2}_{red2}$ (V)	$E^{1/2}_{red1}$ (V)	$E^{1/2}_{ox1}$ (V)	$E^{1/2}_{ox2}$ (V)	$E^{1/2}_{ox1}$-$E^{1/2}_{red1}$ (V)	$E^{1/2}_{ox2}$-$E^{1/2}_{ox1}$ (V)	$E^{1/2}_{red1}$-$E^{1/2}_{red2}$ (V)
3-14	-1.48	-1.18	0.87	1.19	2.05	0.33	0.30
3-27	-1.54	-1.19	0.87	1.41	2.06	0.54	0.37
4-6	-1.34	-1.12	0.52	0.97	1.64	0.45	0.22

In addition, we compared the redox properties of free-base mono- **3-14**, di- **3-27** and tetra- **4-6** pyranoporphyrins (Table 4.1). $E^{1/2}_{red1}$ of **4-6** is cathodically shifted by 50-60 mV compared to $E^{1/2}_{red1}$ of **3-14** and **3-27**. Meanwhile, $E^{1/2}_{ox1}$ of **4-6** is anodically shifted by 350 mV compared to $E^{1/2}_{ox1}$ of **3-14** and **3-27**, thus indicating a more profound perturbation of HOMO when the number of oxygen bridges was increased to four. This behaviour can be

explained considering the non-planar structure of porphyrin **4-6**, which leads to the destabilization of HOMO and the increase of its energy. Hence, the value of $E^{1/2}_{ox1}$-$E^{1/2}_{red1}$ is dramatically decreased from 2.05 V for **3-14**, **3-27** to 1.64 V for **4-6**, indicating the narrowing of the electrochemical HOMO-LUMO gap.

4.1.2 Tetrapyranoporphyrin 4-2

The retrosynthetic analysis towards the synthesis of tetrapyranoporphyrin **4-2** is outlined in Scheme 4.5. It involves the initial synthesis of porphyrin **4-10** using *MacDonald's* condensation, followed by bromination and subsequent *Suzuki* coupling to produce **4-8**. The latter, after demethylation and metallation, should form the corresponding Ni(II) tetrahydroxyporphyrin **4-7**, the precursor of desired O-fused system **4-2**.

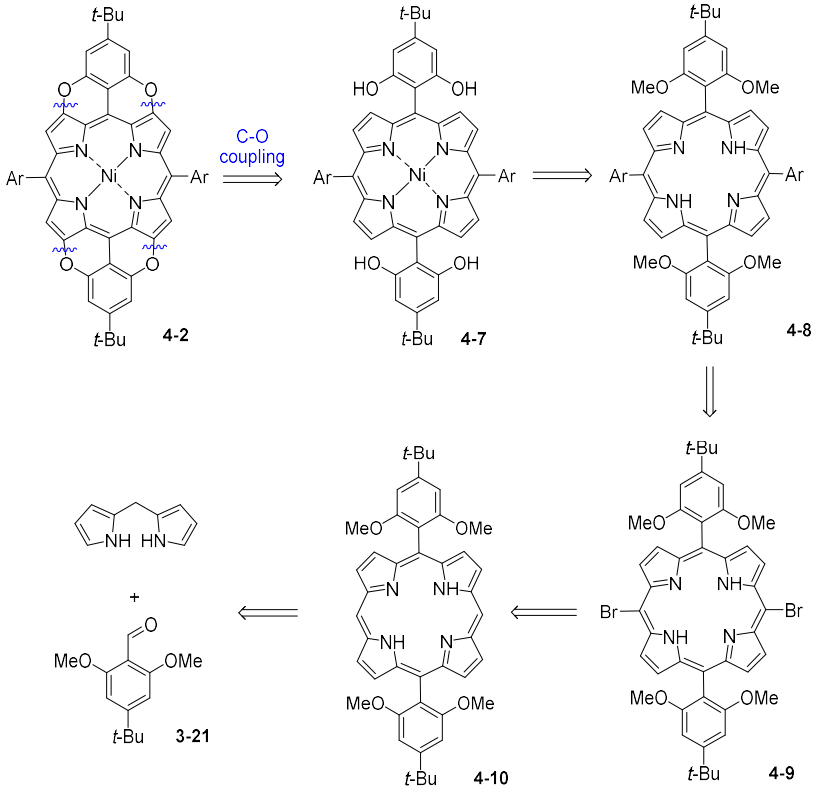

Scheme 4.5 Retrosynthesis of tetrapyranoporphyrin **4-2**.

Similarly to the synthesis of dihydroxyporphyrin **3-29** (details are in Chapter III), tetrahydroxyporphyrin **4-7** was obtained following *MacDonald's* [2+2] porphyrin macrocyclization approach. Accordingly, the condensation of as-prepared dipyrromethane

with dimethoxybenzaldehyde **3-21** in the presence of $BF_3{\cdot}Et_2O$ led to porphyrin precursor **4-10** in 20% yield (Scheme 4.6). Subsequent bromination with NBS, followed by Pd(II)-catalyzed coupling of **4-9** with an excess of 4-*tert*-butylphenylboronic acid afforded free-base tetramethoxyporphyrin **4-8** in 39% yield. Further cleavage of the methyl protecting groups by BBr_3 in CH_2Cl_2, followed by metallation with $Ni(acac)_2$ yielded Ni(II) tetrahydroxyporphyrin **4-7**. All compounds were thoroughly characterized by MASS-spectrometry, ^1H and ^{13}C NMR-, IR- and UV-spectroscopy (Chapter VI).

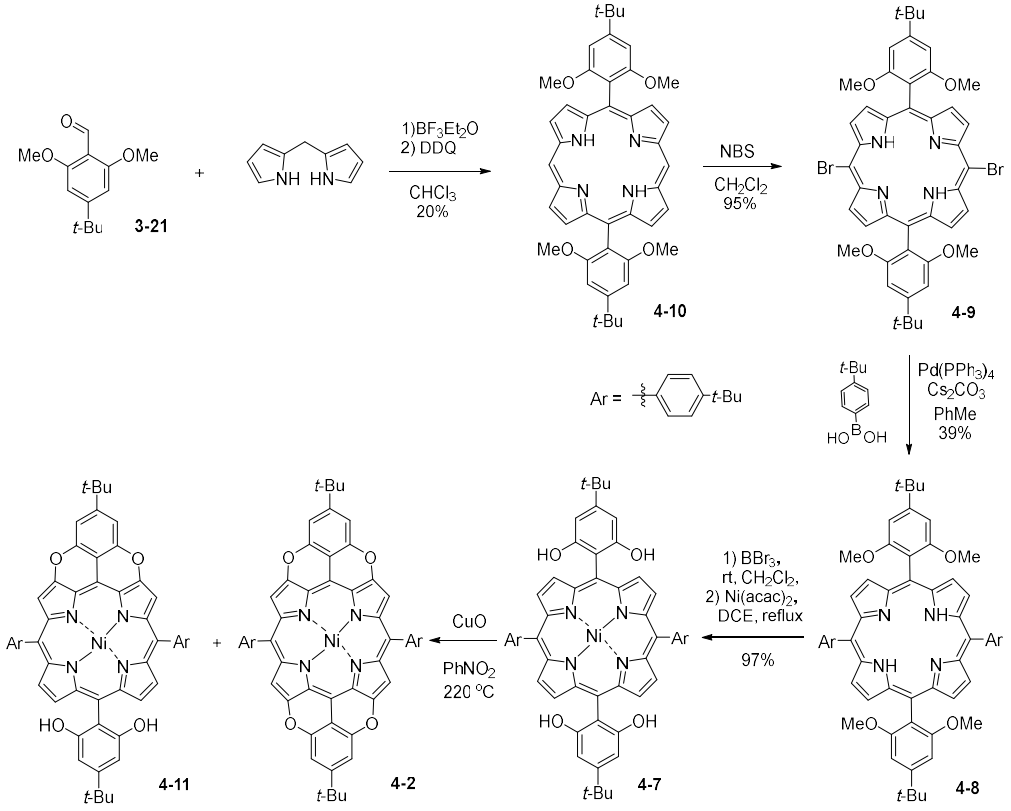

Scheme 4.6 Synthesis of Ni(II) tetrapyranoporphyrin **4-2**.

The chemical structure of Ni(II) tetrahydroxyporphyrin **4-7** was unambiguously identified by ESI-HRMS through detection of the peak corresponding to the molecular ion at m/z 959.4053 (M^+, [$C_{60}H_{61}N_4NiO_4^+$], calc.: 959.4046). The ^1H NMR-spectrum of **4-7** displays a singlet referring to the β-pyrrolic protons at 8.86 ppm, two doublets (7.92 and 7.71 ppm) and one singlet (6.95 ppm) of the *meso*-aryl hydrogen atoms, a singlet of the hydroxyl protons at 4.58 ppm and two singlets of the non-equal *tert*-butyl protons at 1.57 and 1.51 ppm (Figure 4.11).

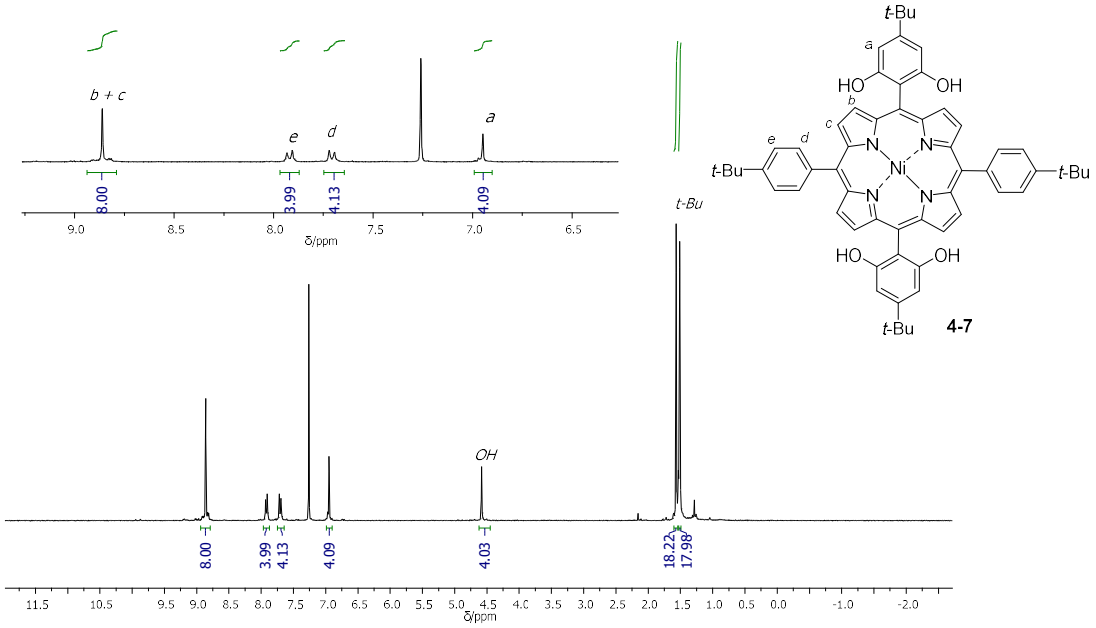

Figure 4.11 ^{1}H NMR-spectrum of Ni(II) tetrahydroxyporphyrin **4-7** (300 MHz, $CDCl_3$).

Subsequent CuO-mediated oxidative ring closure reaction of **4-7** in $PhNO_2$ at 220 °C afforded a complex mixture according to TLC (Scheme 4.6). LRMS-MALDI analysis revealed only traces of desired product **4-2**, while the majority of peaks were corresponding to oxygenated products with higher molecular weights (Figure 4.12).

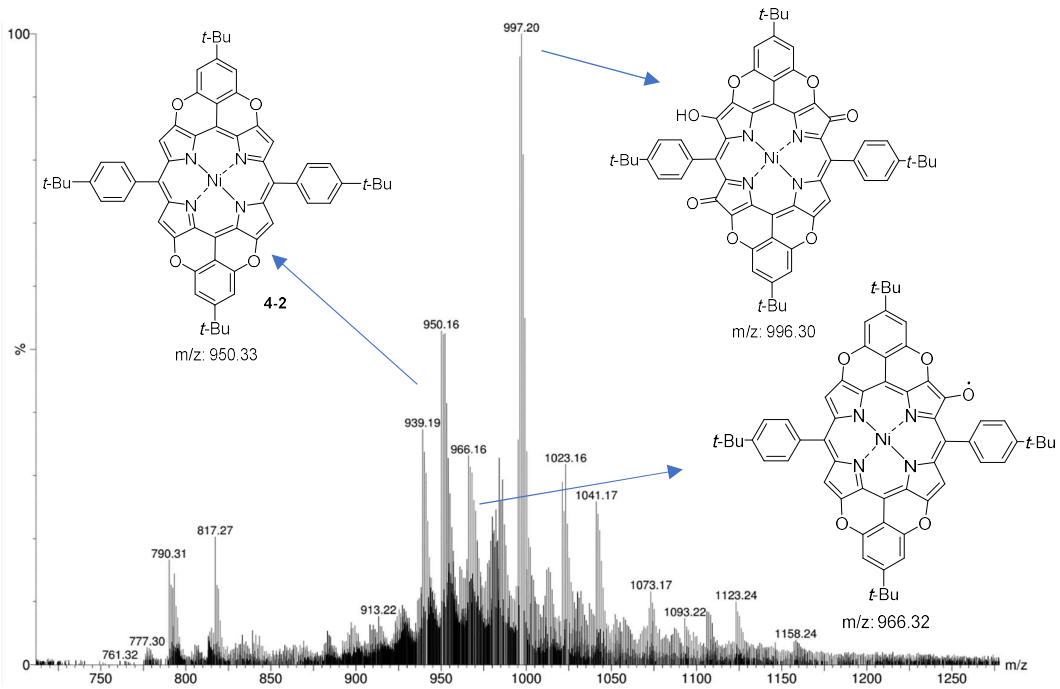

Figure 4.12 LRMS-MALDI spectrum of crude after pyran annulation reaction of **4-7**.

Porphyrin derivatives are known to be highly effective triplet state photosensitizers and capable in generating singlet molecular oxygen $^1O_2$ under illumination and in the presence of oxygen.[184–186] The photosensitizing process includes the initial absorption of a photon by the porphyrin molecule with the following promotion of an electron from the ground state (S_0) to the excited singlet state (S_1) (Figure 4.13). Subsequently, the molecule in S_1 can relax *via* various competing processes. In case of fluorescence and internal conversion, the relaxation of S_1 directly to the ground state S_0 is occurred, while in case of intersystem crossing an excited triplet state T_1 is generated.[187] The energy of the excited triplet state of the porphyrin photosensitizer can be realized through the direct transfer to the molecular oxygen in the triplet ground state ($^3O_2$), resulting in the generation of a singlet molecular oxygen ($^1O_2$).

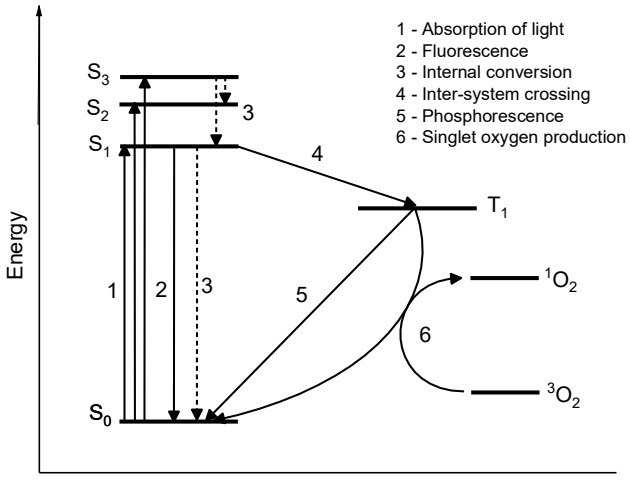

Figure 4.13 Singlet molecular oxygen $^1O_2$ generation by photosensitizing process.

Therefore, we assumed that upon exposure to air, O-fused porphyrin **4-2** behaves as a photosensitizer through producing highly reactive $^1O_2$. Subsequent reaction of $^1O_2$ with the electron saturated porphyrin system leads to the formation of perepoxide **A** (Scheme 4.7).[188] The following rearrangement of **A** gives hydroperoxide **B**, which undergoes hemolytic O-O bond cleavage upon the light irradiation affording porphyrin radical **C**. Subsequent reaction of **C** with $^1O_2$ leads to the formation of **D**, the further rearrangement of which affords oxygenated derivative **E** with m/z 996.30.

All attempts to isolate the target product **4-2** using silica gel or alumina chromatography turned to failure. However, the isolation of product **4-11** was achieved (Scheme 4.6), formed as a result of a not completed O-fusion of **4-7**. The chemical structure of **4-11** was established using NMR-spectroscopy. The ^1H NMR-spectrum of **4-11** displays a

doublet of doublet for $H_{b,c}$ (8.89 ppm) and a singlet for H_f (7.91 ppm) relating to the pyrrole rings; two doublets for $H_{e,d}$ (7.92 and 7.77 ppm) and two singlets for $H_{g,a}$ (7.50 and 7.11 ppm) corresponding to the *meso*-aryl substituents; one singlet for the hydroxyl protons (5.13 ppm) and three singlets (1.64, 1.63 and 1.56 ppm) for the protons of *t*-Bu-groups (Figure 4.14).

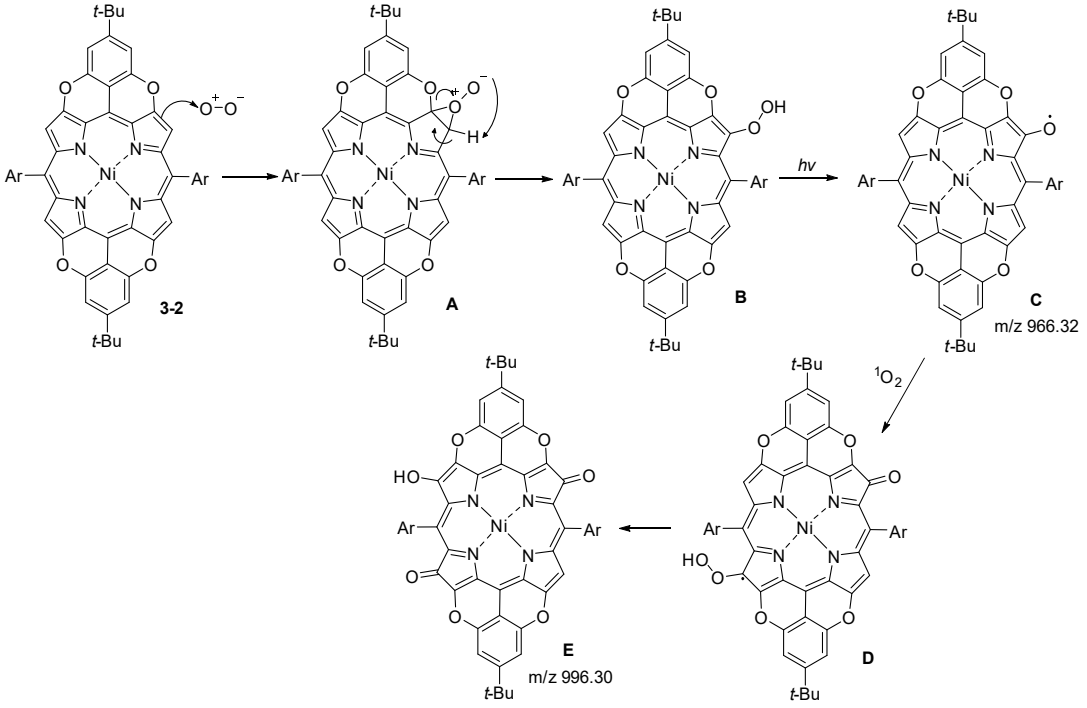

Scheme 4.7 Schematic illustration of the formation of oxygenated products.

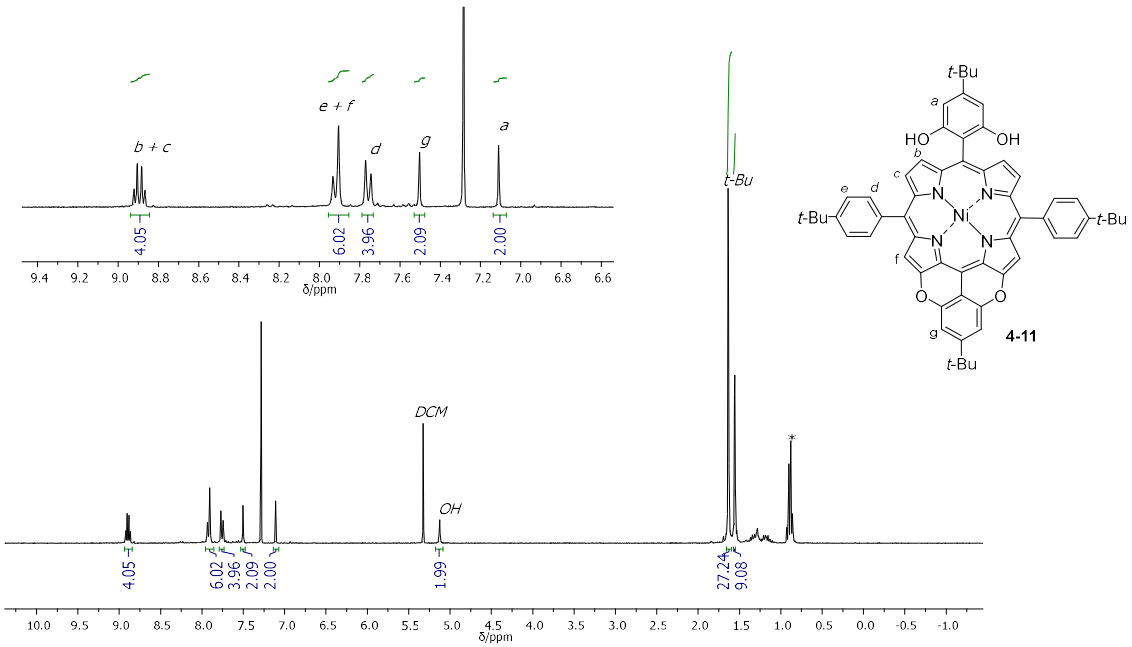

Figure 4.14 ^{1}H NMR-spectrum of **4-11** (300 MHz, $CDCl_3$). *- cyclohexane.

4.2 Synthesis and characterization of octapyranoporphyrin

Finally, our study was extended to the synthesis of full-conjugated octapyranoporphyrin comprising eight six-membered rings with O-bridged bonds (Scheme 4.8). Full-fused porphyrin **4-12** is expected to present a more electron-saturated π-system than as-obtained mono-, di- and tetra- pyranoporphyrins. Therefore, the foreseen extension of the conjugation length will lead to the enhancement of the electron-donating properties and to a decrease of the HOMO-LUMO gap.

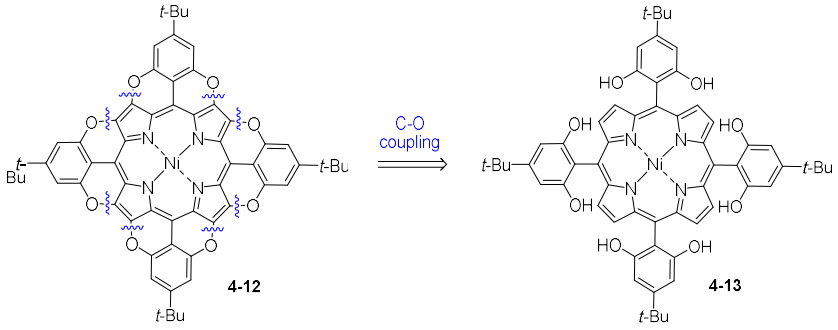

Scheme 4.8 Retrosynthesis of octapyranoporphyrin **4-12**.

On the way to the desired octapyranoporphyrin, we first synthesized Ni(II) octahydroxyporphyrin **4-13** following the same strategy as for the preparation of tetrahydroxyporphyrin **4-3** (Scheme 4.3), but dimethoxybenzaldehyde **3-21** was exploited (Scheme 4.9). Accordingly, condensation of aldehyde **3-21** with pyrrole in $CHCl_3$ in the presence of $BF_3{\cdot}Et_2O$, followed by oxidation with DDQ afforded octamethoxyporphyrin **4-14** in 24% yield. Subsequent BBr_3-cleavage of the methoxy substituents, followed by metallation of **4-15** with $Ni(acac)_2$ in refluxing DCE afforded **4-13** in 95% yield. The structure of Ni(II) octahydroxyporphyrin **4-13** was confirmed by ^{1}H-, ^{13}C-NMR, IR, UV-vis and ESI-HRMS, which displayed the peak corresponding to the molecular ion at m/z 1023.3860 (M^+, [$C_{60}H_{61}N_4O_8Ni^+$], calc.: 1023.3843). The ^{1}H NMR-spectrum of **4-13** is relatively easy to interpretate due to the D_{4h} space group symmetry of the molecule (Figure 4.15). Indeed, the spectrum exhibits only four singlet signals at 8.82, 6.89, 4.70 and 1.48 ppm corresponding to the protons of the pyrrole rings (H_a), the *meso*-aryl substituents (H_b), OH- and the *t*-Bu-groups, respectively.

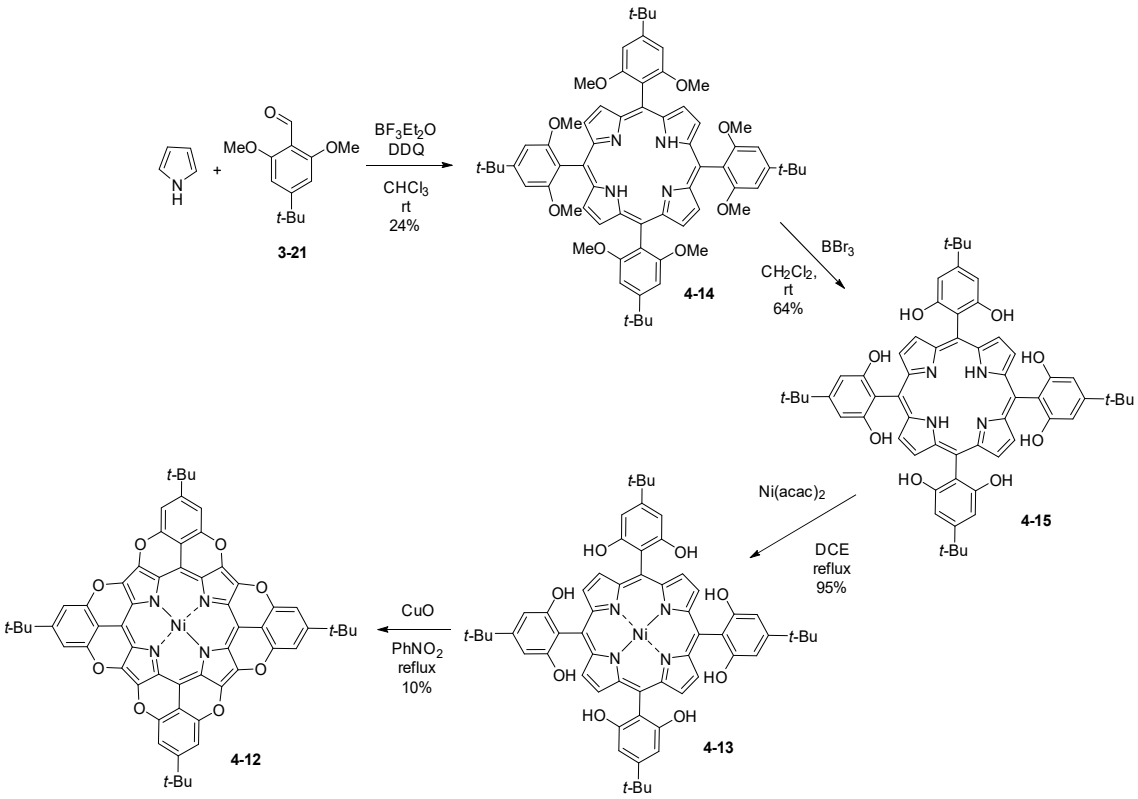

Scheme 4.9 Synthesis of Ni(II) octapyranoporphyrin **4-12**.

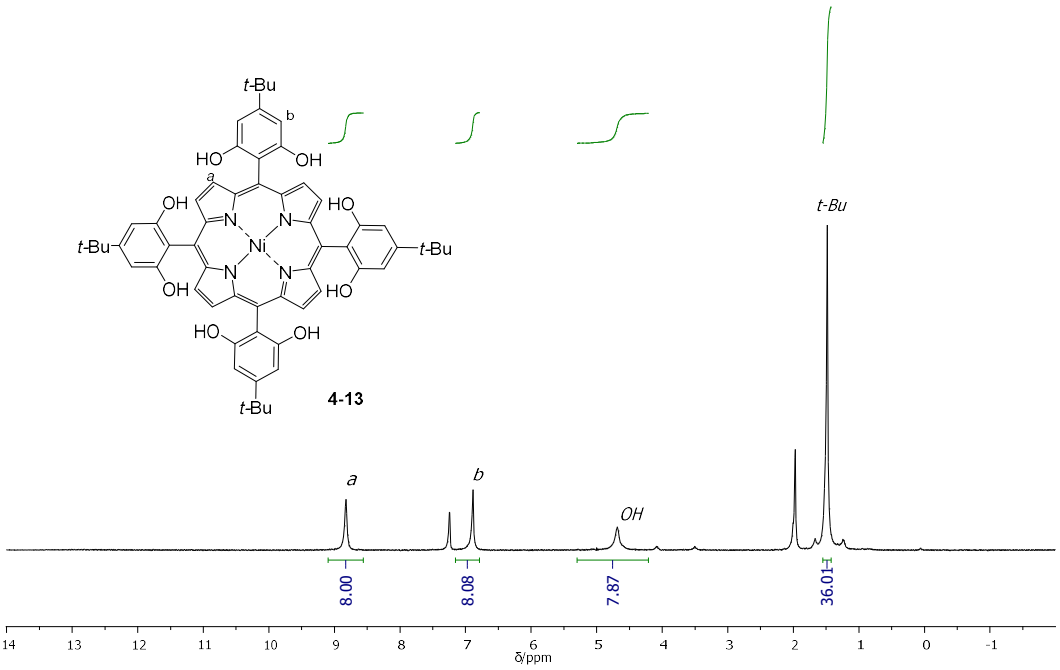

Figure 4.15 ^{1}H NMR-spectrum of Ni(II) octahydroxyporphyrin **4-13** (400 MHz, $CDCl_3$).

In order to accomplish the synthesis of the O-fused porphyrin, the peripheral *meso-o*-hydroxyaryl substituents should undergo an intramolecular ring closure reaction with the β-pyrrolic positions through a diaryl-ether bond formation. Accordingly, octahydroxyporphyrin **4-13** was subjected to the CuO-promoted pyran annulation reaction in refluxing $PhNO_2$ for 12 h affording **4-12** as a green solid (Scheme 4.9). LRMS-MALDI analysis of the material**,** revealed the desired peak corresponding to the molecular ion of **4-12** at m/z 1006 along with other peaks relating to oxygenated products [M+O] (m/z 1022.25), [M+2O] (m/z 1038.24), [M+O+2OH] and [M+4OH] (m/z 1074.26) (Figure 4.16). Noteworthy, while keeping **4-12** under open-air conditions, the intensity of the peaks, corresponding to side products [M+O+2OH] and [M+4OH] was dramatically increased.

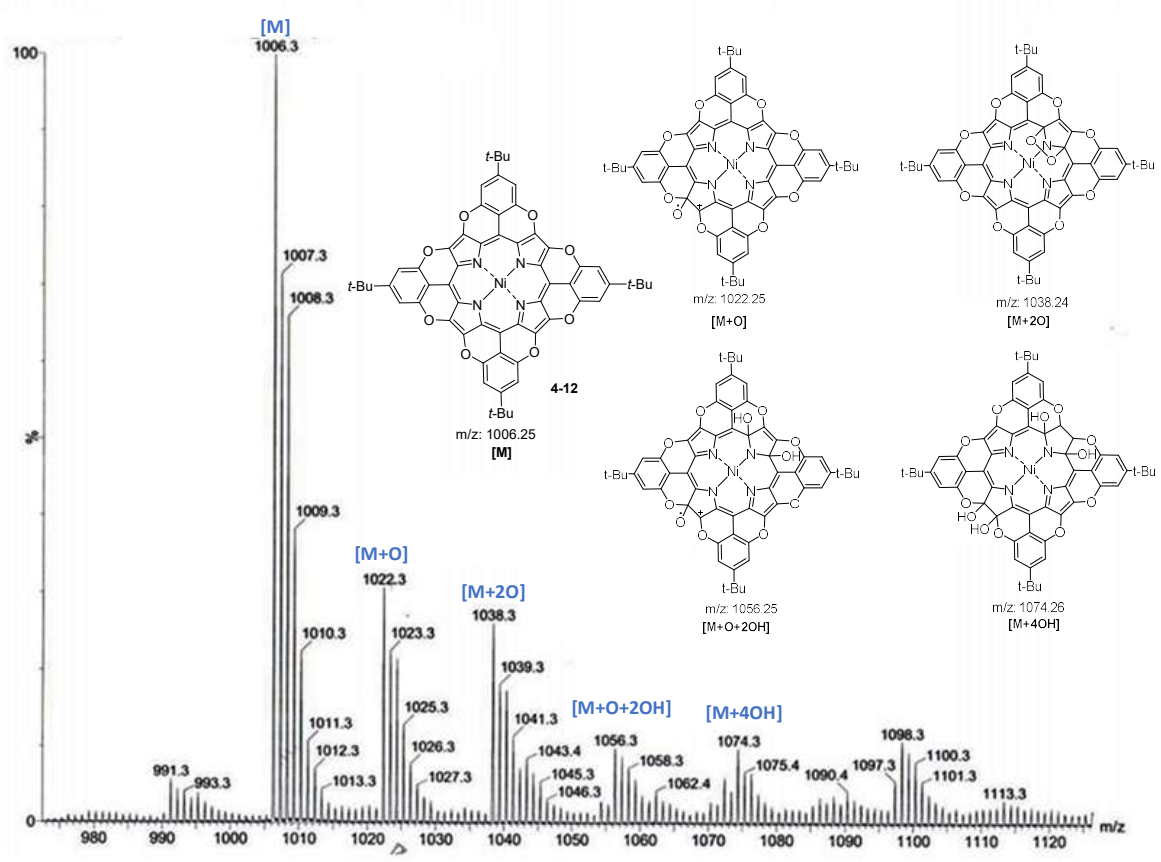

Figure 4.16 LRMS-MALDI spectrum of Ni(II) octapyranoporphyrin **4-12**.

Similarly as in the case of tetrapyranoporphyrin **4-2**, the formation of oxygenated products was attributed to the reaction of molecular singlet oxygen $^1O_2$ with octapyranoporphyrin **4-12**. In this case, the reaction of $^1O_2$ with the aromatic system of porphyrin can be carried out through [2+2] and [2+4] cycloaddition mechanisms yielding

products **B** and **D**, respectively (Scheme 4.10). Subsequent moisture exposure of **B** and **D** results in its hydrolysis to the dihydroxy derivatives (structures **C** and **E)**.

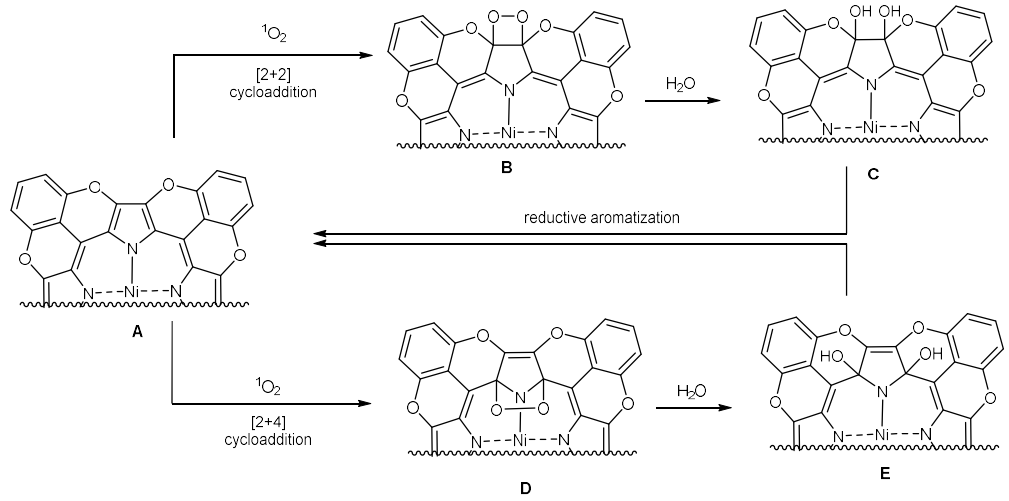

Scheme 4.10 Schematic representation of the formation of oxygenated species.

Metalloporphyrins are known to be highly conjugated systems, where all pyrrole subunits are equal and exhibit local aromaticity. Addition of $^1O_2$ to the double bond of the pyrrole moiety break the conjugation within the cycle, resulting in the loss of the aromaticity. In this manner, each subsequent reaction of the porphyrin macrocycle with $^1O_2$ leads to less conjugated species. Thus, the reductive aromatization of formed oxygenated products in an attempt to recover a desired full-conjugated porphyrin **3-12** was suggested (Scheme 4.10). Among a variety of reducing reagents, our attention was drawn to $SnCl_2$, widely used for the reduction of 1,4-diol derivatives under acid catalysed conditions.[189–192]

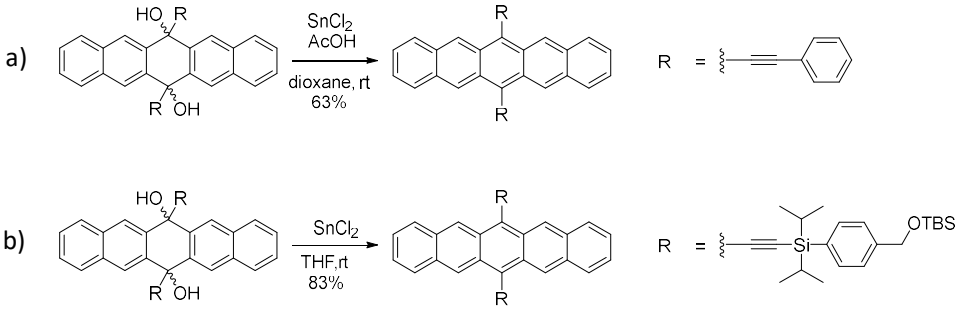

Scheme 4.11 Sn(II)-mediated reductive aromatization: a) acid-catalysed;[193] b) acid-free.[194]

For instance, *Maulding* and *Roberts* reported the Sn(II)-mediated reductive aromatisation of quinol derivative to pentacene in the presence of acetic acid at rt (Scheme 4.11a).[193] On the other hand, *Tykwinski* and co-workers described the $SnCl_2$-promoted acid-free reduction of 6,13-diol affording aromatic pentacene in 83% yield (Scheme 4.11b).[194] Taking into consideration what has been reported so far, crude **4-12** was treated with $SnCl_2$ at rt in THF under inert atmosphere. LRMS-MALDI of the reaction mixture revealed a significant decrease in intensity of peaks corresponding to the oxygenated species (Figure 4.17).

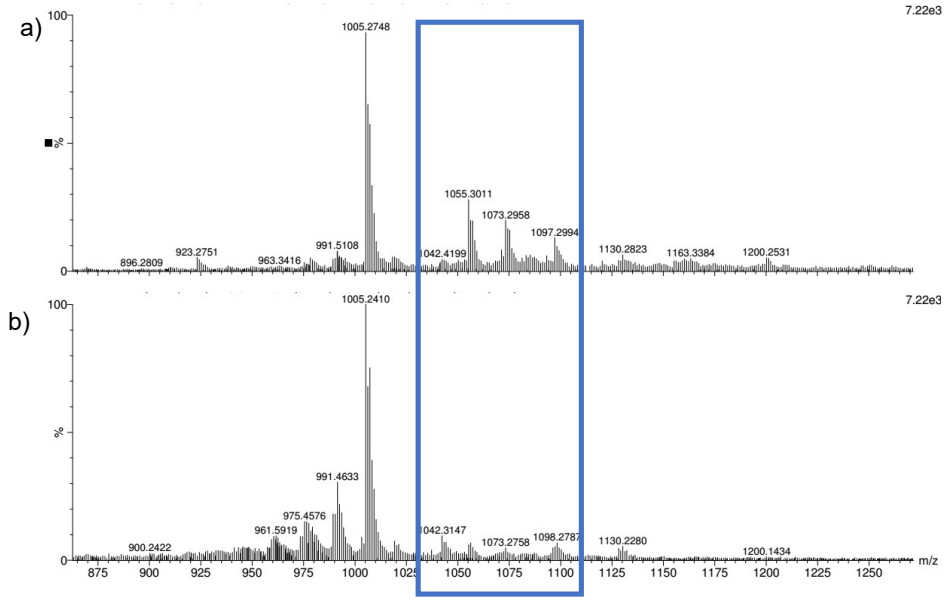

Figure 4.17 LRMS-MALDI experiments of crude **4-12** a) before and b) after the treatment with $SnCl_2$.

In order to isolate the desired product, the use of gel permeation chromatography (GPC) was attempted, since the purification of crude **4-12** by silica gel chromatography is problematic due to irreversible adsorption of the compound on SiO_2. Accordingly, the chromatography column was packed with Bio-Beads™ S-X resin, previously swelled in pyridine, and crude **4-12** was disposed on the top of the column. O_2-free pyridine was used as an eluent and the whole purification method was performed under inert atmosphere. As a result, four different fractions were obtained and LRMS-MALDI analysis of each was carried out (Figure 4.18). It was found, that the fourth fraction consists of pure target octapyranoporphyrin **4-12**, while the third fraction comprises the oxygenated species. Consequently, the success of the CuO-mediated pyran annulation reaction was validated *via* HRMS-MALDI, in which the peak corresponding to the molecular ion at m/z 1006.2473 (M^+,

[$C_{60}H_{44}N_4O_8Ni^+$], calc.: 1006.2513) was observed. Unfortunately, similarly to tetrpyranoporphyrin **4-1**, NMR investigation of **4-12** did not give any conceivable results. On the other hand, UV-vis spectroscopy of **4-12** (fraction 4) in THF displays *Soret* band at 402 nm and low intencity Q bands at near-IR region (730, 750, 832 and 850 nm), thus suggesting the extension of the conjugation system (Figure 3.19a).

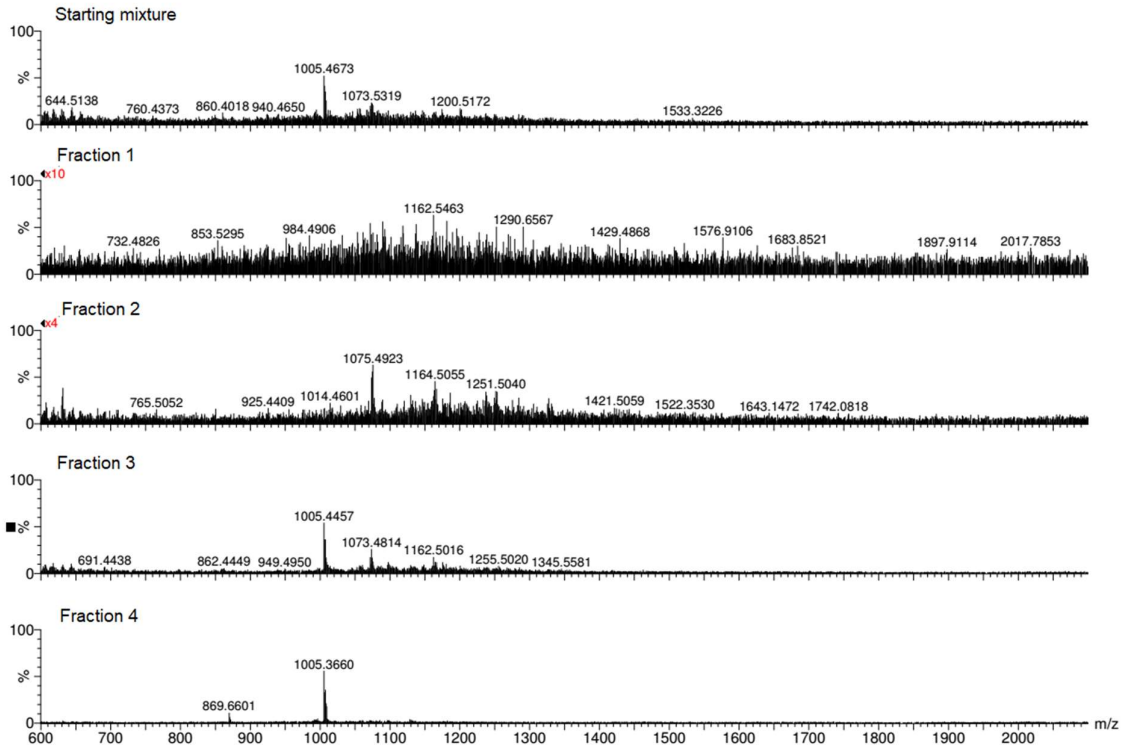

Figure 4.18 LRMS-MALDI analyses of crude mixture and fractions, obtained by gel permeation chromatography of **4-12**.

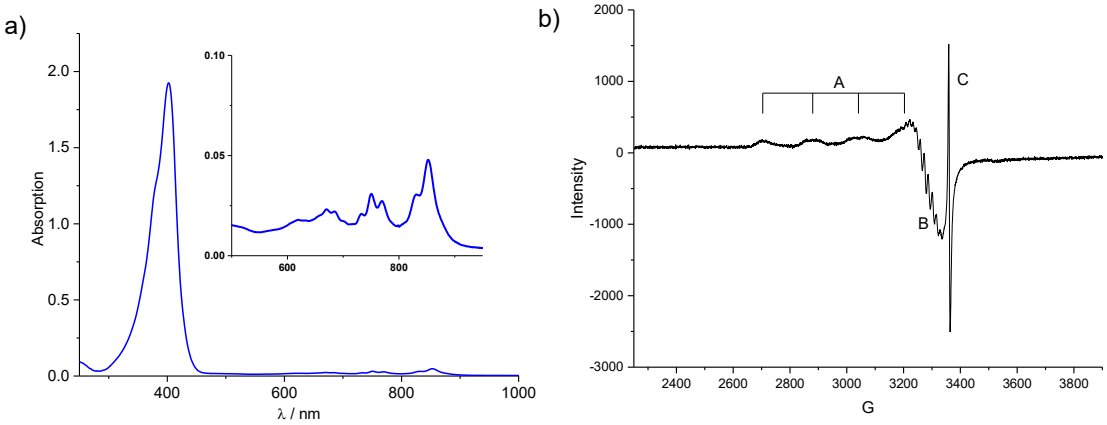

Figure 4.19 a) UV-vis absorption spectrum of **4-12** (fraction 4 after GPC) at rt in THF (inset: zoom of region 500-900 nm); b) EPR analysis of **4-12**.

EPR investigation of **4-12** in CH_2Cl_2 with the addition of pyridine at 120 K revealed the presence of a sharp signal **C** of an organic radical (Figure 4.19b). Besides, the signals relating to Cu(II) porphyrin complex were observed. In particular, the four-line pattern (signals **A**), indicating the hyperfine interaction between the one unpaired electron and the nucleus of Cu atom (I_{Cu} = 3/2), was detected.[195] Moreover, a superhyperfine structure with nine lines (signal **B**), corresponding to the interaction of the unpaired electron of Cu(II) with the nuclear spins of four ^{14}N, was observed. Similarly as for **4-1**, we concluded that along with the intramolecular ring closure reaction of **4-13** the side processes of transmetallation and overoxidation occurred as well.

In order to obtain the free-base octapyranoporphyrin, the demetallation of as-obtained **4-12** was carried out. However, all our attempts to achieve this turned to failure. Specifically, the addition of acid to a suspension of **4-12** in CH_2Cl_2 led to the decomposition of the latter, even at 0 ^oC, according to LRMS-MALDI analysis. It should be noted that the obtained octapyranoporphyrin **4-12** is poorly soluble in common used organic solvents, which can be explained by the strong π-π stacking between the porphyrin macrocycles. Besides, all our attempts to grow up single crystals of **4-12**, suitable for X-ray investigation from a pyridine solution, were unsuccessful and led to amorphous solids.

4.3 Conclusions

In this chapter we extended the use of CuO-mediated pyran annulation reaction to the synthesis of tetra- and octa- pyranoporphyrins, comprising four and eight oxygen bridges, respectively. In the first section, the ring closure reaction of tetrahydroxyporphyrin **4-3** was explored. We confirmed the success implementation of the formerly developed protocol on tetrapyranoporphyrin derivatives through HRMS-MALDI characterizations. The chemical structure of the major tetrapyranoporphyrin isomer **4-1d** was supported by IR-spectroscopy. Further detailed MS/MS investigations of **4-1d** revealed the formation of non-covalent dimers and trimers, suggesting the strong π-π interaction between porphyrin macrocycles Subsequently, the physicochemical properties of free-base tetrapyranoporphyrin **4-6** were thoroughly studied. In contrast to mono- and di- pyranoporphyrin derivatives, UV-vis and electrochemical investigations of **4-6** revealed the narrowing of HOMO-LUMO gap. This was attributed to the HOMO rising effect of **4-6**, caused by the distortion of porphyrin planarity and high electron-donating ability of four oxygen atoms. Finally, EPR analysis of

4-6 established the occurrence of porphyrin radical cation species, possibly formed as a result of one-electron oxidation of **4-6** by O_2. Besides, CuO-promoted pyran annulation reaction of tetrahydroxyporphyrin **4-7** was also studied. However, LRMS-MALDI analysis of crude revealed the formation of only trace amount of expected tetrapyranoporphyrin **4-2** in addition to the oxygenated products with higher molecular weight. This was assigned to the photosensitization of highly reactive singlet molecular oxygen $^1O_2$ and subsequent reaction of $^1O_2$ with **4-2**. Although we didn't manage to isolate desired **4-2**, we have isolated partially fused porphyrin derivative **4-11**, the structure of which was proved by NMR-spectroscopy.

The second section of this chapter focuses on the further exploration of pyran annulation reaction through the increasing of the number of oxygen bridges to eight. CuO-mediated ring closure reaction of octahydroxyporphyrin **4-13** led to the mixture of desired octapyranoporphyrin **4-12** and oxygenated products according to LRMS-MALDI. Similarly as for the synthesis of tetrapyranoporphyrin **4-2**, the formation of side products was associated with the reaction of **4-12** with singlet molecular oxygen $^1O_2$. In both cases, porphyrin macrocycles of **4-2** and **4-12** play role of photosensitizers. Subsequent reductive aromatization of crude **4-12** with $SnCl_2$, followed by GPC purification of reaction mixture resulted in the isolation of full-conjugated porphyrin **4-12**. The chemical structure of **4-12** was unambiguously confirmed through HRMS-MALDI analysis. In addition, EPR investigation supports the formation of highly π-delocalized electron rich system, exhibiting radical character.

5. Conclusions and perspectives

The main goal of the work detailed in this dissertation was to design and synthesize novel π-extended O-embedded porphyrins in order to reveal the emerged structure-property relationships. In this context, the first objective tackled herein focused on the development of synthetic strategy towards the preparation of O-annulated porphyrins. Afterwards, four generations of pyranoporphyrins with a different number of pyran rings were obtained, and the effect of oxygen embedding on their physicochemical properties was investigated.

Initially, we developed a new synthetic methodology to prepare O-embedded porphyrins using CuO as a promouter of intramolecular pyran annulation reaction. The success implementation of the developed protocol was successively demonstrated on the synthesis of mono-, di-, tetra- and octa- pyranoporphyrins (Figure 5.1).

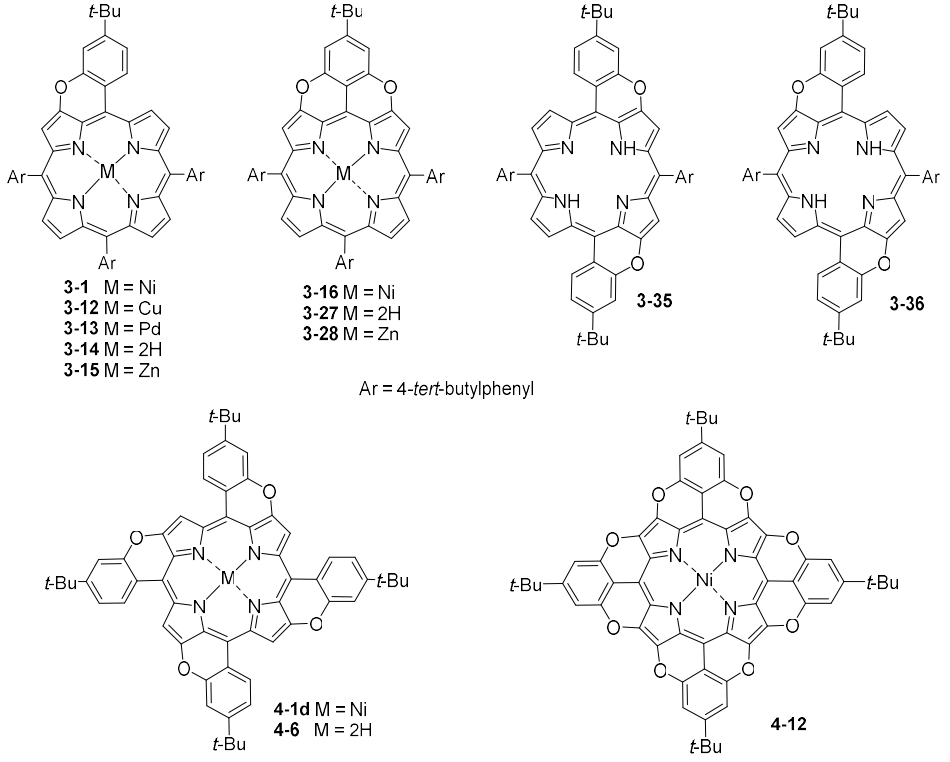

Figure 5.1 Chemical structures of mono-, di-, tetra- and octa- pyranoporphyrins obtained in the present work.

The formation of mono- and di- pyranoporphyrins was unambiguously proved by ^{1}H- and ^{13}C-NMR, IR, UV-vis spectroscopy and HRMS analyses. Moreover, the chemical

structures of mono- **3-1**, **3-14** and di- **3-16**, **3-36** pyranoporphyrins were confirmed by X-ray analysis. Meanwhile, tetra- and octa- pyranoporphyrins exhibited strong π-π interaction and unexpected radical character that makes their structural analysis rather complicated. Therefore, the chemical structures of **4-1d**, **4-6** and **4-12** were confirmed only by HRMS measurments, while their radical character was established by EPR investigations.

The physicochemical investigation of as-prepared O-embedded porphyrins revealed a set of intriguing structure-property relationships. In particular, a slight bathochromic shift of absorption maxima for all O-fused porphyrins compared to non-fused analogues was observed, thus indicating a weak conjugation between the co-planarized *meso*-aryl groups and the porphyrin core. On the other hand, by varying the number and the position of O-bridges along the series of pyranoporphyrins the more pronounced changes of electrochemical properties were revealed. Specifically, the cyclic voltammograms of O-fused porphyrins showed the significant cathodic shift of the first oxidation potential ($E^{1/2}_{ox1}$) with the increased number of the annulated benzopyran rings. This was attributed to the stabilization of the radical cation species, formed upon the first oxidation process, due to the extension of the positive charge delocalization. In addition, CV investigation and NICS calculations of mono- and di- pyranoporphyrins revealed the inverse correlation between the second oxidation potential ($E^{1/2}_{ox2}$) and the antiaromaticity of porphyrin dication species. It was found that the major contribution in the global antiaromaticity of all O-embedded porphyrin dications comes from the 16π antiaromatic circuit. Besides, O-fusion with the pyrrole subunit results in additional aromatic 14π circuit, thus decreasing the antiaromatic character of the dication (Figure 5.2a). On the other hand, O-annulation with the azafulvene subunit increases the antiaromatic character through the emerging of an antiaromatic 24π conjugation pathway (Figure 5.2b). Notably, the global antiaromaticity of dipyranoporphyrin dication is determined by the superposition of aromatic 14π, antiaromatic 24π and 16π conjugated circuits.

The peripheral functionalization of porphyrin core with four or more O-atoms led to the formation of highly electron-saturated pyranoporphyrin systems, which can undergo the reaction with O_2 affording radical cation species. In case of octapyranoporphyrin **4-12**, the formation of oxygenated byproducts along with target macrocycle was observed. This was attributed to the photosensitization of highly reactive singlet molecular oxygen $^1O_2$ and subsequent reaction of $^1O_2$ with **4-12**.

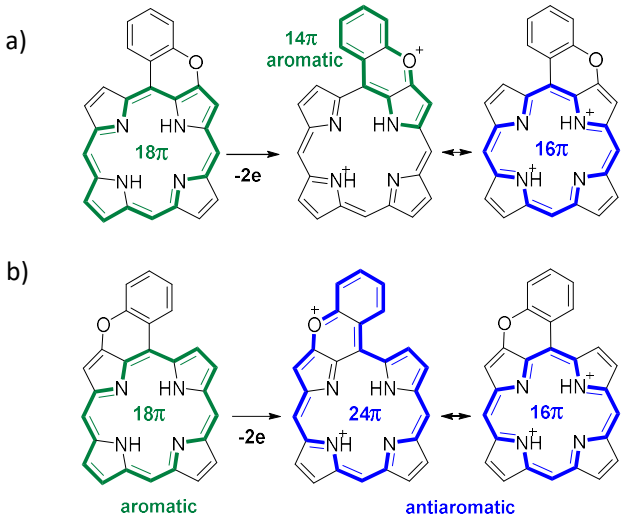

Figure 5.2 Resonance structures of monopyranoporphyrins with aromatic and antiaromatic circuits, demonstrating O-fusion with: a) pyrrole subunit; b) azafulvene subunit.

To conclude, four generations of novel π-extended O-embedded porphyrins have been prepared and the structure-property relationships thoroughly studied. The work presented in this manuscript has expanded the scope of peripheral functionalization of porphyrin macrocycle. Moreover, the obtained results can be used for rational engineering of novel porphyrin-based molecular devices, NLO dyads, photosensitizers *etc*.

6. Experimental part

6.1 Instrumentation

Thin layer chromatography (TLC) was conducted on pre-coated aluminium sheets with 0.20 mm *Merk Millipore* Silica gel 60 with fluorescent indicator F254. ***Column chromatography*** was carried out using *Merck Gerduran* silica gel 60 (particle size 40-63 μm). ***Melting points*** (M.p.) were measured on a *Buchi Melting Point* B-545 in open capillary tubes and have not been corrected. ***Nuclear magnetic resonance*** (NMR) spectra were recorded on a 270 MHz (*Jeol JNM EX-270*), 300 MHz (*Bruker Fourier*), 400 MHz (*Jeol JNM EX-400 or Bruker* AVANCE III HD), 500 MHz (*Jeol JNM EX-500 or Bruker)* or 600 MHz (*Bruker*) NMR at rt otherwise stated. Chemical shifts were reported in ppm according to tetramethylsilane using the solvent residual signal as an internal reference ($CDCl_3$: δ_H = 7.26 ppm, δ_C = 77.16 ppm; CD_2Cl_2: δ_H = 5.32, δ_C = 54.00; DMSO-*d6*: δ_H = 2.50 ppm, δ_C = 39.52 ppm; CD_3OD: δ_H = 3.31 ppm, δ_C = 49.00 ppm). Coupling constants (*J*) were given in Hz. Resonance multiplicity was described as *s* (singlet), *d* (doublet), *t* (triplet), *dd* (doublet of doublets), *dt* (doublet of triplets), *td* (triplet of doublets), *q* (quartet), *m* (multiplet) and *bs* (broad signal). Carbon spectra were acquired with a complete decoupling for the proton. ***Infrared spectra*** (IR) were recorded on *Perkin-Elmer Spectrum II FT-IR System* with *Specac* Silver Gate Evolution single-reflection ATR mounted with a ZnSe crystal or on a *Shimadzu IR Affinity 1S FTIR* spectrometer in ATR mode with a diamond mono-crystal. ***Photophysical analysis***: Absorption spectra of compounds were recorded on air equilibrated solutions at rt with *Agilent Cary 5000* UV-Vis spectrophotometer, using quartz cells with path length of 1.0 cm. Emission spectra were recorded on *Agilent Cary Eclipse* fluorescence spectrofluorometer. ***Mass spectrometry*** was generally performed by *i)* the *Centre de spectrométrie de masse at the Université de Mons in Belgium*. ESI-MS measurements were performed on a *Waters QToF2 mass spectrometer* operating in positive mode. The analyte solutions were delivered to the ESI source by a *Harvard Apparatus* syringe pump at a flow rate of 5 μL/min. Typical ESI conditions were, capillary voltage 3.1 kV; cone voltage 20-50 V; source temperature 80 °C; desolvation temperature 120°C. Dry nitrogen was used as the ESI gas. For the recording of the single-stage ESI-MS spectra, the quadrupole (rf-only mode)

was set to pass ions from 50 to 1000 Th, and all ions were transmitted into the pusher region of the time-of-flight analyzer where they were mass analyzed with 1 s integration time. MALDI-MS were recorded using a *Waters QToF Premier mass spectrometer* equipped with a nitrogen laser, operating at 337 nm with a maximum output of 500 mW delivered to the sample in 4 ns pulses at 20 Hz repeating rate. Time-of-flight analyses were performed in the reflectron mode at a resolution of about 10,000. The matrix solution (1 μL) was applied to a stainless steel target and air-dried. Analyte samples were dissolved in a suitable solvent to obtain 1 mg/mL solutions. 1 μL aliquots of those solutions were applied onto the target area already bearing the matrix crystals, and air-dried. For the recording of the single-stage MS spectra, the quadrupole (rf-only mode) was set to pass ions from 100 to 1000 Th, and all ions were transmitted into the pusher region of the time-of-flight analyzer where they were analyzed with 1 s integration time. *ii) Cardiff University, United Kingdom.* High-resolution ESI mass spectra (HRMS) were performed on a *Waters LCT HR TOF* mass spectrometer in the positive or negative ion mode.

6.2 Materials and general methods

Chemicals were purchased from *Sigma Aldrich, Acros Organics, TCI, Apollo Scientific, ABCR, Alfa Aesar, Carbosynth* and *Fluorochem* and were used as received. Solvents were purchased from *Fluorochem, Fisher Chemical* and *Sigma Aldrich,* while deuterated solvents from *Eurisotop* and *Sigma Aldrich.* THF and PhMe were dried on a Braun MB SPS-800 solvent purification system and further dried over activated 4 Å molecular sieves. $CHCl_3$ and CH_2Cl_2 were distilled from CaH_2 and then stored over 3 Å molecular sieves. Hexane was washed with conc. H_2SO_4 and a $KMnO_4$ solution in a 1M aqueous solution of NaOH (1 g of $KMnO_4$ every 50 mL of NaOH solution) and then distilled from CaH_2 and stored over 3 Å molecular sieves. Sulfuric acid (H_2SO_4 > 95%) was purchased from *Fluorochem*. All distilled solvents were left on CaH_2 overnight prior distillation. Low temperature baths were prepared using different solvent mixtures depending on the desired temperature: -78 °C with acetone/N_2 (liq.) or acetone/dry ice, -40 °C with MeCN/N_2 (liq.), -10 °C with ice-H_2O/NaCl, and 0 °C with ice/H_2O. Anhydrous conditions were achieved by keeping all glassware in oven at 140 °C for at least 12 h and then allowing to cool down under vacuum followed by drying Schlenk tubes or 2-necked flasks by flaming with a heat gun under vacuum and purging with N_2. The inert atmosphere was maintained using N_2-filled balloons equipped

with a syringe and needle that was used to penetrate the silicon stoppers used to close the flask's necks. Additions of liquid reagents were performed using dried plastic or glass syringes. Degassing of solutions was performed using *freeze-pump-thaw* procedure: solutions were frozen using N_2 (liq.) and kept under vacuum for 10 min before thawing. Molecular sieves (3 and 4 Å) were activated by heating at 180 °C under vacuum overnight and by further heating with heat gun under vacuum immediately before use. All reactions were performed in dry conditions and under inert atmosphere unless otherwise stated.

6.3 Experimental procedures

6.3.1 Chapter III

1-(*Tert*-butyl)-3-methoxybenzene 3-6

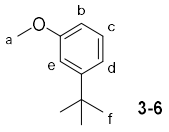

3-6

3-*Tert*-butylphenol (5.00 g, 33.3 mmol) was dissolved in dry THF (20 mL) and added to a stirred suspension of NaH 60% wt. (1.12 g, 46.6 mmol) in dry THF (20 mL) at 0 °C under N_2. The reaction mixture was stirred at 0 °C for 15 min, and methyl iodide (6.85 mL, 109.8 mmol) was added dropwise. The mixture was allowed to reach rt and then stirred for 16 h under reflux. The resulting orange solution was cooled down and quenched with H_2O (40 mL). The layers were separated, and the aqueous layer was extracted with Et_2O (3 × 40 mL). The combined organic extracts were washed with brine (40 mL) and H_2O (40 mL). The combined organic layers were dried over $MgSO_4$ and evaporated *in vacuo*. The residue was purified by SiO_2 column chromatography (eluent: cyclohexane/CH_2Cl_2 1:1) to give **3-6** (5.09 g, 95%) as a colourless oil. M.f.: $C_{11}H_{16}O$. M.w.: 164.25 g/mol. δ_H (400 MHz, $CDCl_3$) 7.25 (t, J = 8.0 Hz, 1H, H_c), 7.06–6.98 (m, 1H, H_d), 6.96 (t, J = 2.2 Hz, 1H, H_e), 6.74 (ddd, J = 8.1, 2.5, 0.8 Hz, 1H, H_b), 3.82 (s, 3H, H_a), 1.33 (s, 9H, H_f). δ_C (100.5 MHz, $CDCl_3$) 159.5, 153.1, 129.1, 118.0, 112.1, 110.0, 55.3, 34.9, 31.4. Spectral data are in agreement with previously reported data.[158]

4-(*Tert*-butyl)-2,6-dimethoxybenzaldehyde 3-4

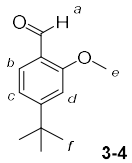

3-4

1-(*Tert*-butyl)-3-methoxybenzene **3-6** (500 mg, 3.12 mmol) was dissolved in MFA (1 mL, 8.11 mmol), and $POCl_3$ (1.06 mL, 11.55 mmol) was added dropwise at rt. The reaction mixture was stirred at 70-80 °C for 4 h. Then the resulting solution was cooled down and treated with a saturated aqueous solution of Na_2CO_3 (5 mL). The solution was diluted in CH_2Cl_2 (10 mL) and the organic phase was washed with H_2O (10 mL) and brine (10 mL). The aqueous phase was extracted with CH_2Cl_2 (2 x 15 mL). The combined organic layers were dried over $MgSO_4$ and evaporated *in vacuo*. The residue was purified by SiO_2 column chromatography (eluent: cyclohexane/CH_2Cl_2 1:1) to give **3-4** (490 mg, 82%) as yellow oil. M.f.: $C_{12}H_{16}O_2$. M.w.: 192.26 g/mol. δ_H (400 MHz, $CDCl_3$) 10.41 (d, 1H, J = 0.92 Hz, H_a), 7.76 (d, 1H, J = 8.24 Hz, H_b), 7.06 (dd, 1H, J = 8.24, 1.37 Hz, H_c), 6.97 (d, 1H, J = 1.37 Hz, H_d), 3.94 (s, 3H, H_e) 1.35 (s, 9H, H_f). δ_C (100.5 MHz, $CDCl_3$) 189.6, 161.9, 160.6, 128.5, 122.7, 118.2, 108.7, 55.6, 35.8, 31.2. Spectral data are in agreement with previously reported data.[159]

(5-(4-(*Tert*-butyl)-2-methoxyphenyl)-10,15,20-tris(4-(*tert*-butyl)phenyl)porphyrin 3-3

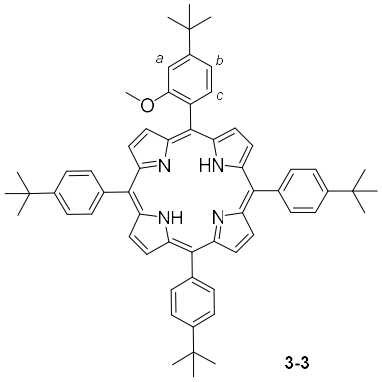

3-3

4-(*Tert*-butyl)-2-methoxybenzaldehyde **3-4** (0.336 g, 1.75 mmol), 4-(*tert*-butyl)benzaldehyde (0.85 g, 5.25 mmol) and pyrrole (490 µL, 7 mmol) were dissolved in freshly distilled CH_2Cl_2 (700 mL), and the resulting solution was degassed for 40 min by purge of Ar. This was followed by the dropwise addition of $BF_3{\cdot}Et_2O$ (130 µl, 1.05 mmol). The reaction mixture was stirred at rt for 1.5 h under Ar, and DDQ (1.27 g, 5.6 mmol) was added. The resulting dark solution was stirred for additional 1 h. The mixture was filtered through silica pad and

the solvent was evaporated *in vacuo*. The residue was purified by SiO_2 column chromatography (eluent: cyclohexane/CH_2Cl_2 2:3), and precipitation from MeOH yielded **3-3** (150 mg, 10%) as a purple solid. M.f.: $C_{61}H_{64}N_4O$. M.w.: 869.21 g/mol. M.p. > 300 °C. λ_{max} (CH_2Cl_2)/nm 419 (ε/mol^{-1} L cm^{-1} 129150), 486 (2875), 516 (15300), 552 (7967), 593 (4258), 647 (3724). ν_{max}/cm^{-1} 3315w (N-H), 2954m(Alk), 2864w(Alk), 1812w, 1607w, 1562w, 1502w, 1475m, 1459m, 1399m, 1361m, 1350m, 1285w, 1267w, 1220m, 1194m, 1132w, 1107m, 1072w, 1042w, 1022m, 993w, 982m, 967s, 915w, 880w, 850w, 839w, 801s, 744s, 731s, 711s, 692w, 655w. δ_H (300 MHz, C_6D_6) 9.06-8.99 (m, 8H, β-*H*), 8.20-8.10 (m, 7H, Ar*H*+H_c), 7.56-7.51 (m, 6H, Ar*H*), 7.24 (dd, J = 4.0, 2.3 Hz, 2H, H_a+H_b), 3.18 (s, 3H, OCH_3), 1.51 (s, 9H, 3CH_3), 1.44 (s, 9H, 3CH_3), 1.43 (s, 16H, 6CH_3), -1.92 (2H, s, N*H*). δ_C (126 MHz, $CDCl_3$) 159.3, 153.4, 150.5, 150.5, 139.5, 139.5, 135.5, 134.6, 128.4, 123.7, 120.3, 120.0, 116.6, 116.2, 108.6, 56.1, 35.5, 35.0, 31.9, 31.9 (10 peaks are missing due to the overlap). HRMS (MALDI): m/z $[M]^+$ calc. for $(C_{61}H_{64}N_4O)^+$: 868.5080, found: 868.5068.

(5-(4-(*Tert*-butyl)-2-hydroxyphenyl)-10,15,20-tris(4-(*tert*-butyl)phenyl)porphyrin 3-7

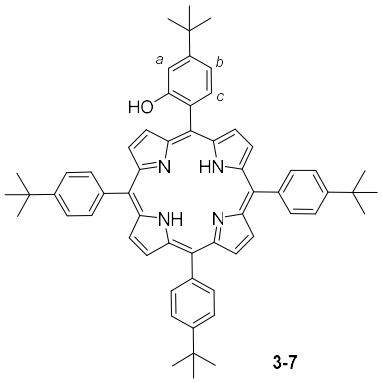

3-7

Porphyrin **3-3** (0.1 g, 0.115 mmol) was dissolved in freshly distilled CH_2Cl_2 (25 mL) and the resulting solution was degassed for 15 min by purge of Ar. This was followed by the dropwise addition of BBr_3 (1.15 mL of 1M solution in CH_2Cl_2, 1.15 mmol). The reaction mixture was stirred for 3 h at rt under Ar, and H_2O (25 mL) was added. The resulting solution was stirred for additional 1 h, and pyridine (2.5 mL) was added. The layers were separated, and the aqueous phase was extracted with CH_2Cl_2 (3 × 10 mL). The combined organic extracts were washed with brine (2 × 40 mL) and H_2O (2 × 40 mL), dried over $MgSO_4$ and evaporated *in vacuo*. The residue was purified by SiO_2 column chromatography (eluent: cyclohexane/CH_2Cl_2 2:3), and precipitation from MeOH afforded **3-7** (88 mg, 90%) as a purple solid. M.f.: $C_{60}H_{62}N_4O$. M.w.: 855.18 g/mol. M.p. > 300 °C. λ_{max} (CH_2Cl_2)/nm 420 (ε/mol^{-1} L cm^{-1} 250759), 487 (2567), 516 (16419), 552 (7994), 591 (4297), 647 (3230).

ν_{max}/cm^{-1} 3510w(O-H), 3314w(N-H), 2953m(Alk), 2863w(Alk), 1614w, 1556w, 1501w, 1473m, 1398m, 1360m, 1349m, 1291m, 1266m, 1217m, 1179m, 1108m, 1022m, 991m, 981m, 966s, 935m, 879m, 850m, 802s, 742m, 728s, 709m, 644m, 582m, 565m, 545m. δ_H (400 MHz, CD_2Cl_2) 9.18-8.66 (m, 8H, β-*H*), 8.15 (d, 6H, *J* = 8.4 Hz, Ar*H*), 7.91 (d, *J* = 8.4 Hz, 1H, H_c), 7.80 (d, *J* = 8.4 Hz, 6H, Ar*H*), 7.44-7.34 (m, 2H, H_a+H_b), 5.05 (s, 1H, O*H*), 1.61 (s, 27H, 9CH_3), 1.59 (s, 9H, 3CH_3), -2.80 (s, 2H, N*H*). HRMS (MALDI): m/z $[M]^+$ calc. for $(C_{60}H_{62}N_4O)^+$: 854.4924, found: 854.4894.

5-(4-(*Tert*-butyl)-2-hydroxyphenyl)-10,15,20-*tris*(4-(*tert*-butyl)phenyl)porphyrinato-N^{21},N^{22},N^{23},N^{24}-nickel(II) 3-2

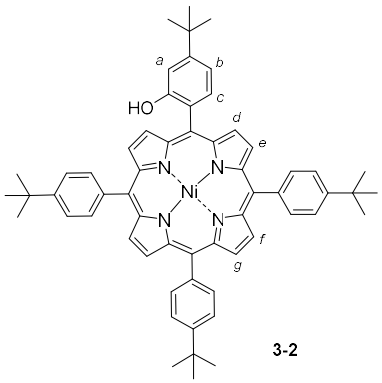

3-2

Porphyrin **3-7** (0.1 g, 0.115 mmol) was dissolved in PhMe (40 mL) and $Ni(acac)_2$ (0.73 g, 2.8 mmol) was added. The reaction mixture was stirred at 100 °C for 5 h under Ar. The mixture was cooled down and washed with H_2O (3 × 20 mL). The organic layer was dried over $MgSO_4$ and evaporated *in vacuo*. The residue was purified by SiO_2 column chromatography (eluent: cyclohexane/CH_2Cl_2 2:3), and precipitation from MeOH afforded **3-2** (236 mg, 93%) as a red solid. M.f.: $C_{60}H_{60}N_4NiO$. M.w.: 911.86 g/mol. M.p. > 300 °C. λ_{max} (CH_2Cl_2)/nm 416 (ε/mol^{-1} L cm^{-1} 177906), 528 (17693). ν_{max}/cm^{-1} 3550w(O-H), 3492w, 3027w, 2960m(Alk), 2901w(Alk), 2867w, 1806w, 1620w, 1559w, 1501w, 1460m, 1430w, 1392m, 1351m, 1297m, 1267m, 1225w, 1202m, 1180m, 1071m, 1004s, 940m, 866w, 852w, 812s, 794s, 741m, 727w, 712s, 696w, 654w, 567m, 519w, 476w. δ_H (500 MHz, $CDCl_3$) 8.82 (d, *J* = 4.9 Hz, 2H, H_d), 8.79 (s, 4H, $H_{f,g}$), 8.78 (d, *J* = 4.9 Hz, 2H, H_e), 7.94 (dd, *J* = 8.2, 1.9 Hz, 6H, Ar*H*), 7.73 (d, *J* = 7.9 Hz, 1H, H_c), 7.70 (d, *J* = 8.3 Hz, 6H, Ar*H*), 7.33 (d, *J* = 1.9 Hz, 1H, H_a), 7.28 (dd, *J* = 7.9, 2.0 Hz, 1H, H_b), 4.89 (br, 1H, O*H*), 1.56 (s, 27H, 3CH_3), 1.54 (s, 9H, CH_3). δ_C (126 MHz, $CDCl_3$) 154.8, 154.1, 150.8, 143.2, 143.0, 142.9, 142.8, 137.8, 137.8, 134.0, 133.7, 133.3, 132.7, 132.5, 131.7, 124.0, 123.7, 119.8, 119.4, 116.9, 112.6,

110.9, 35.1, 35.0, 31.8, 31.7 (5 peaks are missing due to the overlap). HRMS (MALDI): m/z $[M]^+$ calc. for $(C_{60}H_{60}N_4ONi)^+$: 910.4121, found: 910.4125.

10,15,20-*Tris*(4-(*tert*-butyl)phenyl)benzopyrano[a,t]porphyrinato-N^{21},N^{22},N^{23},N^{24}-nickel(II) 3-1

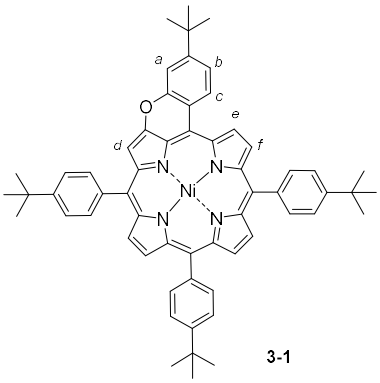

3-1

Porphyrin **3-2** (0.05 g, 0.05 mmol) was dissolved in $PhNO_2$ (2 mL), and CuO (0,026 g, 0.25 mmol) was added. The resulting mixture was stirred at 220 °C for 12 h. The mixture was cooled down, filtrated through celite pad and concentrated *in vacuo*. The residue was purified by SiO_2 column chromatography (eluent: CH_2Cl_2), and precipitation from MeOH afforded **3-1** (0.041 g, 92%) as a purple solid. M.f.: $C_{60}H_{58}N_4NiO$. M.w.: 909.84 g/mol. M.p. > 300 °C. λ_{max} (CH_2Cl_2)/nm 432 (ε/mol^{-1} L cm^{-1} 134000), 550 (9452), 595 (11330). ν_{max}/cm^{-1} 3028w, 2957m, 2622m, 2853m, 1804w, 1740w, 1582m, 1566m, 1505m, 1456m, 1409m, 1361m, 1328w, 1303m, 1268m, 1243m, 1215w, 1191m, 1182m, 1165m, 1143m, 1109m, 1071m, 1005s, 966m, 936w, 871w, 850w, 837w, 813s, 792s, 750m, 740m, 714m, 692m, 675m, 647m, 550m, 497w, 453m. δ_H (500 MHz, $CDCl_3$) 9.55 (d, J = 4.9 Hz, 1H, H_e), 8.95 (d, J = 4.9 Hz, 1H, H_f), 8.75-8.65 (m, 5H, β-H+H_c), 8.29 (s, 1H, H_d), 7.93 (m, 7H, ArH+H_a), 7.72-7.65 (m, 7H, ArH+H_b), 1.57 (s, 9H, 3CH_3), 1.56 (s, 9H, 3CH_3), 1.54 (s, 9H, 3CH_3), 1.54 (s, 9H, 3CH_3). δ_C (126 MHz, $CDCl_3$) 154.9, 152.2, 151.6, 150.7, 150.5, 143.1, 142.8, 142.4, 141.5, 140.5, 139.9, 137.8, 137.7, 137.0, 133.6, 133.4, 132.7, 132.6, 132.4, 131.7, 130.0, 127.3, 124.3, 124.0, 122.2, 120.0, 118.6, 117.7, 117.4, 114.7, 106.7, 104.2, 35.1, 35.0, 34.9, 31.7, 31.5 (9 peaks are missing due to the overlap). HRMS (MALDI): m/z $[M]^+$ calc. for $(C_{60}H_{58}N_4ONi)^+$: 908.3964, found: 908.3987.

5-(4-(*Tert*-butyl)-2-hydroxyphenyl)-10,15,20-*tris*(4-(*tert*-butyl)phenyl)porphyrinato-N^{21},N^{22},N^{23},N^{24}-copper(II) 3-8

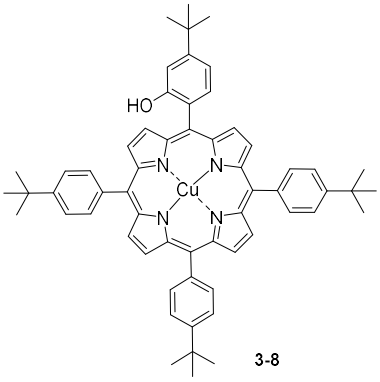

3-8

To the solution of **3-7** (30 mg, 0.035 mmol) in CH_2Cl_2 (14 mL) the solution of $Cu(OAc)_2$ (6.4 mg, 0.35 mmol) in MeOH (3 mL) was added, and the mixture was stirred at 50 °C for 2 h. The mixture was cooled down and the organic phase was washed with H_2O (3 × 10 mL). The aqueous phase was extracted with CH_2Cl_2 (3 × 15 mL). The combined organic layers were dried over $MgSO_4$ and evaporated *in vacuo*. The residue was purified by SiO_2 chromatography (eluent: cyclohexane/CH_2Cl_2 1:1), and precipitation from MeOH afforded **3-8** (30 mg, 94%) as a purple solid. M.f.: $C_{60}H_{60}N_4CuO$. M.w.: 916.71 g/mol. M.p. > 300 °C. λ_{max} (CH_2Cl_2)/nm 417 (ε/mol^{-1} L cm^{-1} 252281), 540 (15665). ν_{max}/cm^{-1} 3558w, 3507w, 2956m, 2863m, 1814w, 1620w, 1561w, 1538w, 1501m, 1461m, 1429w, 1394m, 1361m, 1345m, 1301m, 1265m, 1220w, 1203m, 1179m, 1108m, 1070m, 1012m, 997s, 967m, 937m, 878w, 852m, 800s, 737m, 717s, 697m, 652w, 585m, 566m, 465m. HRMS (MALDI): m/z $[M]^+$ calc. for $(C_{60}H_{60}N_4OCu)^+$: 915.4063, found: 915.4034.

5-(4-(*Tert*-butyl)-2-hydroxyphenyl)-10,15,20-*tris*(4-(*tert*-butyl)phenyl)porphyrinato-N^{21},N^{22},N^{23},N^{24}-silver(II) 3-9

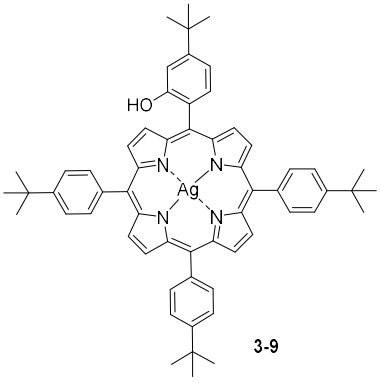

3-9

To the solution of **3-7** (30 mg, 0.035 mmol) in CH_2Cl_2 (14 mL) the solution of AgOAc (5.9 mg, 0.35 mmol) in AcOH (3 mL) was added, and the mixture was stirred at 50 °C for 2 h. The mixture was cooled down and washed with H_2O (3 × 10 mL). The aqueous phase was extracted with CH_2Cl_2 (3 × 15 mL). The combined organic layers were dried over $MgSO_4$ and evaporated *in vacuo*. The residue was purified by SiO_2 column chromatography (eluent: cyclohexane/CH_2Cl_2 1:1), and precipitation from MeOH afforded desired **3-9** (30.2 mg, 90%) as a purple solid. M.f.: $C_{60}H_{60}N_4AgO$. M.w.: 961.03 g/mol. M.p. > 300 °C. λ_{max} (CH_2Cl_2)/nm 427 (ε/mol^{-1} L cm^{-1} 281493), 543 (15116), 578 (841). ν_{max}/cm^{-1} 2958m, 2865m, 1612m, 1561w, 1537w, 1517w, 1460m, 1349m,1362m, 1338m, 1294m, 1264m, 1201m, 1181m, 1107m, 1061m, 1004s, 967m, 937m, 868w, 850m, 806s, 794s, 739m, 714s, 652m, 584m, 564m, 528m, 461w. HRMS (MALDI): m/z $[M]^+$ calc. for $(C_{60}H_{60}N_4OAg)^+$: 959.3818, found: 959.3784.

5-(4-(*Tert*-butyl)-2-hydroxyphenyl)-10,15,20-*tris*(4-(*tert*-butyl)phenyl)porphyrinato-N^{21},N^{22},N^{23},N^{24}-palladium(II) 3-10

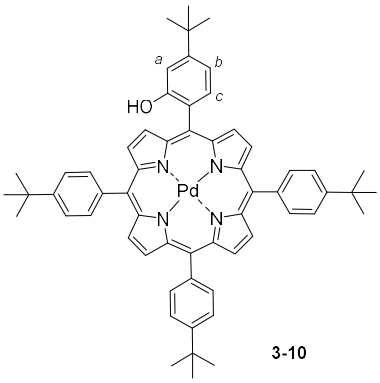

3-10

To the solution of **3-7** (30 mg, 0.035 mmol) in CH_2Cl_2 (14 mL) the solution of $Pd(OAc)_2$ (7.9 mg, 0.35 mmol) in MeOH (3 mL) was added, and the mixture was stirred at 50 °C for 2 h. The mixture was cooled down and the organic phase was washed with H_2O (3 × 10 mL). The aqueous phase was extracted with CH_2Cl_2 (3 × 15 mL). The combined organic layers were dried over $MgSO_4$ and evaporated *in vacuo*. The residue was purified by SiO_2 column chromatography (eluent: cyclohexane/CH_2Cl_2 1:1), and precipitation from MeOH afforded **3-10** (30.8 mg, 92%) as a red solid. M.f.: $C_{60}H_{60}N_4PdO$. M.w.: 909.84 g/mol. M.p. > 300 °C. λ_{max} (CH_2Cl_2)/nm 418 (ε/mol^{-1} L cm^{-1} 269675), 524 (24123). ν_{max}/cm^{-1} 3560w, 3508w, 2955m, 2863m, 1620w, 1561w, 1542w, 1502m, 1461m, 1394m, 1352m, 1302m, 1266m, 1209m, 1179m, 1110m, 1077m, 1010s, 938m, 870w, 853m, 816s, 797s, 735m, 713s, 695m, 653w, 590m, 570m, 514w, 473w. δ_H (500 MHz, $CDCl_3$) 8.88-8.77 (m, 8H, β-*H*), 8.08 (dd, *J*

= 6.4, 2.0 Hz, 6H, Ar*H*), 7.84 (d, *J* = 7.9 Hz, 1H, H_c), 7.73 (d, *J* = 8.3 Hz, 6H, Ar*H*), 7.37 (d, *J* = 1.9 Hz, 1H, H_a), 7.32 (dd, *J* = 7.8, 1.9 Hz, 1H, H_b), 4.96 (br, 1H, O*H*), 1.59 (s, 27H, 9CH_3), 1.57 (s, 9H, 3CH_3). ^{13}C NMR was not reordered due to the low solubility of the compound. HRMS (MALDI): m/z $[M]^+$ calc. for $(C_{60}H_{60}N_4OPd)^+$: 956.3807, found: 956.3768.

5-(4-*Tert*-butyl-2-hydroxyphenyl)-10,15,20-tris(4-tert-butylphenyl)porphyrinato-N^{21},N^{22},N^{23},N^{24}-zinc(II) 3-11

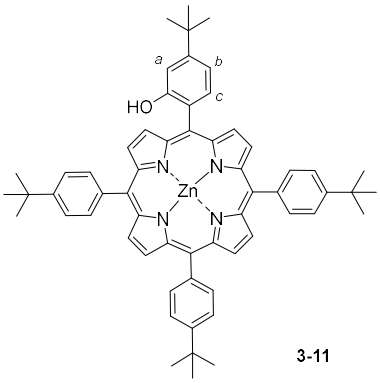

3-11

To the solution of porphyrin **3-7** (30 mg, 0.035 mmol) in CH_2Cl_2 (14 mL) the solution of $Zn(OAc)_2$ (64 mg, 0.35 mmol) in MeOH (3 mL) was added, and the mixture was stirred at 50 °C for 2 h. The reaction solution was cooled down and and the organic phase was washed with H_2O (3 × 10 mL). The aqueous phase was extracted with CH_2Cl_2 (3 × 15 mL). The combined organic layers were dried over $MgSO_4$ and evaporated *in vacuo*. The residue was purified by SiO_2 column chromatography (eluent: cyclohexane/CH_2Cl_2 1:1), and precipitation from MeOH afforded **3-11** (25 mg, 78%) as a red solid. M.f.: $C_{60}H_{60}N_4ZnO$. M.w.: 918.55 g/mol. M.p. > 300 °C. λ_{max} (CH_2Cl_2)/nm 420 (ε/mol^{-1} L cm^{-1} 200439), 548 (24127), 588 (5132). ν_{max}/cm^{-1} 3557w, 2954m, 2862w, 1614w, 1560w, 1527w, 1492m, 1460m, 1428w, 1398w, 1360m, 1338m, 1300m, 1267m, 1205m, 1180m, 1109m, 1073m, 1025m, 996s, 937m, 881w, 852m, 815s, 799s, 734m, 719s, 695m, 652m, 586m, 569m, 549m, 463w. δ_H (300 MHz, C_6D_6) 9.19-9.13 (m, 8H, β-*H*), 8.24 (d, *J* = 8.2 Hz, 6H, Ar*H*), 8.04 (d, *J* = 7.9 Hz, 1H, H_c), 7.56 (d, *J* = 8.4 Hz, 7H, Ar*H*+H_a), 7.24 (dd, *J* = 7.9, 1.9 Hz, 1H, H_b), 1.41 (s, 36H, 12CH_3); δ_C (75 MHz, C_6D_6) 155.9, 153.2, 150.9, 150.8, 150.6, 149.7, 140.8, 140.7, 134.8, 132.8, 132.2, 132.1, 131.3, 126.7, 123.4, 121.9, 121.3, 116.3, 112.7, 112.5, 34.7, 34.5, 31.4, 31.3 (one peak is missing due to the overlap); HRMS (MALDI): m/z $[M]^+$ calc. for $(C_{60}H_{59}N_4OZn)^+$: 915.3980, found: 915.3952.

10,15,20-*Tris*(4-(*tert*-butyl)phenyl)benzopyrano[a,t]porphyrinato-N^{21},N^{22},N^{23},N^{24}-copper(II) 3-12

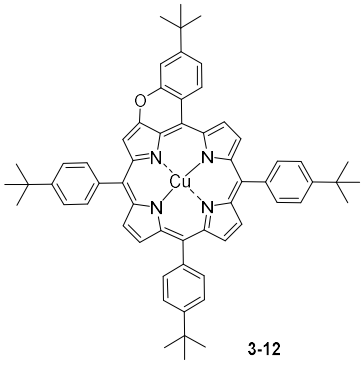

3-12

Cu(II) porphyrin **3-8** (15 mg, 0.0163 mmol) was dissolved in $PhNO_2$ (2 mL), and CuO (12 mg, 0.163 mmol) was added. The resulting mixture was stirred at 220 °C for 16 h. The reaction solution was cooled down, filtrated through celite pad and concentrated *in vacuo*. The residue was purified by SiO_2 column chromatography (eluent: CH_2Cl_2), and precipitation from MeOH afforded **3-12** (13 mg, 87%) as a purple solid. M.f.: $C_{60}H_{58}N_4CuO$. M.w.: 914.70 g/mol. M.p. > 300 °C. λ_{max} (CH_2Cl_2)/nm 434 (ε/mol^{-1} L cm^{-1} 225368), 559 (14879), 608 (22682). ν_{max}/cm^{-1} 2957m, 2924m, 2864m, 1737w, 1573m, 1494m, 1461m, 1408m, 1392m, 1362m, 1297m, 1267m, 1240m, 1191m, 1179m, 1162m, 1142m, 1108m, 1070m, 1000s, 963m, 936w, 871w, 863w, 849w, 812m, 794s, 740m, 717m, 694m, 680w, 650m, 568m, 470w. HRMS (MALDI): m/z $[M]^+$ calc. for $(C_{60}H_{58}N_4OCu)^+$: 913.3907, found: 913.3927.

10,15,20-*Tris*(4-(*tert*-butyl)phenyl)benzopyrano[a,t]porphyrinato-N^{21},N^{22},N^{23},N^{24}-palladium(II) 3-13

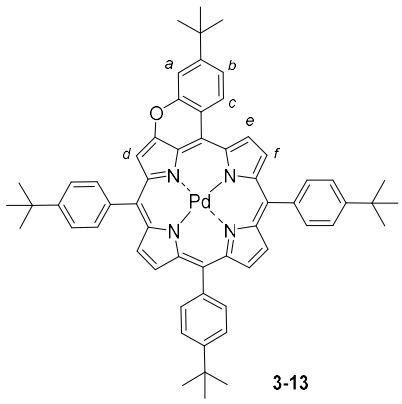

3-13

Pd(II) porphyrin **3-10** (15 mg, 0.0156 mmol) was dissolved in $PhNO_2$ (2 mL) and CuO (11 mg, 0.156 mmol) was added. The resulting mixture was stirred at 220 °C for 16 h. The

reaction solution was cooled down, filtrated through celite pad and concentrated *in vacuo*. The residue was purified by SiO_2 column chromatography (eluent: CH_2Cl_2), and precipitation from MeOH afforded **3-13** (14 mg, 93%) as a purple solid. M.f.: $C_{60}H_{58}N_4PdO$. M.w.: 957.57 g/mol. M.p. > 300 °C. λ_{max} (CH_2Cl_2)/nm 435 (ε/mol^{-1} L cm^{-1} 166502), 544 (7442), 590 (14636). ν_{max}/cm^{-1} 3028w, 2958m, 2901m, 2865m, 1803w, 1624w, 1572m, 1501m, 1461m, 1443m, 1408m, 1393m, 1361m, 1352m, 1329m, 1303m, 1267m, 1247m, 1182m, 1163m, 1142m, 1108m, 1072m, 1041w, 1012s, 969m, 936m, 870m, 849m, 812m, 791s, 749m, 739m, 714m, 693m, 677m, 648m, 603w, 568m, 552m, 470m. δ_H (500 MHz, $CDCl_3$) 9.77 (d, J = 4.9 Hz, 1H, H_e), 9.14 (d, J = 8.4 Hz, 1H, H_c), 8.99 (d, J = 4.9 Hz, 1H, H_f), 8.88-8.73 (m, 4H, β-*H*), 8.42 (s, 1H, H_d), 8.13-8.04 (m, 6H, Ar*H*), 8.01 (d, J = 2.0 Hz, 1H, 7.79-7.64 (m, 7H, Ar*H*+ H_b), 1.61 (s, 18H, 6CH_3), 1.58 (s, 9H, 3CH_3), 1.58 (s, 9H, 3CH_3). δ_C (126 MHz, $CDCl_3$) 153.5, 152.3, 151.7, 150.7, 150.5, 142.0, 141.5, 140.6, 139.6, 139.3, 138.9, 138.8, 138.7, 136.4, 134.1, 133.8, 133.3, 131.9, 131.6, 131.3, 131.2, 130.6, 127.9, 126.9, 124.1, 123.8, 123.7, 123.5, 122.2, 120.4, 119.7, 114.9, 110.1, 103.0, 35.1, 35.0, 31.8, 31.5 (5 peaks are missing due to the overlap). HRMS (MALDI): m/z [M]$^+$ calc. for $(C_{60}H_{58}N_4OPd)^+$: 954.3651, found: 954.3666.

10,15,20-*Tris*(4-(*tert*-butyl)phenyl)benzopyrano[a,t]porphyrin 3-14

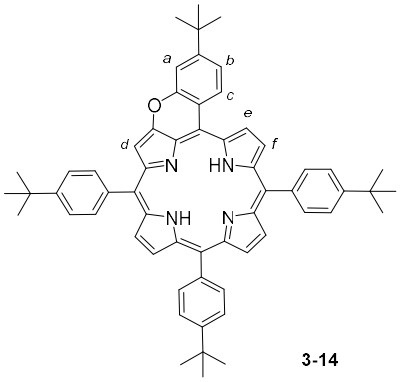

3-14

Ni(II) porphyrin **3-1** (60 mg, 0.066 mmol) was dissolved in CH_2Cl_2 (3mL), TFA (12 mL) and conc. H_2SO_4 (1 mL) were sequentially added slowly at 0 ºC. The resulting solution was stirred at 0 ºC for 15 min, poured into iced water and neutralized with saturated aqueous solution of $NaHCO_3$ (20 mL). The aqueous phase was separated and extracted with CH_2Cl_2 (3 × 15 mL). The combined organic layers were washed with H_2O (3 × 15 mL), dried over $MgSO_4$ and evaporated *in vacuo*. The residue was purified by SiO_2 column chromatography (eluent: cyclohexane/CH_2Cl_2 1:1), and precipitation from MeOH afforded **3-14** (47 mg, 84%) as a purple solid. M.f.: $C_{60}H_{60}N_4O$. M.w.: 853.17 g/mol. M.p. > 300 °C. λ_{max} (CH_2Cl_2)/nm

431 (ε/mol^{-1} L cm^{-1} 145716), 506 (1655), 541 (3790), 580 (15270), 602 (5293), 655 (3620). ν_{max}/cm^{-1}2956m, 2864m, 1588m, 1557m, 1538m, 1504w, 1470m, 1403m, 1360m, 1314m, 1260m, 1235m, 1193w, 1172w, 1153m, 1108m, 1021m, 997w, 979m, 964m, 871w, 849m, 799s, 720s, 689m, 650m, 577m, 566w. δ_H (300 MHz, C_6D_6) 9.65 (d, J = 4.8 Hz, 1H, H_e), 9.24 (d, J = 8.6 Hz, 1H, H_c), 9.12-8.92 (m, 5H, β-H+H_f), 8.81 (s, 1H, H_d), 8.17 (ddd, J = 17.8, 10.3, 5.1 Hz, 7H, ArH+H_a), 7.59 (ddd, J = 8.2, 6.9, 3.3 Hz, 7H, ArH+H_b), 1.48 (s, 18H, 6CH_3), 1.43 (s, 9H, 3CH_3), 1.42 (s, 9H, 3CH_3), -1.38 (s, 2H, NH). δ_C (126 MHz, $CDCl_3$) 152.1, 150.9, 150.7, 150.5, 139.4, 139.2, 139.1, 134.8, 134.5, 134.2, 132.8, 124.2, 123.7, 122.4, 122.0, 120.0, 119.4, 118.9, 114.9, 108.1, 105.1, 35.2, 35.0, 31.8, 31.5 (19 peaks are missing due to the overlap). HRMS (MALDI): m/z [M]$^+$ calc. for $(C_{60}H_{61}N_4O)^+$: 853.4845, found: 853.4843.

10,15,20-*Tris*(4-(*tert*-butyl)phenyl)benzopyrano[a,t]porphyrinato-N^{21},N^{22},N^{23},N^{24}-zinc(II) 3-15

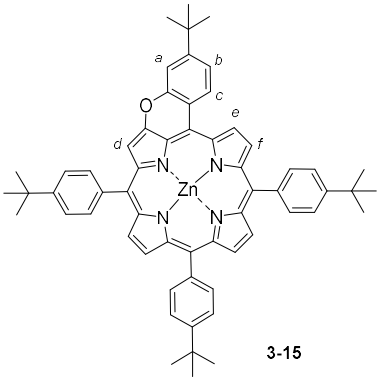

3-15

Free-base porphyrin **3-14** (25 mg, 0.029 mmol) was dissolved in CH_2Cl_2 (10 mL), and the solution of $Zn(OAc)_2$ (53 mg, 0.29 mmol) in MeOH (3 mL) was added. The resulting mixture was stirred at 50 °C for 2 h. The reaction solution was cooled down and washed with H_2O (3 × 10 mL). Organic layer was dried over $MgSO_4$ and evaporated *in vacuo*. The residue was purified by SiO_2 column chromatography (eluent: cyclohexane/CH_2Cl_2 1:1), and precipitation from MeOH yielded **3-15** (23 mg, 90%) as a green solid. M.f.: $C_{60}H_{58}N_4ZnO$. M.w.: 916.53 g/mol. M.p. > 300 °C. λ_{max} (CH_2Cl_2)/nm 437 (ε/mol^{-1} L cm^{-1} 333299), 565 (16336), 618 (34033). ν_{max}/cm^{-1} 2955m, 2864w, 1697w, 1566m, 1542w, 1482m, 1460m, 1393m, 1361m, 1334m, 1307m, 1292m, 1266m, 1231m, 1193m, 1175m, 1140m, 1108m, 1069m, 996s, 935w, 865w, 849m, 810s, 794s, 724s, 697m, 684m, 647m, 568m, 469w. δ_H (500 MHz, C_6D_6) 9.54 (d, J = 4.5 Hz, 1H, H_e), 9.26 (d, J = 8.4 Hz, 1H, H_c), 9.08 (dd, J = 6.0, 2.7 Hz, 4H, β-H), 8.93 (d, J = 4.5 Hz, 1H, H_f), 8.72 (s, 1H, H_d), 8.33-8.18 (m, 7H, ArH), 8.11 (d, J = 2.0

Hz, 1H, H_a), 7.65 (dd, J = 8.2, 6.4 Hz, 4H, Ar*H*), 7.60 (d, J = 8.2 Hz, 2H, Ar*H*), 7.56 (dd, J = 8.4, 2.0 Hz, 1H, H_b), 1.48 (s, 9H, 3CH_3), 1.48 (s, 9H, 3CH_3), 1.44 (s, 9H, 3CH_3), 1.39 (s, 9H, 3CH_3. δ_C (126 MHz, C_6D_6) 155.0, 152.0, 151.3, 151.0, 150.9, 150.1, 150.0, 149.9, 148.7, 148.4, 147.5, 145.2, 140.7, 140.6, 140.5, 134.8, 134.7, 134.4, 134.3, 133.7, 132.3, 131.8, 131.2, 124.1, 123.7, 123.6, 123.2, 122.0, 121.2, 119.9, 119.8, 115.1, 109.2, 104.3, 34.6, 34.6, 31.5, 31.2 (13 peaks are missing due to the overlap). HRMS (MALDI): m/z $[M]^+$ calc. for $(C_{60}H_{59}N_4OZn)^+$: 915.3980, found: 915.3980.

4-(*Tert*-butyl)-2,6-dimethoxyphenol 3-23

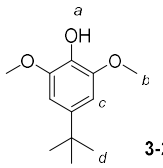

3-23

2,6-Dimethoxyphenol **3-22** (1.01 g, 6.48 mmol) was dissolved in methanesulfonic acid (1.6 mL). The resulting mixture was heated at 40 °C and *tert*-BuOH (1.81 mL, 19.44 mmol) was slowly added during 1.5 h, keeping the temperature of the solution around 50-55 °C. The reaction solution was further stirred for 2 h at 50 °C. The mixture was poured into ice and extracted with Et_2O (3 × 20 mL). The combined extracts were washed with H_2O (3 × 10 mL), saturated aqueous solution of $NaHCO_3$ (2 × 20 mL) and H_2O (2 × 10 mL), dried over $MgSO_4$ and evaporated *in vacuo*. The residue was purified by SiO_2 column chromatography (eluent: cyclohexane/EtOAc 1:1) to afford **3-23** (1.06 g, 78%) as a pale-yellow oil. M.f.: $C_{12}H_{18}O_3$. M.w.: 210.27 g/mol. δ_H (400 MHz, $CDCl_3$) 6.60 (s, 2H, H_c), 5.48 (s, 1H, H_a), 3.87 (s, 6H, H_b), 1.30 (s, 9H, H_d); δ_C (100.5 MHz, $CDCl_3$) 146.6, 142.7, 132.7, 102.5, 56.5, 34.9, 31.7. Spectral data are in agreement with previously reported data.[158]

4-(*Tert*-butyl)-2,6-dimethoxybenzaldehyde 3-24

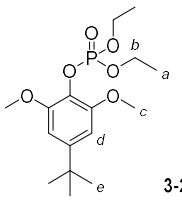

3-24

4-(*Tert*-butyl)-2,6-dimethoxyphenol **3-23** (3.88 g, 18.46 mmol) was dissolved in a mixture of CCl_4 (1 mL) and $HPO(OEt)_2$ (3.56 mL, 27.66 mmol) in anhydrous condition at 0 °C. Et_3N

(4.11 mL, 29.54 mmol) was added slowly in order to keep the temperature under 10 °C, and the resulting solution was stirred for 16 h at rt. The mixture was then concentrated, and the crude was diluted with 5 mL of Et_2O and 5 mL of H_2O. The aqueous phase was separated and extracted with Et_2O (3 × 5 mL). The combined organic phases were washed with H_2O (20 mL), 1M aqueous solution of HCl (2 × 15 mL), H_2O (15 mL), 4M aqueous solution of NaOH (2 × 15 mL) and dried over $MgSO_4$. After evaporation to dryness, hot recrystallization from *n*-hexane yielded **3-24** (3.60 g, 39%) as a pale white-yellow flakes. M.f.: $C_{16}H_{27}O_6P$. M.w.: 346.36 g/mol. M.p.: 72-74 °C. δ_H (400 MHz, $CDCl_3$) 6.59 (s, 2H, H_d), 4.29 (q, 4H, J = 7.10 Hz, H_b), 3.84 (s, 6H, C H_c), 1.37 (td, 6H, J = 7.10 Hz, H_a), 1.28 (s, 9H, H_e). δ_C (100.5 MHz, $CDCl_3$) 151.3, 148.5, 127.6, 102.7, 64.3, 56.2, 35.1, 31.5, 16.2. Spectral data are in agreement with previously reported data. [158]

1,3-Dimethoxy-5-(*tert*-butyl)benzene 3-25

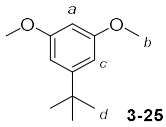

3-25

To a 250-mL three-necked round-bottom flask charged with NH_3 (liq.) (30 mL, 1.20 mol) activated Li (300 mg, 43.22 mmol) was added in anhydrous conditions, under Ar and at -78 °C, resulting in a blue solution. This was followed by the addition of **3-24** (5 g, 14.36 mmol) in dry THF (20 mL) at -78 °C. If the blue color of solution disappeared after the addition of the reagent, more Li (100 mg, 14.40 mmol) was added until the blue coloration remained. Once the addition was completed, the blue mixture was stirred for 20 min at reflux. The reaction mixture was then quenched with NH_4Cl. After evaporation of NH_3, the crude was diluted with Et_2O. Subsequently, the aqueous phase was extracted with Et_2O (3 × 15 mL) and the combined organic phases were washed with H_2O (2 × 15 mL), 2M aqueous solution of NaOH (2 × 20 mL), H_2O (2 × 15 mL), dried over $MgSO_4$ and evaporated *in vacuo*. The residue was recrystallized twice from cyclohexane yielding **3-25** (2.73 g, 93%) as a white solid. M.f.: $C_{12}H_{18}O_2$. M.w.: 194.27 g/mol. M.p.: 47-49 °C. δ_H (400 MHz, $CDCl_3$) 6.55 (d, 2H, J = 2.29 Hz, H_c), 6.31 (t, 1H, J = 2.29 Hz, H_a), 3.80 (s, 6H, H_b), 1.30 (s, 9H, H_d). δ_C (100.5 MHz, $CDCl_3$) 160.6, 153.9, 104.2, 96.8, 55.3, 35.1, 31.4. Spectral data are in agreement with previously reported data. [158]

4-(*Tert*-butyl)-2,6-dimethoxybenzaldehyde 3-21

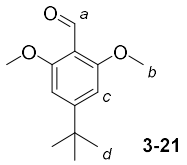

3-21

1,3-Dimethoxy-5-(*tert*-butyl)benzene **3-25** (250 mg, 1.29 mmol) was dissolved in dry THF (25 mL), and *n*-BuLi (0.95 mL, 1.42 mmol, 1.5M in hexane) was added dropwise at -40 °C under Ar and in anhydrous conditions. The resulting mixture was stirred for 15 min at -40 °C and 5 min at rt allowing the colour of the reaction to turn yellowish. This was followed by the addition of anhydrous DMF (110 µL, 1.42 mmol) at -40 °C. The resulting mixture was cooled down and stirred for 16 h at rt. Then Et_2O (20 mL) was added and the mixture was washed with H_2O (20 mL). The aqueous phase was extracted with Et_2O (3 × 20 mL). The combined organic layers were dried over $MgSO_4$ and evaporated *in vacuo*. The residue was purified by SiO_2 column chromatography (eluent: cyclohexane/EtOAc 8:2) to give **3-21** (112 mg, 39%) as a yellow solid. M.f.: $C_{13}H_{18}O_3$. M.w.: 222.28 g/mol. M.p.: 73-74 °C. δ_H (400 MHz, $CDCl_3$) 10.45 (s, 1H, H_a), 6.57 (s, 2H, H_c), 3.90 (s, 6H, H_b), 1.33 (s, 9H, H_d). δ_C (75 MHz, $CDCl_3$) 189.2, 162.2, 160.8, 112.2, 101.3, 56.0, 36.1, 31.1.

5-(4-(*Tert*-butyl)-2,6-dimethoxyphenyl)-10,15,20-*tris*(4-(*tert*-butyl)phenyl)porphyrin 3-20

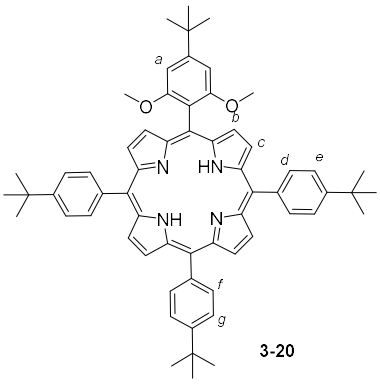

3-20

4-(*Tert*-butyl)-2,6-dimethoxybenzaldehyde **3-21** (500 mg, 2.24 mmol), 4-(*tert*-butyl)-benzaldehyde (1.13 mL, 6.72 mmol) and pyrrole (622 µl, 8.97 mmol) were dissolved in freshly distilled CH_2Cl_2 (700 mL) and the resulting solution was degassed for 40 min by purge of Ar. This was followed by the dropwise addition of $BF_3 \cdot Et_2O$ (160 µl, 1.25 mmol). The reaction mixture was stirred at rt for 1.5 h under Ar, and DDQ (1.52 g, 6.72 mmol) was added. The resulting dark solution was stirred for additional 1 h. The mixture was filtered through silica pad and the solvent was evaporated *in vacuo*. The residue was purified by SiO_2

column chromatography (eluent: cyclohexane/CH_2Cl_2 2:3), and precipitation from MeOH yielded **3-20** (280 mg, 14%) as a purple solid. M.f.: $C_{62}H_{66}N_4O_2$. M.w.: 899.24 g/mol. M.p. > 300 °C. ν_{max}/cm^{-1} 2957w, 2925w, 2903w, 2864w, 2850w, 1604w, 1567w, 1473w, 1461w, 1406m, 1361w, 1347w, 1316w, 1266w, 1241m, 1220w, 1195w, 1183w, 1127s, 1107s, 1069w, 1046w, 1023.0505w, 992w, 981w, 966s, 925w, 848w, 835w, 797s, 732m, 709m, 664w, 622w, 577w, 555w. δ_H (500 MHz, C_6D_6) 9.08 (d, J = 4.7 Hz, 2H, H_b), 8.92-8.96 (m, 6H; β-H+H_c), 8.08 (d, J = 8.2 Hz, 2H, H_g), 8.00 (d, J = 8.3 Hz, 4H, H_e), 7.50 (d, J = 8.3 Hz, 2H, H_f), 7.47 (d, J = 8.3 Hz, 4H, H_d), 6.97 (s, 2H, ArH), 3.11 (s, 6H, OCH_3), 1.50 (s, 9H, 3CH_3), 1.37 (s, 9H, 3CH_3), 1.36 (s, 18H, 6CH_3), -1.95 (s, 2H, NH). δ_C (126 MHz, $CDCl_3$) 160.2, 154.0, 150.4, 139.6, 139.5, 134.6, 123.6, 120.2, 119.6, 117.5, 112.3, 101.9, 56.2, 35.8, 35.0, 31.8, 31.7; HRMS (MALDI): m/z $[M]^+$ calc. for $(C_{62}H_{66}N_4O_2)^+$: 898.5186, found: 898.5198.

5-(4-(*Tert*-butyl)-2,6-dihydroxyphenyl)-10,15,20-*tris*(4-(*tert*-butyl)phenyl)porphyrin 3-26

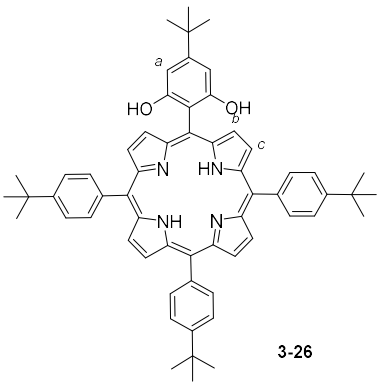

3-26

Porphyrin **3-20** (50 mg, 0.056 mmol) was dissolved in freshly distilled CH_2Cl_2 (10 mL) and the resulting solution was degassed for 30 min by purge of Ar. This was followed by the dropwise addition of BBr_3 (0.6 mL of 1 M solution in CH_2Cl_2, 0.6 mmol). The reaction mixture was stirred for 3 h at rt under Ar, and H_2O (10 mL) was added. The resulting solution was stirred for additional 1 h, and pyridine (1 mL) was added. The layers were separated, and the aqueous phase was extracted with CH_2Cl_2 (3 × 10 mL). The combined organic extracts were washed with brine (2 × 40 mL) and H_2O (2 × 40 mL), dried over $MgSO_4$ and evaporated *in vacuo*. The residue was purified by SiO_2 column chromatography (eluent: cyclohexane/CH_2Cl_2 2:3), and precipitation from MeOH afforded **3-26** (42 mg, 86%) as a purple solid. M.f.: $C_{60}H_{62}N_4O_2$. M.w.: 871.18 g/mol. M.p. > 300 °C. λ_{max} (CH_2Cl_2)/nm 420 (ε/mol^{-1} L cm^{-1} 84101), 516 (3196), 552 (656). ν_{max}/cm^{-1} 3315w, 2955m, 1630w, 1562m, 1504w, 1474m, 1396m, 1361m, 1347m, 1266m, 1221m, 1194m, 1161m, 1107m, 1044m,

1020m, 992m, 980m, 966s, 879w, 848m, 799s, 729s, 644m, 578m, 547m. δ_H (500 MHz, C_6D_6) δ 9.00 (d, J = 4.9 Hz, 2H, H_b), 8.98-8.91 (m, 4H, β-*H*), 8.82 (d, J = 4.6 Hz, 2H, H_c), 8.10-7.96 (m, 6H, Ar*H*), 7.52–7.43 (m, 6H, Ar*H*), 7.11 (s, 2H, H_a), 1.39 (s, 9H, 3CH_3), 1.37 (s, 27H, 9CH_3), -2.15 (s, 2H, N*H*); δ_C (126 MHz, $CDCl_3$) 155.8, 155.2, 150.9, 139.0, 138.7, 134.6, 123.8, 123.7, 122.2, 120.9, 112.9, 105.1, 103.8, 35.0, 31.8, 31.7.

5-(4-(*Tert*-butyl)-2,6-hydroxyphenyl)-10,15,20-*tris*(4-(*tert*-butyl)phenyl)porphyrinato-N^{21},N^{22},N^{23},N^{24}-nickel(II) 3-19

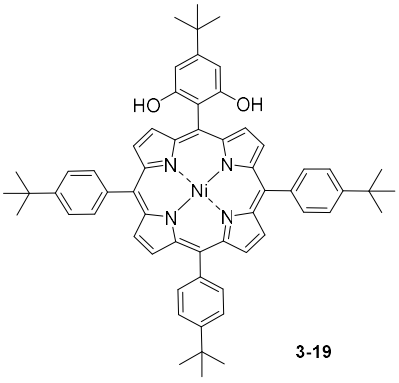

3-19

Porphyrin **3-26** (90 mg, 0.10 mmol) was dissolved in PhMe (20 mL) and $Ni(acac)_2$ (256 mg, 1.03 mmol) was added. The reaction mixture was stirred at 100 °C for 5 h under Ar. The mixture was cooled down and washed with H_2O (3 × 20 mL). The organic layer was dried over $MgSO_4$ and evaporated *in vacuo*. The residue was purified by SiO_2 column chromatography (eluent: cyclohexane/CH_2Cl_2 1:1), and precipitation from MeOH afforded **3-19** (236 mg, 85%) as a purple solid. M.f.: $C_{60}H_{60}N_4NiO_2$. M.w.: 927.86 g/mol. M.p. > 300 °C. λ_{max} (CH_2Cl_2)/nm 415 (ε/mol^{-1} L cm^{-1} 131087), 527 (16603). ν_{max}/cm^{-1} 3538w, 2959m, 2901w, 2865w, 1634w, 1564w, 1506w, 1460w, 1394w, 1361m, 1353m, 1344m, 1312w, 1266w, 1247w, 1207w, 1193w, 1161m, 1109m, 1075m, 1044w, 1015w, 1002s, 845w, 813s, 801s, 41w, 730w, 715s, 571w, 454w. δ_H (500 MHz, $CDCl_3$) 8.92-8.73 (m, 8H, β-*H*), 7.92 (d, J = 7.0 Hz, 6H, Ar*H*), 7.69 (d, J = 7.9 Hz, 6H, Ar*H*), 6.95 (d, J = 1.4 Hz, 2H, Ar*H*), 4.61 (br, 1H, O*H*), 1.56 (s, 27H, 9CH_3), 1.51 (s, 9H, 3CH_3). δ_C (126 MHz, $CDCl_3$) 155.4, 155.2, 150.9, 143.5, 143.2, 143.0, 143.0, 137.6, 137.5, 134.0, 133.6, 132.9, 132.6, 131.1, 124.0, 120.6, 119.7, 111.6, 105.1, 103.1, 35.2, 35.0, 31.7, 31.5. HRMS (MALDI): m/z $[M]^+$ calc. for $(C_{60}H_{60}N_4O_2Ni)^+$: 926.4070, found: 926.4043.

Ni(II) dipyranoporphyrin 3-16

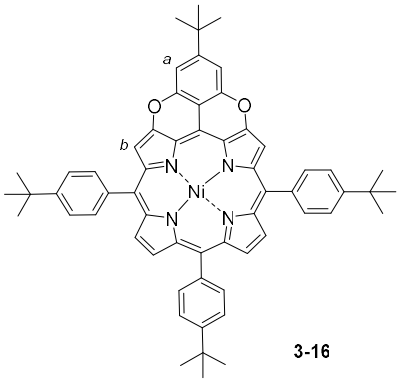

3-16

Porphyrin **3-19** (50 mg, 0.054 mmol) was dissolved in $PhNO_2$ (2 mL) and CuO (41 mg, 0.54 mmol) was added. The resulting mixture was stirred at 220 °C for 12 h. The mixture was cooled down, filtrated through celite pad and concentrated *in vacuo*. The residue was purified by SiO_2 column chromatography (eluent: CH_2Cl_2), and precipitation from MeOH afforded **3-16** (45 mg, 91%) as a purple solid. M.f.: $C_{60}H_{56}N_4NiO_2$. M.w.: 923.83 g/mol. M.p. > 300 °C. λ_{max} (CH_2Cl_2)/nm 426 (ε/mol^{-1} L cm^{-1} 92976), 537 (16057), 570 (12945). ν_{max}/cm^{-1} 2959m, 1621w, 1505m, 1461m, 1392w, 1361m, 1352m, 1267m, 1191w, 1167w, 1108s, 1071m, 1004s, 865w, 852w, 813s, 794s, 742m, 712s, 676w, 665w, 587w, 567m. δ_H (400 MHz, C_6D_6) 9.03 (d, J = 4.9 Hz, 2H, β-*H*), 8.97 (d, J = 4.9 Hz, 2H, β-*H*), 8.43 (s, 2H, H_b), 8.08 (d, 2H, Ar*H*), 8.00 (d, 2H, Ar*H*), 7.49-7.56 (m, 8H, Ar*H*+H_a), 1.40 (s, 27H, 9CH_3), 1.27 (s, 9H, 3CH_3). δ_C (126 MHz, $CDCl_3$) 153.7, 152.5, 151.4, 150.6, 150.4, 144.0, 142.6, 140.9, 139.1, 138.2, 133.9, 133.7, 132.1, 131.0, 124.2, 123.7, 123.3, 119.9, 117.8, 108.3, 106.0, 105.3, 104.8, 102.7, 36.0, 35.0, 31.8 (3 peaks are missing due to the overlap). HRMS (MALDI): m/z $[M]^+$ calc. for $(C_{60}H_{56}N_4O_2Ni)^+$: 922.3757, found: 922.3734.

Free-base dipyranoporphyrin 3-27

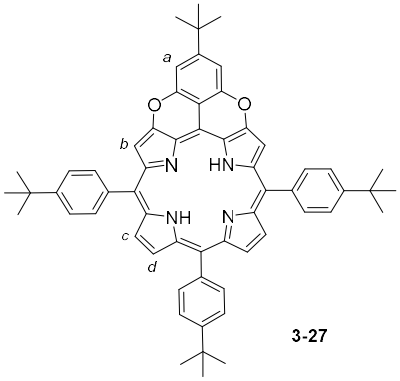

3-27

Ni(II) dipyranoporphyrin **3-16** (30 mg, 0.033 mmol) was dissolved in CH_2Cl_2 (4 mL), and TFA(10 mL) and conc. H_2SO_4 (1 mL) were sequentially added slowly at 0 ºC. The resulting solution was stirred at 0 ºC for 15 min. Then the reaction mixture was poured into iced water and neutralized with saturated aqueous solution of $NaHCO_3$ (20 mL). The aqueous phase was separated and washed with CH_2Cl_2 (3 × 15 mL). The combined organic layers were washed with H_2O (3 × 15 mL), dried over $MgSO_4$ and evaporated *in vacuo*. The residue was purified by SiO_2 column chromatography (eluent: cyclohexane/CH_2Cl_2 1:1), and precipitation from MeOH afforded **3-27** (24 mg, 84%) as a purple solid. M.f.: $C_{60}H_{58}N_4O_2$. M.w.: 867.15 g/mol. M.p. > 300 °C. λ_{max} (CH_2Cl_2)/nm 438 (ε/mol^{-1} L cm^{-1} 183867), 502 (3887), 538 (11923), 577 (26185) 605 (5898), 662 (18041). ν_{max}/cm^{-1} 2959s, 2901w, , 2865w, 1584m, 1563w, 1557w, 1546m, 506m, 1479m, 1455m, 1416m, 1396m, 1362m, 1282m, 1267m, 1247m, 1197m, 1174m, 1158m, 1131m, 1109m, 1041m, 1021m, 1001m, 994m, 983m, 964m, 849s, 800s, 765m, 748s, 730m, 13m, 674m, 664m, 581m, 568m, 556w. δ_H (500 MHz, C_6D_6) 9.07 (d, *J* = 4.7 Hz, 2H, *H*$_d$), 8.97 (d, *J* = 4.7 Hz, 2H, *H*$_c$), 8.65 (s, 2H, *H*$_b$), 8.22 (d, *J* = 8.2 Hz, 4H, Ar*H*), 8.16 (d, *J* = 8.2 Hz, 2H, Ar*H*), 7.72 (s, 2H, Ar*H*), 7.61 (d, *J* = 8.2 Hz, 4H, Ar*H*), 7.53 (d, *J* = 8.2 Hz, 2H, *H*$_a$), 1.42 (s, 27H, 9C*H*$_3$), 1.32 (s, 9H, 3C*H*$_3$), -1.10 (s, 2H, N*H*). δ_C (126 MHz, $CDCl_3$) 153.8, 153.4, 151.7, 150.7, 150.4, 147.1, 146.6, 145.4, 140.7, 138.0, 134.6, 134.4, 131.6, 130.5, 124.9, 124.5, 123.4, 120.6, 117.8, 108.7, 103.3, 35.9, 35.0, 31.8, 31.7 (5 peaks are missing due to the overlap). HRMS (MALDI): m/z [M]$^+$ calc. for $(C_{60}H_{58}N_4O_2)^+$: 867.4638, found: 867.4647.

Zn(II) dipyranoporphyrin 3-28

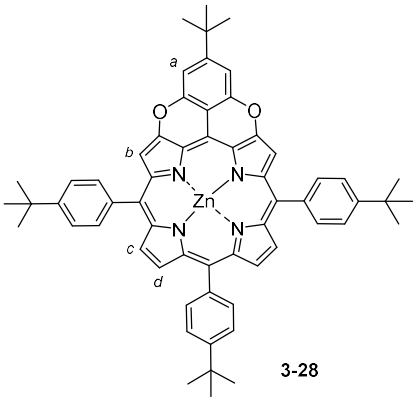

3-28

Free-base dipyranoporphyrin **3-27** (20 mg, 0.023 mmol) was dissolved in CH_2Cl_2 (10 mL), and the solution of $Zn(OAc)_2$ (42 mg, 0.23 mmol) in MeOH (3 mL) was added. The resulting mixture was stirred at 50 °C for 2 h. The reaction solution was cooled down and washed with H_2O (3 × 10 mL). The organic layer was dried over $MgSO_4$ and evaporated *in vacuo*. The

residue was purified by SiO_2 column chromatography (eluent: cyclohexane/CH_2Cl_2 1:1), and precipitation from MeOH afforded **3-28** (18 mg, 85%) as a red solid. M.f.: $C_{60}H_{56}N_4ZnO_2$. M.w.: 930.51 g/mol. M.p. > 300 °C. λ_{max} (CH_2Cl_2)/nm 416 (ε/mol^{-1} L cm^{-1} 92736), 436 (295125), 521 (1296), 561 (14574), 602 (22702). ν_{max}/cm^{-1} 2957m, 2866m, 1660w, 1633m, 1592s, 1560m, 1507m, 1480s, 1412m, 1392m, 1361m, 1348m, 1268s, 1224m, 1201m, 1164s, 1148m, 1108s, 1073m, 1000s, 941m, 886w, 864m, 849m, 823m, 793s, 766m, 741m, 725m, 713s, 676m, 668m, 660m, 630m, 580m, 556m, 480w. δ_H (500 MHz, $CDCl_3$) 9.17 (d, J = 4.6 Hz, 2H, H_d), 9.11 (d, J = 4.6 Hz, 2H, H_c), 8.48 (s, 2H, H_b), 8.35 (d, J = 8.1 Hz, 2H, Ar*H*), 8.26 (d, J = 8.0 Hz, 4H, Ar*H*), 7.76 (s, 2H, Ar*H*), 7.68 (d, J = 8.2 Hz, 4H, Ar*H*), 7.66 (d, J = 8.2 Hz, 2H, H_a), 1.49 (s, 18H, 6CH_3), 1.48 (s, 9H, 3CH_3), 1.35 (s, 9H, 3CH_3). δ_C (126 MHz, $CDCl_3$) 153.4, 152.4, 151.9, 151.1, 150.0, 149.8, 149.7, 147.6, 141.1, 140.5, 140.0, 134.9, 134.7, 132.4, 131.2, 128.4, 124.2, 123.6, 122.0, 121.3, 118.9, 108.7, 108.3, 104.5, 35.5, 34.6, 31.5, 31.4 (2 peaks are missing due to the overlap). HRMS (MALDI): m/z [M]$^+$ calc. for ($C_{60}H_{56}N_4O_2Zn$)$^+$: 929.3773, found: 929.3760.

5,15-*Bis*(4-(*tert*-butyl)-2-methoxyphenyl)porphyrin 3-33

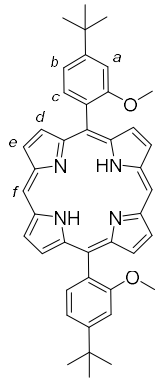

3-33

4-(*Tert*-butyl)-2-methoxybenzaldehyde **3-4** (1.34 g, 7 mmol) and dipyrromethane (1.02 g, 7 mmol) were dissolved in freshly distilled CH_2Cl_2 (700 mL) and the resulting solution was degassed for 40 min by purge of Ar. This was followed by the dropwise addition of $BF_3{\cdot}Et_2O$ (130 µl, 1.05 mmol). The reaction mixture was stirred for 5 h at rt under Ag, and DDQ (1.27 g, 5.6 mmol) was added. The resulting dark solution was stirred for additional 1 h. The mixture was filtered through silica pad and the solvent was evaporated *in vacuo*. The residue was purified by SiO_2 column chromatography (eluent: cyclohexane/CH_2Cl_2 2:3), and precipitation from MeOH afforded **3-33** (440 mg, 20%) as a purple solid. M.f.: $C_{42}H_{42}N_4O_2$. M.w.: 634.82 g/mol. M.p. > 300 °C. λ_{max} (CH_2Cl_2)/nm 407(ε/mol^{-1} L cm^{-1} 382930), 502 (17687), 536 (5069), 576 (5376), 629 (802). ν_{max}/cm^{-1} 3279w, 3111w, 2951m, 2900m,

2864w, 2824w, 1606w, 1561m, 1541w, 1515w, 1492w, 1458m, 1400m, 1391m, 1360m, 1336w, 1282m, 1229s, 1199m, 1177w, 1148w, 1134m, 1108w, 1063m, 1040s, 988m, 957s, 914m, 904m, 860m, 846m, 802m, 780s, 739s, 717m, 689s, 651m, 636m. δ_H (300 MHz, $CDCl_3$) 10.26 (s, 2H, H_f), 9.36 (d, J = 4.5 Hz, 4H, H_e), 9.06 (d, J = 4.5 Hz, 4H, H_d), 8.01 (d, J = 7.7 Hz, 2H, H_c), 7.45 (d, J = 8.0 Hz, 2H, H_b), 7.42 (s, 2H, H_a), 3.65 (s, 6H, OCH_3), 1.68 (s, 18H, CH_3), -3.02 (s, 2H, NH). δ_C (101 MHz, $CDCl_3$) 159.1, 153.4, 147.5, 145.2, 135.5, 131.2, 130.9, 127.5, 116.7, 115.3, 108.7, 104.7, 56.0, 35.4, 31.8. HRMS (ES): m/z $[M]^+$ calc. for $(C_{42}H_{43}N_4O_2)^+$: 635.3386, found: 635.3380.

5,15-Dibromo-10,20-*bis*(4-(*tert*-butyl)-2-methoxyphenyl)porphyrin 3-32

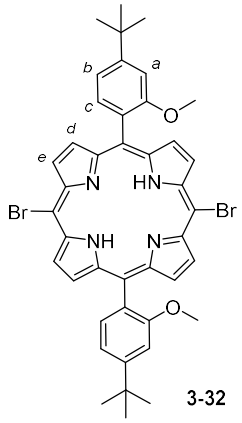

3-32

Porphyrin **3-33** (100 mg, 0.16 mmol) was dissolved in the mixture of CH_2Cl_2 (9 mL) and MeOH (1 mL). NBS (60 mg, 0.34 mmol) was added and the resulting solution was stirred at rt for 15 min. The reaction mixture was quenched by the addition of acetone (1.5 mL) and solvents were evaporated *in vacuo*. The residue was purified by SiO_2 column chromatography (eluent: petroleum ether/CH_2Cl_2 1:1), and precipitation from MeOH afforded **3-32** (127 mg, 95%) as a purple solid. M.f.: $C_{42}H_{40}Br_2N_4O_2$. M.w.: 792.62 g/mol. M.p. > 300 °C. λ_{max} (CH_2Cl_2)/nm 423(ε/mol^{-1} L cm^{-1} 320255), 521 (14986), 556 (8507), 601 (3505), 658 (3615). ν_{max}/cm^{-1} 3320w, 2951m, 2900w, 2860w, 2828w, 1607w, 1561w, 1495w, 1462m, 1398m, 1361w, 1336m, 1284m, 1230s, 1214m, 1180m, 1136m, 1107w, 1073w, 1041m, 998m, 981m, 964s, 912m, 847m, 805m, 790s, 780s, 729s, 706s, 689s, 652m, 628m. δ_H (300 MHz, $CDCl_3$) 9.48 (d, J = 4.8 Hz, 4H, H_e), 8.74 (d, J = 4.6 Hz, 4H, H_d), 7.80 (d, J = 7.6 Hz, 2H, H_c), 7.31 (d, J = 7.9 Hz, 2H, H_b), 7.27 (s, 2H, H_a), 3.54 (s, 6H, OCH_3), 1.56 (s, 18H, CH_3), -2.71 (s, 2H, NH). δ_C (101 MHz, $CDCl_3$) 159.0, 153.7, 135.1, 127.4, 117.7, 116.6, 108.4, 103.1, 55.8, 35.4, 31.7 (4 peaks are missing due to the overlap). HRMS (ES): m/z $[M]^+$ calc. for $(C_{42}H_{41}N_4O_2Br_2)^+$: 791.1596, found: 791.1599.

5,15-*Bis*(4-(*tert*-butyl)-2-methoxyphenyl)-10,20-*bis*(4-(*tert*-butyl)phenyl)porphyrin 3-30

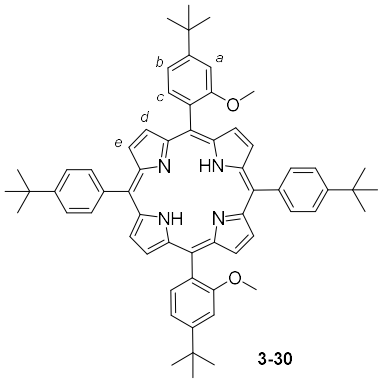

3-30

A mixture of dibromoporphyrin **3-32** (60 mg, 0.076 mmol), 4-*tert*-butylphenylboronic acid (68 mg, 0.38 mmol) and Cs_2CO_3 (124 mg, 0.38 mmol) in dry PhMe (10 mL) were degassed by freeze-thaw-pump cycle. $Pd(PPh_3)_4$ (7 mg, 0.006 mmol) was added and the mixture was degassed one more time. The resulting solution was stirred at 120 °C under reflux for 5 h. The reaction mixture was cooled down, filtered through celite pad and concentrated *in vacuo*. The residue was purified by SiO_2 column chromatography (eluent: petroleum ether/CH_2Cl_2 1:1), and precipitation from MeOH afforded **3-30** (33 mg, 49%) as a purple solid. M.f.: $C_{62}H_{66}N_4O_2$. M.w.: 899.23 g/mol. M.p.: > 300 °C. λ_{max} (CH_2Cl_2)/nm 420(ε/mol^{-1} L cm^{-1} 490492), 516 (19041), 551(8899), 591 (5992), 674(5135). ν_{max}/cm^{-1} 3310w, 2956m, 2901w, 2864w, 2829w, 1608w, 1561w, 1499w, 1460w, 1400m, 1362w, 1348w, 1286m, 1233w, 1221w, 1180w, 1137w, 1108w, 1071w, 1041m, 993w, 982w, 966s, 914w, 849w, 796s, 731s, 708m, 693w, 654w, 637w, 571m. δ_H (400 MHz, $CDCl_3$) 8.86 (d, J = 4.6 Hz, 4H, H_e), 8.82 (d, J = 4.5 Hz, 4H, H_d), 8.17 (d, J = 8.2 Hz, 4H, Ar*H*), 7.96 (dd, J = 7.7, 3.4 Hz, 2H, H_c), 7.77 (d, J = 8.1 Hz, 4H, Ar*H*), 7.39 (dd, J = 7.8, 1.6 Hz, 2H, H_b), 7.37 (s, 2H, H_a), 3.60 (s, 6H, 2OCH_3), 1.64 (s, 18H, 6CH_3), 1.63 (s, 18H, 6CH_3). δ_C (101 MHz, $CDCl_3$) 159.2, 159.1, 153.2, 150.3, 139.4, 135.3, 134.4, 128.4, 123.5, 119.6, 116.5, 116.1, 108.6, 108.5, 56.0, 35.3, 34.9, 31.7, 31.7 (2 peaks are missing due to the overlap)**.** HRMS (ES): m/z $[M]^+$ calc. for $(C_{62}H_{67}N_4O_2)^+$: 899.5264, found: 899.5282.

5,15-*Bis*(4-(*tert*-butyl)-2-hydroxyphenyl)-10,20-*bis*(4-(*tert*-butyl)phenyl)porphyrin 3-34

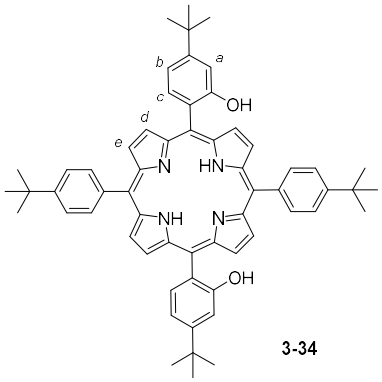

3-34

Porphyrin **3-30** (30 mg, 0.033 mmol) was dissolved in freshly distilled CH_2Cl_2 (10 mL) and the resulting solution was degassed for 15 min by purge of Ar. This was followed by the dropwise addition of BBr_3 (0.66 mL of 1M solution in CH_2Cl_2, 0.66 mmol). The reaction mixture was stirred for 4 h at rt under Ar, and H_2O (10 mL) was added. The resulting solution was stirred for additional 1 h, and pyridine (0.5 mL) was added. The layers were separated, and the aqueous layer was extracted with CH_2Cl_2 (3 × 5 mL). The combined organic extracts were washed with brine (2 × 10 mL) and H_2O (2 × 10 mL), dried over $MgSO_4$ and evaporated *in vacuo*. The residue was purified by SiO_2 column chromatography (eluent: petroleum ether/CH_2Cl_2 1:1), and precipitation from MeOH afforded **3-34** (25 mg, 86%) as a purple solid. M.f.: $C_{60}H_{62}N_4O_2$. M.w.: 871.18 g/mol. M.p.: > 300 °C. λ_{max} (CH_2Cl_2)/nm 420(ε/mol^{-1} L cm^{-1} 409741), 516 (17021), 552(7689), 591 (5746), 648(5808). ν_{max}/cm^{-1} 3555w, 505m, 3321w, 2951m, 2901m, 2862m, 1618w, 1560w, 1500w, 1474m, 1461m, 1427w, 1399m, 1360m, 1349m, 1291m, 1266w, 1216m, 1178s, 1109m, 1098w, 1023w, 991w, 981m, 966s, 935m, 908w, 867w, 851w, 835w, 799s, 727s, 695m, 652w, 644w, 584m, 566m, 544w. δ_H (400 MHz, $CDCl_3$) 8.82 (d, J = 4.8 Hz, 4H, H_e), 8.80 (d, J = 4.8 Hz, 4H, H_d), 8.03 (d, J = 8.1 Hz, 4H, Ar*H*), 7.82 (dd, J = 9.9, 7.9 Hz, 2H, H_c), 7.67 (d, J = 8.2 Hz, 4H, Ar*H*), 7.30 (t, J = 2.1 Hz, 2H, H_b), 7.28-7.23 (m, 2H, H_a), 4.91 (d, J = 16.5 Hz, 2H, O*H*), 1.51 (s, 18H, 6CH_3), 1.49 (s, 18H, 6CH_3). δ_C (101 MHz, $CDCl_3$) 155.1, 154.2, 150.8, 138.6, 134.7, 134.6, 124.9, 123.7, 120.8, 116.7, 112.7, 112.5, 35.1, 34.9, 31.7, 31.6 (2 peaks are missing due to the overlap). HRMS (ES): m/z $[M]^+$ calc. for $(C_{60}H_{63}N_4O_2)^+$: 871.4951, found: 871.4949.

5,15-bis(4-(*tert*-butyl)-2-hydroxyphenyl)-10,20-bis(4-*tert*-butylphenyl)porphyrinato-N^{21},N^{22},N^{23},N^{24}-nickel(II) 3-29

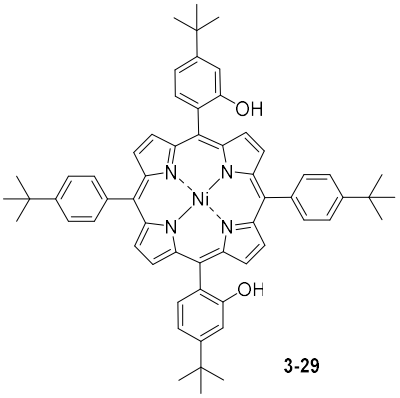

3-29

Porphyrin **3-34** (30 mg, 0.034 mmol) was dissolved in PhMe (10 mL) and $Ni(acac)_2$ (88 mg, 0.34 mmol) was added. The reaction mixture was stirred at 100 °C for 5 h under Ar. The mixture was cooled down and washed with H_2O (3 × 10 mL). The organic layer was dried over $MgSO_4$ and evaporated *in vacuo*. The residue was purified by SiO_2 column chromatography (eluent: petroleum ether/CH_2Cl_2 1:1), and precipitation from MeOH yielded **3-29** (30 mg, 97%) as a red solid. M.f.: $C_{60}H_{60}N_4NiO_2$. M.w.: 927.86 g/mol. M.p.: > 300 °C. λ_{max} (CH_2Cl_2)/nm 416(ε/mol^{-1} L cm^{-1} 255729), 528 (18443), 557(4971). ν_{max}/cm^{-1} 3550w, 3492m, 3325w, 2960m, 2901w, 2866w, 1620w, 1560w, 1500m, 1474w, 1460m, 1427w, 1392w, 1361m, 1350s, 1296m, 1265m, 1224w, 1201w, 1178s, 1108m, 1100m, 1071m, 1003s, 939s, 907w, 864w, 851w, 812s, 795s, 739m, 729w, 696m, 653m, 581w, 567m, 548w. δ_H (400 MHz, $CDCl_3$) 8.72 (d, *J* = 4.9 Hz, 4H, β-*H*), 8.70 (d, *J* = 4.9 Hz, 4H, β-*H*), 7.83 (d, *J* = 8.0 Hz, 4H, Ar*H*), 7.69-7.55 (m, 6H, Ar*H*), 7.29-.17 (m, 4H, Ar*H*), 4.75 (d, *J* = 13.9 Hz, 2H, O*H*), 1.47 (s, 18H, 6C*H*$_3$), 1.44 (s, 18H, 6C*H*$_3$). δ_C (101 MHz, $CDCl_3$) 154.7, 154.1, 150.8, 143.3, 142.8, 137.4, 133.9, 133.3, 131.9, 123.9, 123.5, 119.6, 116.8, 112.5, 111.7, 35.0, 34.9, 31.6, 31.5 (1 peak is missing due to the overlap). HRMS (ES): m/z $[M]^+$ calc. for $(C_{60}H_{61}N_4O_2Ni)^+$: 927.4148, found: 927.4127.

***Cis*- and *trans*-like dipyranoporphyrins 3-35 and 3-36**

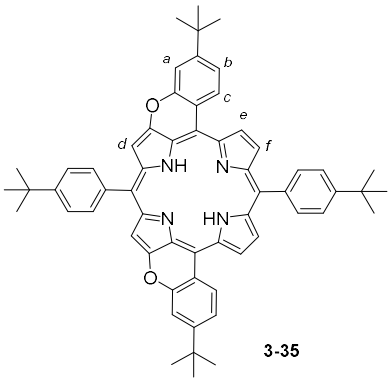

3-35

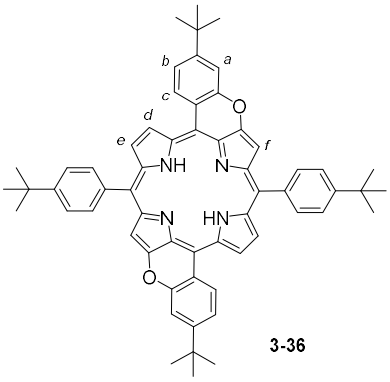

3-36

Porphyrin **3-29** (30 mg, 0.032 mmol) was dissolved in $PhNO_2$ (2 mL) and CuO (26 mg, 0.064 mmol) was added. The resulting mixture was stirred at 220 ºC for 12 h. The mixture was cooled down, filtrated through celite pad and concentrated *in vacuo*. The residue was purified by SiO_2 column chromatography (eluent: CH_2Cl_2) to yield inseparable mixture of Ni(II) porphyrin isomers **3-17** and **3-18** (22 mg, 78%). Subsequently, the mixture (22 mg, 0.025 mmol) was dissolved in CH_2Cl_2 (1.5 mL), and TFA (6 mL) and conc. H_2SO_4 (0.5 mL) were sequentially added slowly at 0 ºC. The solution was stirred at 0 ºC for 15 min, and the reaction mixture poured into iced water and neutralized with saturated aqueous solution of $NaHCO_3$ (10 mL). The aqueous phase was separated and extracted with CH_2Cl_2 (3 × 10 mL). The combined organic phases were washed with H_2O (3 × 15 mL), dried over $MgSO_4$ and evaporated *in vacuo*. The isomers were separated by SiO_2 column chromatography (eluent: cyclohexane/CH_2Cl_2 1:1), and precipitation from MeOH yielded **3-36** (9 mg, 32 %) and **3-35** (8 mg, 29 %).

10,20-*Bis*(4-(*tert*-butyl)phenyl)dibenzopyrano[a,t,j,k]porphyrin 3-36

Purple solid. M.f.: $C_{60}H_{58}N_4O_2$. M.w.: 867.15 g/mol. M.p.: > 300 °C. λ_{max} (CH_2Cl_2)/nm 443(ε/mol^{-1} L cm^{-1} 212940), 563(9414), 576 (10738), 607(37066), 620 (40605), 670(30300). ν_{max}/cm^{-1} 3279w, 2959m, 2900w, 2863w, 1625w, 1580m, 1566m, 1543m, 1497w, 1459m, 1404s, 1361m, 1311m, 1298m, 1269m, 1256m, 1230m, 1202w, 1185m, 1153m, 1134s, 1107m, 1057m, 1026w, 997w, 983s, 941m, 872m, 851w, 827w, 806m, 791s, 731s, 687m, 656w, 644m, 589w, 567m, 547w. δ_H (300 MHz, $CDCl_3$) 9.85 (d, J = 5.0 Hz, 2H, H_d), 9.21 (d, J = 8.5 Hz, 2H, H_c), 9.05 (d, J = 5.0 Hz, 2H, H_e), 8.49 (s, 2H, H_f), 8.20 (d, J = 8.1 Hz, 4H, Ar*H*), 8.10 (d, J = 1.7 Hz, 2H, H_a), 7.85 (d, J = 8.0 Hz, 6H, Ar*H*+H_b), 1.67 (s, 18H, 6CH_3), 1.64 (s, 18H, 6CH_3), -1.66 (s, 2H, N*H*). δ_C (75 MHz, $CDCl_3$) 156.4, 151.9, 151.6, 150.7, 138.9, 137.9, 136.2, 134.1, 132.9, 126.0, 125.3, 124.1, 121.9, 121.1, 119.9, 114.8, 106.4,

106.0, 35.1, 35.0, 31.7, 31.5 (2 peaks are missing due to the overlap). HRMS (ES): m/z $[M]^+$ calc. for $(C_{60}H_{59}N_4O_2)^+$: 867.4638, found: 867.4656.

10,20-*Bis*(4-(*tert*-butyl)phenyl)dibenzopyrano[a,t,h,i]porphyrin 3-35

Purple solid. M.f.: $C_{60}H_{58}N_4O_2$. M.w.: 867.15 g/mol. M.p.: > 300 °C. λ_{max} (CH_2Cl_2)/nm 445(ε/mol^{-1} L cm^{-1} 276675), 524 (4817), 564 (9450), 605 (52816), 625 (18909), 681(28705). ν_{max}/cm^{-1} 3325w, 2951m, 2902m, 2864m, 1578w, 1557m, 1532s, 1485m, 1458m, 1443s, 1405s, 1360s, 1322m, 1306m, 1279m, 1268m, 1229m, 1192m, 1167m, 1155s, 1141m, 1124m, 1108m, 1073w, 1022w, 999m, 976m, 941w, 866m, 843w, 824w, 789s, 742m, 718m, 704s, 691s, 679s, 644s, 589w, 569m, 554m. δ_H (300 MHz, $CDCl_3$) 9.51 (d, *J* = 4.7 Hz, 2H, H_e), 9.10 (d, *J* = 8.4 Hz, 2H, H_c), 8.80 (d, *J* = 4.7 Hz, 2H, H_f), 8.37 (s, 2H, H_d), 8.14 (t, *J* = 7.6 Hz, 4H, Ar*H*), 8.02 (d, *J* = 1.8 Hz, 2H, H_a), 7.81 (dd, *J* = 10.9, 8.0 Hz, 6H, H_b), 1.64 (s, 18H, 6CH_3), 1.60 (s, 18H, 6CH_3), -0.97 (s, 2H, N*H*). δ_C (75 MHz, $CDCl_3$) 155,0, 151.7, 151.2, 150.8, 150.7, 139.0, 138.4, 134.1, 133.7, 133.0, 131.7, 126.8, 124.8, 124.6, 123.7, 122.3, 120.4, 117.1, 114.7, 113.5, 106.8, 102.6, 35.1, 35.0, 31.7, 31.5 (3 peaks are missing due to the overlap). HRMS (ES): m/z $[M]^+$ calc. for $(C_{60}H_{59}N_4O_2)^+$: 867.4638, found: 867.4660.

6.3.2 Chapter IV

5,10,15,20-*Tetrakis*(4-(*tert*-butyl)-2-methoxyphenyl)porphyrin 4-4

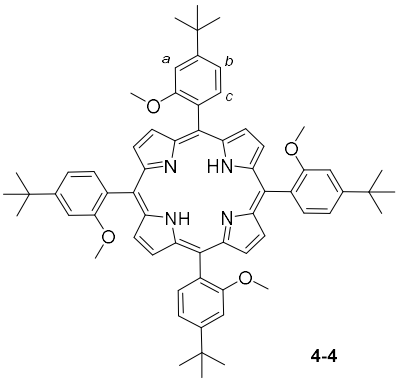

4-4

4-(*Tert*-butyl)-2-methoxybenzaldehyde **3-4** (1.92 g, 9.99 mmol) and pyrrole (542 µl, 7.81 mmol) were dissolved in freshly distilled $CHCl_3$ (700 mL) and the resulting solution was degassed for 40 min by purge of Ar. This was followed by the dropwise addition of $BF_3{\cdot}Et_2O$ (156 µl, 1.27 mmol). The reaction mixture was stirred for 1.5 h at rt under Ar, and DDQ (1.7 g, 7.5 mmol) was added. The resulting dark solution was stirred for additional 1 h, and Et_3N (5 mL) was added. The mixture was filtered through silica pad and the solvent was

evaporated *in vacuo*. The residue was purified by SiO_2 column chromatography (eluents: from CH_2Cl_2 to EtOAc), and precipitation from cold pentane yielded **4-4** (420 mg, 18%) as a purple solid. M.f.: $C_{64}H_{70}N_4O_4$. M.w.: 959.29 g/mol. M.p. > 300 °C. λ_{max} (CH_2Cl_2)/nm 420(ε/mol^{-1} L cm^{-1} 310119), 515 (13457), 549 (5456), 590 (4707), 645 (3000). ν_{max}/cm^{-1} 3314w, 2957m, 2902w, 2864w, 2831w, 1606w, 1561m, 1499m, 1460m, 1400m, 1361w, 1347w, 1285m, 1268m, 1229s, 1179m, 1153w, 1136m, 1106w, 1035m, 992w, 981m, 966s, 906s, 868m, 855m, 797s, 725s, 693s, 648m, 577m. δ_H (300 MHz, $CDCl_3$) 8.80 (s, 8H, β-*H*), 7.97 (td, *J* = 13.8, 8.1 Hz, 4H, H_c), 7.41 (d, *J* = 1.5 Hz, 2H, H_b), 7.38 (s, 6H, H_a+H_b), 3.77-3.44 (m, 12H, OCH_3), 1.66 (s, 36H, 12CH_3), -2.52 (s, 2H, N*H*). δ_C (75 MHz, $CDCl_3$) 159.2, 159.1, 153.0, 135.3, 128.6, 116.4, 115.6, 108.6, 56.0, 35.3, 31.8 (1 peak is missing due to the overlap). HRMS (ES): m/z $[M]^+$ calc. for $(C_{64}H_{71}N_4O_4)^+$: 959.5475, found: 959.5497.

5,10,15,20-*Tetrakis*(4-(*tert*-butyl-2-hydroxyphenyl)porphyrin 4-5

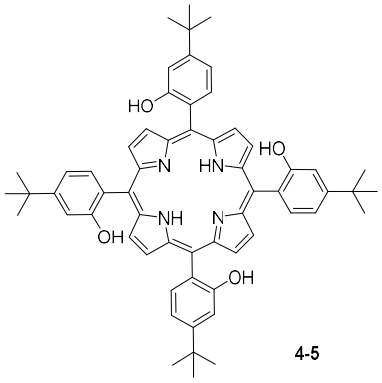

4-5

Porphyrin **4-4** (160mg, 0.17 mmol) was dissolved in freshly distilled CH_2Cl_2 (40 mL) and the resulting solution was degassed for 15 min by purge of Ar. This was followed by the dropwise addition of BBr_3 (3.4 mL of 1M solution in CH_2Cl_2, 3.4 mmol). The reaction mixture was stirred for 5 h at rt under Ar, and H_2O (40 mL) was added. The resulting solution was stirred for additional 1 h. The layers were separated, and the aqueous layer was extracted with CH_2Cl_2 (3 × 20 mL). The combined organic extracts were washed with brine (2 × 40 mL) and H_2O (2 × 40 mL), dried over $MgSO_4$ and evaporated *in vacuo*. Precipitation from cold pentane yielded **4-5** (147 mg, 96%) as a purple solid. M.f.: $C_{60}H_{62}N_4O_4$. M.w.: 903.18 g/mol. M.p. > 300 °C. λ_{max} (CH_2Cl_2)/nm 421(ε/mol^{-1} L cm^{-1} 324413), 515(20471), 550(9688), 588(9215), 645(6288). ν_{max}/cm^{-1} 3553w, 3510w, 3318w, 2952m, 2902w, 2864w, 1616w, 1558m, 1499w, 1475m, 1460w, 1427m, 1407m, 1362m, 1348w, 1292s, 1263w, 1215m, 1178s, 1126m, 1097m, 1073w, 991w, 981m, 967s, 933s, 868m, 798s, 724s, 695s, 651m, 573w. δ_H (300 MHz, $CDCl_3$) 8.93 (s, 8H, β-*H*), 7.89 (dd, *J* = 7.7, 3.7 Hz, 4H, Ar*H*), 7.37 (d, *J*

= 9.7 Hz, 8H, Ar*H*), 4.91 (s, 4H, O*H*), 1.59 (s, 36H, C*H*$_3$), -2.72 (s, 2H, N*H*). δ_C (126 MHz, $CDCl_3$) δ 155.0, 154.4, 134.7, 124.3, 116.9, 113.6, 112.6, 35.1, 31.6 (2 peaks are missing due to the overlap)**.** HRMS (ES): m/z $[M]^+$ calc. for $(C_{60}H_{63}N_4O_4)^+$: 903.4849, found: 903.4830.

5,10,15,20-*Tetrakis*(4-*tert*-butyl-2-hydroxyphenyl)porphyrinato-N^{21},N^{22},N^{23},N^{24}-nickel(II) 4-3

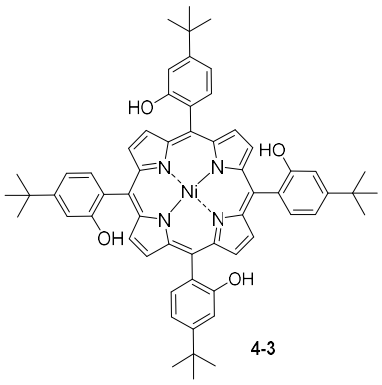

4-3

To the solution of porphyrin **4-5** (100 mg, 0.11 mmol) in DCE (20 mL), degassed for 30 min by purge of Ar, $Ni(acac)_2$ (143 mg, 0.55 mmol) was added, and the resulting mixture was stirred for 3 h under reflux. The reaction mixture was cooled down and washed with brine (5 × 10 mL). The organic layer was dried over $MgSO_4$ and concentrated *in vacuo*. The residue was purified by SiO_2 column chromatography (eluent: EtOAc/petroleum ether 1:1), and precipitation from cold pentane yielded **4-3** (100 mg, 95%) as a red solid. M.f.: $C_{60}H_{60}N_4NiO_4$. M.w.: 959.86 g/mol. M.p. > 300 °C. λ_{max} (CH_2Cl_2)/nm 415(ε/mol^{-1} L cm^{-1} 256359), 527(19890), 557(5424). ν_{max}/cm^{-1} 3558w, 3497w, 2953m, 2903w, 2866w, 1619w, 1561m, 1502w, 1460w, 1427m, 1407m, 1353m, 1292m, 1265m, 1221m, 1178s, 1128m, 1100m, 1076m, 998s, 936m, 871m, 814m, 801s, 733m, 715s, 697m, 652m, 583w. δ_H (300 MHz, $CDCl_3$) 8.84 (s, 8H, β-*H*), 7.79–7.58 (m, 4H, Ar*H*), 7.30 (m, 8H, Ar*H*), 4.86 (s, 4H, O*H*), 1.54 (s, 36H, C*H*$_3$). δ_C (75 MHz, $CDCl_3$) 154.6, 154.4, 143.4, 133.9, 133.0, 123.1, 117.0, 112.6, 112.6, 35.0, 31.5. HRMS (ES): m/z $[M]^+$ calc. for $(C_{60}H_{61}N_4O_4Ni)^+$: 959.4046, found: 959.4059.

Ni(II) tetrapyranoporphyrin 4-1d

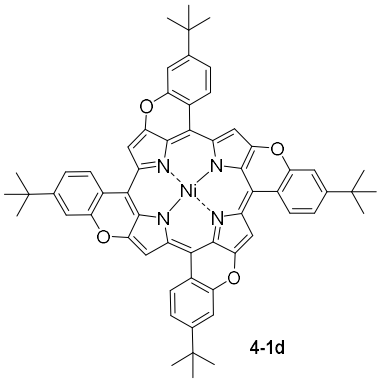

4-1d

Porphyrin **4-3** (30 mg, 0.031 mmol) was dissolved in $PhNO_2$ (2 mL) and CuO (48 mg, 0.62 mmol) was added. The resulting mixture was stirred at 220 ºC for 12 h. The mixture was cooled down, filtrated through celite pad and concentrated *in vacuo*. The residue was purified by SiO_2 column chromatography (eluent: CH_2Cl_2/Py 1:1), and precipitation from MeOH afforded **4-1d** (18 mg, 62%) as a green solid. M.f.: $C_{60}H_{52}N_4NiO_4$. M.w.: 951.79 g/mol. M.p. > 300 °C. ν_{max}/cm^{-1} 467w, 648m, 700m, 718w, 791s, 871m, 939m, 971w, 1013s, 1099m, 1142w, 1181m, 1260m, 1303m, 1362w, 1410m, 1462w, 1562w, 1710w, 2850m, 2918m, 2955m, 3541w.HRMS (MALDI): m/z $[M]^+$ calc. for $(C_{60}H_{52}N_4O_4Ni)^+$: 950.3342, found: 950.3344.

Free-base tetrapyranoporphyrin 4-6

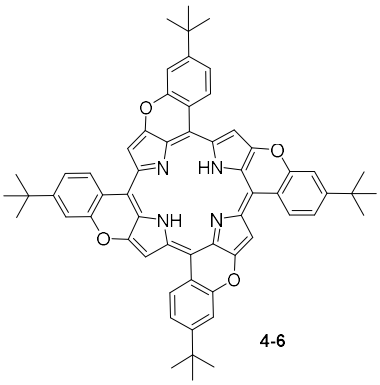

4-6

Ni(II) tetrapyranoporphyrin **4-1d** (15 mg, 0.015 mmol) was dissolved in CH_2Cl_2 (1 mL), and TFA (2 mL) and conc. H_2SO_4 (two drops) were sequentially added slowly at 0 ºC. The resulting solution was stirred at 0 ºC for 1 h. Then the reaction mixture was poured into iced water and neutralized with saturated aqueous solution of $NaHCO_3$ (10 mL). The aqueous phase was separated and washed with CH_2Cl_2 (3 × 10 mL). The combined organic layers were washed with H_2O (3 × 10 mL), dried over $MgSO_4$ and evaporated *in vacuo*. The residue was purified by SiO_2 column chromatography (eluent: CH_2Cl_2), and precipitation from

MeOH afforded **4-6** (4 mg, 30%) as a green solid. M.f.: $C_{60}H_{54}N_4O_2$. M.w.: 895.12 g/mol. M.p. > 300 °C.

5,15-*Bis*(4-(*tert*-butyl)-2,6-dimethoxyphenyl)porphyrin 4-10

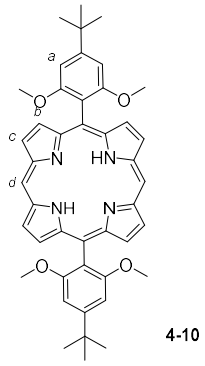

4-10

4-(*Tert*-butyl)-2,6-dimethoxybenzaldehyde **3-21** (1.55 g, 7 mmol) and dipyrromethane (1.02 g, 7 mmol) were dissolved in freshly distilled CH_2Cl_2 (700 mL) and the resulting solution was degassed for 40 min by purge of Ar. This was followed by the dropwise addition of $BF_3{\cdot}Et_2O$ (130 µl, 1.05 mmol). The reaction mixture was stirred for 5 h at rt under Ar, and DDQ (1.27 g, 5.6 mmol) was added. The resulting dark solution was stirred for additional 1 h. The mixture was filtered through silica pad and the solvent was evaporated *in vacuo*. The residue was purified by SiO_2 column chromatography (eluent: cyclohexane/CH_2Cl_2 2:3), and precipitation from MeOH yielded **4-10** (410 mg, 17%) as a purple solid. M.f.: $C_{44}H_{46}N_4O_4$. M.w.: 694.88 g/mol. M.p. > 300 °C. λ_{max} (CH_2Cl_2)/nm 408(ε/mol^{-1} L cm^{-1} 388678), 502 (19174), 535 (5874), 576 (6643), 629 (1918). ν_{max}/cm^{-1} 3291w, 3101w, 2951w, 2933w, 2862w, 2833w, 1786w, 1690w, 1603m, 1570m, 1450m, 1405s, 1358w, 1315m, 1267m, 1237s, 1196m, 1181w, 1121s, 1056m, 1042m, 987m, 971m, 955s, 924m, 846m, 830s, 788s, 747s, 721m, 689s, 663m, 617m, 555m. δ_H (300 MHz, $CDCl_3$) 10.15 (s, 2H, H_d), 9.28 (d, J = 4.6 Hz, 4H, H_c), 8.98 (d, J = 4.5 Hz, 4H, H_b), 7.06 (s, 4H, H_a), 3.52 (s, 12H, OCH_3), 1.64 (s, 18H, CH_3), -3.00 (s, 2H, NH). δ_C (75 MHz, $CDCl_3$) δ 160.1, 154.0, 147.6, 145.0, 131.1, 130.4, 116.8, 111.3, 104.1, 102.1, 77.5, 56.1, 35.7, 31.8. HRMS (AP): m/z $[M]^+$ calc. for $(C_{44}H_{47}N_4O_4)^+$: 695.3597, found: 695.3596.

5,15-Dibromo-10,20-*bis*(4-(*tert*-butyl)-2,6-dimethoxyphenyl)porphyrin 4-9

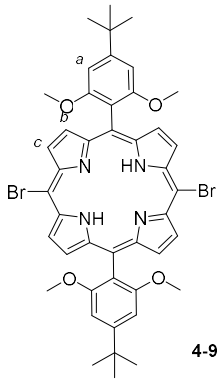

4-9

Porphyrin **4-10** (100 mg, 0.14 mmol) was dissolved in the mixture of CH_2Cl_2 (9 mL) and MeOH (1 mL). NBS (57 mg, 0.32 mmol) was added and the resulting solution was stirred at rt for 15 min. The reaction mixture was quenched by the addition of acetone (1.5 mL) and solvents were evaporated *in vacuo*. The residue was purified by SiO_2 column chromatography (eluent: petroleum ether/CH_2Cl_2 1:1), and precipitation from MeOH afforded **4-9** (113 mg, 95%) as a purple solid. M.f.: $C_{44}H_{44}Br_2N_4O_4$. M.w.: 852.67 g/mol. M.p. > 300 °C. λ_{max} (CH_2Cl_2)/nm 423(ε/mol^{-1} L cm^{-1} 360818), 520 (20965), 555 (11994), 600 (7887), 657 (6726). ν_{max}/cm^{-1} 2957m, 2934m, 2902w, 2862w, 2836w, 1604m, 1568s, 1460m, 1451m, 1404s, 1360w, 1336m, 1317m, 1263w, 1239s, 1215m, 1193w, 1183m, 1120s, 1074w, 1051w, 1037m, 997m, 979m, 962s, 926m, 870w, 849w,832m, 795s, 737s, 718s, 691m, 664m, 623m, 556w. δ_H (300 MHz, $CDCl_3$) 9.54 (d, J = 4.8 Hz, 4H, H_c), 8.82 (d, J = 4.7 Hz, 4H, H_b), 7.05 (s, 4H, H_a), 3.56 (s, 12H, OCH_3), 1.66 (s, 18H, CH_3), -2.53 (s, 2H, NH). δ_C (75 MHz, $CDCl_3$) 159.9, 154.3, 116.6, 114.0, 102.4, 101.8, 56.0, 35.8, 31.7 (4 peaks are missing due to the overlap). HRMS (APCI): m/z $[M]^+$ calc. for $(C_{44}H_{45}N_4O_4Br_2)^+$: 851.1808, found: 851.1800.

5,15-*Bis*(4-(*tert*-butyl)-2,6-dimethoxyphenyl)-10,20-*bis*(4-(*tert*-butyl)phenyl)porphyrin

4-8

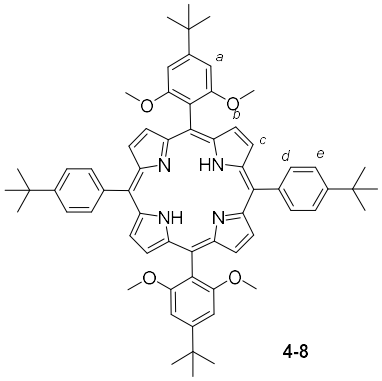

4-8

A mixture of dibromoporphyrin **4-9** (100 mg, 170 mmol), 4-*tert*-butylphenylboronic acid (104 mg, 0.59 mmol) and Cs_2CO_3 (190 mg, 0.59 mmol) in dry PhMe (20 mL) were degassed by freeze-thaw-pump cycle. $Pd(PPh_3)_4$ (10 mg, 0.009 mmol) was added and the mixture was degassed one more time. The resulting solution was stirred at 120 °C under reflux for 5 h. The reaction mixture was cooled down, filtered through celite pad and concentrated *in vacuo*. The residue was purified by SiO_2 column chromatography (eluent: CH_2Cl_2), and precipitation from MeOH yielded **4-8** (44 mg, 39%) as a purple solid. M.f.: $C_{64}H_{70}N_4O_4$. M.w.: 959.29 g/mol. M.p. > 300 °C. λ_{max} (CH_2Cl_2)/nm 417(ε/mol^{-1} L cm^{-1} 351726), 431 (297995), 518 (44067), 555 (30303), 594 (22890), 651 (13111). ν_{max}/cm^{-1} 3467w, 3314w, 29547, 2902m, 2863m, 2832m, 1707w, 1605m, 1566s, 1458m, 1404m, 1361m, 1341m, 1314m, 1269w, 1239s, 1182m, 1121s, 1099s, 1024m, 980m, 964s, 925m, 833m, 795s, 725m, 691s, 665m, 575m, 511m. δ_H (300 MHz, $CDCl_3$) 8.80 (d, J = 4.7 Hz, 4H, H_c), 8.77 (d, J = 4.7 Hz, 4H, H_b), 8.14 (d, J = 7.9 Hz, 4H, H_d), 7.72 (d, J = 8.0 Hz, 4H, H_e), 7.02 (s, 4H, H_a), 3.50 (s, 12H, 4OCH_3), 1.61 (s, 18H, 6CH_3), 1.60 (s, 18H, 6CH_3), -2.60 (s, 2H, NH). δ_C (126 MHz, $CDCl_3$) 160.1, 153.8, 150.1, 139.5, 134.4, 130.1, 128.7, 123.4, 118.9, 117.8, 112.2, 102.0, 56.1, 35.7, 34.9, 31.7 (3 peaks are missing due to the overlap). HRMS (ES): m/z $[M]^+$ calc. for $(C_{64}H_{71}N_4O_4)^+$: 959.5475, found: 959.5516.

5,15-*Bis*(4-(*tert*-butyl)-2,6-dimethoxyphenyl)-10,20-*bis*(4-(*tert*-butyl)phenyl)-porphyrinato-N^{21},N^{22},N^{23},N^{24}-nickel(II) 4-7

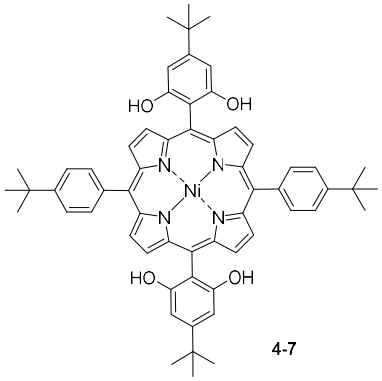

4-7

Porphyrin **4-8** (30 mg, 0.032 mmol) was dissolved in freshly distilled CH_2Cl_2 (10 mL) and the resulting solution was degassed for 15 min by purge of Ar. This was followed by the dropwise addition of BBr_3 (1.2 mL of 1 M solution in CH_2Cl_2, 1.2 mmol). The reaction mixture was stirred for 5 h at rt under Ar, and H_2O (10 mL) was added. The resulting solution was stirred for additional 1 h, and pyridine (0.5 mL) was added. The layers were separated, and the aqueous layer was extracted with CH_2Cl_2 (3 × 5 mL). The combined organic extracts were washed with brine (2 × 10 mL) and H_2O (2 × 10 mL), dried over $MgSO_4$ and evaporated *in vacuo*. The residue was dissolved in DCE (10 mL) and $Ni(acac)_2$ (82 mg, 0.32 mmol) was added. The reaction mixture was stirred at 100 °C for 5 h under N_2. The mixture was cooled down and washed H_2O (4 × 5 mL). The organic layer was dried over $MgSO_4$ and evaporated *in vacuo*. The residue was purified by SiO_2 column chromatography (eluent: CH_2Cl_2), and precipitation from MeOH yielded **4-7** (25 mg, 82%) as a purple solid. M.f.: $C_{60}H_{60}N_4NiO_4$. M.w.: 959.86 g/mol. M.p. > 300 °C. λ_{max} (CH_2Cl_2)/nm 415(ε/mol^{-1} L cm^{-1} 571100), 527(39962), 556(16394). ν_{max}/cm^{-1} 3553w, 3497w, 2957m, 2903w, 2866w, 1719w, 1630m, 1561m, 1508w, 1459m, 1425m, 1394w, 1361m, 1352s, 1313m, 1267s, 1162s, 1109m, 1074m, 1042s, 1002s, 944w, 921w, 844s, 797s, 740m, 717s, 701m, 668w, 573m. δ_H(300 MHz, $CDCl_3$) 8.86 (s, 8H, Py*H*), 7.92 (d, *J* = 8.1 Hz, 4H, Ar*H*), 7.71 (d, *J* = 8.1 Hz, 4H, Ar*H*), 6.95 (s, 4H, Ar*H*), 4.58 (s, 4H, O*H*), 1.57 (s, 18H, 6C*H*$_3$), 1.51 (s, 18H, 6C*H*$_3$). δ_C (75 MHz, $CDCl_3$) 155.3, 151.1, 143.8, 143.1, 137.0, 134.2, 133.6, 131.7, 124.0, 120.1, 111.3, 105.2, 105.0, 35.2, 34.9, 31.6, 31.4 (1 peak is missing due to the overlap). HRMS (ES): m/z $[M]^+$ calc. for $(C_{60}H_{61}N_4O_8Ni)^+$: 959.4046, found: 959.4053.

5,10,15,20-*Tetrakis*(4-(*tert*-butyl)-2,6-dimethoxyphenyl)porphyrin 4-14

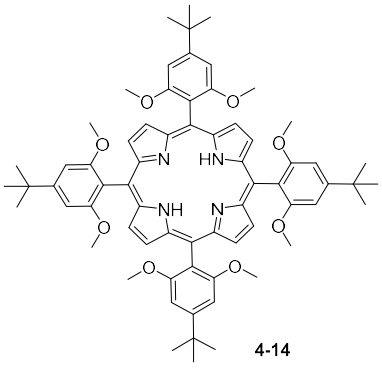

4-14

4-(*Tert*-butyl)-2,6-dimethoxybenzaldehyde **3-21** (1.5 g, 6.73 mmol) and pyrrole (470 µl, 6.73 mmol) were dissolved in freshly distilled $CHCl_3$ (700 mL) and the resulting solution was degassed for 40 min by purge of Ar. This was followed by the dropwise addition of $BF_3{\cdot}Et_2O$ (120 µl, 0.94 mmol). The reaction mixture was stirred at for 1.5 h at rt under Ar, and DDQ (1.145 g, 5.05 mmol) was added. The resulting dark solution was stirred for additional 1 h, and Et_3N (5 mL) was added. The mixture was filtered through silica pad and the solvent was evaporated *in vacuo*. The residue was purified by SiO_2 column chromatography (eluents: from CH_2Cl_2 to EtOAc), and precipitation from cold pentane yielded **4-14** (425 mg, 24%) as a purple solid. M.f.: $C_{68}H_{78}N_4O_8$. M.w.: 1078.58 g/mol. M.p. > 300 °C. λ_{max} (CH_2Cl_2)/nm 419(ε/mol^{-1} L cm^{-1} 106301), 514 (4145), 546(1082), 589(1275), 643(220). ν_{max}/cm^{-1} 3316w, 2953m, 2903w, 2862w, 2832w, 1603m, 1566s, 1457m, 1451m, 1404s, 1360w, 1346w, 1316w, 1280w, 1239s, 1217m, 1180m, 1122s, 1043m, 992w, 981w, 965s, 924m, 871w, 833m, 811w, 797s, 741m, 731m, 710m, 665w, 622m. δ_H (300 MHz, $CDCl_3$) 8.70 (s, 8H, β-*H*), 7.01 (s, 8H, Ar*H*), 3.50 (s, 24H, OC*H*$_3$), 1.61 (s, 36H, C*H*$_3$), -2.43 (s, 2H, N*H*). δ_C (75 MHz, $CDCl_3$) 160.1, 153.4, 118.1, 110.9, 102.1, 56.2, 35.6, 31.7 (2 peaks are missing due to the overlap). HRMS (AP): m/z $[M]^+$ calc. for $(C_{68}H_{79}N_4O_8)^+$: 1079.5898, found: 1079.5890.

5,10,15,20-*Tetrakis*(4-(*tert*-butyl)-2,6-dihydroxyphenyl)porphyrin 4-15

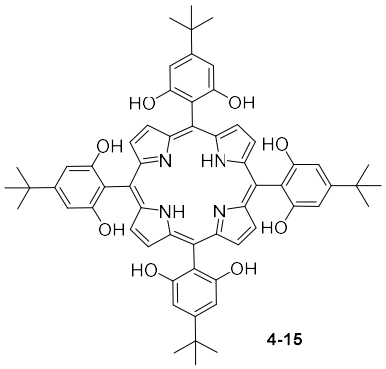

4-15

Octamethoxyporphyrin **4-14** (100 mg, 0.093 mmol) was dissolved in freshly distilled CH_2Cl_2 (20 mL) and the resulting solution was degassed for 15 min by purge of Ar. This was followed by the dropwise addition of BBr_3 (3.72 mL of 1M solution in CH_2Cl_2, 3.72 mmol). The reaction mixture was stirred for 16 h at rt under Ar, and H_2O (30 mL) was added. The resulting solution was stirred for additional 1 h, and pyridine (0.2 mL) was added. The layers were separated, and the aqueous layer was extracted with EtOAc (4 × 20 mL). The combined organic extracts were washed with brine (4 × 40 mL), dried over $MgSO_4$ and evaporated *in vacuo*. Precipitation from cold pentane yielded **4-15** (56 mg, 64%) as a purple solid. M.f.: $C_{60}H_{62}N_4O_8$. M.w.: 967.16 g/mol. M.p. > 300 °C. ν_{max}/cm^{-1} 3549br, 3316br, 2960m, 2905w, 2868w, 1702w, 1627m, 1562m, 1478w, 1416m, 1363m, 1337m, 1312m, 1255m, 1166s, 1043s, 1018m, 994m, 979m, 967s, 943w, 870w, 842m, 802s, 731m, 667m, 586m. δ_H (500 MHz, $(CD_3)_2CO$) 8.93 (s, 8H, β-*H*), 7.84 (bs, 6H, O*H*, 2 protons are missing due to the proton exchange), 7.00 (s, 8H, Ar*H*), 1.58 (s, 36H, C*H*$_3$), -2.60 (s, 2H, N*H*). δ_C (126 MHz, $(CD_3)_2CO$) 157.8, 153.5, 116.8, 114.1, 110.8, 104.3, 34.6, 31.1 (1 peak is missing due to the overlap). HRMS (ES): m/z $[M]^+$ calc. for $(C_{60}H_{63}N_4O_8)^+$: 967.4646, found: 967.4654.

5,10,15,20-*Tetrakis*(4-(*tert*-butyl)-2,6-dihydroxyphenyl)porphyrinato-N^{21},N^{22},N^{23},N^{24}-nickel(II) 4-13

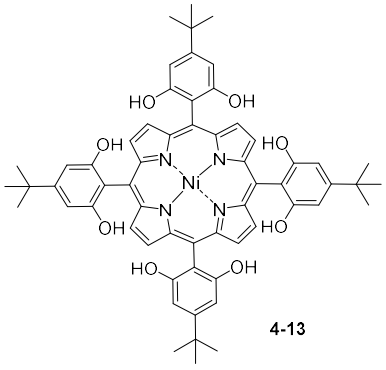

4-13

To the solution of porphyrin **4-15** (0.1 g, 0.1 mmol) in DCE (30 mL), previously degassed under Ar for 30 min, $Ni(acac)_2$ (266 mg, 1.03 mmol) was added, and the resulting mixture was stirred for 3 h under reflux. The reaction mixture was cooled down and washed with brine (4 × 20 mL). The organic layer was dried over $MgSO_4$ and concentrated *in vacuo*. The residue was purified by SiO_2 column chromatography (eluent: acetone/petroleum ether 1:1), and precipitation from pentane yielded **4-13** (97 mg, 95%) as a red solid. M.f.: $C_{60}H_{60}N_4NiO_8$. M.w.: 1023.85 g/mol. M.p. > 300 °C. λ_{max} (CH_2Cl_2)/nm 413(ε/mol^{-1} L cm^{-1} 65000), 527(8924), 559(6101). ν_{max}/cm^{-1} 3329br, 2962w, 2905w, 2868w, 1705w, 1618m,

1561m, 1522m, 1459m, 1414m, 1390m, 1362m, 1341m, 1265m, 1240m, 1171m, 1110m, 1072m, 1044m, 1002s, 944m, 921m, 874w, 844m, 797m, 738m, 715m, 668m, 596s. δ_H (400 MHz, $CDCl_3$) 8.82 (s, 8H, β-*H*), 6.89 (s, 8H, Ar*H*), 4.70 (s, 8H, O*H*), 1.48 (s, 36H, C*H*$_3$). HRMS (ES): m/z $[M]^+$ calc. for $(C_{60}H_{61}N_4O_8Ni)^+$: 1023.3843, found: 1023.3860.

Ni(II) octapyranoporphyrin 4-12

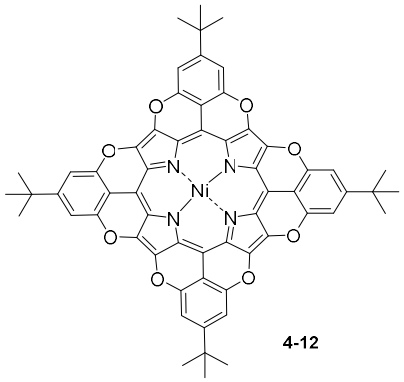

4-12

Porphyrin **4-13** (30 mg, 0.029 mmol) was dissolved in $PhNO_2$ (2 mL) and CuO (93 mg, 0.12 mmol) was added. The resulting mixture was stirred at 220 ºC for 12 h. The mixture was cooled down, filtrated through celite pad and concentrated *in vacuo*. The residue was purified by GPC (eluent: Py) affording **4-12** (3 mg, 10 %) as a green solid. M.f.: $C_{60}H_{44}N_4NiO_8$. M.w.: 1007.73 g/mol. M.p. > 300 °C. HRMS (MALDI): m/z $[M]^+$ calc. for $(C_{60}H_{44}N_4O_8Ni)^+$: 1006.2513, found: 1006.2473.

APPENDIX

Selected ^{1}H and ^{13}C NMR spectra

(5-(4-(*Tert*-butyl)-2-methoxyphenyl)-10,15,20-tris(4-(*tert*-butyl)phenyl)porphyrin 3-3

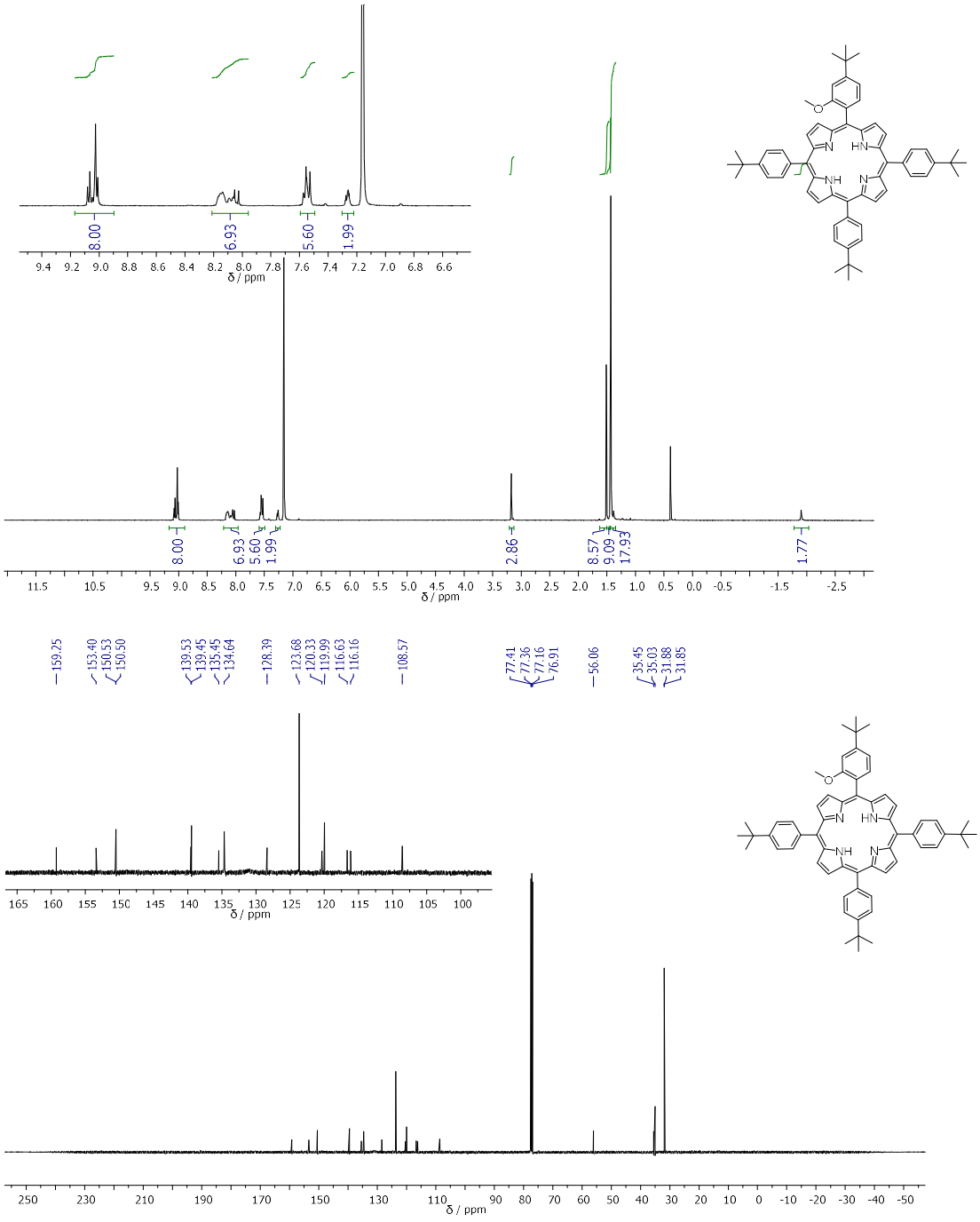

5-(4-(*Tert*-butyl)-2-hydroxyphenyl)-10,15,20-tris(4-(*tert*-butyl)phenyl)porphyrin 3-7

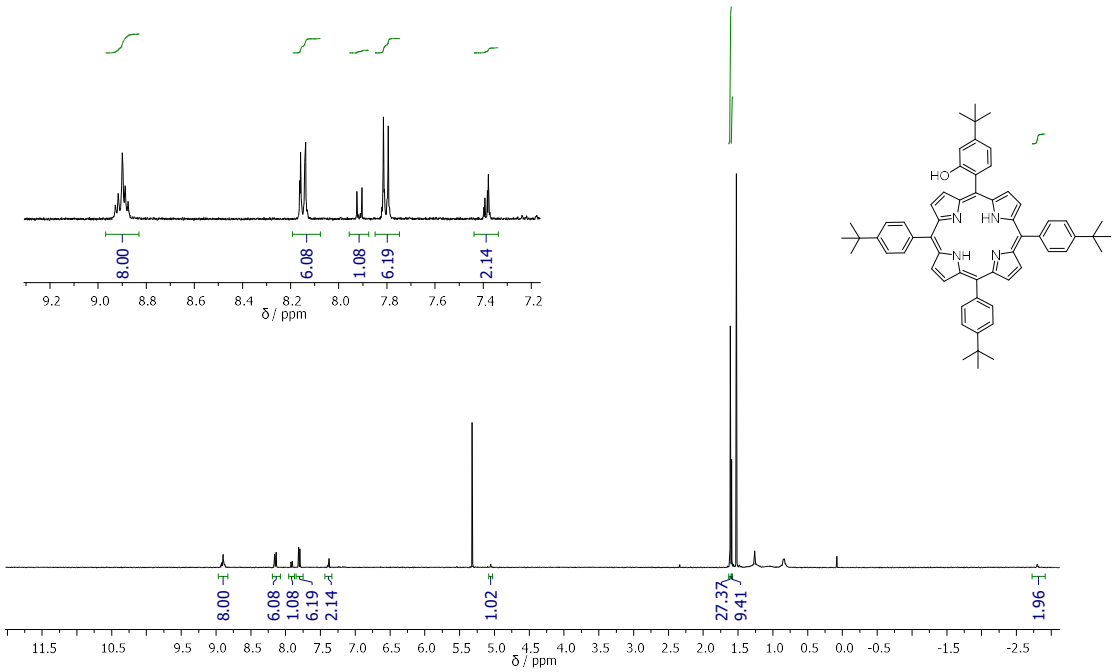

5-(4-(*Tert*-butyl)-2-hydroxyphenyl)-10,15,20-*tris*(4-(*tert*-butyl)phenyl)porphyrinato-N^{21},N^{22},N^{23},N^{24}-nickel(II) 3-2

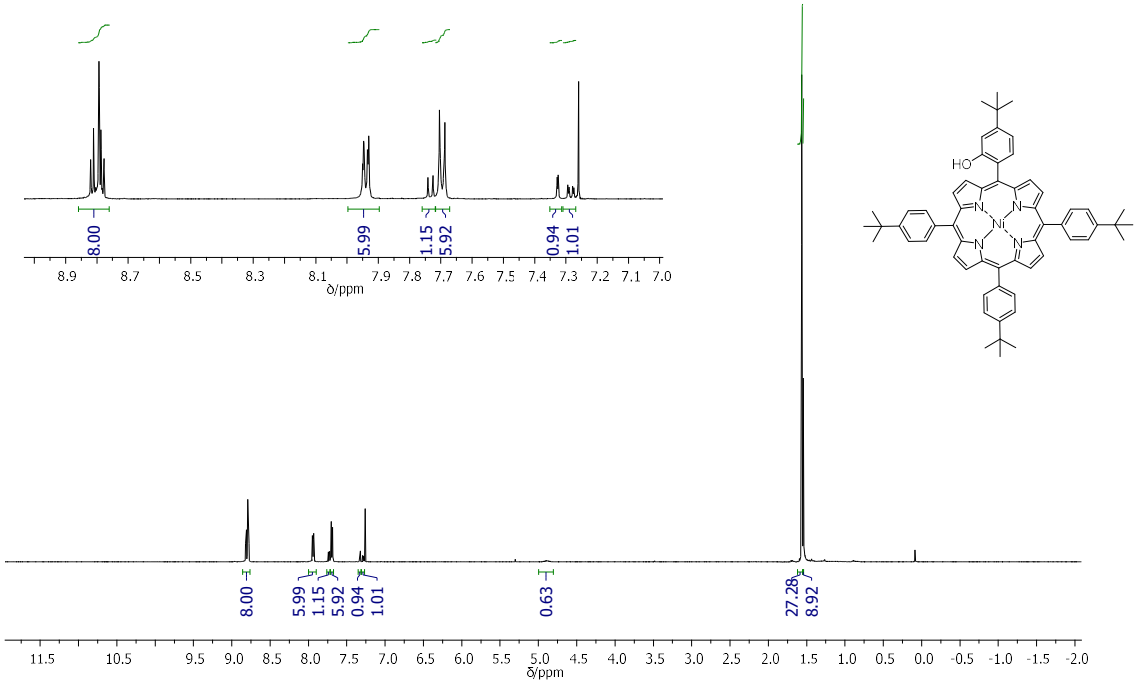

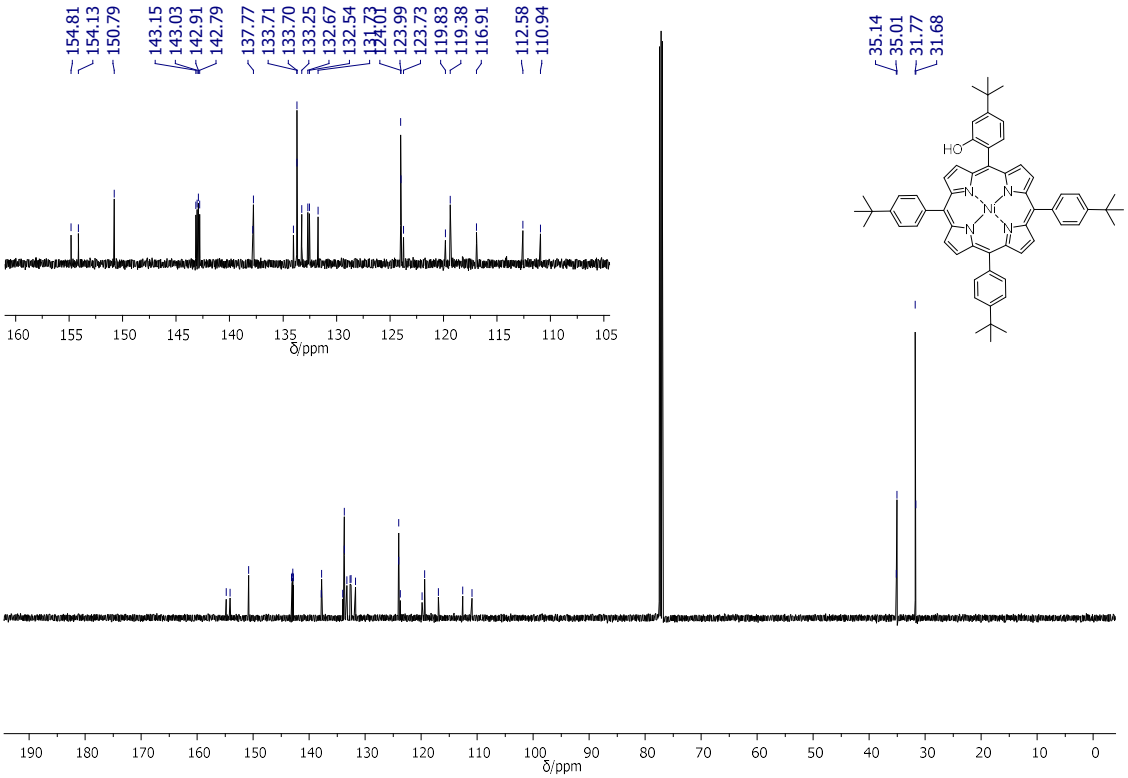

10,15,20-*Tris*(4-*tert*-butylphenyl)benzopyrano[a,t]porphyrinato-N^{21},N^{22},N^{23},N^{24}-nickel(II) 3-1

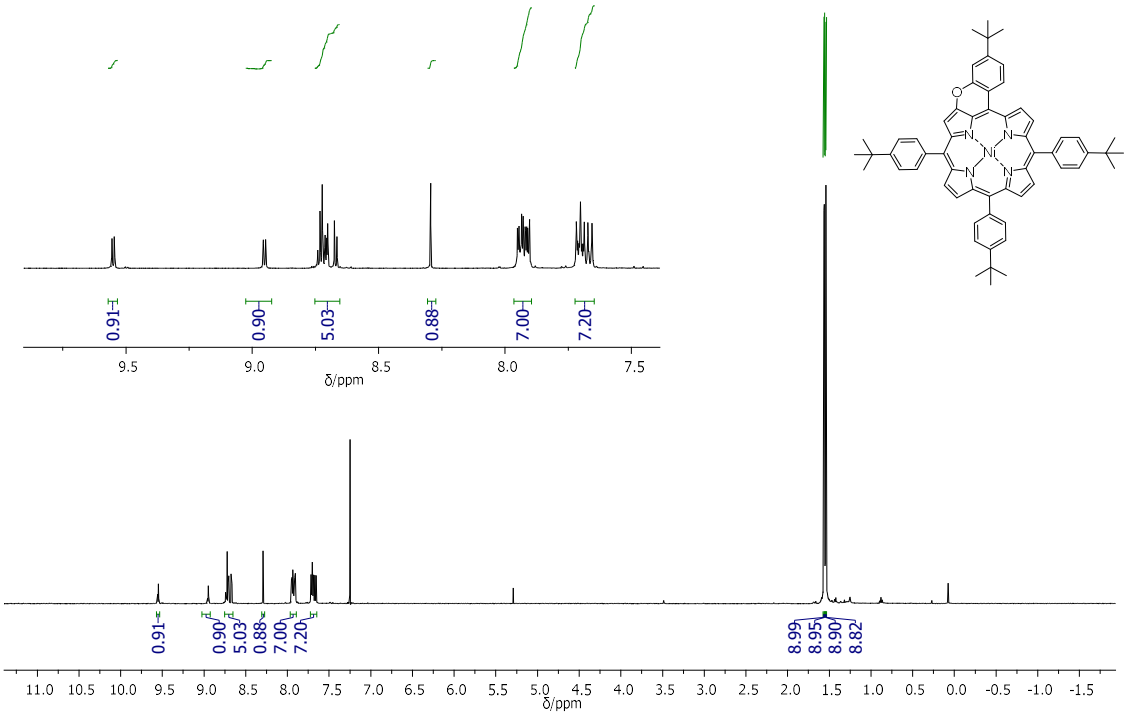

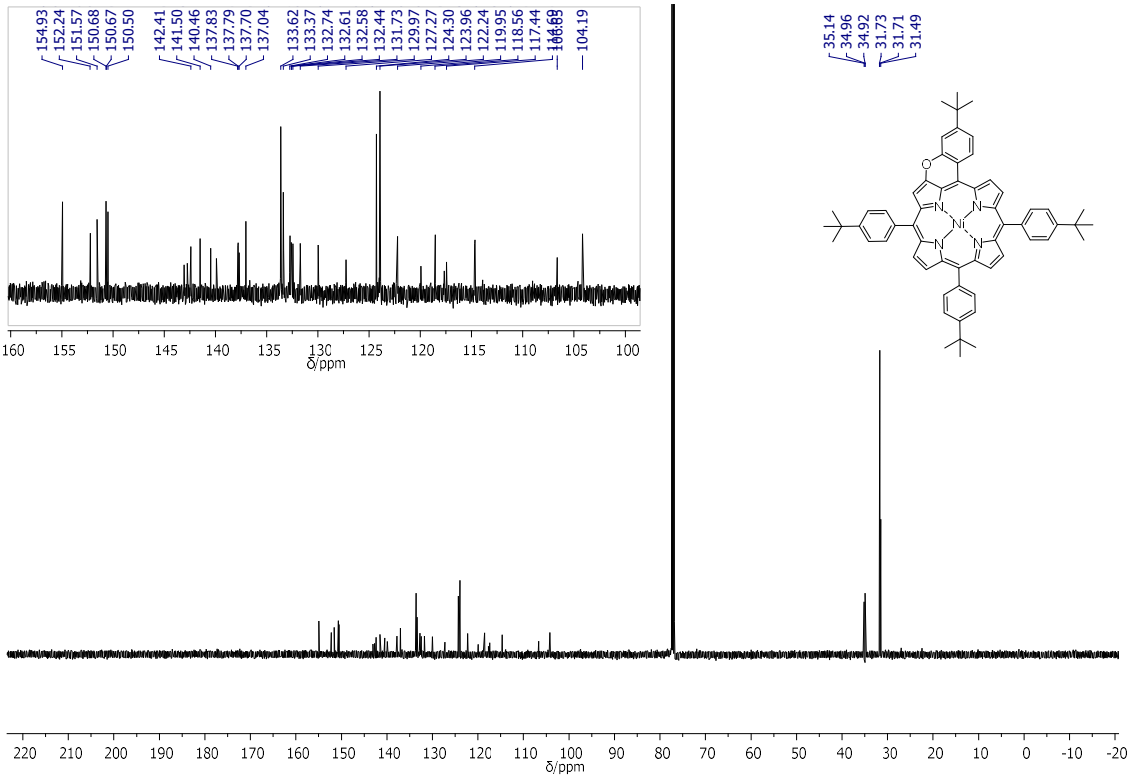

5-(4-(*Tert*-butyl)-2-hydroxyphenyl)-10,15,20-*tris*(4-(*tert*-butyl)phenyl)porphyrinato-N^{21},N^{22},N^{23},N^{24}-palladium(II) 3-10

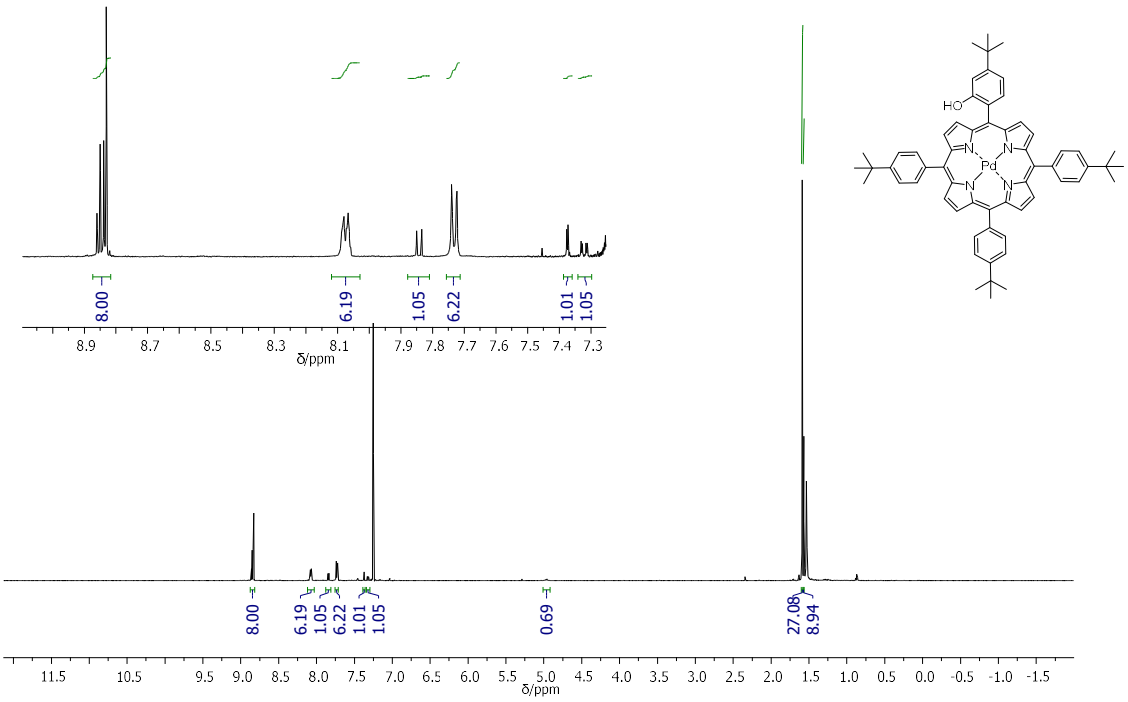

5-(4-*Tert*-butyl-2-hydroxyphenyl)-10,15,20-tris(4-tert-butylphenyl)porphyrinato-N^{21},N^{22},N^{23},N^{24}-zinc(II) 3-11

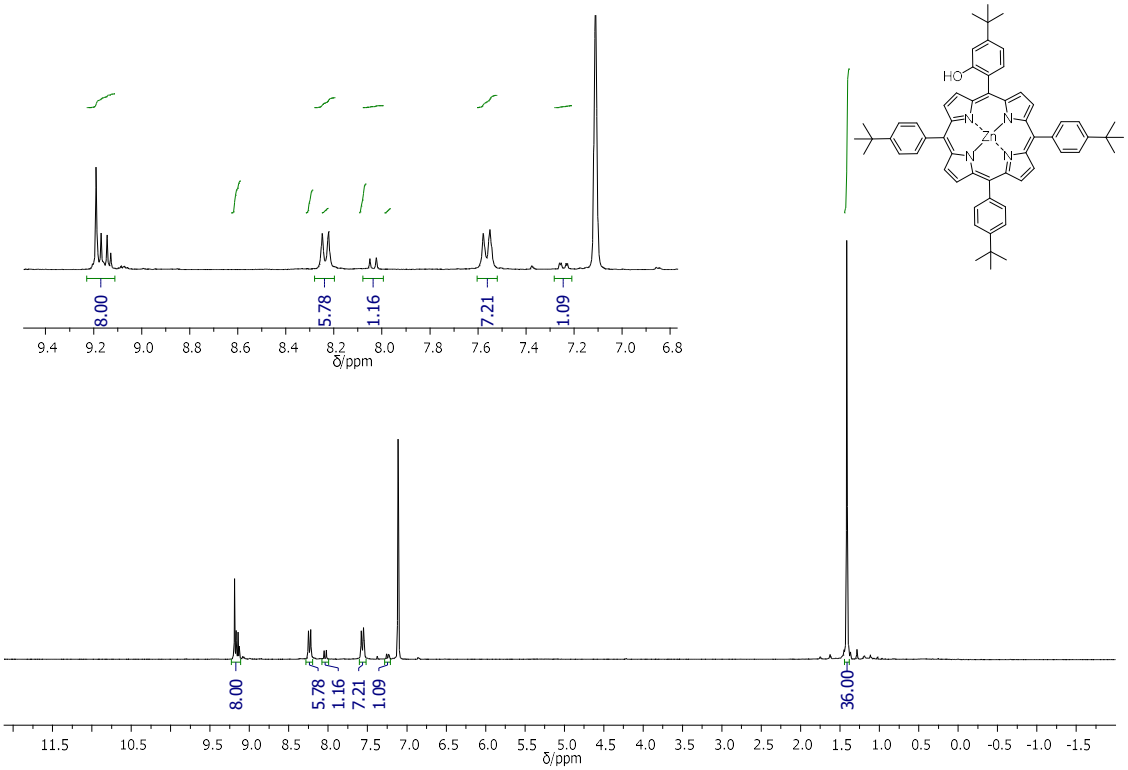

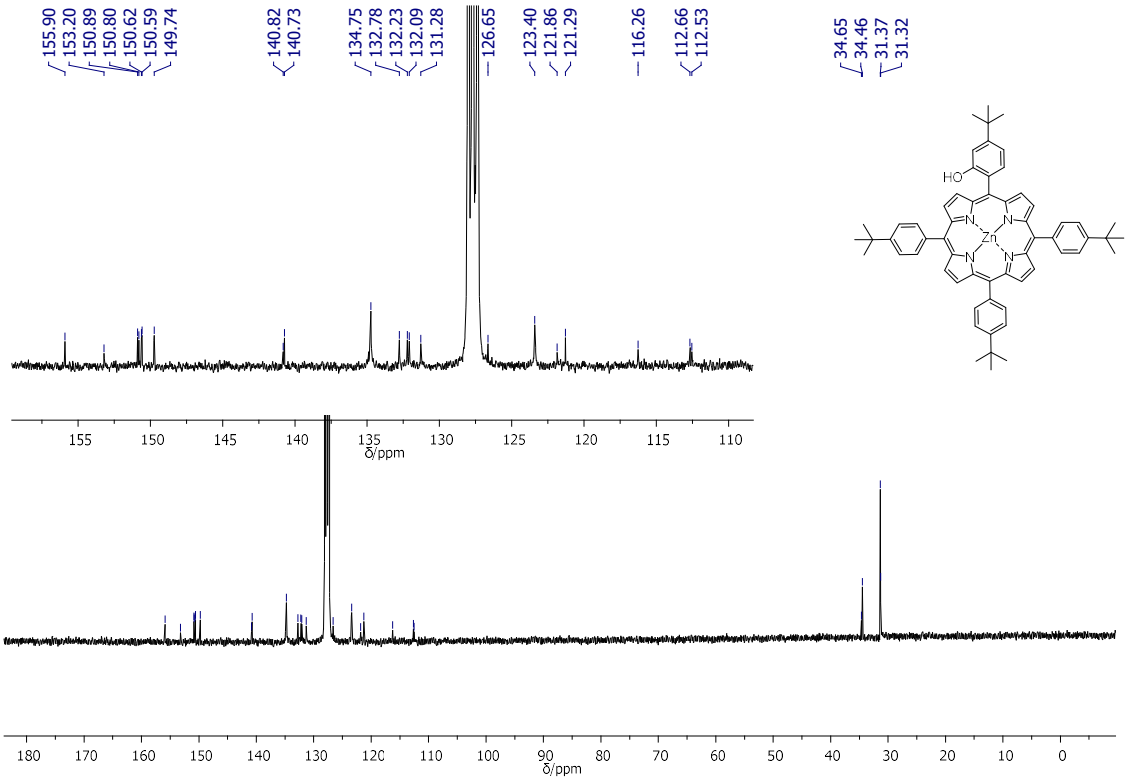

10,15,20-*Tris*(4-(*tert*-butyl)phenyl)benzopyrano[a,t]porphyrinato-N^{21},N^{22},N^{23},N^{24}-palladium(II) 3-13

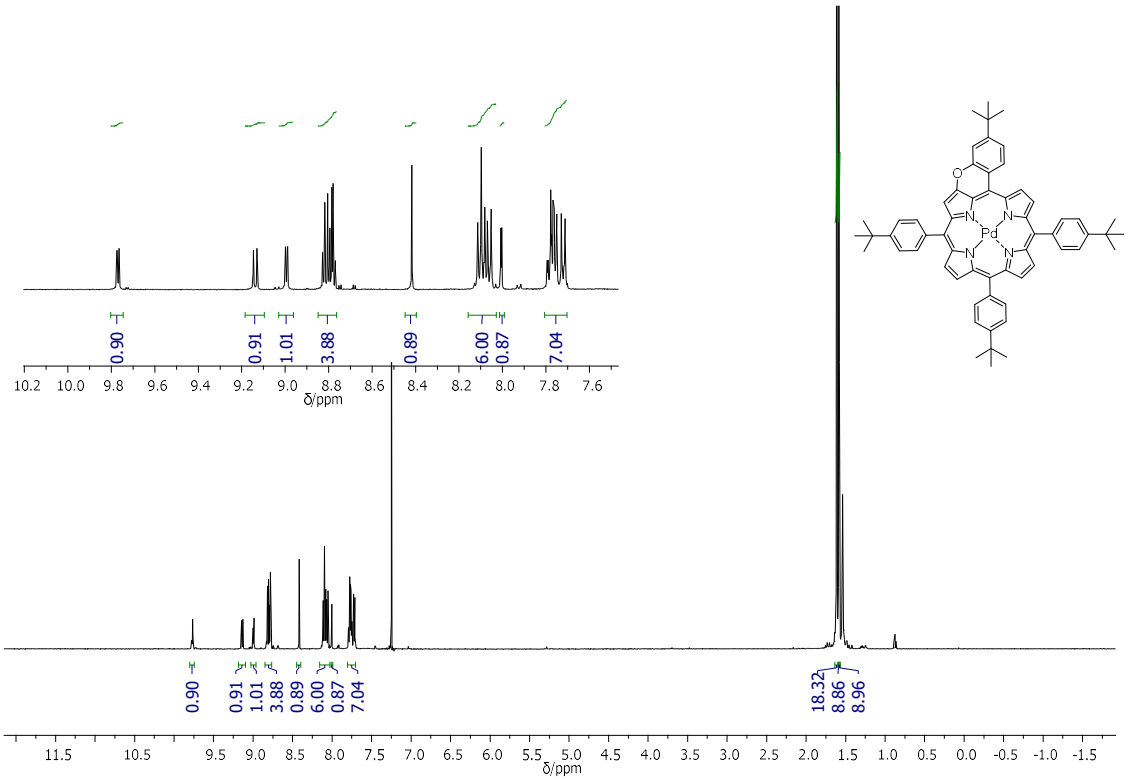

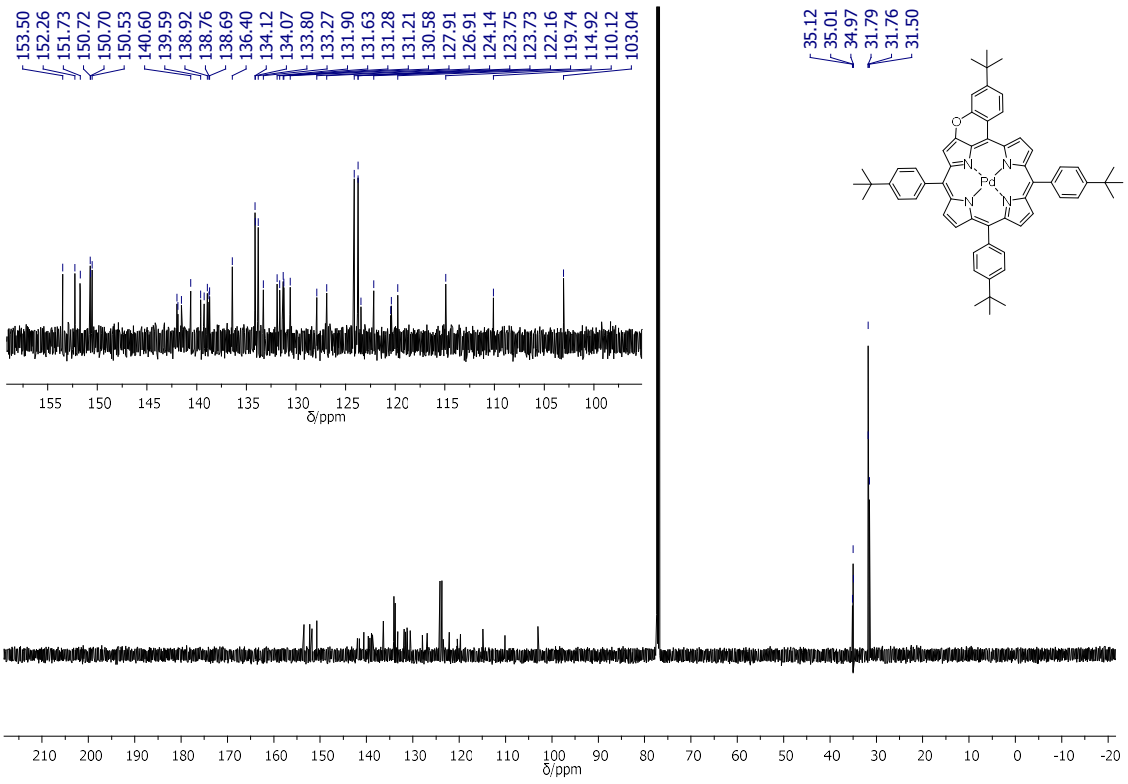

10,15,20-*Tris*(4-(*tert*-butyl)phenyl)benzopyrano[a,t]porphyrin 3-14

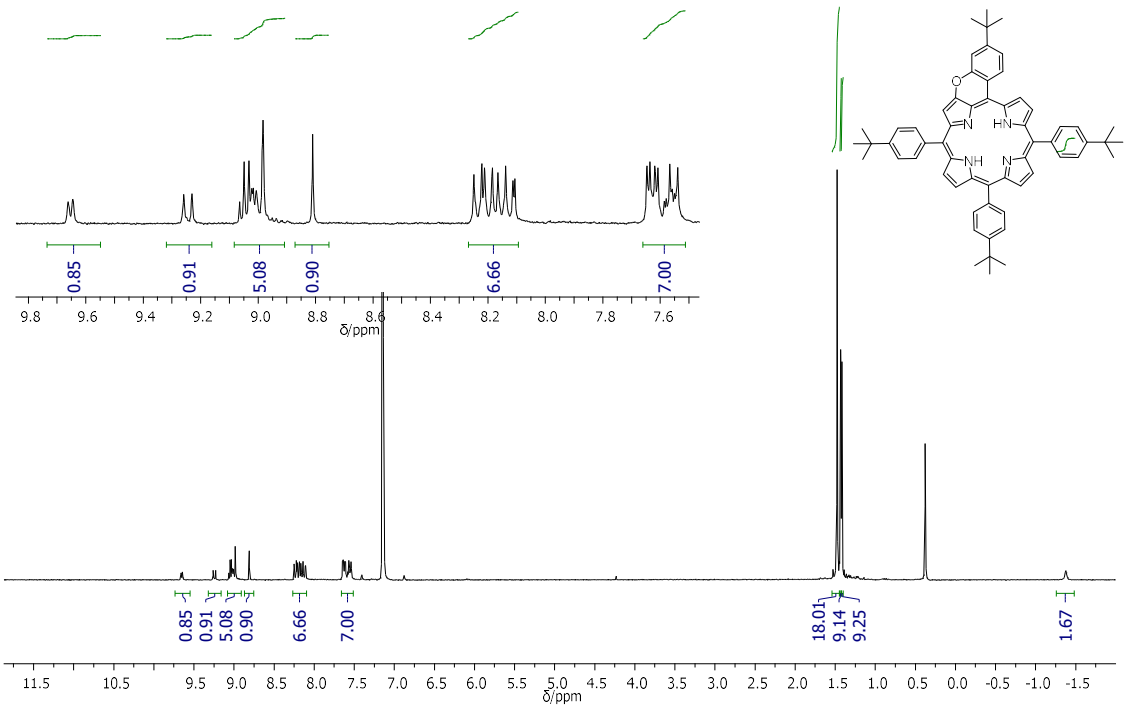

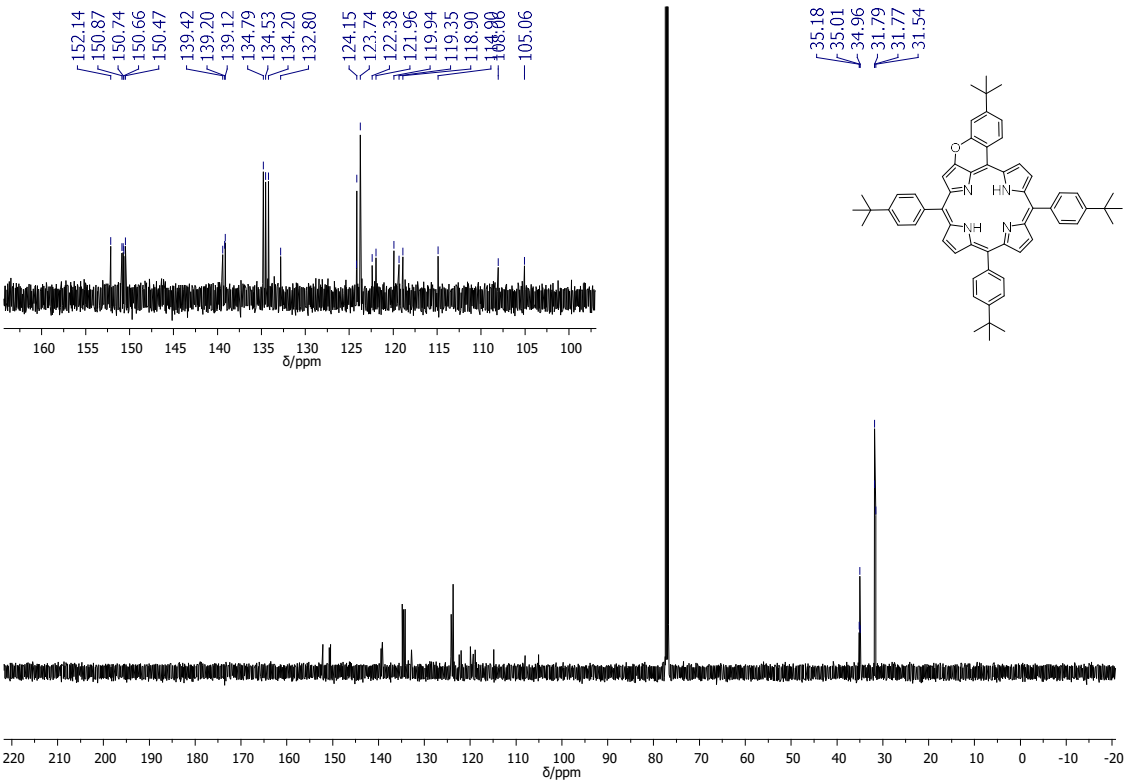

10,15,20-*Tris*(4-(*tert*-butyl)phenyl)benzopyrano[a,t]porphyrinato-N^{21},N^{22},N^{23},N^{24}-zinc(II) 3-15

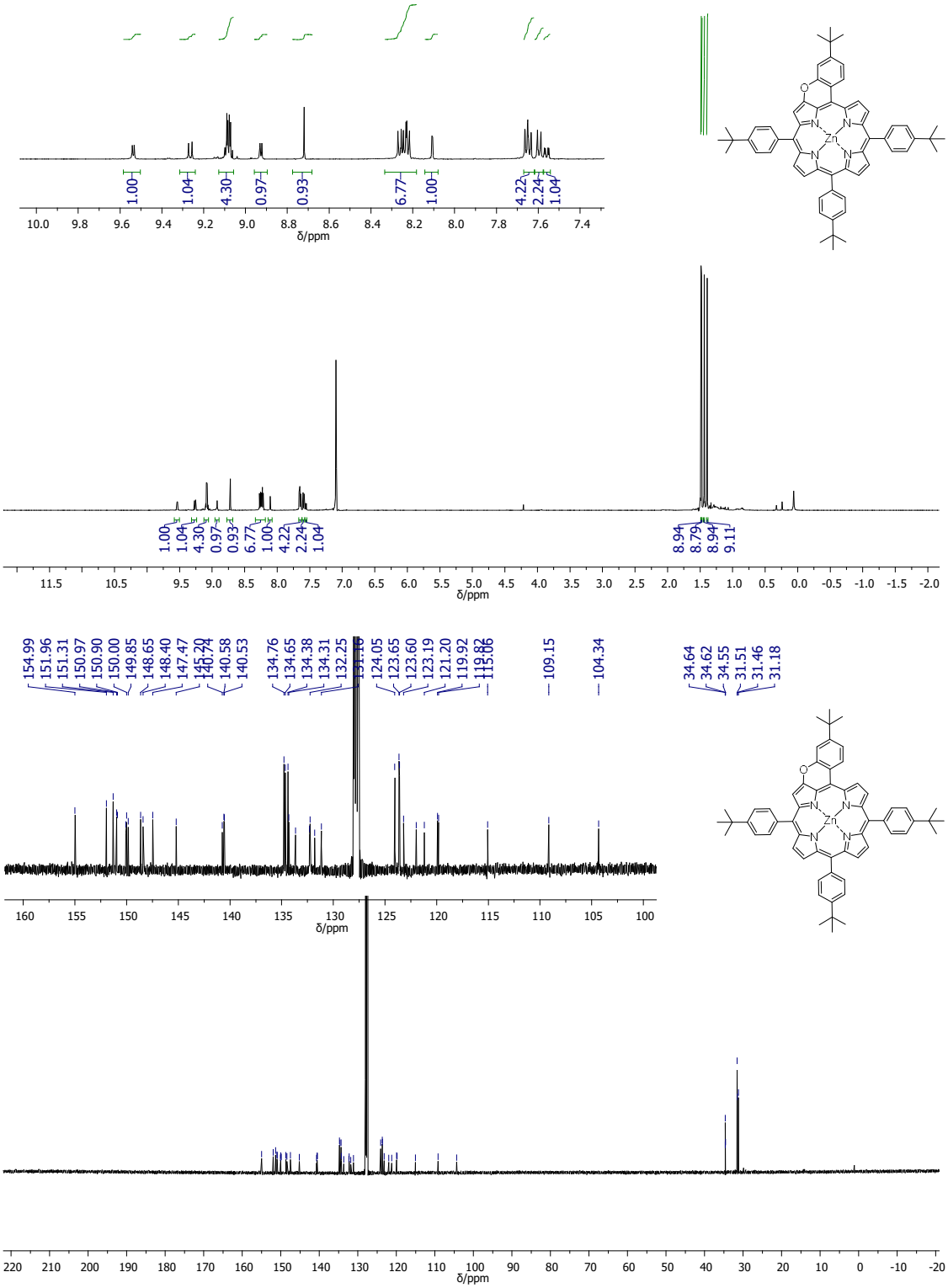

5-(4-(*Tert*-butyl)-2,6-dimethoxyphenyl)-10,15,20-*tris*(4-(*tert*-butyl)phenyl)porphyrin 3-20

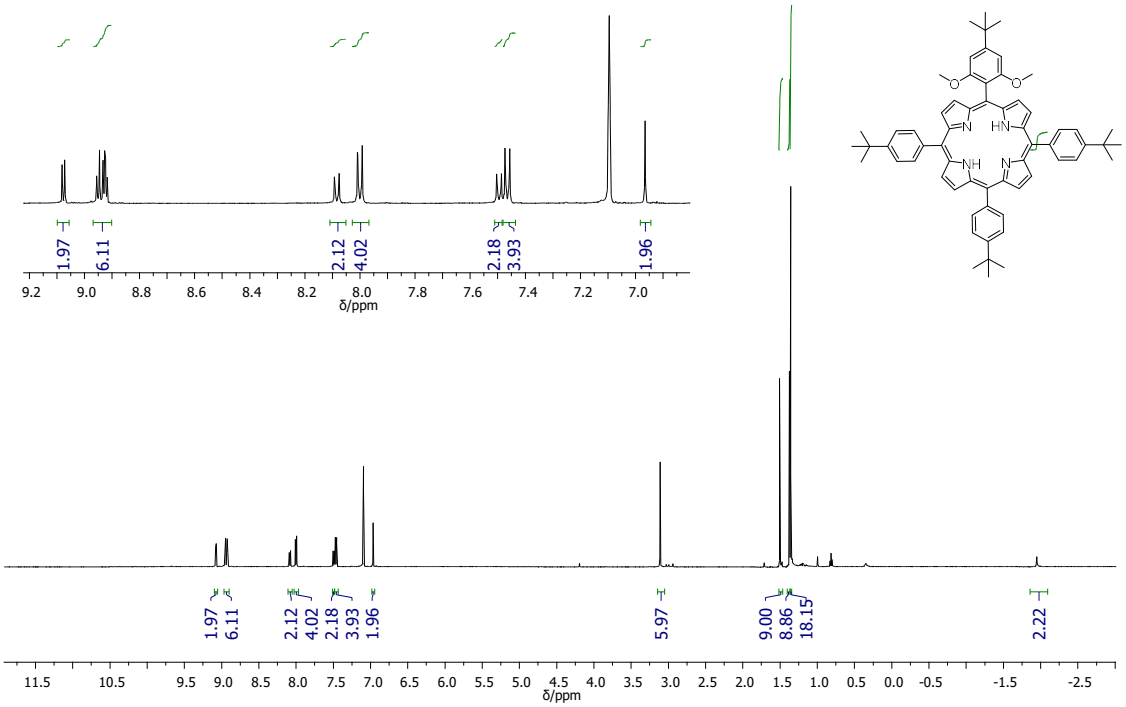

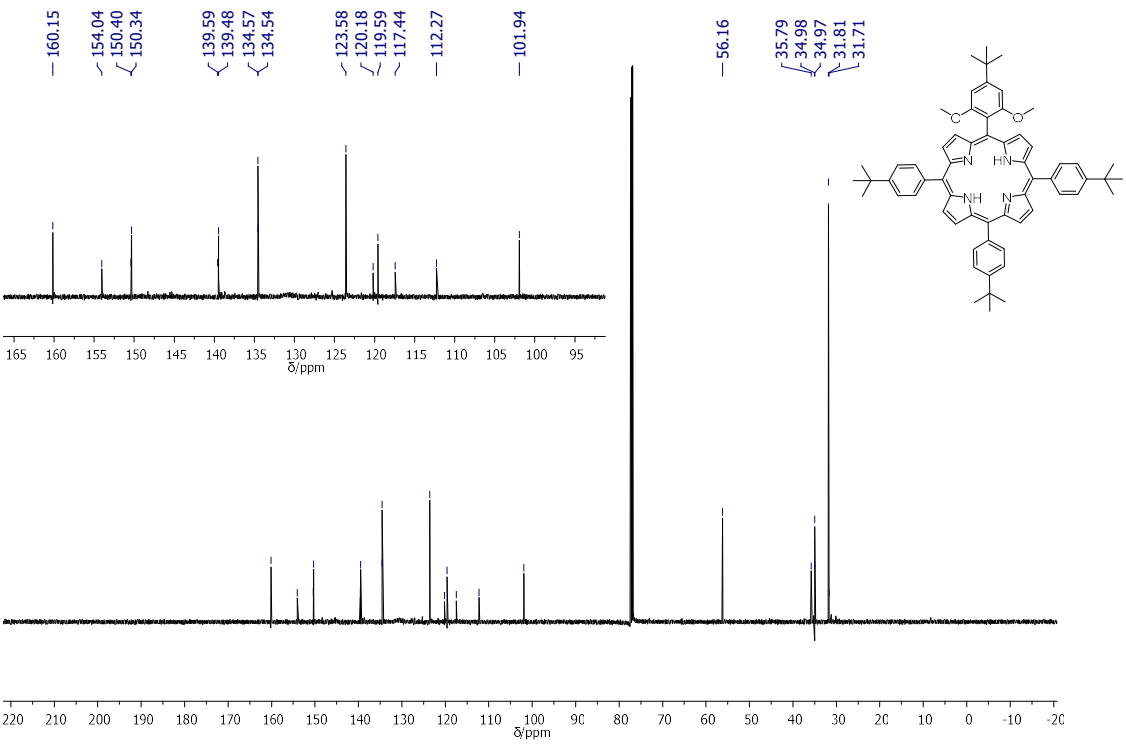

5-(4-(*Tert*-butyl)-2,6-dihydroxyphenyl)-10,15,20-*tris*(4-(*tert*-butyl)phenyl)porphyrin 3-26

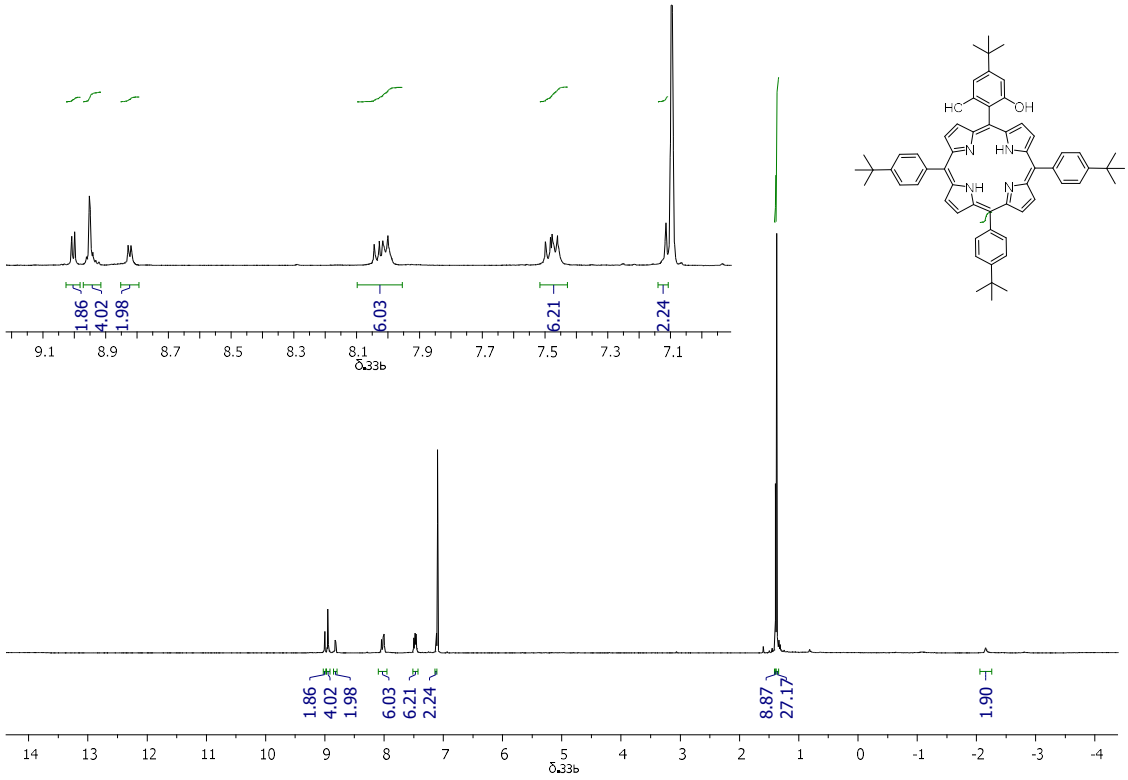

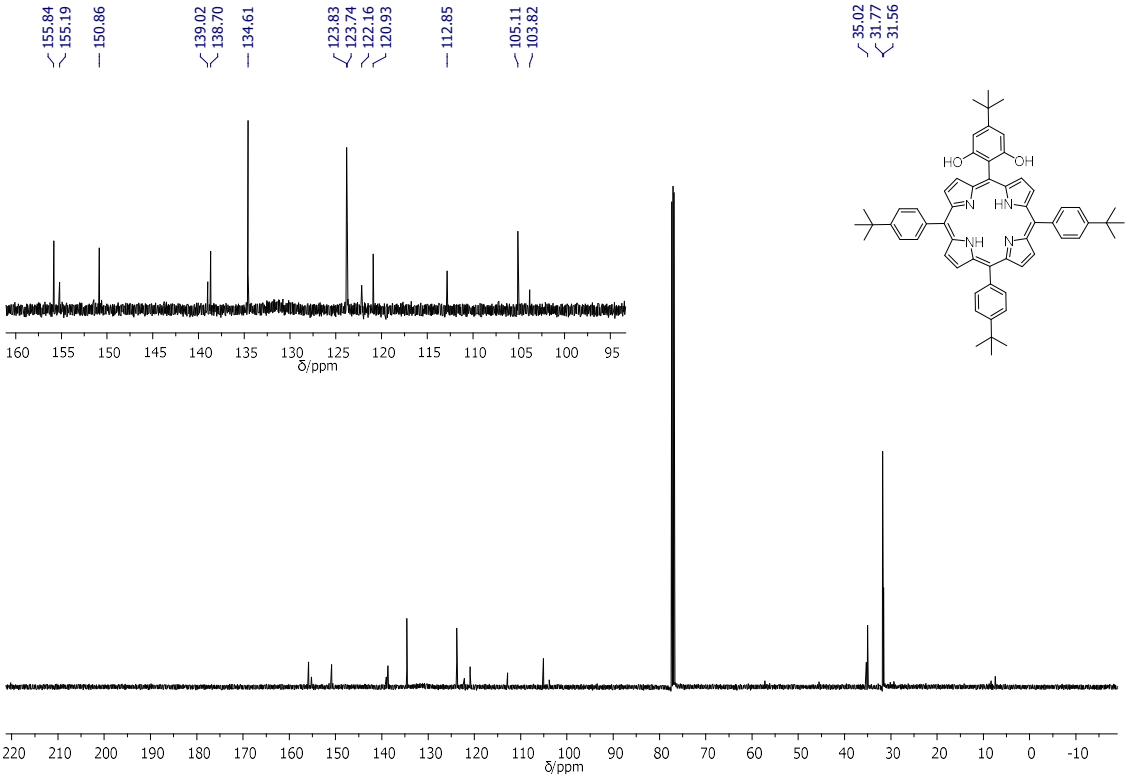

5-(4-(*Tert*-butyl)-2,6-hydroxyphenyl)-10,15,20-*tris*(4-(*tert*-butyl)phenyl)porphyrinato-N^{21},N^{22},N^{23},N^{24}-nickel(II) 3-19

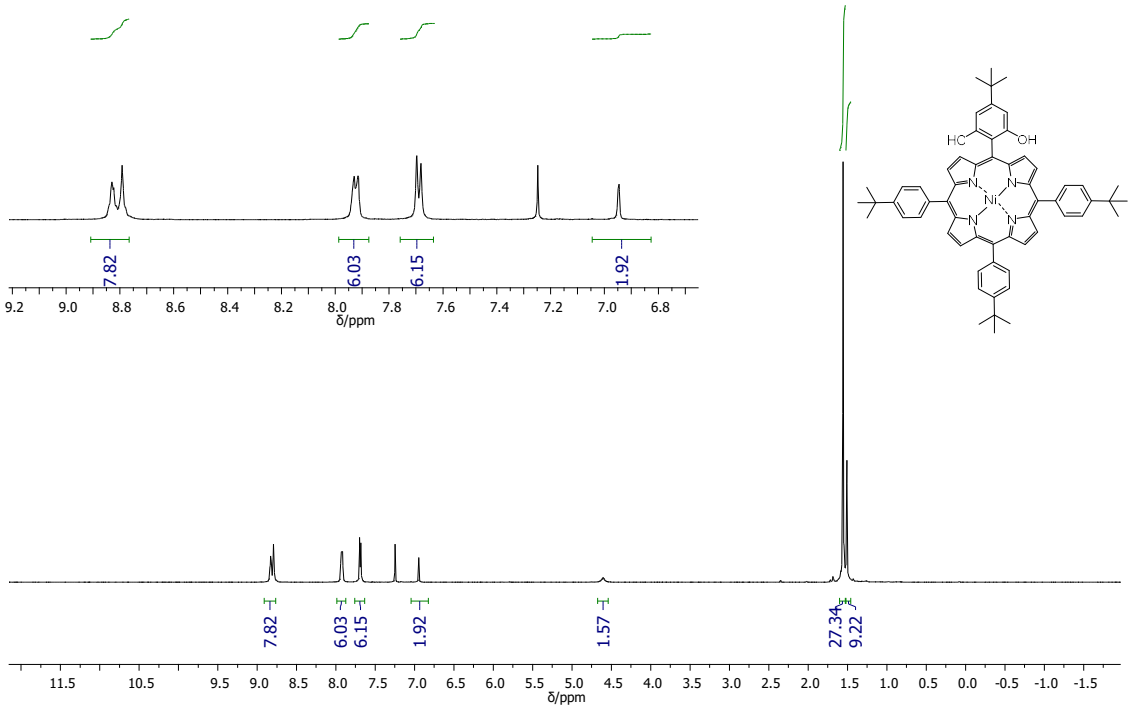

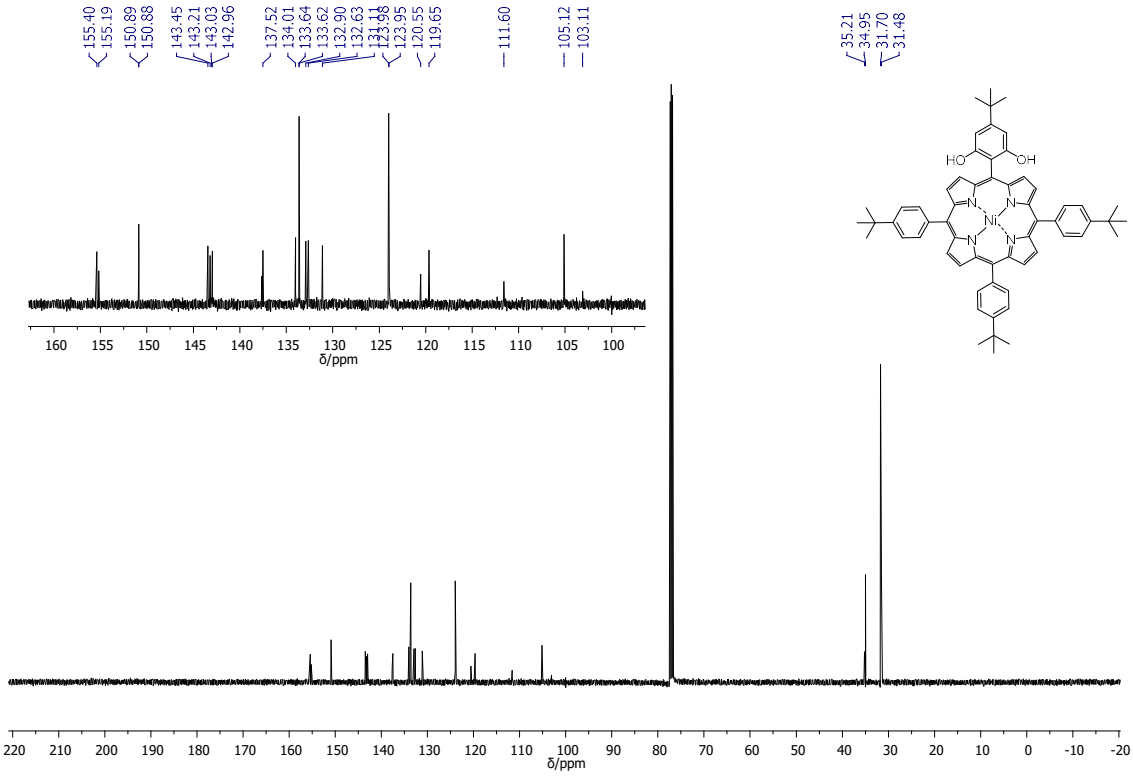

5-(4-(*Tert*-butyl)-2,6-dipyranophenyl)-10,15,20-(4-*tert*-butylphenyl)porphyrinato-N^{21},N^{22},N^{23},N^{24}-nickel(II) 3-16

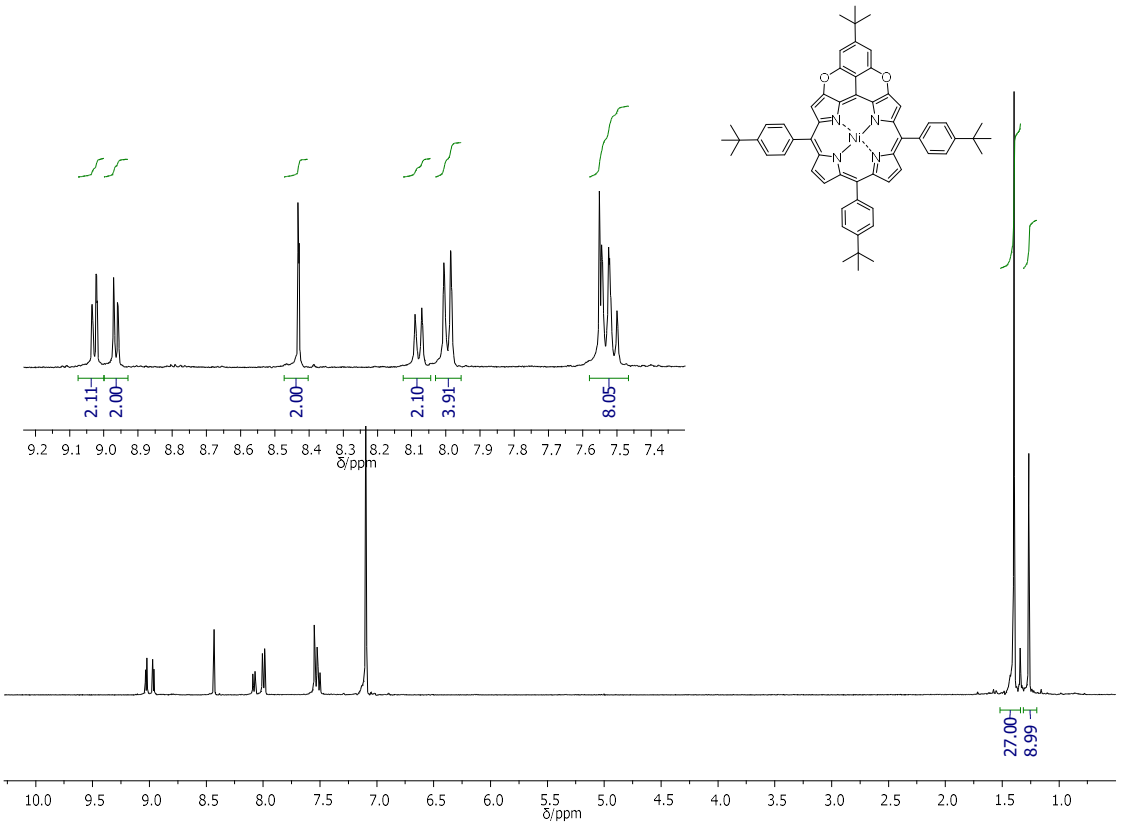

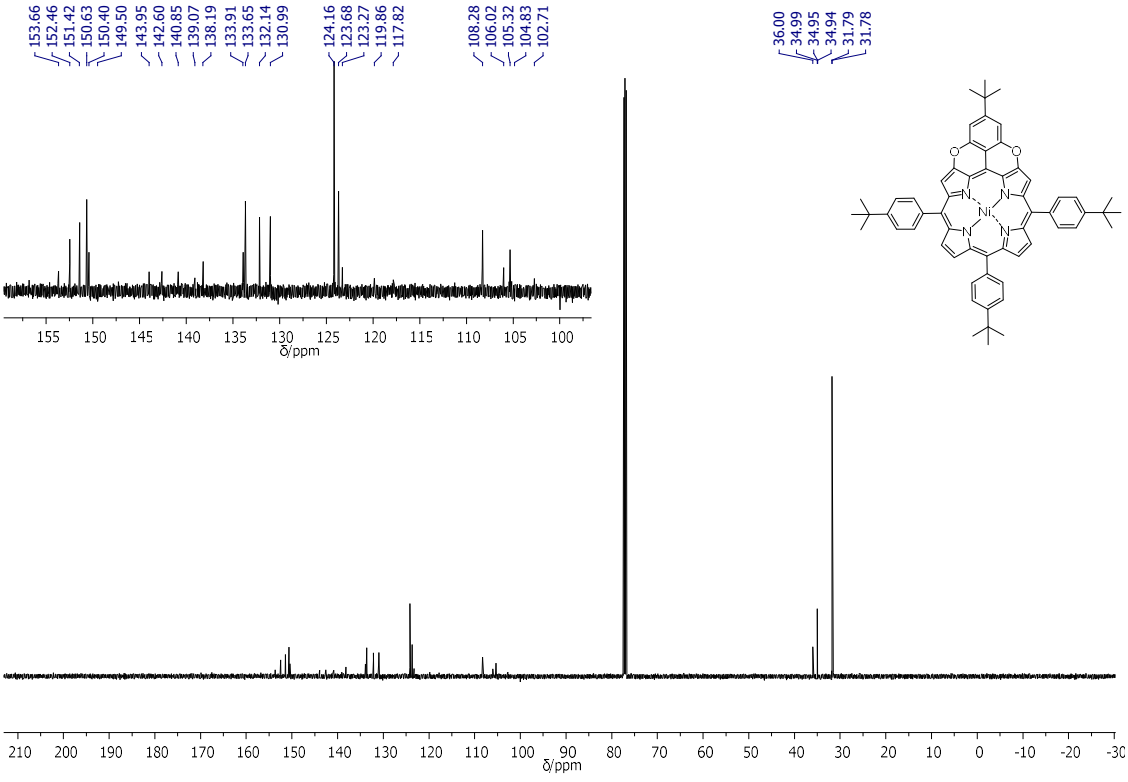

5-(4-(*Tert*-butyl)-2,6-dipyranophenyl)-10,15,20-(4-*tert*-butylphenyl)porphyrin 3-27

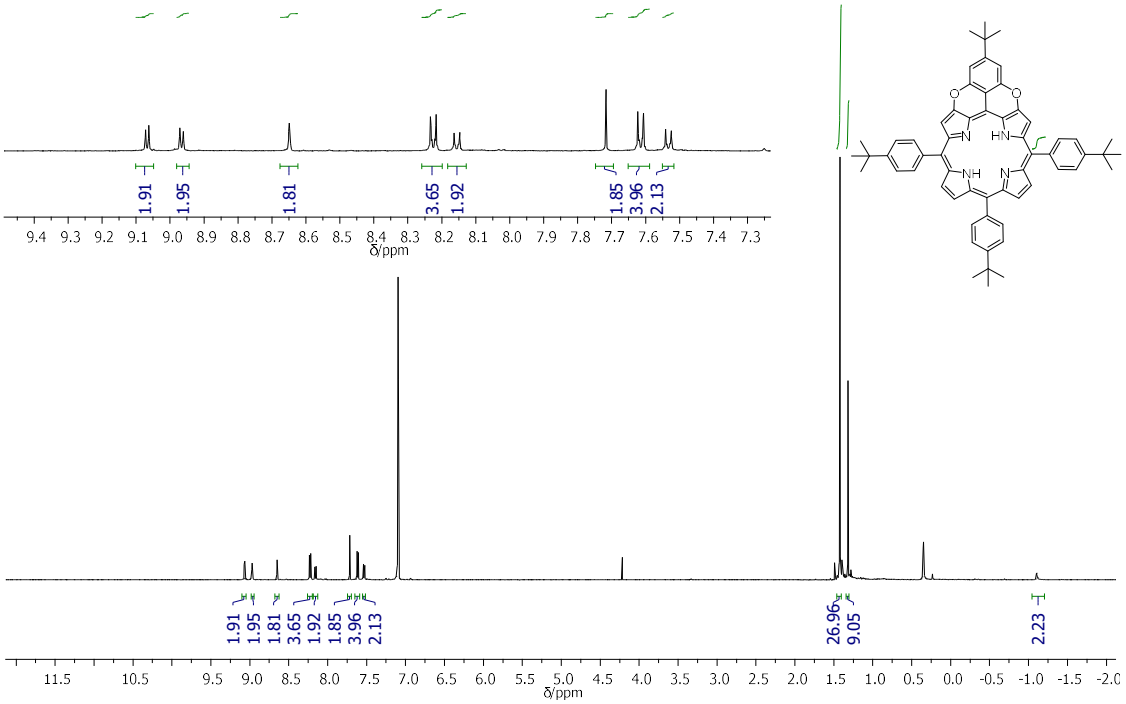

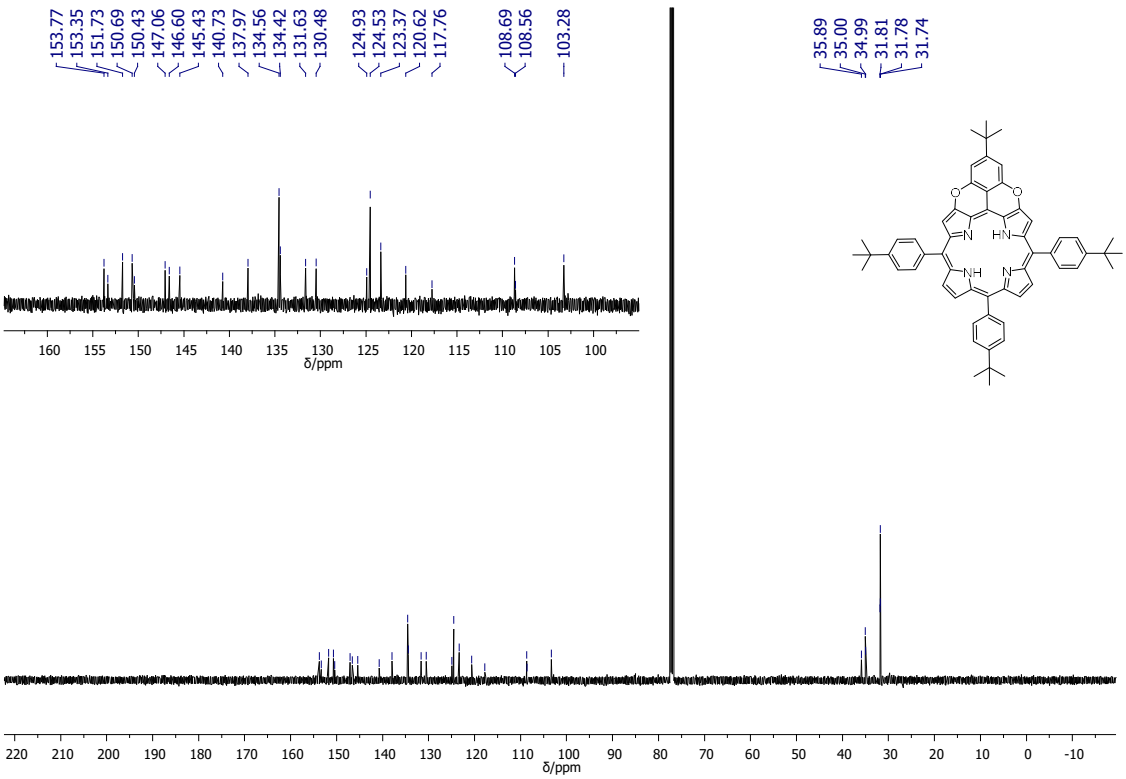

5-(4-(*Tert*-butyl)-2,6-dipyranophenyl)-10,15,20-(4-*tert*-butylphenyl)porphyrinato-N^{21},N^{22},N^{23},N^{24}-zinc(II) 3-28

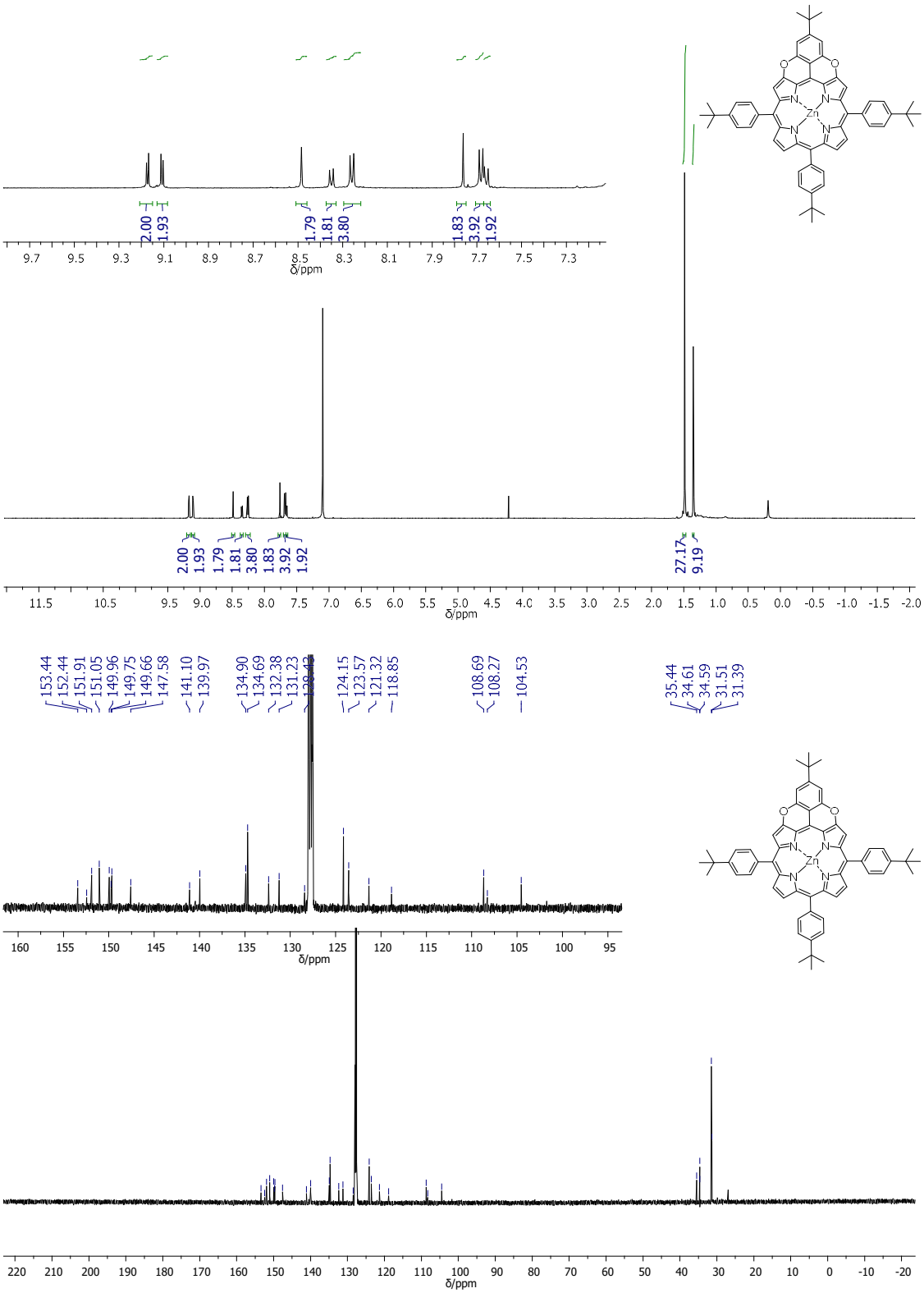

5,15-*Bis*(4-(*tert*-butyl)-2-methoxyphenyl)porphyrin 3-33

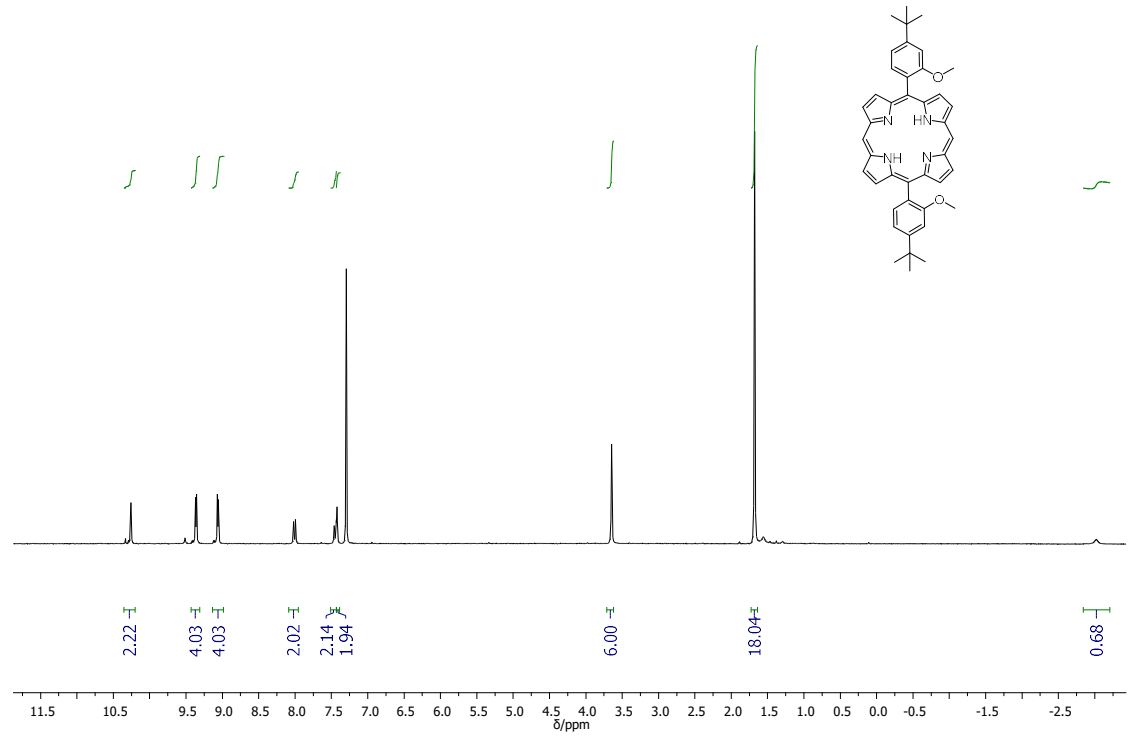

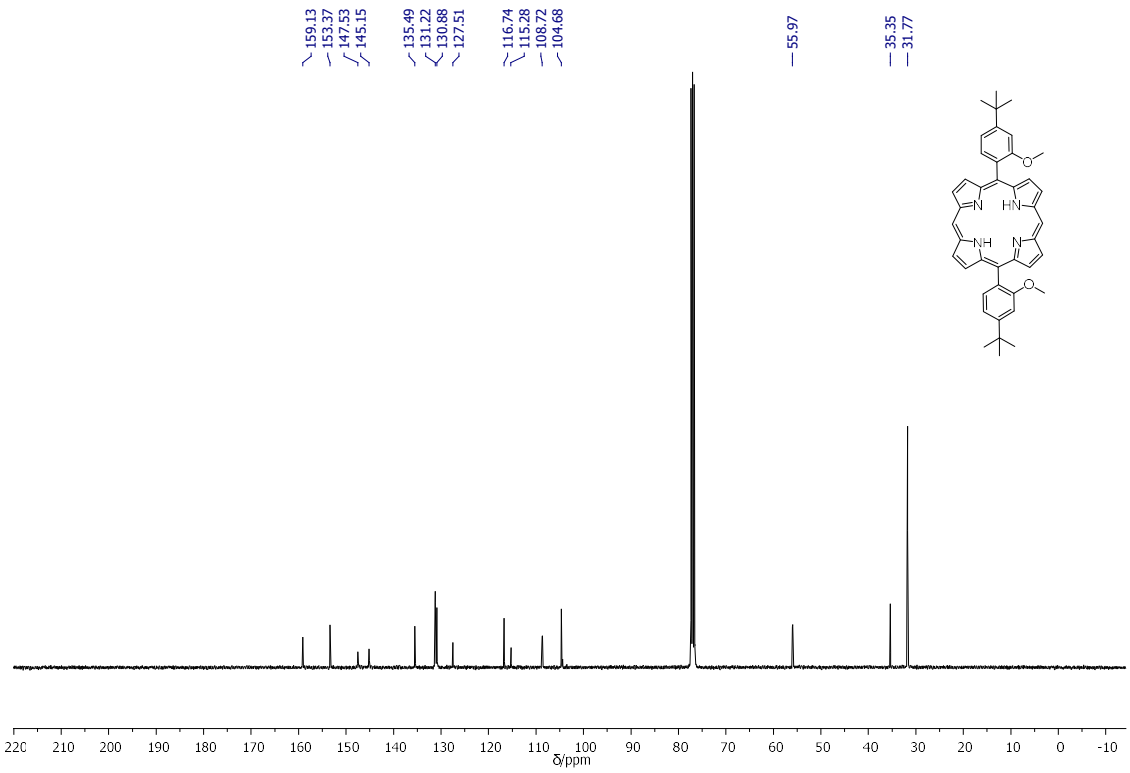

5,15-Dibromo-10,20-*bis*(4-(*tert*-butyl)-2-methoxyphenyl)porphyrin 3-32

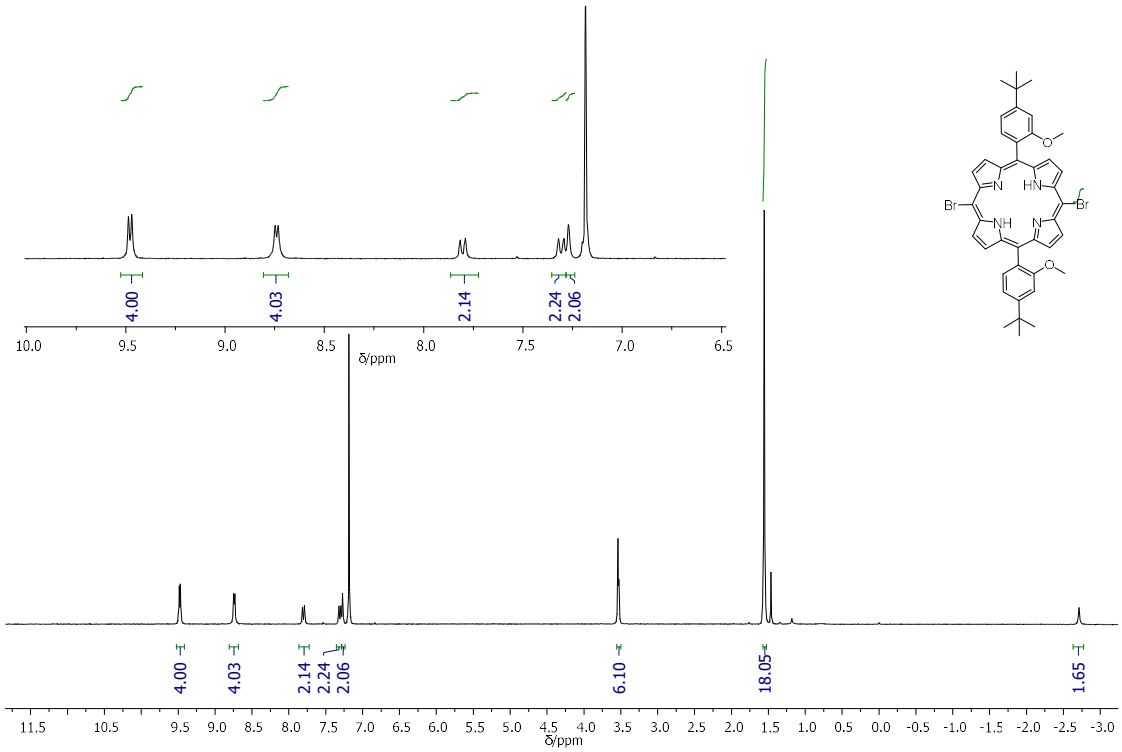

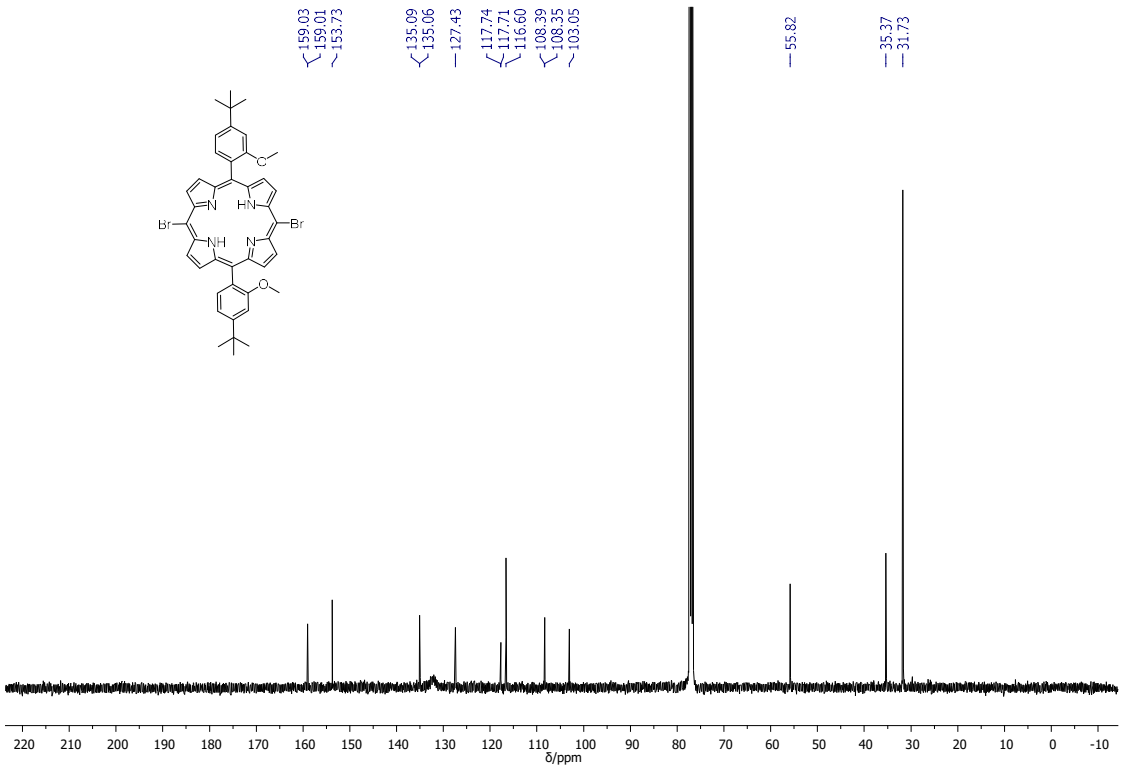

5,15-*Bis*(4-(*tert*-butyl)-2-methoxyphenyl)-10,20-*bis*(4-(*tert*-butyl)phenyl)porphyrin 3-30

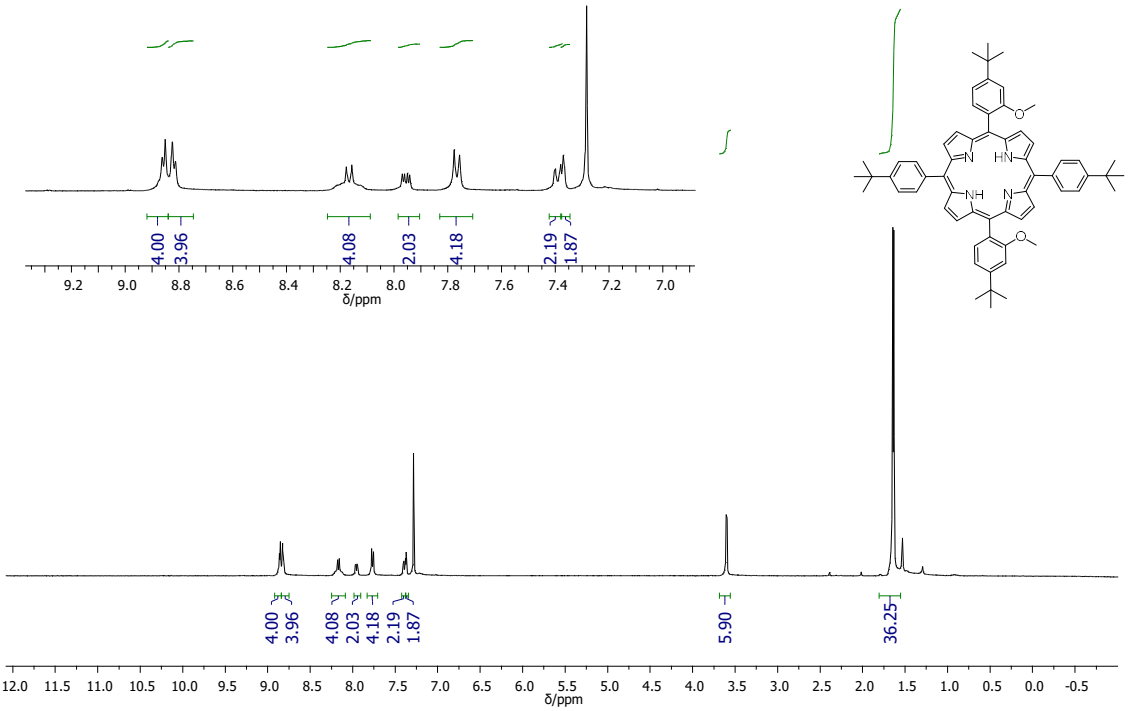

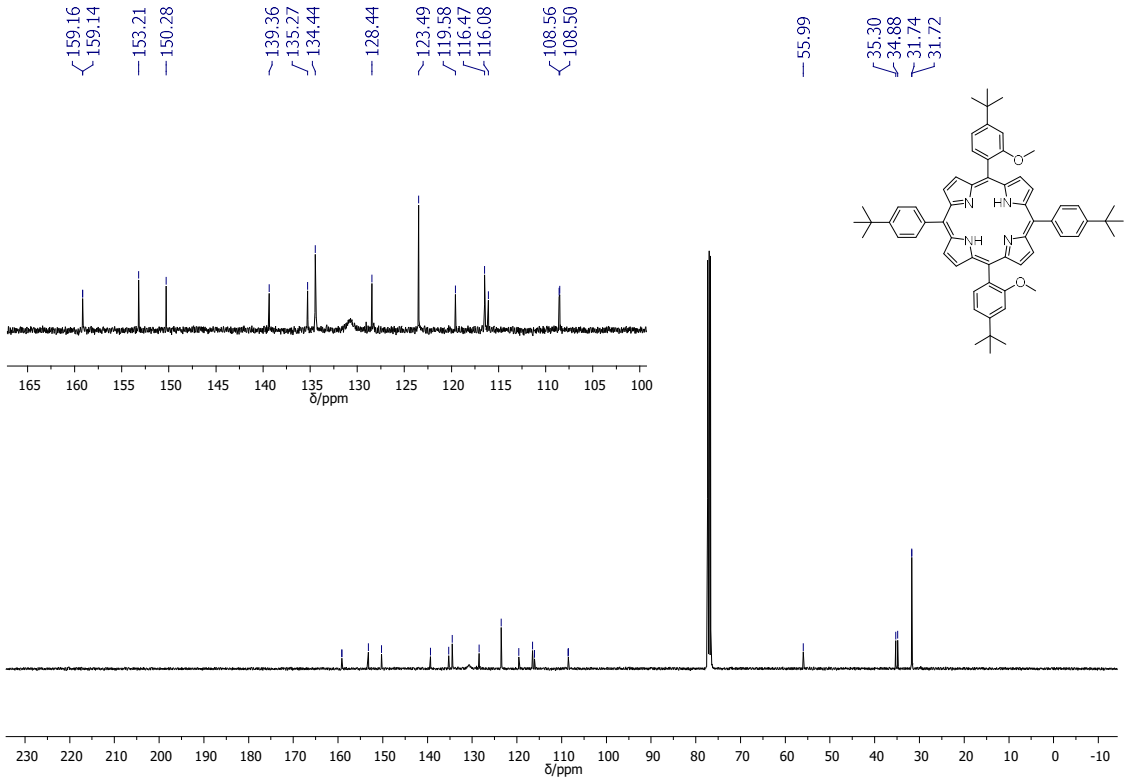

5,15-*Bis*(4-(*tert*-butyl)-2-hydroxyphenyl)-10,20-*bis*(4-(*tert*-butyl)phenyl)porphyrin 3-34

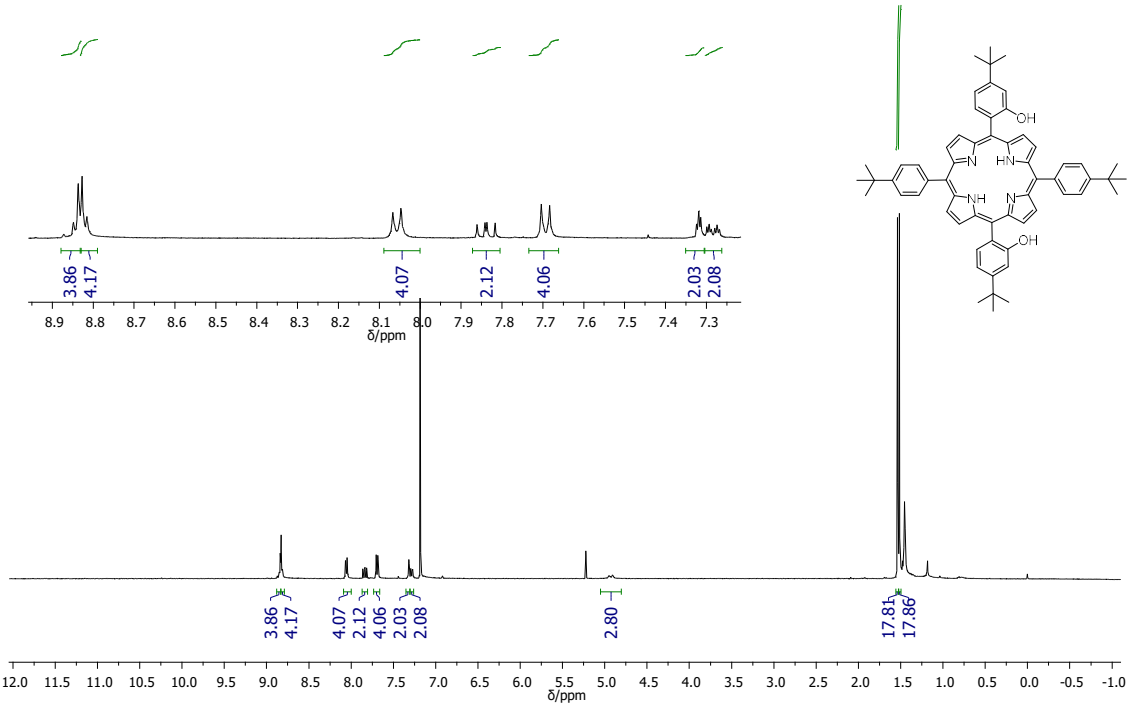

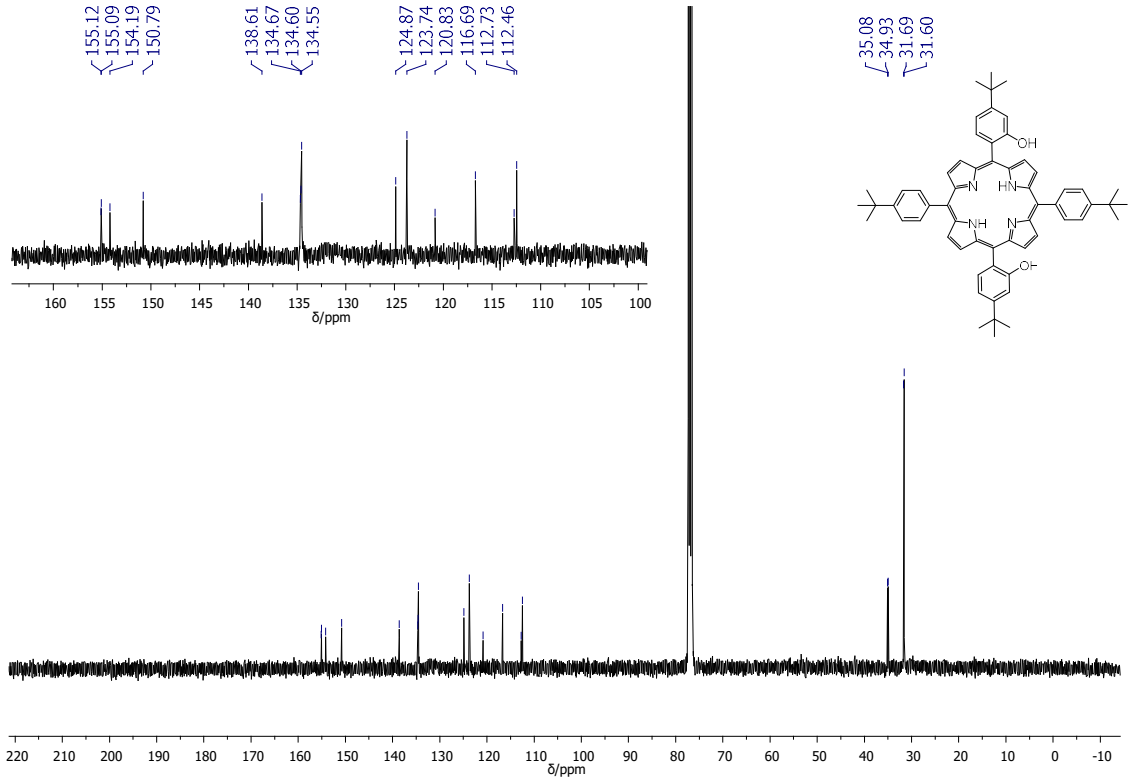

5,15-bis(4-(*tert*-butyl)-2-hydroxyphenyl)-10,20-bis(4-*tert*-butylphenyl)porphyrinato-N^{21},N^{22},N^{23},N^{24}-nickel(II) 3-29

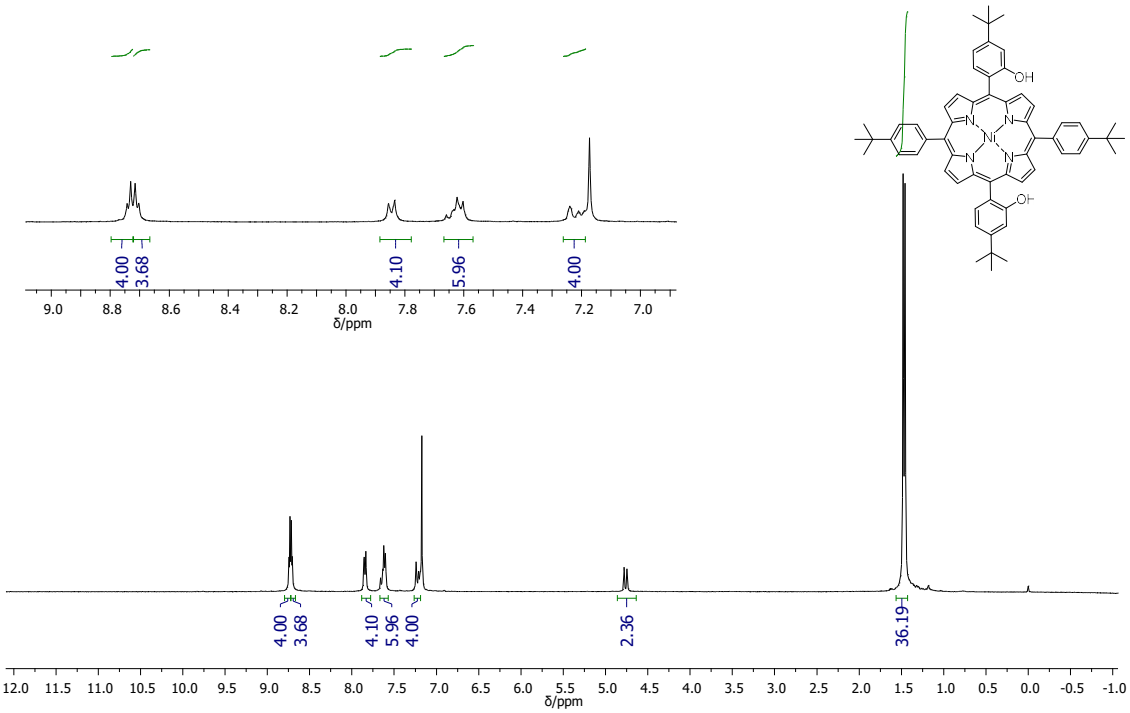

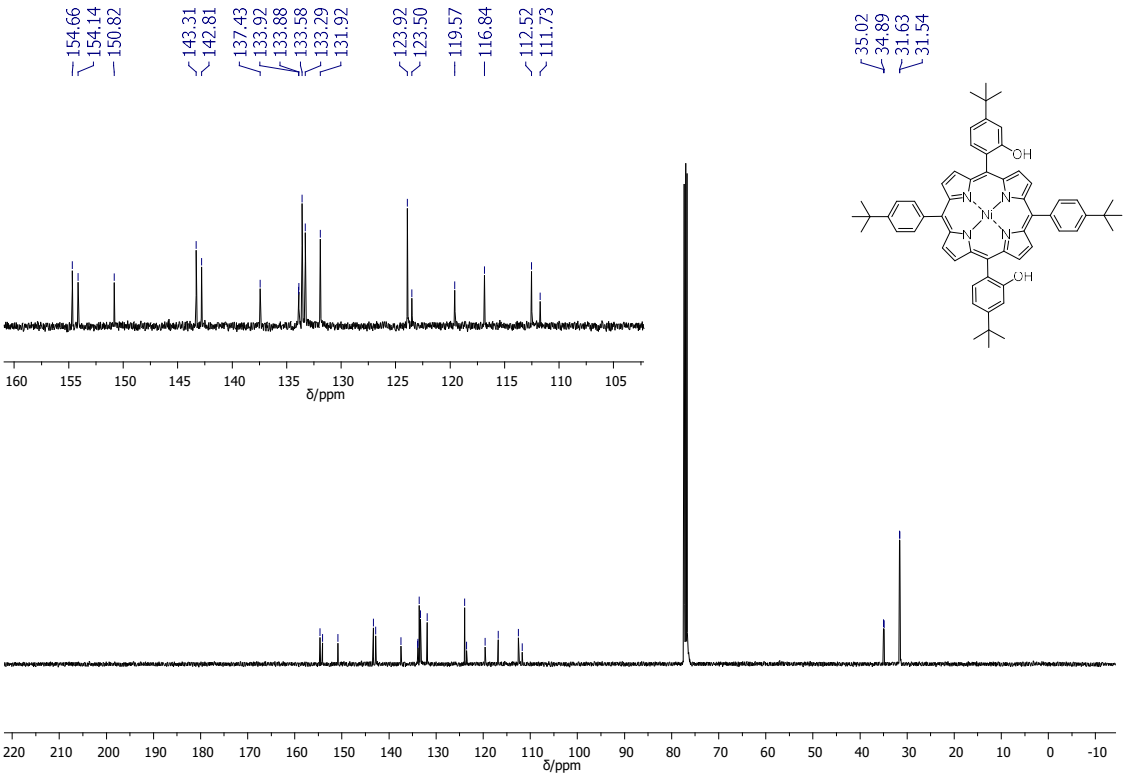

10,20-*Bis*(4-(*tert*-butyl)phenyl)dibenzopyrano[a,t,j,k]porphyrin 3-36

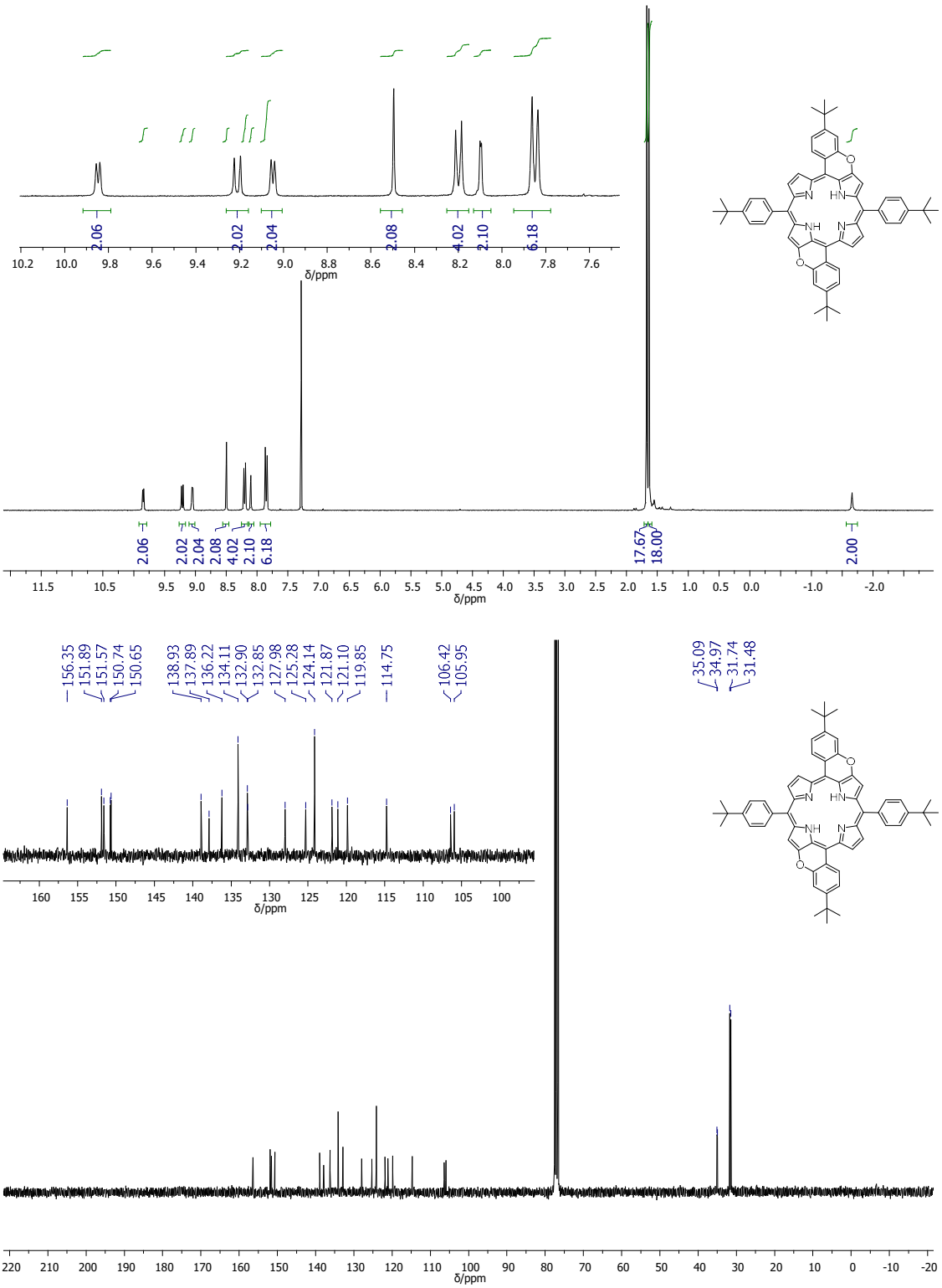

10,20-*Bis*(4-(*tert*-butyl)phenyl)dibenzopyrano[a,t,h,i]porphyrin 3-35

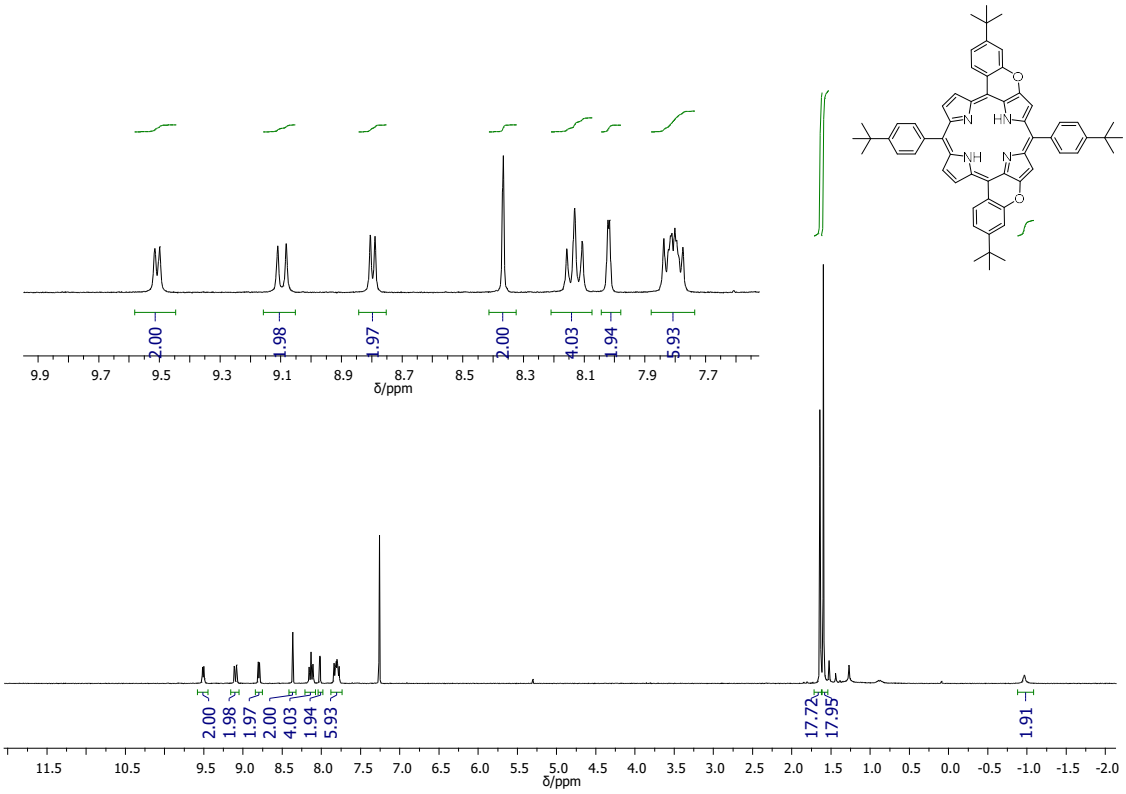

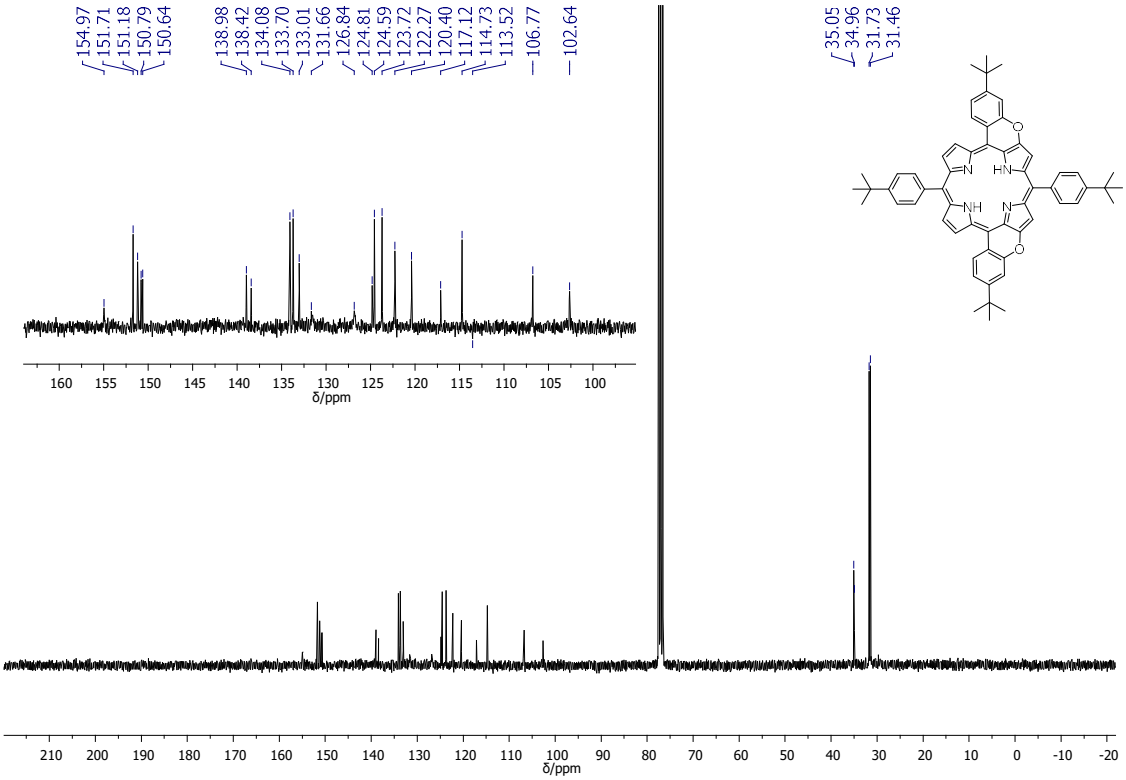

5,10,15,20-*Tetrakis*(4-(*tert*-butyl)-2-methoxyphenyl)porphyrin 4-4

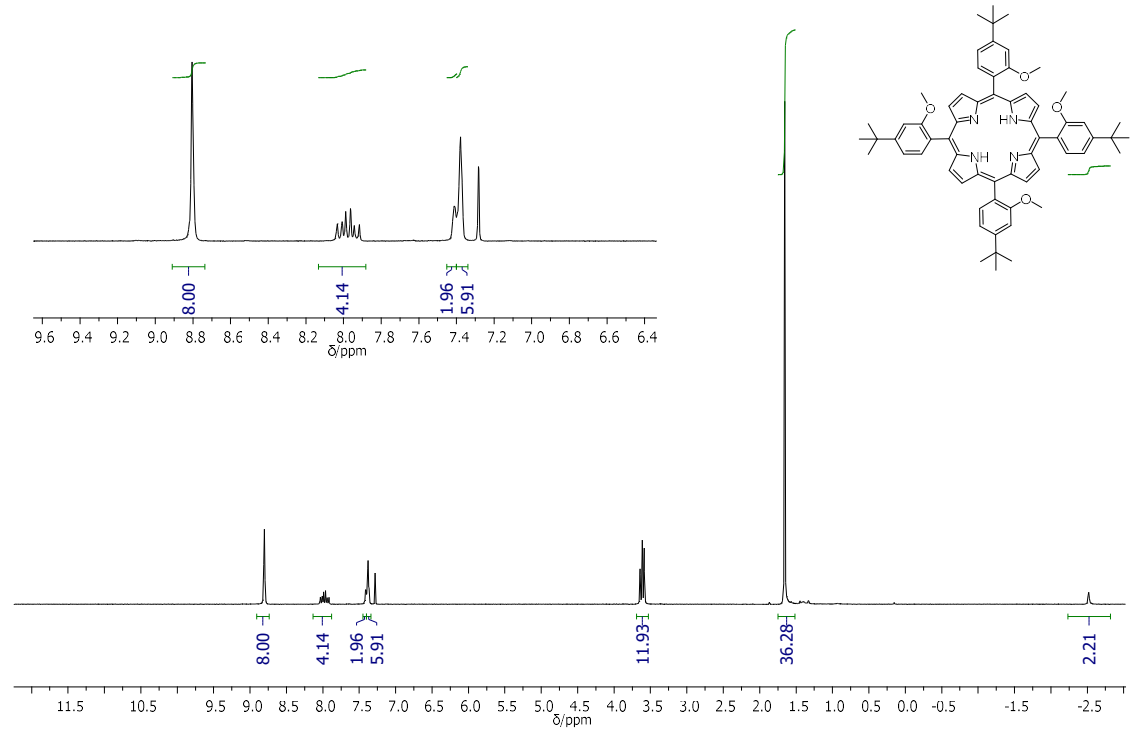

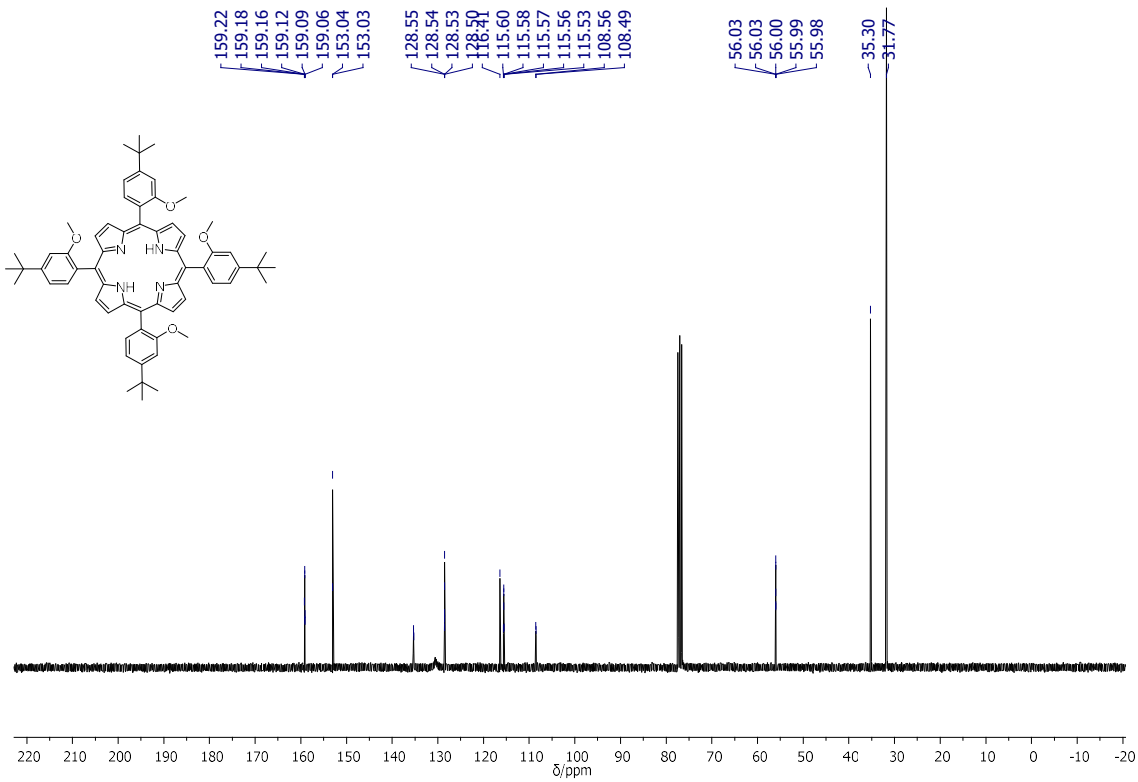

5,10,15,20-*Tetrakis*(4-(*tert*-butyl-2-hydroxyphenyl)porphyrin 4-5

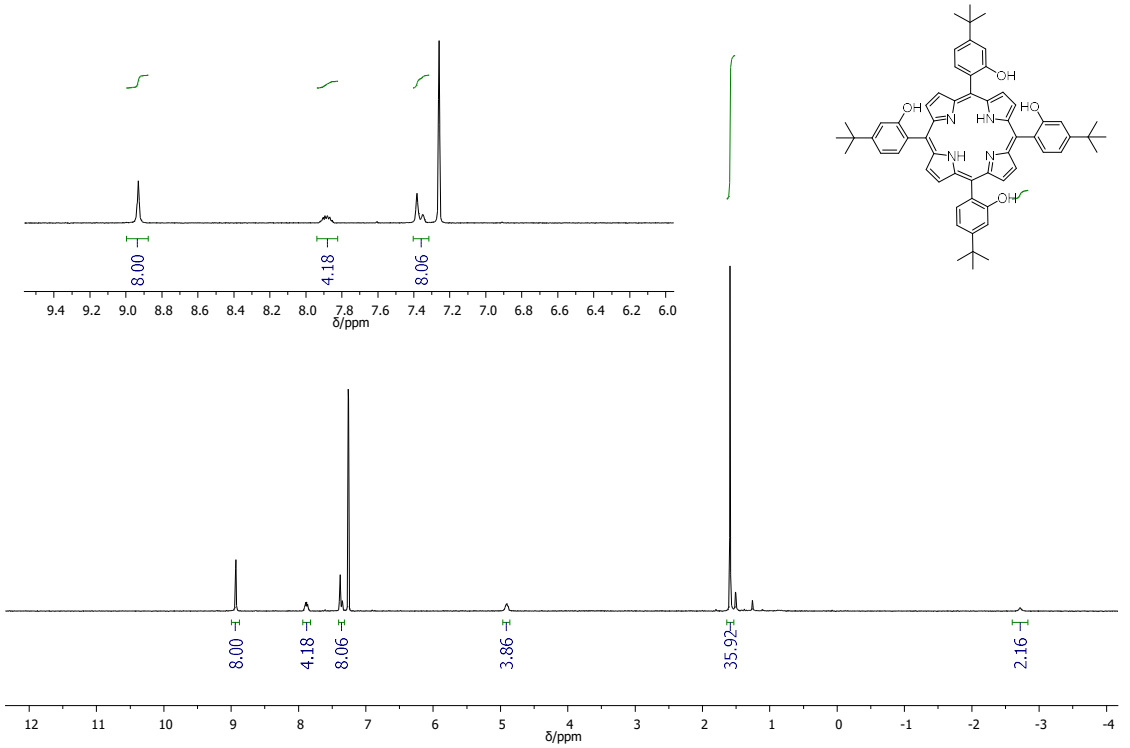

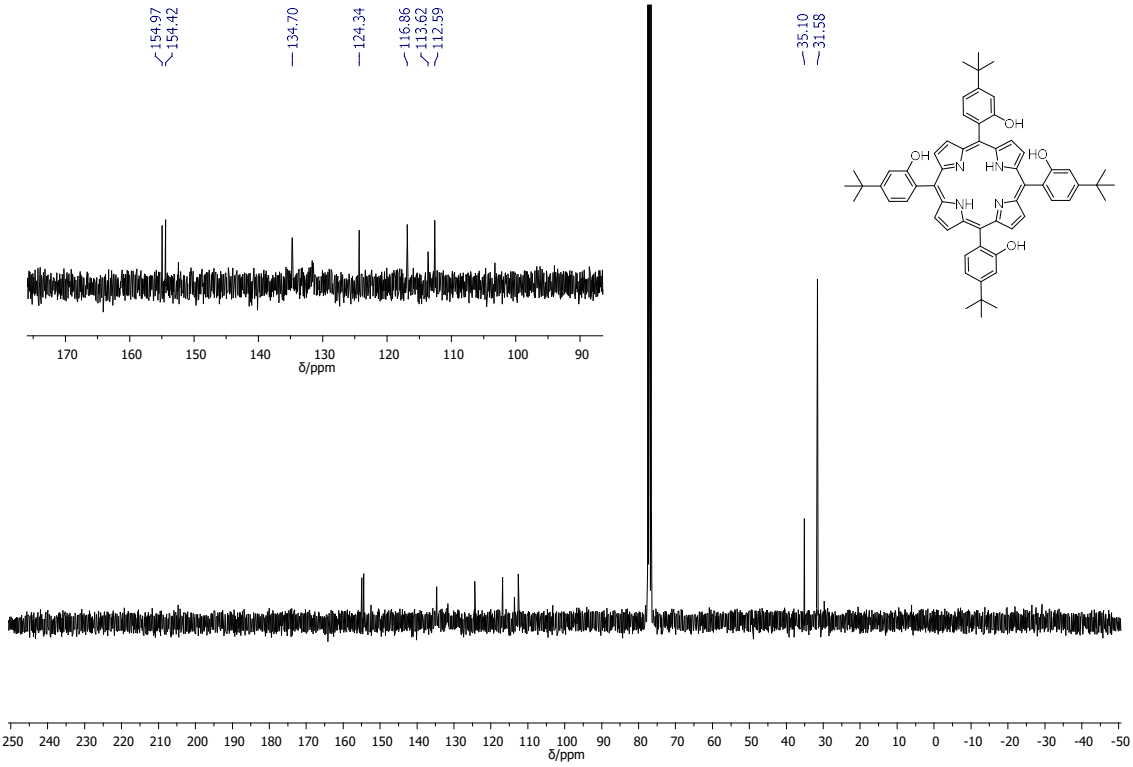

5,10,15,20-*Tetrakis*(4-*tert*-butyl-2-hydroxyphenyl)porphyrinato-N^{21},N^{22},N^{23},N^{24}-nickel(II) 4-3

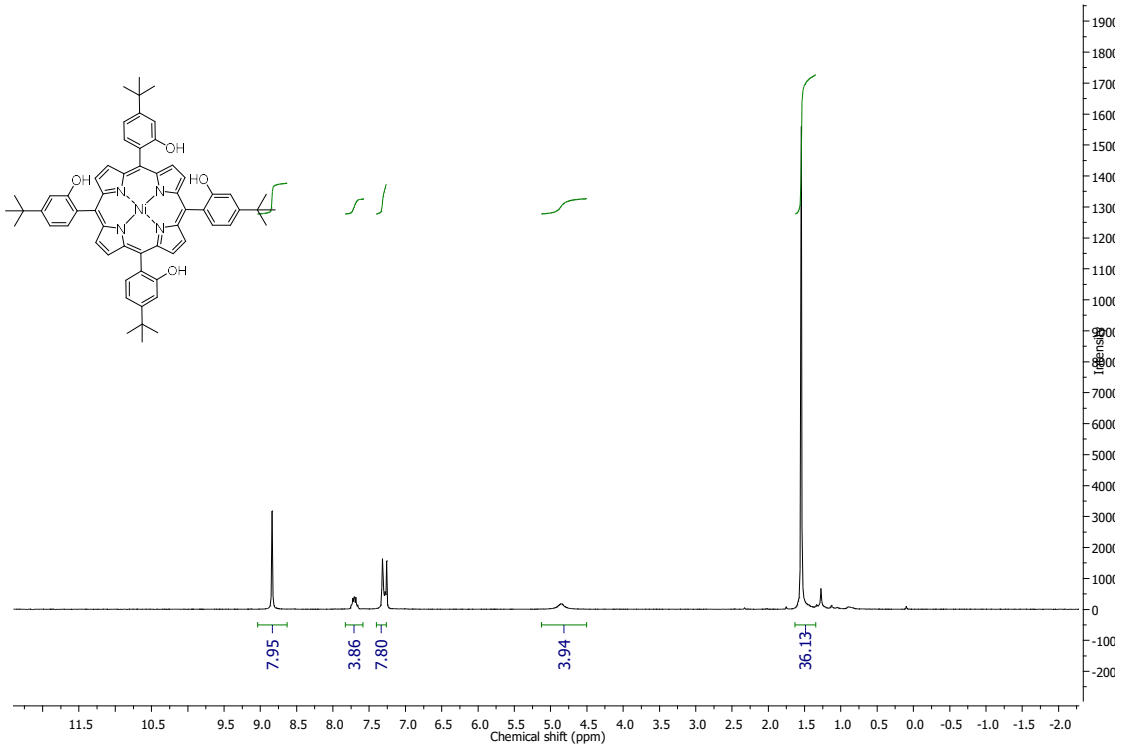

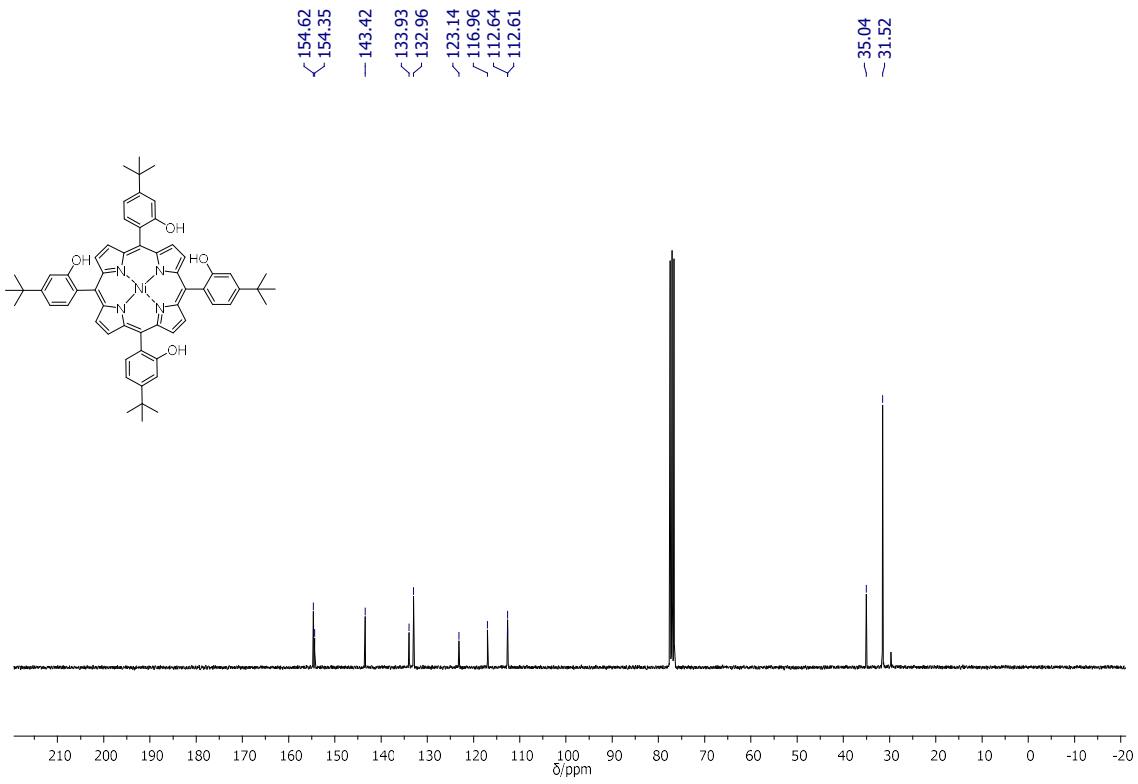

5,15-*Bis*(4-(*tert*-butyl)-2,6-dimethoxyphenyl)porphyrin 4-10

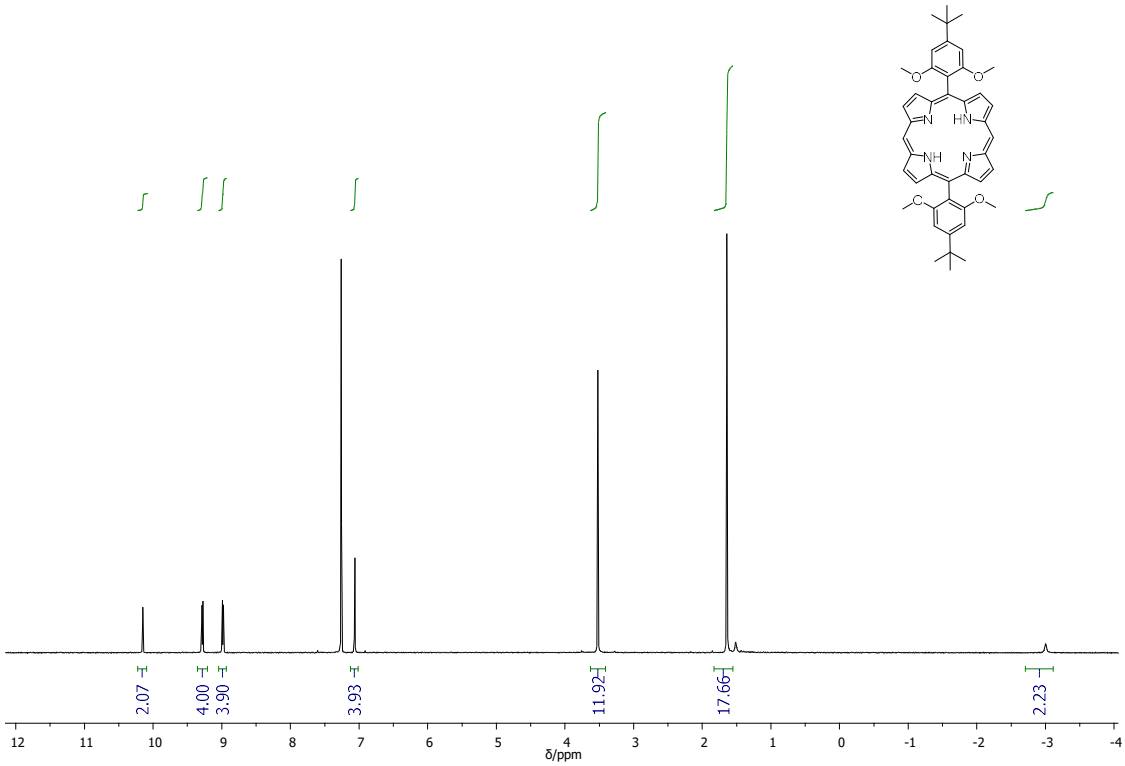

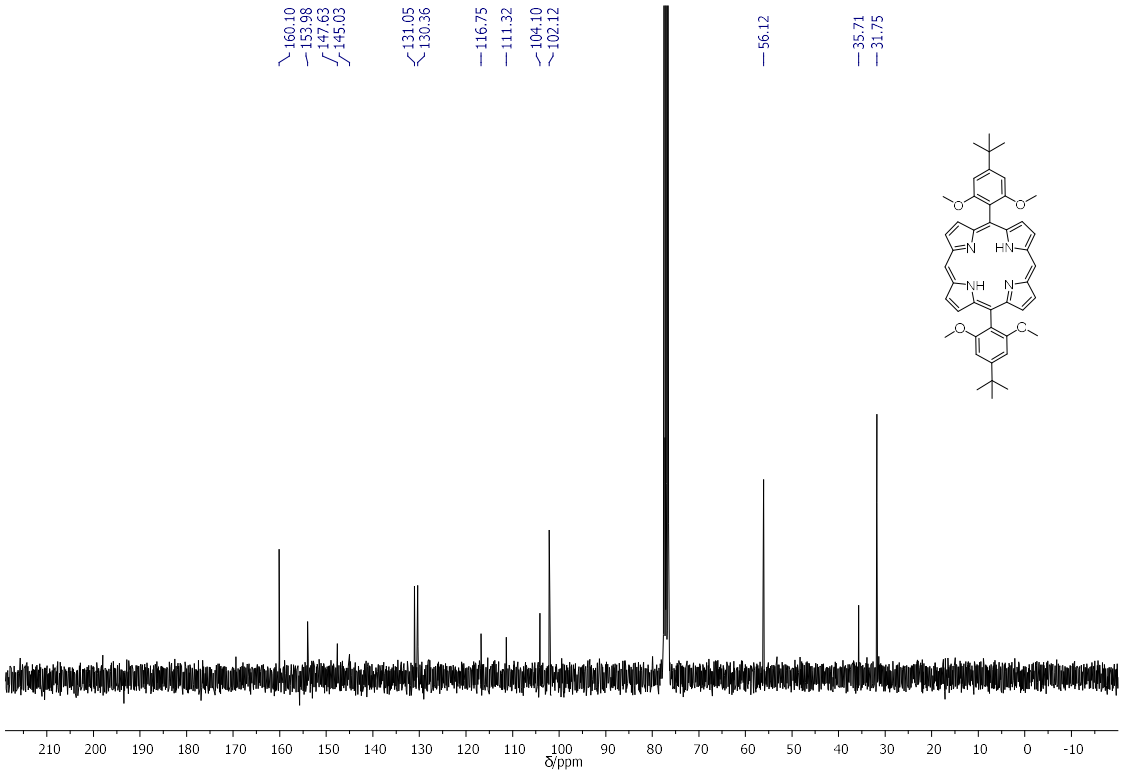

5,15-Dibromo-10,20-*bis*(4-(*tert*-butyl)-2,6-dimethoxyphenyl)porphyrin 4-9

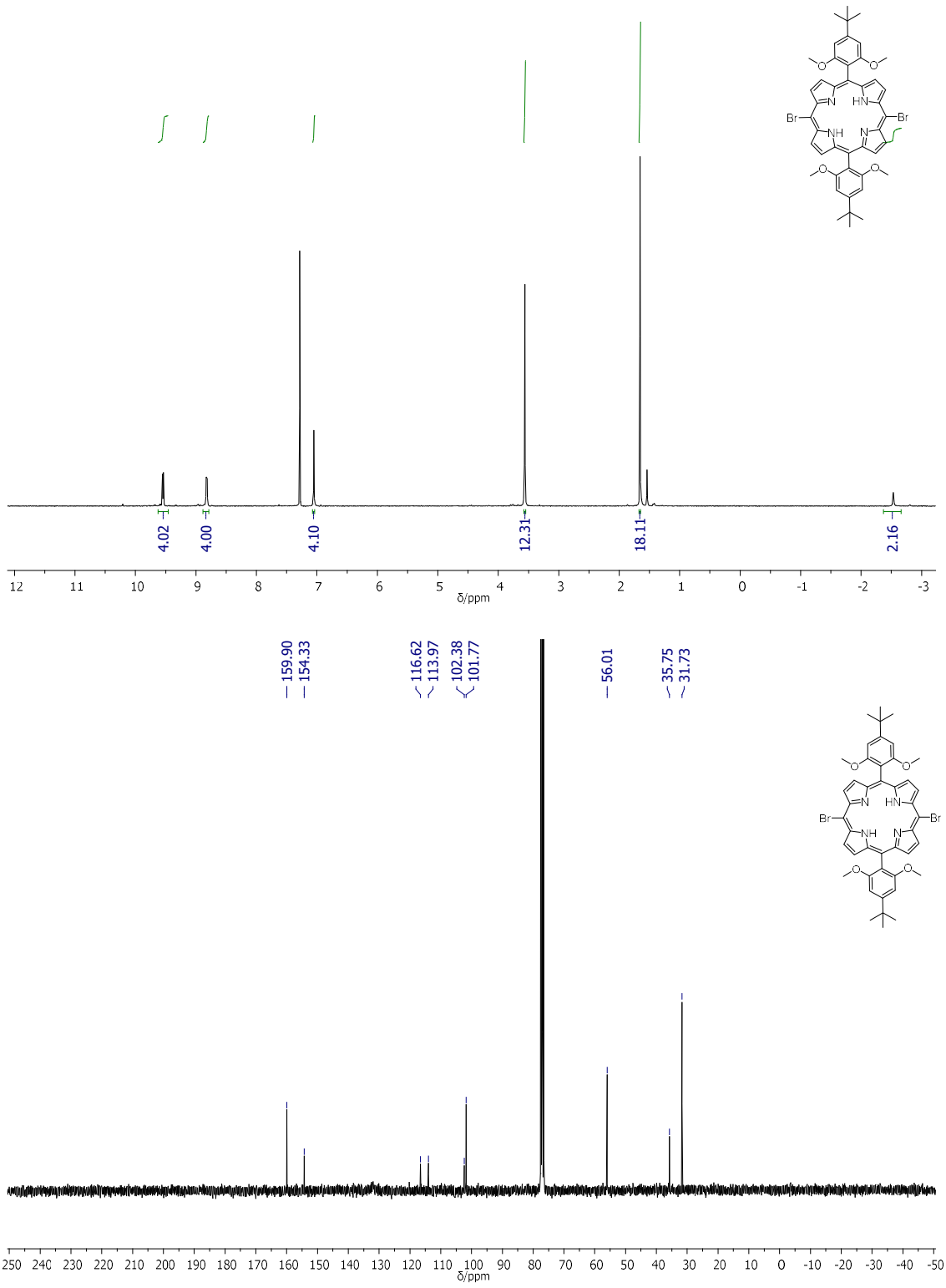

5,15-*Bis*(4-(*tert*-butyl)-2,6-dimethoxyphenyl)-10,20-*bis*(4-(*tert*-butyl)phenyl)porphyrin 4-8

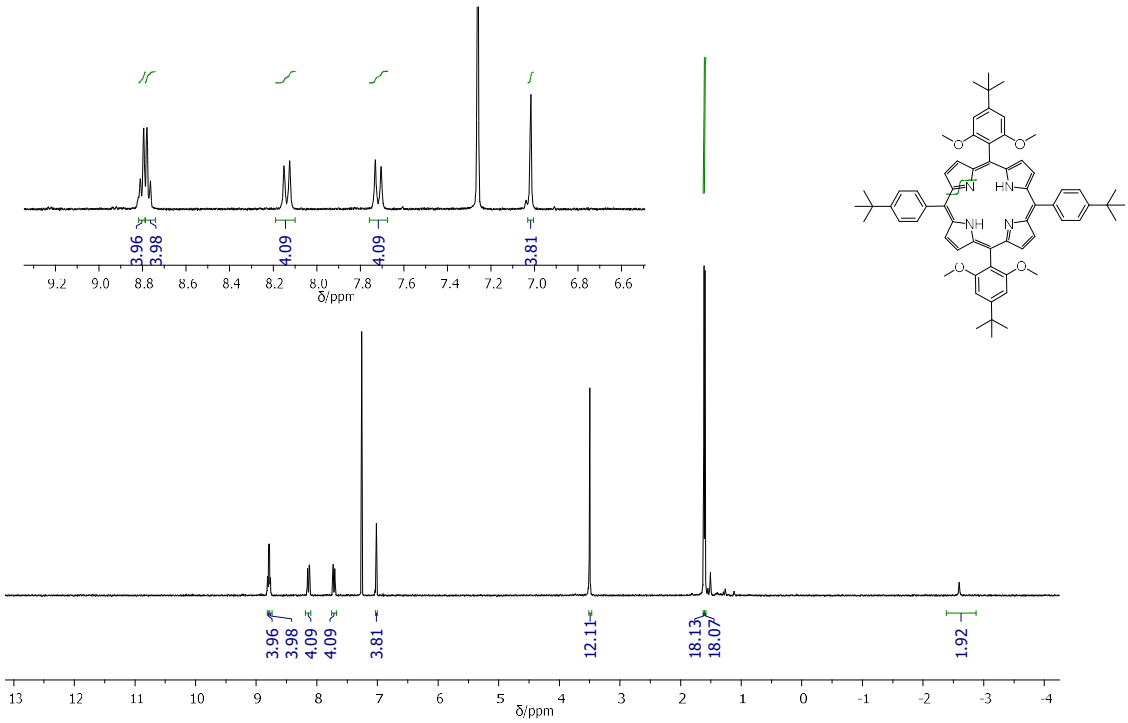

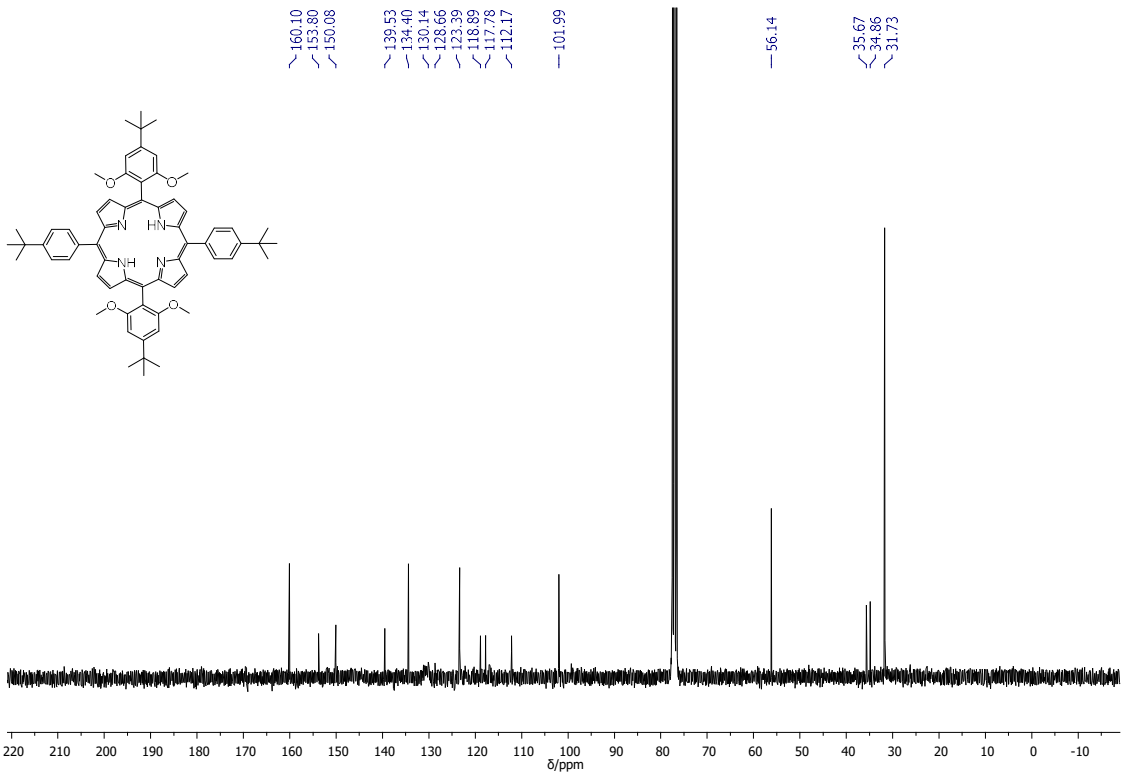

5,15-*Bis*(4-(*tert*-butyl)-2,6-dimethoxyphenyl)-10,20-*bis*(4-(*tert*-butyl)phenyl)-porphyrinato-N^{21},N^{22},N^{23},N^{24}-nickel(II) 4-7

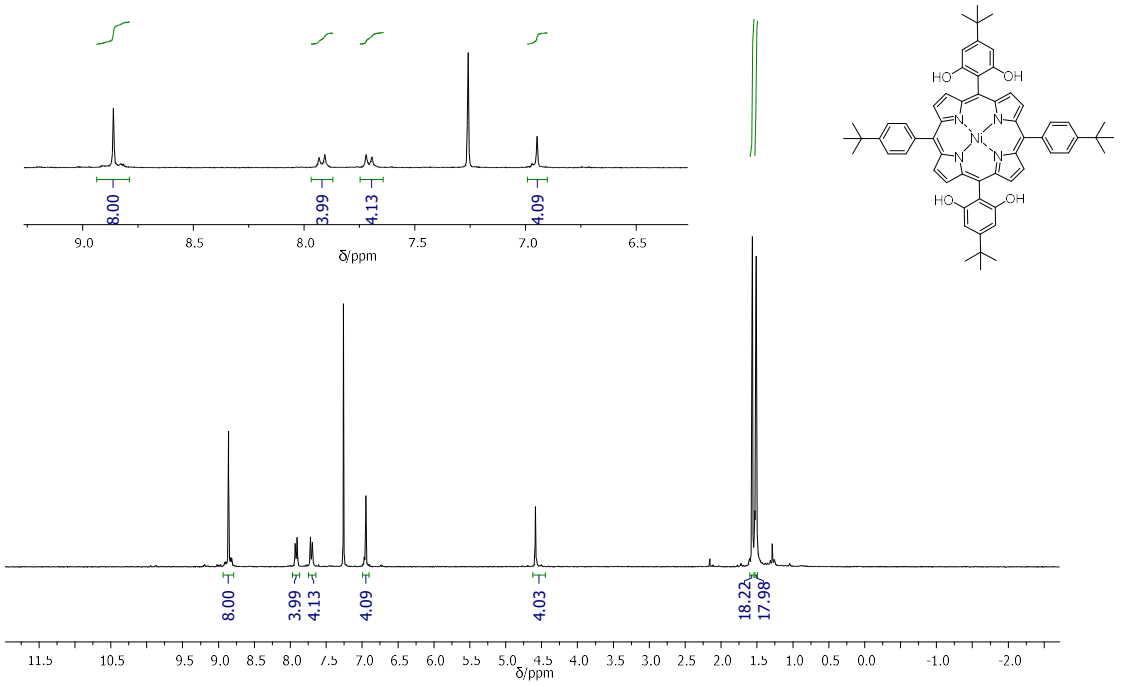

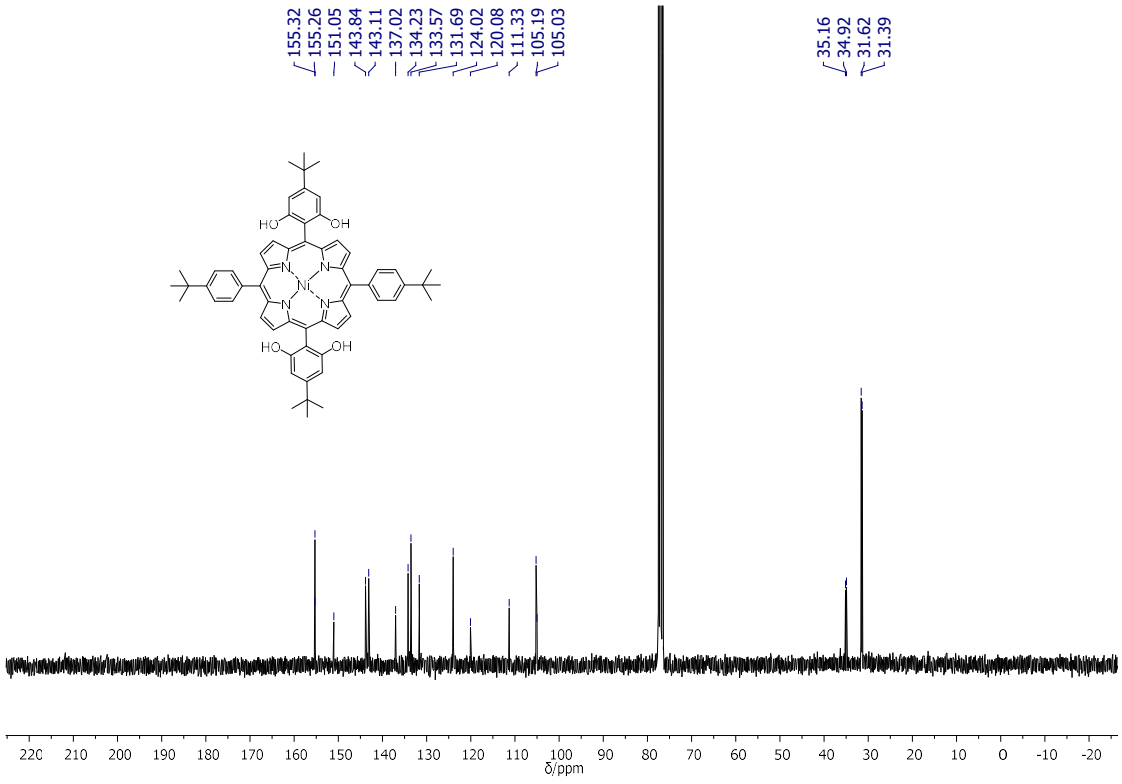

5,10,15,20-*Tetrakis*(4-(*tert*-butyl)-2,6-dimethoxyphenyl)porphyrin 4-14

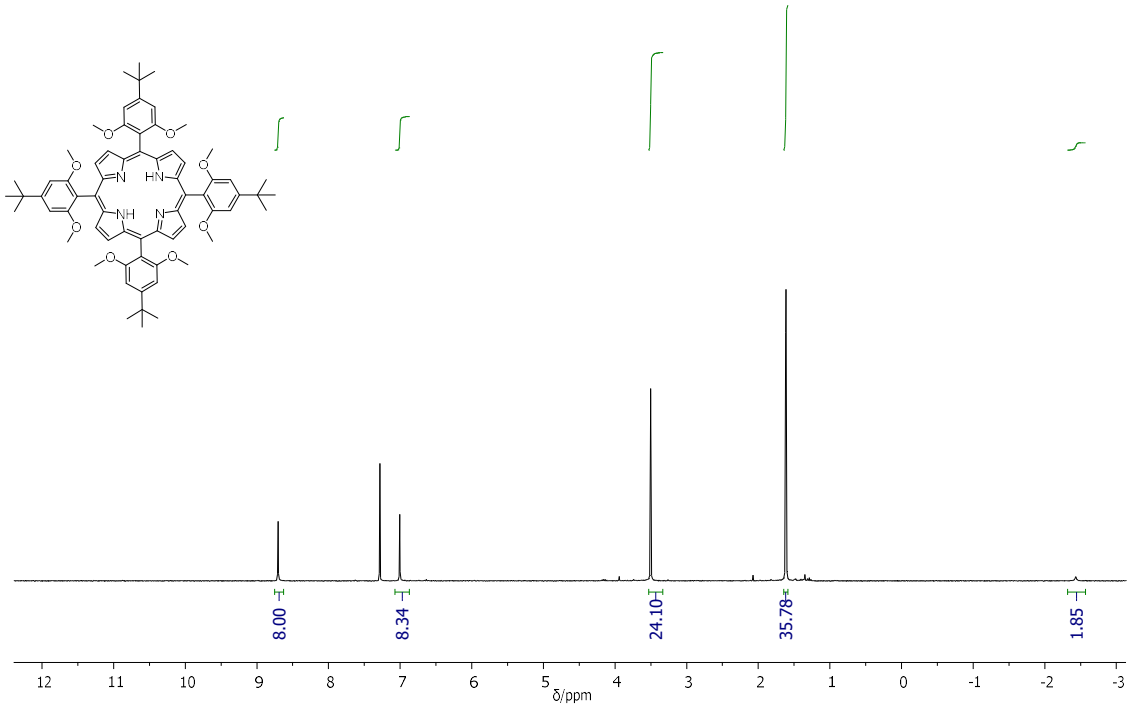

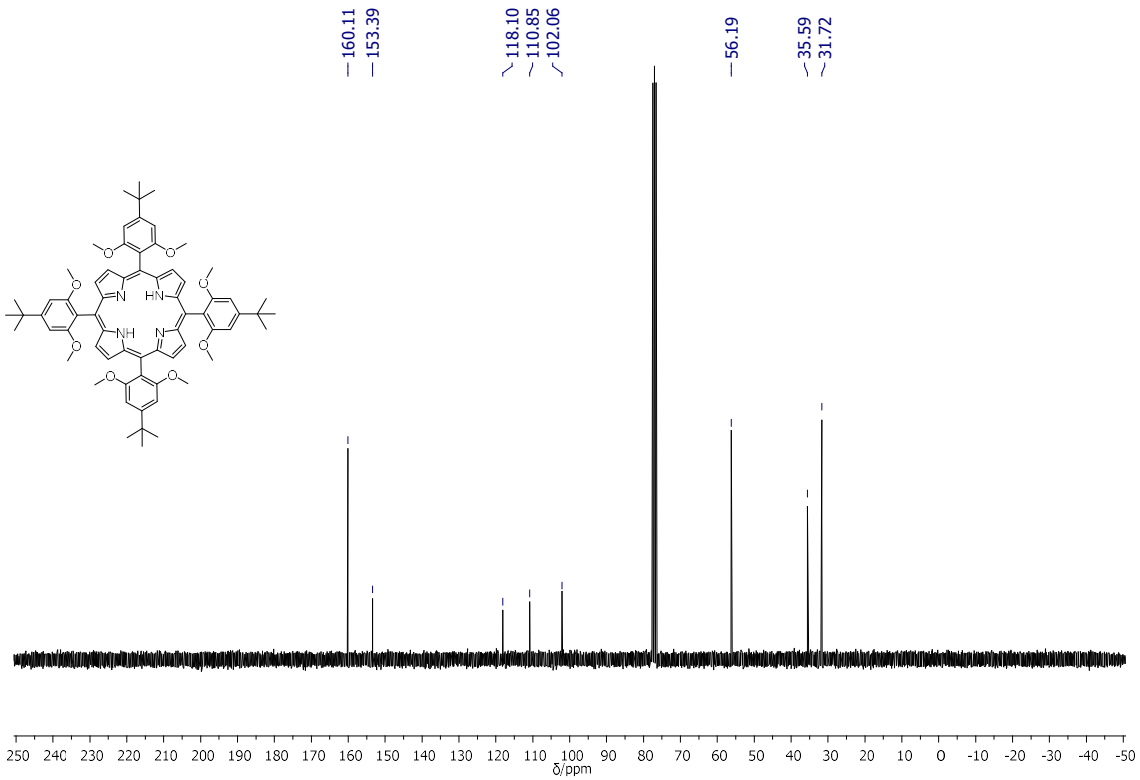

5,10,15,20-*Tetrakis*(4-(*tert*-butyl)-2,6-dihydroxyphenyl)porphyrin 4-15

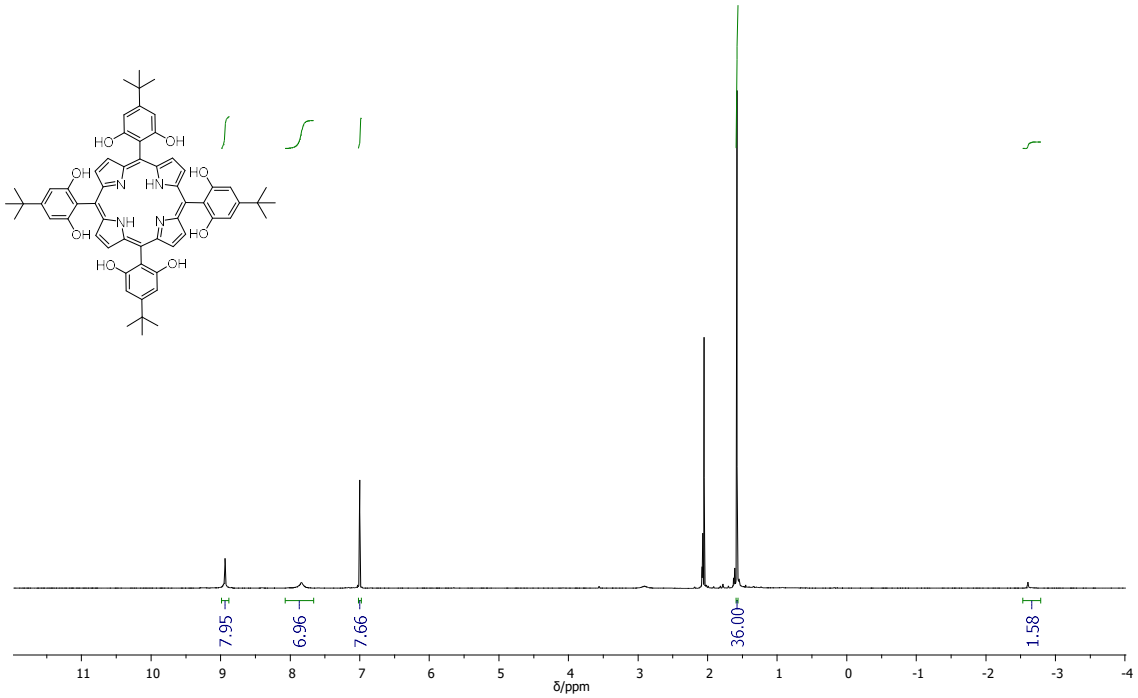

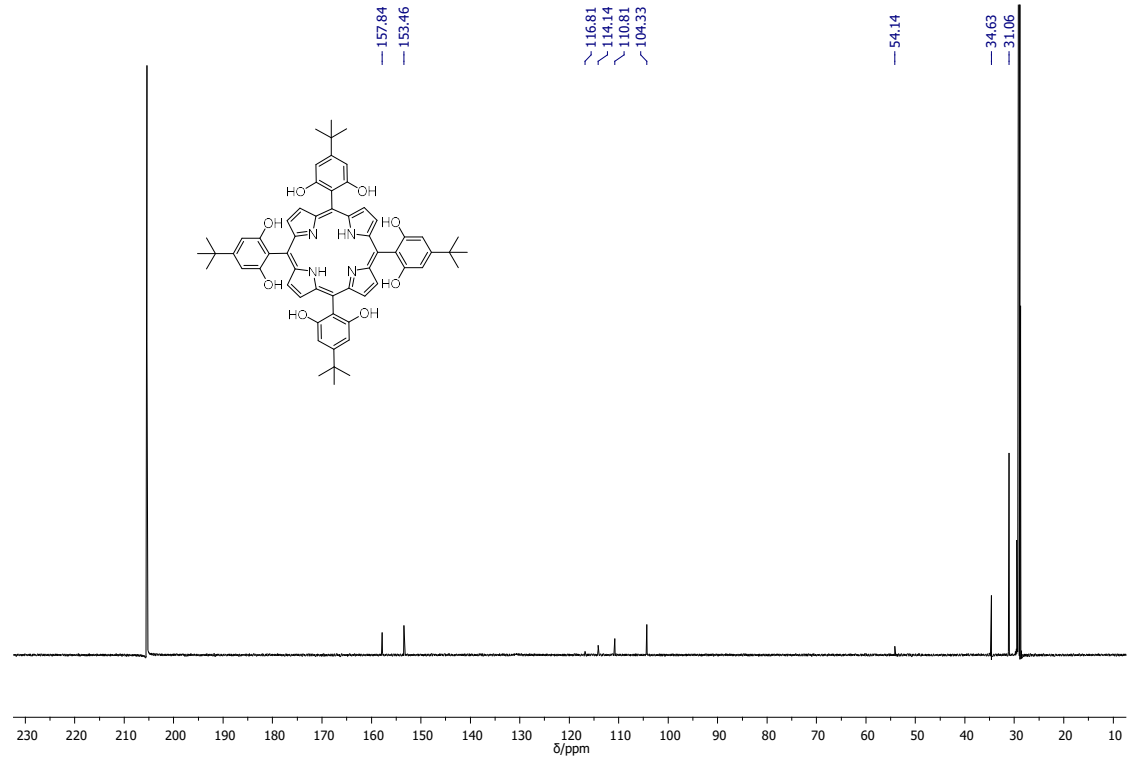

5,10,15,20-*Tetrakis*(4-(*tert*-butyl)-2,6-dihydroxyphenyl)porphyrinato-N^{21},N^{22},N^{23},N^{24}-nickel(II) 4-13

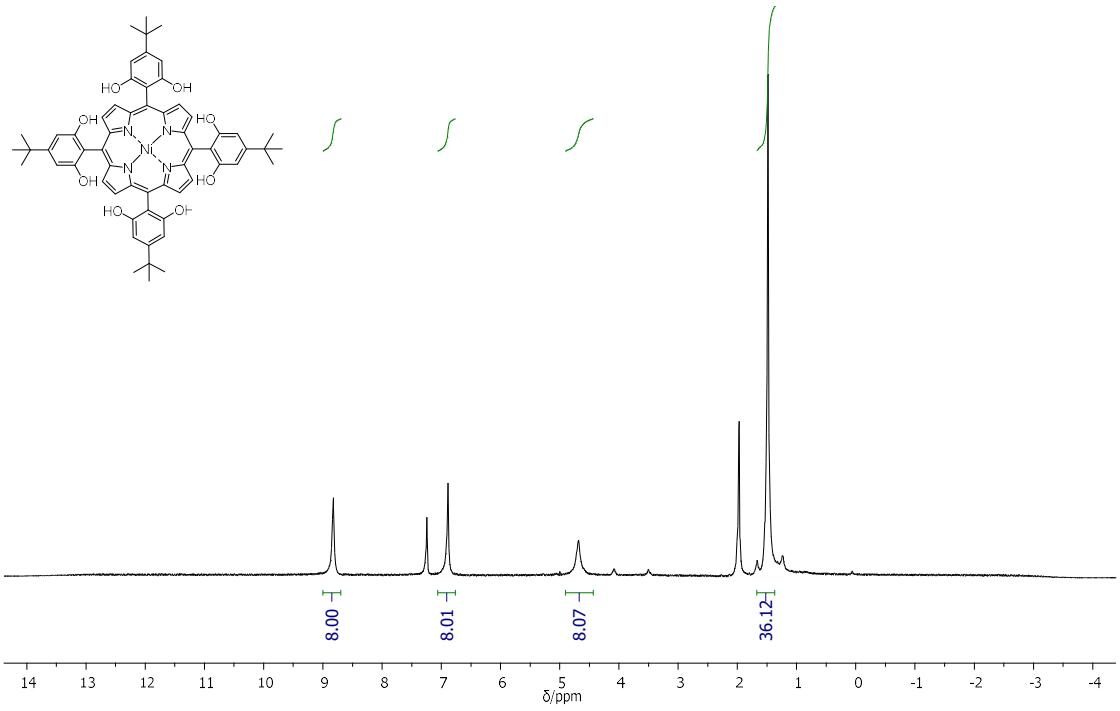

X-Ray analysis of 3-1

Crystal data and structure refinement

Identification code: **3-1**

Empirical formula: C11.43 H11.05 N0.76 Ni0.19 O0.19

Formula weight: 173.30

Temperature: 150(2) K

Crystal system,space group: Monoclinic, I 2/a

Unit cell dimensions:

a = 16.8035(13) Å, a= 90°

b = 9.3834(8) Å, b= 97.326(9)°

c = 31.026(3) Å, g = 90°

Volume: 4852.1(7) $Å^3$

Z, calculated density:21, 1.245 g/cm^3

F(000): 1928

Crystal size: 0.181 × 0.121 × 0.080 mm^3

θ range for data collection: 2.893 to 29.744°

Index ranges: -18<=h<=23, -9<=k<=12, -41<=l<=34

Refl. collected: 12496

Independent refl.: 5846 [R(int) = 0.0966]

Completeness to θ = 25.242, 99.8 %

Refinement method: Full-matrix least-squares on F^2

Data/restraints/parameters: 5846/29/384

Goodness-of-fit on F^2: 0.991

Final R indices [I>2σ(I)]: R1 = 0.0883, wR2 = 0.1672

R indices (all data): R1 = 0.2702, wR2 = 0.2401

Largest diff. peak and hole: 0.462 and -0.264 $Å^{-3}$

Table 1 Atomic coordinates (× 10^4) and equivalent isotropic displacement parameters (A^2 × 10^3) for **3-1**. U(eq) is defined as one third of the trace of the orthogonalized U^{ij} tensor.

Atom	x	y	z	U(eq)	Atom	x	y	z	U(eq)
C(1)	5736(3)	7069(5)	4825(2)	56(2)	C(23A)	8673(9)	6080(20)	7296(5)	85(5)
C(2)	5632(3)	7208(5)	5258(2)	52(1)	C(24A)	9079(12)	4850(30)	7378(6)	75(7)
C(3)	6236(3)	6850(6)	5581(2)	54(1)	C(25A)	9196(16)	3970(40)	7034(10)	115(11)
C(4)	6110(3)	6636(6)	6024(2)	69(2)	C(26A)	8932(9)	4400(20)	6594(7)	76(5)
C(5)	6803(4)	6179(7)	6225(2)	76(2)	C(27)	9418(13)	4150(40)	7805(6)	138(15)
C(5A)	6803(4)	6179(7)	6225(2)	76(2)	C(28)	9280(40)	5350(40)	8106(13)	178(14)
C(6)	7394(3)	6194(6)	5937(2)	63(2)	C(29)	9020(30)	2790(40)	7922(18)	161(17)
C(7)	8220(3)	6052(6)	6052(2)	61(2)	C(30)	10316(12)	4000(50)	7902(13)	169(16)
C(8)	8752(3)	6401(6)	5767(2)	62(2)	C(21)	8504(4)	5578(7)	6497(2)	72(2)
C(9)	9585(3)	6659(7)	5894(2)	74(2)	C(22)	7967(7)	5692(16)	6793(4)	159(11)
C(10)	9893(3)	7114(7)	5531(2)	74(2)	C(23)	8151(11)	5160(20)	7210(4)	168(10)
C(11)	4836(3)	7645(6)	5383(2)	58(2)	C(24)	8889(13)	4510(30)	7336(5)	170(20)
C(12)	4746(3)	8930(7)	5580(3)	91(2)	C(25)	9432(10)	4390(20)	7035(6)	101(12)
C(13)	4034(4)	9329(7)	5732(2)	88(2)	C(26)	9238(6)	4922(17)	6617(5)	103(9)

C(14)	3385(3)	8435(6)	5691(2)	74(2)	C(27A)	9140(20)	4140(40)	7860(7)	250(30)
C(15)	3462(4)	7167(7)	5481(2)	84(2)	C(28A)	9060(40)	5250(50)	8201(14)	179(12)
C(16)	4184(3)	6762(6)	5326(2)	68(2)	C(29A)	8680(40)	2770(60)	7850(20)	330(50)
C(17)	2609(4)	8855(8)	5872(3)	104(3)	C(30A)	10040(30)	3920(90)	7905(16)	410(60)
C(18)	2084(5)	9703(10)	5525(5)	205(7)	N(1)	7024(2)	6563(4)	5527(2)	50(1)
C(19)	2798(6)	9815(15)	6242(5)	276(10)	N(2)	8550(2)	6664(4)	5329(1)	50(1)
C(20)	2115(4)	7611(7)	5963(2)	92(2)	O(1)	7112(9)	6039(14)	6636(5)	144(4)
C(21A)	8504(4)	5578(7)	6497(2)	72(2)	Ni(1)	7500	6612(1)	5000	51(1)
C(22A)	8395(7)	6444(19)	6860(6)	79(5)					

Table 2 Bond lengths (Å) for **3-1.**

Bond	A	Bond	A	Bond	A
C(1)-C(2)	1.383(7)	C(15)-C(16)	1.413(8)	C(29)-H(29B)	0.98
C(1)-N(2)#1	1.400(6)	C(15)-H(15)	0.95	C(29)-H(29C)	0.98
C(1)-C(10)#1	1.428(7)	C(16)-H(16)	0.95	C(30)-H(30A)	0.98
C(2)-C(3)	1.374(7)	C(17)-C(19)	1.463(11)	C(30)-H(30B)	0.98
C(2)-C(11)	1.497(7)	C(17)-C(20)	1.480(8)	C(30)-H(30C)	0.98
C(3)-N(1)	1.383(6)	C(17)-C(18)	1.526(13)	C(21)-C(22)	1.373(8)
C(3)-C(4)	1.430(8)	C(18)-H(18A)	0.98	C(21)-C(26)	1.387(8)
C(4)-C(5A)	1.319(8)	C(18)-H(18B)	0.98	C(22)-C(23)	1.381(8)
C(4)-C(5)	1.319(8)	C(18)-H(18C)	0.98	C(22)-O(1)	1.494(18)
C(4)-H(4)	0.95	C(19)-H(19A)	0.98	C(23)-C(24)	1.397(9)
C(5)-O(1)	1.323(14)	C(19)-H(19B)	0.98	C(23)-H(23)	0.95
C(5)-C(6)	1.418(8)	C(19)-H(19C)	0.98	C(24)-C(25)	1.391(9)
C(5A)-C(6)	1.418(8)	C(20)-H(20A)	0.98	C(24)-C(27A)	1.66(3)
C(5A)-H(5A)	0.95	C(20)-H(20B)	0.98	C(25)-C(26)	1.389(9)
C(6)-N(1)	1.388(7)	C(20)-H(20C)	0.98	C(25)-H(25)	0.95
C(6)-C(7)	1.395(8)	C(21A)-C(26A)	1.330(19)	C(26)-H(26)	0.95
C(7)-C(8)	1.374(8)	C(21A)-C(22A)	1.420(19)	C(27A)-C(28A)	1.503(10)
C(7)-C(21)	1.472(8)	C(22A)-C(23A)	1.42(2)	C(27A)-C(30A)	1.503(10)
C(7)-C(21A)	1.472(8)	C(22A)-H(22A)	0.95	C(27A)-C(29A)	1.507(10)
C(8)-N(2)	1.379(7)	C(23A)-C(24A)	1.34(3)	C(28A)-H(28D)	0.98
C(8)-C(9)	1.427(7)	C(23A)-H(23A)	0.95	C(28A)-H(28E)	0.98
C(9)-C(10)	1.368(8)	C(24A)-C(25A)	1.38(4)	C(28A)-H(28F)	0.98
C(9)-H(9)	0.95	C(24A)-C(27)	1.52(3)	C(29A)-H(29D)	0.98
C(10)-C(1)#1	1.429(7)	C(25A)-C(26A)	1.44(3)	C(29A)-H(29E)	0.98
C(10)-H(10)	0.95	C(25A)-H(25A)	0.95	C(29A)-H(29F)	0.98
C(11)-C(16)	1.367(7)	C(26A)-H(26A)	0.95	C(30A)-H(30D)	0.98
C(11)-C(12)	1.369(8)	C(27)-C(28)	1.501(10)	C(30A)-H(30E)	0.98
C(12)-C(13)	1.392(8)	C(27)-C(29)	1.508(10)	C(30A)-H(30F)	0.98
C(12)-H(12)	0.95	C(27)-C(30)	1.509(10)	N(1)-Ni(1)	1.910(4)
C(13)-C(14)	1.369(8)	C(28)-H(28A)	0.98	N(2)-C(1)#1	1.400(6)
C(13)-H(13)	0.95	C(28)-H(28B)	0.98	N(2)-Ni(1)	1.924(4)
C(14)-C(15)	1.370(8)	C(28)-H(28C)	0.98	Ni(1)-N(1)#1	1.910(4)

C(14)-C(17)	1.536(8)	C(29)-H(29A)	0.98	Ni(1)-N(2)#1	1.924(4)

Table 3 Angles (◦) for **3-1**.

Angle	◦	Angle	◦	Angle	◦
C(2)-C(1)-N(2)#1	125.3(5)	C(20)-C(17)-C(18)	104.9(7)	C(27)-C(30)-H(30A)	109.4
C(2)-C(1)-C(10)#1	125.2(5)	C(19)-C(17)-C(14)	109.6(7)	C(27)-C(30)-H(30B)	109.6
N(2)#1-C(1)-C(10)#1	109.0(5)	C(20)-C(17)-C(14)	113.0(5)	H(30A)-C(30)-H(30B)	109.5
C(3)-C(2)-C(1)	120.9(5)	C(18)-C(17)-C(14)	108.5(7)	C(27)-C(30)-H(30C)	109.5
C(3)-C(2)-C(11)	118.6(5)	C(17)-C(18)-H(18A)	109.5	H(30A)-C(30)-H(30C)	109.5
C(1)-C(2)-C(11)	120.3(5)	C(17)-C(18)-H(18B)	109.5	H(30B)-C(30)-H(30C)	109.5
C(2)-C(3)-N(1)	126.0(5)	H(18A)-C(18)-H(18B)	109.5	C(22)-C(21)-C(26)	119.5(7)
C(2)-C(3)-C(4)	123.4(5)	C(17)-C(18)-H(18C)	109.5	C(22)-C(21)-C(7)	116.3(7)
N(1)-C(3)-C(4)	110.5(5)	H(18A)-C(18)-H(18C)	109.5	C(26)-C(21)-C(7)	123.9(8)
C(5A)-C(4)-C(3)	105.7(5)	H(18B)-C(18)-H(18C)	109.5	C(21)-C(22)-C(23)	120.7(7)
C(5)-C(4)-C(3)	105.7(5)	C(17)-C(19)-H(19A)	109.5	C(21)-C(22)-O(1)	119.1(11)
C(5)-C(4)-H(4)	127.2	C(17)-C(19)-H(19B)	109.5	C(23)-C(22)-O(1)	118.3(11)
C(3)-C(4)-H(4)	127.2	H(19A)-C(19)-H(19B)	109.5	C(22)-C(23)-C(24)	120.5(7)
C(4)-C(5)-O(1)	134.6(9)	C(17)-C(19)-H(19C)	109.5	C(22)-C(23)-H(23)	119.8
C(4)-C(5)-C(6)	110.3(6)	H(19A)-C(19)-H(19C)	109.5	C(24)-C(23)-H(23)	119.7
O(1)-C(5)-C(6)	112.9(8)	H(19B)-C(19)-H(19C)	109.5	C(25)-C(24)-C(23)	118.7(7)
C(4)-C(5A)-C(6)	110.3(6)	C(17)-C(20)-H(20A)	109.5	C(25)-C(24)-C(27A)	122.1(19)
C(4)-C(5A)-H(5A)	124.9	C(17)-C(20)-H(20B)	109.5	C(23)-C(24)-C(27A)	118.4(19)
C(6)-C(5A)-H(5A)	124.9	H(20A)-C(20)-H(20B)	109.5	C(26)-C(25)-C(24)	120.3(7)
N(1)-C(6)-C(7)	125.0(6)	C(17)-C(20)-H(20C)	109.5	C(26)-C(25)-H(25)	119.8
N(1)-C(6)-C(5)	108.1(5)	H(20A)-C(20)-H(20C)	109.5	C(24)-C(25)-H(25)	119.9
C(7)-C(6)-C(5)	126.4(6)	H(20B)-C(20)-H(20C)	109.5	C(21)-C(26)-C(25)	120.3(7)
N(1)-C(6)-C(5A)	108.1(5)	C(26A)-C(21A)-C(22A)	114.5(12)	C(21)-C(26)-H(26)	119.8
C(7)-C(6)-C(5A)	126.4(6)	C(26A)-C(21A)-C(7)	124.4(11)	C(25)-C(26)-H(26)	119.9
C(8)-C(7)-C(6)	121.4(6)	C(22A)-C(21A)-C(7)	120.8(8)	C(28A)-C(27A)-C(30A)	103(5)
C(8)-C(7)-C(21)	121.1(5)	C(21A)-C(22A)-C(23A)	124.0(14)	C(28A)-C(27A)-C(29A)	120(4)
C(6)-C(7)-C(21)	117.5(6)	C(21A)-C(22A)-H(22A)	118	C(30A)-C(27A)-C(29A)	113(5)
C(8)-C(7)-C(21A)	121.1(5)	C(23A)-C(22A)-H(22A)	118	C(28A)-C(27A)-C(24)	121(3)
C(6)-C(7)-C(21A)	117.5(6)	C(24A)-C(23A)-C(22A)	119.1(17)	C(30A)-C(27A)-C(24)	104(2)
C(7)-C(8)-N(2)	125.3(5)	C(24A)-C(23A)-H(23A)	120.5	C(29A)-C(27A)-C(24)	96(3)
C(7)-C(8)-C(9)	123.9(6)	C(22A)-C(23A)-H(23A)	120.4	C(27A)-C(28A)-H(28D)	109.5
N(2)-C(8)-C(9)	110.6(6)	C(23A)-C(24A)-C(25A)	118.9(19)	C(27A)-C(28A)-H(28E)	109.4
C(10)-C(9)-C(8)	106.6(6)	C(23A)-C(24A)-C(27)	131(2)	H(28D)-C(28A)-H(28E)	109.5
C(10)-C(9)-H(9)	126.7	C(25A)-C(24A)-C(27)	110(2)	C(27A)-C(28A)-H(28F)	109.5
C(8)-C(9)-H(9)	126.7	C(24A)-C(25A)-C(26A)	120(2)	H(28D)-C(28A)-H(28F)	109.5
C(9)-C(10)-C(1)#1	107.9(5)	C(24A)-C(25A)-H(25A)	119.7	H(28E)-C(28A)-H(28F)	109.5
C(9)-C(10)-H(10)	126	C(26A)-C(25A)-H(25A)	119.8	C(27A)-C(29A)-H(29D)	109.5
C(1)#1-C(10)-H(10)	126	C(21A)-C(26A)-C(25A)	122.8(18)	C(27A)-C(29A)-H(29E)	109.5
C(16)-C(11)-C(12)	117.4(5)	C(21A)-C(26A)-H(26A)	118.6	H(29D)-C(29A)-H(29E)	109.5
C(16)-C(11)-C(2)	121.9(5)	C(25A)-C(26A)-H(26A)	118.6	C(27A)-C(29A)-H(29F)	109.5

C(12)-C(11)-C(2)	120.7(5)	C(28)-C(27)-C(29)	112(3)	H(29D)-C(29A)-H(29F)	109.5
C(11)-C(12)-C(13)	122.4(5)	C(28)-C(27)-C(30)	101(4)	H(29E)-C(29A)-H(29F)	109.5
C(11)-C(12)-H(12)	118.8	C(29)-C(27)-C(30)	109(3)	C(27A)-C(30A)-H(30D)	109.5
C(13)-C(12)-H(12)	118.8	C(28)-C(27)-C(24A)	98(3)	C(27A)-C(30A)-H(30E)	109.4
C(14)-C(13)-C(12)	120.8(6)	C(29)-C(27)-C(24A)	117(2)	H(30D)-C(30A)-H(30E)	109.5
C(14)-C(13)-H(13)	119.6	C(30)-C(27)-C(24A)	118(2)	C(27A)-C(30A)-H(30F)	109.5
C(12)-C(13)-H(13)	119.6	C(27)-C(28)-H(28A)	109.5	H(30D)-C(30A)-H(30F)	109.5
C(13)-C(14)-C(15)	117.0(5)	C(27)-C(28)-H(28B)	109.4	H(30E)-C(30A)-H(30F)	109.5
C(13)-C(14)-C(17)	120.8(6)	H(28A)-C(28)-H(28B)	109.5	C(3)-N(1)-C(6)	105.1(5)
C(15)-C(14)-C(17)	122.2(5)	C(27)-C(28)-H(28C)	109.5	C(3)-N(1)-Ni(1)	127.8(4)
C(14)-C(15)-C(16)	122.2(6)	H(28A)-C(28)-H(28C)	109.5	C(6)-N(1)-Ni(1)	127.1(4)
C(14)-C(15)-H(15)	118.9	H(28B)-C(28)-H(28C)	109.5	C(8)-N(2)-C(1)#1	105.8(4)
C(16)-C(15)-H(15)	118.9	C(27)-C(29)-H(29A)	109.5	C(8)-N(2)-Ni(1)	127.7(4)
C(11)-C(16)-C(15)	120.0(5)	C(27)-C(29)-H(29B)	109.5	C(1)#1-N(2)-Ni(1)	126.4(4)
C(11)-C(16)-H(16)	120	H(29A)-C(29)-H(29B)	109.5	C(5)-O(1)-C(22)	125.4(10)
C(15)-C(16)-H(16)	120	C(27)-C(29)-H(29C)	109.4	N(1)#1-Ni(1)-N(1)	177.2(2)
C(19)-C(17)-C(20)	114.0(9)	H(29A)-C(29)-H(29C)	109.5	N(1)#1-Ni(1)-N(2)	89.91(17)
C(19)-C(17)-C(18)	106.3(9)	H(29B)-C(29)-H(29C)	109.5	N(1)-Ni(1)-N(2)	90.16(17)
N(2)-Ni(1)-N(2)#1	177.1(3)	N(1)-Ni(1)-N(2)#1	89.91(17)	N(1)#1-Ni(1)-N(2)#1	90.16(17)

Table 4 Anisotropic displacement parameters (A^2 × 10^2) for **3-1**. The anisotropic displacement factor exponent takes the form: –2 pi2 [h^2a*^2 U11 + ... + 2 h k a* b*U12].

Atom	U11	U22	U33	U23	U13	U12
C(1)	30(3)	61(4)	77(5)	12(3)	4(3)	-2(2)
C(2)	40(3)	50(3)	68(4)	-3(3)	10(3)	-4(2)
C(3)	44(3)	62(4)	57(4)	-5(3)	10(3)	-3(3)
C(4)	41(3)	88(4)	80(5)	-11(4)	17(3)	7(3)
C(5)	76(5)	107(5)	46(4)	-6(4)	10(4)	5(4)
C(5A)	76(5)	107(5)	46(4)	-6(4)	10(4)	5(4)
C(6)	49(4)	68(4)	70(4)	-5(3)	3(3)	5(3)
C(7)	53(4)	74(4)	54(4)	-12(3)	2(3)	18(3)
C(8)	44(3)	82(4)	57(4)	-9(3)	-1(3)	12(3)
C(9)	40(3)	106(5)	70(4)	-16(4)	-11(3)	18(3)
C(10)	37(3)	87(5)	94(5)	-22(4)	0(4)	3(3)
C(11)	34(3)	50(3)	93(5)	-4(3)	16(3)	-1(3)
C(12)	37(4)	77(5)	162(7)	-26(5)	28(4)	-14(3)
C(13)	53(4)	67(4)	148(7)	-26(4)	24(4)	-6(3)
C(14)	40(3)	62(4)	123(6)	-13(4)	22(4)	-1(3)
C(15)	49(4)	80(5)	125(6)	-20(4)	18(4)	-9(3)
C(16)	45(3)	68(4)	92(5)	-12(4)	19(3)	0(3)
C(17)	58(4)	83(5)	182(9)	-32(5)	55(5)	-6(4)
C(18)	90(7)	117(8)	430(20)	79(10)	136(10)	58(6)
C(19)	118(8)	353(18)	387(19)	-308(17)	150(11)	-127(10)
C(20)	50(4)	97(5)	135(7)	-7(5)	39(4)	4(4)

C(21A)	64(4)	96(5)	57(5)	-2(4)	8(4)	6(4)
C(22A)	35(7)	120(12)	81(11)	25(10)	-7(7)	7(8)
C(23A)	57(9)	120(14)	77(12)	-8(10)	12(8)	-3(9)
C(24A)	62(11)	127(17)	38(12)	-1(12)	9(9)	-21(13)
C(25A)	66(14)	170(20)	110(20)	42(18)	15(15)	2(16)
C(26A)	40(9)	121(13)	66(12)	17(10)	4(8)	16(10)
C(27)	131(19)	250(40)	32(12)	43(17)	-4(13)	-40(20)
C(28)	220(40)	300(20)	30(16)	37(16)	47(18)	-50(20)
C(29)	160(20)	210(40)	100(30)	80(30)	-15(19)	10(20)
C(30)	94(15)	300(50)	100(30)	60(30)	-23(14)	-10(20)
C(21)	64(4)	96(5)	57(5)	-2(4)	8(4)	6(4)
C(22)	91(16)	320(40)	82(15)	18(18)	62(14)	71(18)
C(23)	190(30)	250(30)	81(16)	33(19)	53(17)	60(20)
C(24)	250(50)	180(30)	90(30)	30(20)	40(30)	90(30)
C(25)	55(13)	190(30)	64(16)	18(14)	14(10)	44(17)
C(26)	36(10)	200(30)	70(13)	5(14)	-4(10)	23(12)
C(27A)	410(70)	260(50)	110(30)	20(30)	90(40)	250(50)
C(28A)	220(30)	280(20)	60(20)	-12(18)	88(16)	-50(20)
C(29A)	660(140)	230(50)	70(20)	70(30)	-40(60)	-140(60)
C(30A)	530(100)	540(120)	110(40)	-20(50)	-190(50)	310(90)
N(1)	29(2)	56(3)	66(3)	-7(2)	9(2)	3(2)
N(2)	31(2)	63(3)	56(3)	-2(2)	6(2)	6(2)
O(1)	136(11)	176(12)	129(11)	-12(9)	55(10)	6(9)
Ni(1)	33(1)	56(1)	63(1)	0	5(1)	0

X-Ray analysis of 3-14

Crystal data and structure refinement

Identification code: **3-14**

Empirical formula: C60 H59 N4 O

Formula weight: 852.11

Temperature: 150(2) K

Crystal system, space group: Monoclinic, I 2/a

Unit cell dimensions:

a = 17.5653(8) Å, a= 90°

b = 12.1918(5) Å,b= 96.300(5)°

c = 22.3229(13) Å, g = 90°

Volume: 4751.6(4) $Å^3$

Z, calculated density: 4, 1.191 g/cm^3

F(000): 1820

Crystal size: 0.203 × 0.112 × 0.091 mm^3

θ range for data collection: 2.934 to 29.575°.

Index ranges: -23<=h<=18, -16<=k<=16, -30<=l<=26

Refl. Collected: 12336

Independent refl.: 5666 [R(int) = 0.0262]

Completeness to θ = 25.242, 99.8 %

Refinement method: Full-matrix least-squares on F^2

Data/restraints/parameters: 5666/20/392

Goodness-of-fit on F^2: 1.297

Final R indices [I>2σ(I)]: R1 = 0.1091, wR2 = 0.3365

R indices (all data): R1 = 0.1639, wR2 = 0.3796

Largest diff. peak and hole: 0.795 and -0.348 $Å^{-3}$

Table 1 Atomic coordinates (× 10^4) and equivalent isotropic displacement parameters ($Å^2$ × 10^3) for **3-14**. U(eq) is defined as one third of the trace of the orthogonalized U^{ij} tensor.

Atom	x	y	z	U(eq)	Atom	x	y	Z	U(eq)
C(1)	5872(2)	7162(3)	5098(2)	54(1)	C(17)	6406(8)	12188(16)	6100(7)	49(3)
C(2)	6411(2)	7775(3)	4783(2)	59(1)	C(18)	6886(12)	12306(19)	6702(7)	53(4)
C(3)	6673(2)	7099(3)	4366(2)	58(1)	C(19)	5701(7)	12892(11)	6056(6)	59(3)
C(4)	6302(2)	6061(3)	4426(2)	51(1)	C(20)	6881(8)	12559(11)	5615(7)	49(2)
C(5)	6425(2)	5145(3)	4064(2)	49(1)	C(11A)	5629(14)	8786(10)	5733(10)	54(6)
C(6)	6017(2)	4165(3)	4058(2)	51(1)	C(12A)	6359(5)	9049(6)	5972(4)	66(2)
C(7)	6165(2)	3203(3)	3722(2)	67(1)	C(13A)	6555(4)	10138(7)	6098(4)	58(2)
C(8)	5644(2)	2435(3)	3827(2)	68(1)	C(14A)	6003(12)	10939(17)	6044(11)	54(5)
C(9)	5153(2)	2892(3)	4226(2)	52(1)	C(15A)	5286(4)	10681(6)	5821(4)	60(2)
C(10)	5460(2)	7620(3)	5534(2)	54(1)	C(16A)	5072(4)	9626(5)	5675(4)	55(2)
C(11)	5759(16)	8725(11)	5740(10)	67(7)	C(17A)	6250(9)	12116(16)	6220(7)	61(4)
C(12)	6321(6)	9251(9)	5407(5)	93(3)	C(18A)	6759(11)	12199(18)	6812(7)	52(4)
C(13)	6550(6)	10343(8)	5529(7)	101(4)	C(19A)	5522(9)	12769(16)	6237(10)	115(7)
C(14)	6221(13)	10960(20)	6001(10)	62(6)	C(20A)	6653(11)	12512(18)	5700(8)	110(7)
C(15)	5913(7)	10311(8)	6371(4)	92(3)	C(21)	7022(2)	5265(3)	3654(2)	52(1)
C(16)	5648(7)	9228(7)	6231(4)	90(3)	C(22)	6856(2)	5183(3)	3034(2)	63(1)

Table 2 Bond lengths (Å) for **3-14**.

Bond	Å	Bond	Å	Bond	Å
C(1)-N(2)	1.380(4)	C(12)-C(13)	1.409(13)	C(13A)-H(13A)	0.95
C(1)-C(10)	1.392(5)	C(13)-C(14)	1.47(2)	C(14A)-C(15A)	1.34(2)
C(1)-C(2)	1.447(5)	C(13)-H(13)	0.95	C(14A)-C(17A)	1.54(3)
C(2)-O(1)	1.290(7)	C(14)-C(15)	1.30(3)	C(15A)-C(16A)	1.369(9)
C(2)-C(3)	1.361(5)	C(14)-C(17)	1.54(3)	C(15A)-H(15A)	0.95
C(3)-C(4)	1.437(5)	C(15)-C(16)	1.424(12)	C(16A)-H(16A)	0.95
C(3)-H(3)	0.95	C(15)-H(15)	0.95	C(17A)-C(20A)	1.503(9)
C(4)-N(2)	1.377(4)	C(16)-H(16)	0.95	C(17A)-C(19A)	1.510(9)
C(4)-C(5)	1.410(5)	C(17)-C(19)	1.502(9)	C(17A)-C(18A)	1.517(9)
C(5)-C(6)	1.392(5)	C(17)-C(20)	1.507(8)	C(18A)-H(18D)	0.98
C(5)-C(21)	1.472(5)	C(17)-C(18)	1.514(9)	C(18A)-H(18E)	0.98
C(6)-N(1)	1.362(4)	C(18)-H(18A)	0.98	C(18A)-H(18F)	0.98
C(6)-C(7)	1.432(5)	C(18)-H(18B)	0.98	C(19A)-H(19D)	0.98

C(7)-C(8)	1.347(5)	C(18)-H(18C)	0.98	C(19A)-H(19E)	0.98
C(7)-H(7)	0.95	C(19)-H(19A)	0.98	C(19A)-H(19F)	0.98
C(8)-C(9)	1.420(5)	C(19)-H(19B)	0.98	C(20A)-H(20D)	0.98
C(8)-H(8)	0.95	C(19)-H(19C)	0.98	C(20A)-H(20E)	0.98
C(9)-N(1)	1.375(4)	C(20)-H(20A)	0.98	C(20A)-H(20F)	0.98
C(9)-C(10)#1	1.401(5)	C(20)-H(20B)	0.98	C(21)-C(22)	1.387(5)
C(10)-C(9)#1	1.401(5)	C(20)-H(20C)	0.98	C(21)-C(26)	1.411(5)
C(10)-C(11)	1.499(9)	C(11A)-C(12A)	1.37(2)	C(22)-C(23)	1.389(5)
C(10)-C(11A)	1.509(8)	C(11A)-C(16A)	1.41(2)	C(22)-H(22)	0.95
C(11)-C(16)	1.29(2)	C(12A)-C(13A)	1.392(11)	C(23)-C(24)	1.381(5)
C(11)-C(12)	1.45(2)	C(12A)-H(12A)	0.95	C(23)-H(23)	0.95
C(12)-O(1)	1.399(11)	C(13A)-C(14A)	1.37(2)	C(24)-C(25)	1.393(5)
C(24)-C(27)	1.536(5)	C(27)-C(29)	1.518(7)	C(28)-H(28C)	0.98
C(25)-C(26)	1.372(5)	C(27)-C(28)	1.537(7)	C(29)-H(29A)	0.98
C(25)-H(25)	0.95	C(27)-C(30)	1.539(7)	C(29)-H(29B)	0.98
C(26)-H(26)	0.95	C(28)-H(28A)	0.98	C(29)-H(29C)	0.98
C(30)-H(30A)	0.98	C(28)-H(28B)	0.98	C(30)-H(30B)	0.98
C(30)-H(30C)	0.98	N(1)-H(1)	0.93(7)		

Table 3 Angles (◦) for **3-14**.

Angle	◦	Angle	◦	Angle	◦
N(2)-C(1)-C(10)	127.6(3)	C(18)-C(17)-C(14)	107.9(14)	C(17A)-C(20A)-H(20D)	109.5
N(2)-C(1)-C(2)	108.9(3)	C(17)-C(18)-H(18A)	109.5	C(17A)-C(20A)-H(20E)	109.5
C(10)-C(1)-C(2)	123.4(3)	C(17)-C(18)-H(18B)	109.5	H(20D)-C(20A)-H(20E)	109.5
O(1)-C(2)-C(3)	128.4(4)	H(18A)-C(18)-H(18B)	109.5	C(17A)-C(20A)-H(20F)	109.5
O(1)-C(2)-C(1)	123.7(4)	C(17)-C(18)-H(18C)	109.5	H(20D)-C(20A)-H(20F)	109.5
C(3)-C(2)-C(1)	108.0(3)	H(18A)-C(18)-H(18C)	109.5	H(20E)-C(20A)-H(20F)	109.5
C(2)-C(3)-C(4)	106.2(3)	H(18B)-C(18)-H(18C)	109.5	C(22)-C(21)-C(26)	116.8(3)
C(2)-C(3)-H(3)	126.9	C(17)-C(19)-H(19A)	109.5	C(22)-C(21)-C(5)	121.8(3)
C(4)-C(3)-H(3)	126.9	C(17)-C(19)-H(19B)	109.5	C(26)-C(21)-C(5)	121.4(3)
N(2)-C(4)-C(5)	126.4(3)	H(19A)-C(19)-H(19B)	109.5	C(21)-C(22)-C(23)	121.2(3)
N(2)-C(4)-C(3)	110.6(3)	C(17)-C(19)-H(19C)	109.5	C(21)-C(22)-H(22)	119.4
C(5)-C(4)-C(3)	123.0(3)	H(19A)-C(19)-H(19C)	109.5	C(23)-C(22)-H(22)	119.4
C(6)-C(5)-C(4)	125.0(3)	H(19B)-C(19)-H(19C)	109.5	C(24)-C(23)-C(22)	122.2(4)
C(6)-C(5)-C(21)	118.7(3)	C(17)-C(20)-H(20A)	109.5	C(24)-C(23)-H(23)	118.9
C(4)-C(5)-C(21)	116.2(3)	C(17)-C(20)-H(20B)	109.5	C(22)-C(23)-H(23)	118.9
N(1)-C(6)-C(5)	127.0(3)	H(20A)-C(20)-H(20B)	109.5	C(23)-C(24)-C(25)	116.6(3)
N(1)-C(6)-C(7)	107.2(3)	C(17)-C(20)-H(20C)	109.5	C(23)-C(24)-C(27)	122.4(4)
C(5)-C(6)-C(7)	125.8(3)	H(20A)-C(20)-H(20C)	109.5	C(25)-C(24)-C(27)	121.0(3)
C(8)-C(7)-C(6)	108.2(3)	H(20B)-C(20)-H(20C)	109.5	C(26)-C(25)-C(24)	122.2(3)
C(8)-C(7)-H(7)	125.9	C(12A)-C(11A)-C(16A)	118.4(6)	C(26)-C(25)-H(25)	118.9
C(6)-C(7)-H(7)	125.9	C(12A)-C(11A)-C(10)	118.6(16)	C(24)-C(25)-H(25)	118.9
C(7)-C(8)-C(9)	107.9(3)	C(16A)-C(11A)-C(10)	123.0(14)	C(25)-C(26)-C(21)	121.0(4)
C(7)-C(8)-H(8)	126	C(11A)-C(12A)-C(13A)	120.1(9)	C(25)-C(26)-H(26)	119.5

C(9)-C(8)-H(8)	126	C(11A)-C(12A)-H(12A)	120	C(21)-C(26)-H(26)	119.5
N(1)-C(9)-C(10)#1	124.8(3)	C(13A)-C(12A)-H(12A)	120	C(29)-C(27)-C(24)	109.0(4)
N(1)-C(9)-C(8)	107.5(3)	C(14A)-C(13A)-C(12A)	120.3(10)	C(29)-C(27)-C(28)	108.8(5)
C(10)#1-C(9)-C(8)	127.6(3)	C(14A)-C(13A)-H(13A)	119.9	C(24)-C(27)-C(28)	112.4(3)
C(1)-C(10)-C(9)#1	124.7(3)	C(12A)-C(13A)-H(13A)	119.9	C(29)-C(27)-C(30)	111.9(5)
C(1)-C(10)-C(11)	112.5(10)	C(15A)-C(14A)-C(13A)	119.4(15)	C(24)-C(27)-C(30)	110.2(3)
C(9)#1-C(10)-C(11)	122.8(10)	C(15A)-C(14A)-C(17A)	122.8(16)	C(28)-C(27)-C(30)	104.6(4)
C(1)-C(10)-C(11A)	118.9(10)	C(13A)-C(14A)-C(17A)	117.7(15)	C(27)-C(28)-H(28A)	109.5
C(9)#1-C(10)-C(11A)	116.2(9)	C(14A)-C(15A)-C(16A)	122.1(11)	C(27)-C(28)-H(28B)	109.5
C(16)-C(11)-C(12)	113.6(10)	C(14A)-C(15A)-H(15A)	119	H(28A)-C(28)-H(28B)	109.5
C(16)-C(11)-C(10)	127.3(16)	C(16A)-C(15A)-H(15A)	119	C(27)-C(28)-H(28C)	109.5
C(12)-C(11)-C(10)	118.5(15)	C(15A)-C(16A)-C(11A)	119.3(7)	H(28A)-C(28)-H(28C)	109.5
O(1)-C(12)-C(13)	115.2(8)	C(15A)-C(16A)-H(16A)	120.3	H(28B)-C(28)-H(28C)	109.5
O(1)-C(12)-C(11)	123.2(9)	C(11A)-C(16A)-H(16A)	120.3	C(27)-C(29)-H(29A)	109.5
C(13)-C(12)-C(11)	121.0(10)	C(20A)-C(17A)-C(19A)	108.8(12)	C(27)-C(29)-H(29B)	109.5
C(12)-C(13)-C(14)	119.9(13)	C(20A)-C(17A)-C(18A)	111.6(13)	H(29A)-C(29)-H(29B)	109.5
C(12)-C(13)-H(13)	120	C(19A)-C(17A)-C(18A)	111.3(15)	C(27)-C(29)-H(29C)	109.5
C(14)-C(13)-H(13)	120	C(20A)-C(17A)-C(14A)	104.3(16)	H(29A)-C(29)-H(29C)	109.5
C(15)-C(14)-C(13)	111.5(18)	C(19A)-C(17A)-C(14A)	106.4(14)	H(29B)-C(29)-H(29C)	109.5
C(15)-C(14)-C(17)	126.5(16)	C(18A)-C(17A)-C(14A)	114.0(15)	C(27)-C(30)-H(30A)	109.5
C(13)-C(14)-C(17)	120.6(17)	C(17A)-C(18A)-H(18D)	109.5	C(27)-C(30)-H(30B)	109.5
C(14)-C(15)-C(16)	125.0(12)	C(17A)-C(18A)-H(18E)	109.5	H(30A)-C(30)-H(30B)	109.5
C(14)-C(15)-H(15)	117.5	H(18D)-C(18A)-H(18E)	109.5	C(27)-C(30)-H(30C)	109.5
C(16)-C(15)-H(15)	117.5	C(17A)-C(18A)-H(18F)	109.5	H(30A)-C(30)-H(30C)	109.5
C(11)-C(16)-C(15)	123.5(10)	H(18D)-C(18A)-H(18F)	109.5	H(30B)-C(30)-H(30C)	109.5
C(11)-C(16)-H(16)	118.3	H(18E)-C(18A)-H(18F)	109.5	C(6)-N(1)-C(9)	109.2(3)
C(15)-C(16)-H(16)	118.3	C(17A)-C(19A)-H(19D)	109.5	C(6)-N(1)-H(1)	123(4)
C(19)-C(17)-C(20)	107.4(11)	C(17A)-C(19A)-H(19E)	109.5	C(9)-N(1)-H(1)	120(4)
C(19)-C(17)-C(18)	112.2(14)	H(19D)-C(19A)-H(19E)	109.5	C(4)-N(2)-C(1)	106.4(3)
C(20)-C(17)-C(18)	108.2(13)	C(17A)-C(19A)-H(19F)	109.5	C(2)-O(1)-C(12)	116.8(6)
C(19)-C(17)-C(14)	112.7(14)	H(19D)-C(19A)-H(19F)	109.5		
C(20)-C(17)-C(14)	108.3(14)	H(19E)-C(19A)-H(19F)	109.5		

Table 4 Anisotropic displacement parameters (A^2 × 10^2) for **3-14** . The anisotropic displacement factor exponent takes the form: –2 pi2 [h^2a*^2 U11 + ... + 2 h k a* b*U12]

Atom	U11	U22	U33	U23	U13	U12
C(1)	67(2)	38(2)	56(2)	-4(1)	1(2)	-5(2)
C(2)	67(2)	41(2)	69(2)	-9(2)	8(2)	-12(2)
C(3)	58(2)	45(2)	71(2)	-1(2)	9(2)	-10(2)
C(4)	52(2)	38(2)	62(2)	1(2)	-2(2)	0(1)
C(5)	48(2)	40(2)	58(2)	-1(1)	-2(1)	1(1)
C(6)	52(2)	42(2)	58(2)	-8(2)	0(2)	3(1)
C(7)	56(2)	51(2)	96(3)	-24(2)	14(2)	1(2)
C(8)	67(2)	42(2)	96(3)	-26(2)	9(2)	-4(2)

C(9)	62(2)	38(2)	55(2)	-5(1)	2(2)	-4(1)
C(10)	72(2)	33(2)	58(2)	-7(1)	5(2)	-8(1)
C(11)	110(15)	48(8)	50(10)	3(6)	34(9)	7(7)
C(12)	99(7)	74(6)	116(9)	-17(6)	51(7)	-19(5)
C(13)	86(7)	76(7)	146(12)	-26(7)	28(7)	-22(5)
C(14)	86(14)	52(8)	47(6)	-6(5)	0(8)	-21(8)
C(15)	165(11)	53(5)	65(5)	-17(4)	45(6)	-29(6)
C(16)	147(9)	49(5)	82(6)	-2(4)	52(6)	-32(5)
C(17)	76(7)	39(5)	36(4)	0(4)	18(4)	-21(5)
C(18)	67(6)	44(6)	51(7)	11(5)	12(5)	-17(5)
C(19)	62(6)	48(5)	65(5)	-13(4)	5(4)	-22(4)
C(20)	72(6)	36(4)	45(4)	1(3)	27(4)	-8(4)
C(11A)	70(8)	29(6)	62(10)	-16(5)	-2(6)	-27(6)
C(12A)	59(4)	46(4)	85(6)	-17(4)	-31(4)	9(3)
C(13A)	45(3)	52(5)	72(5)	-24(4)	-14(3)	7(3)
C(14A)	55(8)	29(5)	81(9)	-14(5)	14(5)	-14(5)
C(15A)	44(3)	41(4)	92(5)	-17(4)	1(3)	1(3)
C(16A)	44(3)	33(3)	89(5)	-15(3)	12(3)	-3(3)
C(17A)	67(7)	39(6)	74(10)	4(6)	-7(6)	-12(6)
C(18A)	82(9)	39(6)	35(5)	-8(5)	7(5)	-19(5)
C(19A)	80(9)	98(13)	166(18)	-33(11)	5(9)	25(8)
C(20A)	152(18)	94(10)	85(12)	-11(8)	17(10)	-60(11)
C(21)	52(2)	36(2)	67(2)	-5(2)	4(2)	4(1)
C(22)	55(2)	66(2)	65(2)	-9(2)	1(2)	-1(2)
C(23)	66(2)	62(2)	64(2)	-4(2)	5(2)	1(2)
C(24)	59(2)	42(2)	74(2)	0(2)	10(2)	1(2)
C(25)	58(2)	53(2)	80(3)	-3(2)	2(2)	-2(2)
C(26)	58(2)	51(2)	71(2)	-6(2)	-2(2)	-2(2)
C(27)	70(2)	71(3)	80(3)	5(2)	18(2)	-6(2)
C(28)	94(3)	118(4)	91(4)	-1(3)	28(3)	-10(3)
C(29)	168(6)	92(4)	154(6)	-4(4)	55(5)	-54(4)
C(30)	72(3)	184(6)	109(4)	45(4)	37(3)	19(3)
N(1)	61(2)	34(1)	52(2)	-2(1)	5(1)	-3(1)
N(2)	64(2)	34(1)	51(2)	-4(1)	6(1)	-3(1)
O(1)	120(5)	71(4)	101(5)	-16(3)	40(4)	-8(3)

X-Ray analysis of 3-16

Crystal data and structure refinement

Identification code: **3-16**

Empirical formula: C60 H56 N4 Ni O2

Formula weight: 923.79

Temperature: 293(2) K

Crystal system, space group: Monoclinic, P 21/c

Unit cell dimensions:

a = 22.337(3) Å, a= 90°

b = 12.1971(12) Å, b= 96.801(13)°

c = 17.498(3) Å, g = 90°

Volume: 4733.8(11) Å^3

Z, calculated density: 4, 1.296 g/cm^3

F(000): 1952

θ range for data collection: 2.936 to 29.481°

Index ranges: -30<=h<=22, -14<=k<=16, -16<=l<=23

Refl. collected: 24303

Independent refl.: 10829 [R(int) = 0.2119]

Completeness to θ = 25.242, 97.6 %

Refinement method: Full-matrix least-squares on F^2

Data/restraints/parameters:10829 / 0 / 604

Goodness-of-fit on F^2: 0.978

Final R indices [I>2.0 σ(I)]: R1 = 0.1585, wR2 = 0.3410

R indices (all data):R1 = 0.4297, wR2 = 0.5104

Largest diff. peak and hole:1.316 and -0.563 Å^{-3}

Table 1 Atomic coordinates (× 10^4) and equivalent isotropic displacement parameters (Å^2 × 10^3) for **3-16**. U(eq) is defined as one third of the trace of the orthogonalized U^{ij} tensor.

Atom	x	y	z	U(eq)	Atom	x	y	z	U(eq)
Ni(1)	2491(1)	2482(1)	7368(1)	45(1)	C(25)	3051(6)	1444(10)	6057(9)	55(4)
N(1)	3091(4)	3433(7)	6978(6)	40(3)	C(26)	3072(6)	415(10)	5617(9)	65(4)
N(2)	1917(4)	1522(7)	7765(6)	41(3)	C(27)	1905(7)	3480(9)	8640(8)	56(4)
N(3)	2636(5)	1423(7)	6581(7)	50(3)	C(28)	3798(6)	4220(12)	6282(8)	60(4)
N(4)	2338(5)	3527(8)	8133(6)	51(3)	C(29)	1991(6)	-54(9)	6895(8)	51(4)
C(1)	1551(5)	2566(9)	8793(7)	36(3)	C(30)	136(7)	2831(11)	9813(9)	66(4)
O(1)	2413(6)	-1206(9)	5596(8)	116(4)	C(31)	2562(6)	4598(10)	8237(8)	56(4)
C(2)	1757(6)	438(8)	7491(8)	44(3)	C(32)	3644(7)	9542(9)	8732(8)	58(4)
C(3)	1568(6)	1612(9)	8331(8)	49(4)	C(33)	4844(8)	2066(12)	4999(10)	70(5)
C(4)	3428(6)	3300(10)	6404(8)	44(3)	C(34)	1345(7)	-52(9)	7919(8)	59(4)
O(2)	1167(6)	-1150(9)	7679(8)	113(4)	C(35)	4642(7)	1928(11)	4241(11)	67(5)
C(5)	373(8)	3072(10)	10550(8)	55(4)	C(36)	4455(8)	2232(12)	5568(10)	72(5)
C(6)	1378(7)	2873(9)	10174(8)	52(4)	C(37)	4019(8)	1933(10)	4057(10)	71(5)
C(7)	3236(6)	4486(10)	7235(7)	48(4)	C(38)	-32(8)	3357(13)	11161(9)	75(5)
C(8)	3684(6)	4985(10)	6834(8)	53(4)	C(39)	4245(7)	9619(10)	9233(9)	77(5)
C(9)	2271(6)	5193(9)	8798(8)	61(4)	C(40)	3630(7)	2112(10)	4589(11)	68(5)
C(10)	2400(6)	392(9)	6462(8)	50(4)	C(41)	5074(8)	1671(12)	3622(11)	80(5)
C(11)	989(7)	3052(10)	10712(8)	52(4)	C(42)	3139(7)	9900(13)	9248(10)	93(6)
C(12)	1782(7)	-1147(10)	6696(8)	54(4)	C(43)	1303(11)	-2823(14)	6962(10)	136(10)
C(13)	1146(6)	2667(10)	9402(9)	53(4)	C(44)	151(9)	2699(15)	11876(8)	104(7)
C(14)	3430(6)	2350(10)	5956(7)	45(3)	C(45)	-709(8)	3153(17)	10895(11)	113(7)
C(15)	3016(6)	5037(9)	7820(9)	51(4)	C(46)	761(8)	-4642(12)	5532(10)	99(7)
C(16)	1874(6)	4514(10)	9045(8)	59(4)	C(47)	1500(13)	-1770(16)	7129(13)	174(14)
C(17)	3206(7)	6182(9)	8041(8)	53(4)	C(48)	44(8)	4587(13)	11350(11)	111(7)
C(18)	3502(6)	8369(10)	8482(9)	53(4)	C(49)	5734(8)	1873(17)	3918(10)	114(7)
C(19)	535(6)	2632(9)	9228(8)	50(3)	C(50)	5005(9)	452(14)	3370(12)	125(8)

C(20)	1218(6)	638(11)	8458(7)	52(4)	C(51)	3594(9)	10320(14)	8062(10)	116(8)
C(21)	3844(6)	2233(9)	5353(8)	48(4)	C(52)	1856(8)	-5071(12)	5874(14)	139(10)
C(22)	2640(7)	-182(10)	5894(9)	63(4)	C(53)	1762(11)	-2740(11)	5875(9)	132(10)
C(23)	1430(6)	-3335(10)	6348(8)	55(4)	C(54)	1175(12)	-5153(12)	6840(11)	155(11)
C(24)	1282(7)	-4550(11)	6142(8)	62(4)	C(55)	3145(14)	6988(15)	7544(11)	194(15)
C(58)	3626(9)	7534(13)	8920(11)	111(7)	C(56)	3220(9)	8119(12)	7769(11)	108(7)
C(59)	4917(8)	2418(15)	2914(11)	112(7)	C(57)	3446(14)	6462(13)	8724(12)	209(17)
C(60)	1870(13)	-1664(13)	6055(10)	153(12)					

Table 2 Bond lengths (Å) of **3-16**.

Bond	A	Bond	A	Bond	A
Ni(1)-N(4)	1.909(11)	C(13)-C(19)	1.365(18)	C(39)-H(39A)	0.96
Ni(1)-N(2)	1.925(10)	C(14)-C(25)	1.417(17)	C(39)-H(39B)	0.96
Ni(1)-N(3)	1.943(10)	C(14)-C(21)	1.490(19)	C(39)-H(39C)	0.96
Ni(1)-N(1)	1.955(10)	C(15)-C(31)	1.421(18)	C(40)-H(40)	0.93
N(1)-C(4)	1.336(16)	C(15)-C(17)	1.497(15)	C(41)-C(49)	1.52(2)
N(1)-C(7)	1.387(14)	C(16)-C(27)	1.451(17)	C(41)-C(59)	1.54(2)
N(2)-C(3)	1.337(16)	C(16)-H(16)	0.93	C(41)-C(50)	1.55(2)
N(2)-C(2)	1.438(14)	C(17)-C(57)	1.296(19)	C(42)-H(42A)	0.96
N(3)-C(10)	1.371(13)	C(17)-C(55)	1.31(2)	C(42)-H(42B)	0.96
N(3)-C(25)	1.379(17)	C(18)-C(58)	1.29(2)	C(42)-H(42C)	0.96
N(4)-C(27)	1.389(17)	C(18)-C(56)	1.36(2)	C(43)-C(47)	1.38(2)
N(4)-C(31)	1.403(14)	C(18)-C(32)	1.517(16)	C(43)-H(43)	0.93
C(1)-C(27)	1.411(16)	C(19)-C(30)	1.454(19)	C(44)-H(44A)	0.96
C(1)-C(3)	1.420(17)	C(19)-H(19)	0.93	C(44)-H(44B)	0.96
C(1)-C(13)	1.482(18)	C(20)-C(34)	1.321(18)	C(44)-H(44C)	0.96
O(1)-C(22)	1.423(15)	C(20)-H(20)	0.93	C(45)-H(45A)	0.96
O(1)-C(60)	1.63(3)	C(21)-C(36)	1.372(19)	C(45)-H(45B)	0.96
C(2)-C(29)	1.361(17)	C(21)-C(40)	1.373(19)	C(45)-H(45C)	0.96
C(2)-C(34)	1.387(18)	C(22)-C(26)	1.344(18)	C(46)-H(46A)	0.96
C(3)-C(20)	1.453(16)	C(23)-C(43)	1.30(2)	C(46)-H(46B)	0.96
C(4)-C(14)	1.398(17)	C(23)-C(53)	1.38(2)	C(46)-H(46C)	0.96
C(4)-C(28)	1.424(17)	C(23)-C(24)	1.552(18)	C(48)-H(48A)	0.96
O(2)-C(34)	1.445(14)	C(24)-C(54)	1.47(2)	C(48)-H(48B)	0.96
O(2)-C(47)	1.49(2)	C(24)-C(46)	1.487(17)	C(48)-H(48C)	0.96
C(5)-C(30)	1.367(19)	C(24)-C(52)	1.55(2)	C(49)-H(49A)	0.96
C(5)-C(11)	1.372(19)	C(25)-C(26)	1.476(18)	C(49)-H(49B)	0.96
C(5)-C(38)	1.52(2)	C(26)-H(26)	0.93	C(49)-H(49C)	0.96
C(6)-C(11)	1.372(18)	C(28)-H(28)	0.93	C(50)-H(50A)	0.96
C(6)-C(13)	1.412(18)	C(30)-H(30)	0.93	C(50)-H(50B)	0.96
C(6)-H(6)	0.93	C(32)-C(51)	1.502(19)	C(50)-H(50C)	0.96
C(7)-C(15)	1.364(18)	C(32)-C(39)	1.518(17)	C(51)-H(51A)	0.96
C(7)-C(8)	1.425(18)	C(32)-C(42)	1.59(2)	C(51)-H(51B)	0.96
C(8)-C(28)	1.388(19)	C(33)-C(35)	1.36(2)	C(51)-H(51C)	0.96

C(8)-H(8)	0.93	C(33)-C(36)	1.41(2)	C(52)-H(52A)	0.96
C(9)-C(16)	1.323(17)	C(33)-H(33)	0.93	C(52)-H(52B)	0.96
C(9)-C(31)	1.438(18)	C(35)-C(37)	1.392(19)	C(52)-H(52C)	0.96
C(9)-H(9)	0.93	C(35)-C(41)	1.56(2)	C(53)-C(60)	1.365(19)
C(10)-C(29)	1.369(18)	C(36)-H(36)	0.93	C(53)-H(53)	0.93
C(10)-C(22)	1.375(18)	C(37)-C(40)	1.36(2)	C(54)-H(54A)	0.96
C(11)-H(11)	0.93	C(37)-H(37)	0.93	C(54)-H(54B)	0.96
C(12)-C(47)	1.29(2)	C(38)-C(44)	1.50(2)	C(54)-H(54C)	0.96
C(12)-C(60)	1.32(2)	C(38)-C(48)	1.54(2)	C(55)-C(56)	1.44(2)
C(12)-C(29)	1.441(16)	C(38)-C(45)	1.55(2)	C(55)-H(55)	0.93
C(56)-H(56)	0.93	C(58)-H(58)	0.93	C(59)-H(59B)	0.96
C(57)-C(58)	1.40(2)	C(59)-H(59A)	0.96	C(59)-H(59C)	0.96
C(57)-H(57)	0.93				

Table 3 Angles (◦) of **3-16**.

Angle	◦	Angel	◦	Angle	◦
N(4)-Ni(1)-N(2)	88.3(4)	C(3)-C(20)-H(20)	127.9	C(32)-C(42)-H(42A)	109.5
N(4)-Ni(1)-N(3)	179.2(5)	C(36)-C(21)-C(40)	119.2(15)	C(32)-C(42)-H(42B)	109.5
N(2)-Ni(1)-N(3)	91.5(5)	C(36)-C(21)-C(14)	119.1(13)	H(42A)-C(42)-H(42B)	109.5
N(4)-Ni(1)-N(1)	92.1(5)	C(40)-C(21)-C(14)	121.7(13)	C(32)-C(42)-H(42C)	109.5
N(2)-Ni(1)-N(1)	178.5(4)	C(26)-C(22)-C(10)	110.0(12)	H(42A)-C(42)-H(42C)	109.5
N(3)-Ni(1)-N(1)	88.2(5)	C(26)-C(22)-O(1)	125.7(14)	H(42B)-C(42)-H(42C)	109.5
C(4)-N(1)-C(7)	103.0(10)	C(10)-C(22)-O(1)	124.0(13)	C(23)-C(43)-C(47)	121.7(17)
C(4)-N(1)-Ni(1)	131.4(8)	C(43)-C(23)-C(53)	115.3(14)	C(23)-C(43)-H(43)	119.1
C(7)-N(1)-Ni(1)	125.5(10)	C(43)-C(23)-C(24)	126.0(14)	C(47)-C(43)-H(43)	119.1
C(3)-N(2)-C(2)	100.2(10)	C(53)-C(23)-C(24)	118.6(14)	C(38)-C(44)-H(44A)	109.5
C(3)-N(2)-Ni(1)	133.6(8)	C(54)-C(24)-C(46)	111.6(15)	C(38)-C(44)-H(44B)	109.5
C(2)-N(2)-Ni(1)	126.2(9)	C(54)-C(24)-C(23)	109.7(12)	H(44A)-C(44)-H(44B)	109.5
C(10)-N(3)-C(25)	101.0(11)	C(46)-C(24)-C(23)	111.4(12)	C(38)-C(44)-H(44C)	109.5
C(10)-N(3)-Ni(1)	128.7(10)	C(54)-C(24)-C(52)	105.6(16)	H(44A)-C(44)-H(44C)	109.5
C(25)-N(3)-Ni(1)	129.8(9)	C(46)-C(24)-C(52)	110.9(15)	H(44B)-C(44)-H(44C)	109.5
C(27)-N(4)-C(31)	102.8(11)	C(23)-C(24)-C(52)	107.4(11)	C(38)-C(45)-H(45A)	109.5
C(27)-N(4)-Ni(1)	128.1(8)	N(3)-C(25)-C(14)	123.8(12)	C(38)-C(45)-H(45B)	109.5
C(31)-N(4)-Ni(1)	128.4(9)	N(3)-C(25)-C(26)	113.4(12)	H(45A)-C(45)-H(45B)	109.5
C(27)-C(1)-C(3)	119.2(12)	C(14)-C(25)-C(26)	122.8(14)	C(38)-C(45)-H(45C)	109.5
C(27)-C(1)-C(13)	118.3(12)	C(22)-C(26)-C(25)	101.8(13)	H(45A)-C(45)-H(45C)	109.5
C(3)-C(1)-C(13)	122.5(11)	C(22)-C(26)-H(26)	129.1	H(45B)-C(45)-H(45C)	109.5
C(22)-O(1)-C(60)	112.0(12)	C(25)-C(26)-H(26)	129.1	C(24)-C(46)-H(46A)	109.5
C(29)-C(2)-C(34)	124.2(11)	N(4)-C(27)-C(1)	127.0(11)	C(24)-C(46)-H(46B)	109.5
C(29)-C(2)-N(2)	123.9(11)	N(4)-C(27)-C(16)	110.7(12)	H(46A)-C(46)-H(46B)	109.5
C(34)-C(2)-N(2)	111.9(11)	C(1)-C(27)-C(16)	122.3(14)	C(24)-C(46)-H(46C)	109.5
N(2)-C(3)-C(1)	123.1(11)	C(8)-C(28)-C(4)	105.6(13)	H(46A)-C(46)-H(46C)	109.5
N(2)-C(3)-C(20)	114.8(12)	C(8)-C(28)-H(28)	127.2	H(46B)-C(46)-H(46C)	109.5
C(1)-C(3)-C(20)	122.1(13)	C(4)-C(28)-H(28)	127.2	C(12)-C(47)-C(43)	126.3(17)

N(1)-C(4)-C(14)	124.2(12)	C(2)-C(29)-C(10)	126.3(11)	C(12)-C(47)-O(2)	113.3(16)
N(1)-C(4)-C(28)	113.9(12)	C(2)-C(29)-C(12)	116.8(13)	C(43)-C(47)-O(2)	116.0(18)
C(14)-C(4)-C(28)	121.9(14)	C(10)-C(29)-C(12)	116.9(12)	C(38)-C(48)-H(48A)	109.5
C(34)-O(2)-C(47)	121.2(13)	C(5)-C(30)-C(19)	120.0(14)	C(38)-C(48)-H(48B)	109.5
C(30)-C(5)-C(11)	117.2(14)	C(5)-C(30)-H(30)	120	H(48A)-C(48)-H(48B)	109.5
C(30)-C(5)-C(38)	121.2(16)	C(19)-C(30)-H(30)	120	C(38)-C(48)-H(48C)	109.5
C(11)-C(5)-C(38)	121.6(14)	N(4)-C(31)-C(15)	123.4(12)	H(48A)-C(48)-H(48C)	109.5
C(11)-C(6)-C(13)	119.7(14)	N(4)-C(31)-C(9)	112.0(12)	H(48B)-C(48)-H(48C)	109.5
C(11)-C(6)-H(6)	120.2	C(15)-C(31)-C(9)	124.6(12)	C(41)-C(49)-H(49A)	109.5
C(13)-C(6)-H(6)	120.2	C(51)-C(32)-C(18)	112.1(12)	C(41)-C(49)-H(49B)	109.5
C(15)-C(7)-N(1)	127.5(13)	C(51)-C(32)-C(39)	112.9(12)	H(49A)-C(49)-H(49B)	109.5
C(15)-C(7)-C(8)	119.7(12)	C(18)-C(32)-C(39)	111.4(10)	C(41)-C(49)-H(49C)	109.5
N(1)-C(7)-C(8)	112.8(12)	C(51)-C(32)-C(42)	106.2(13)	H(49A)-C(49)-H(49C)	109.5
C(28)-C(8)-C(7)	104.6(12)	C(18)-C(32)-C(42)	106.6(12)	H(49B)-C(49)-H(49C)	109.5
C(28)-C(8)-H(8)	127.7	C(39)-C(32)-C(42)	107.1(12)	C(41)-C(50)-H(50A)	109.5
C(7)-C(8)-H(8)	127.7	C(35)-C(33)-C(36)	123.0(15)	C(41)-C(50)-H(50B)	109.5
C(16)-C(9)-C(31)	106.4(11)	C(35)-C(33)-H(33)	118.5	H(50A)-C(50)-H(50B)	109.5
C(16)-C(9)-H(9)	126.8	C(36)-C(33)-H(33)	118.5	C(41)-C(50)-H(50C)	109.5
C(31)-C(9)-H(9)	126.8	C(20)-C(34)-C(2)	108.8(11)	H(50A)-C(50)-H(50C)	109.5
C(29)-C(10)-N(3)	123.4(12)	C(20)-C(34)-O(2)	136.4(15)	H(50B)-C(50)-H(50C)	109.5
C(29)-C(10)-C(22)	122.8(11)	C(2)-C(34)-O(2)	114.8(13)	C(32)-C(51)-H(51A)	109.5
N(3)-C(10)-C(22)	113.7(13)	C(33)-C(35)-C(37)	115.6(17)	C(32)-C(51)-H(51B)	109.5
C(6)-C(11)-C(5)	124.2(13)	C(33)-C(35)-C(41)	122.7(14)	H(51A)-C(51)-H(51B)	109.5
C(6)-C(11)-H(11)	117.9	C(37)-C(35)-C(41)	121.5(16)	C(32)-C(51)-H(51C)	109.5
C(5)-C(11)-H(11)	117.9	C(21)-C(36)-C(33)	118.8(14)	H(51A)-C(51)-H(51C)	109.5
C(47)-C(12)-C(60)	110.4(14)	C(21)-C(36)-H(36)	120.6	H(51B)-C(51)-H(51C)	109.5
C(47)-C(12)-C(29)	124.7(15)	C(33)-C(36)-H(36)	120.6	C(24)-C(52)-H(52A)	109.5
C(60)-C(12)-C(29)	124.8(15)	C(40)-C(37)-C(35)	122.9(16)	C(24)-C(52)-H(52B)	109.5
C(19)-C(13)-C(6)	117.6(14)	C(40)-C(37)-H(37)	118.6	H(52A)-C(52)-H(52B)	109.5
C(19)-C(13)-C(1)	121.2(13)	C(35)-C(37)-H(37)	118.6	C(24)-C(52)-H(52C)	109.5
C(6)-C(13)-C(1)	121.1(13)	C(44)-C(38)-C(5)	109.7(14)	H(52A)-C(52)-H(52C)	109.5
C(4)-C(14)-C(25)	122.3(13)	C(44)-C(38)-C(48)	109.3(14)	H(52B)-C(52)-H(52C)	109.5
C(4)-C(14)-C(21)	121.3(12)	C(5)-C(38)-C(48)	108.3(14)	C(60)-C(53)-C(23)	117.4(19)
C(25)-C(14)-C(21)	116.4(12)	C(44)-C(38)-C(45)	108.9(16)	C(60)-C(53)-H(53)	121.3
C(7)-C(15)-C(31)	122.8(11)	C(5)-C(38)-C(45)	113.1(13)	C(23)-C(53)-H(53)	121.3
C(7)-C(15)-C(17)	122.5(13)	C(48)-C(38)-C(45)	107.4(15)	C(24)-C(54)-H(54A)	109.5
C(31)-C(15)-C(17)	114.6(13)	C(32)-C(39)-H(39A)	109.5	C(24)-C(54)-H(54B)	109.5
C(9)-C(16)-C(27)	108.2(13)	C(32)-C(39)-H(39B)	109.5	H(54A)-C(54)-H(54B)	109.5
C(9)-C(16)-H(16)	125.9	H(39A)-C(39)-H(39B)	109.5	C(24)-C(54)-H(54C)	109.5
C(27)-C(16)-H(16)	125.9	C(32)-C(39)-H(39C)	109.5	H(54A)-C(54)-H(54C)	109.5
C(57)-C(17)-C(55)	114.5(14)	H(39A)-C(39)-H(39C)	109.5	H(54B)-C(54)-H(54C)	109.5
C(57)-C(17)-C(15)	123.9(13)	H(39B)-C(39)-H(39C)	109.5	C(17)-C(55)-C(56)	122.6(17)
C(55)-C(17)-C(15)	121.6(13)	C(37)-C(40)-C(21)	120.3(15)	C(17)-C(55)-H(55)	118.7
C(58)-C(18)-C(56)	114.3(14)	C(37)-C(40)-H(40)	119.8	C(56)-C(55)-H(55)	118.7
C(58)-C(18)-C(32)	123.5(13)	C(21)-C(40)-H(40)	119.8	C(18)-C(56)-C(55)	119.4(17)
C(56)-C(18)-C(32)	122.1(13)	C(49)-C(41)-C(59)	107.1(15)	C(18)-C(56)-H(56)	120.3

C(13)-C(19)-C(30)	121.2(13)	C(49)-C(41)-C(50)	108.1(15)	C(55)-C(56)-H(56)	120.3
C(13)-C(19)-H(19)	119.4	C(59)-C(41)-C(50)	109.4(15)	C(17)-C(57)-C(58)	123.2(17)
C(30)-C(19)-H(19)	119.4	C(49)-C(41)-C(35)	112.6(14)	C(17)-C(57)-H(57)	118.4
C(34)-C(20)-C(3)	104.3(12)	C(59)-C(41)-C(35)	109.8(13)	C(58)-C(57)-H(57)	118.4
C(34)-C(20)-H(20)	127.9	C(50)-C(41)-C(35)	109.8(14)	C(18)-C(58)-C(57)	124.1(16)
C(18)-C(58)-H(58)	118	C(41)-C(59)-H(59C)	109.5	C(12)-C(60)-C(53)	128.0(17)
C(57)-C(58)-H(58)	118	H(59A)-C(59)-H(59C)	109.5	C(12)-C(60)-O(1)	116.6(14)
C(41)-C(59)-H(59A)	109.5	H(59B)-C(59)-H(59C)	109.5	C(53)-C(60)-O(1)	110(2)
C(41)-C(59)-H(59B)	109.5	H(59A)-C(59)-H(59B)	109.5		

Table 4 Anisotropic displacement parameters (A^2 × 10^2) for **3-16** . The anisotropic displacement factor exponent takes the form: –2 pi2 [h^2a*^2 U11 + ... + 2 h k a* b*U12]

Atom	U_{11}	U_{22}	U_{33}	U_{23}	U_{13}	U_{12}
Ni(1)	54(1)	22(1)	60(1)	3(1)	9(1)	-1(1)
N(1)	38(7)	29(5)	50(7)	7(5)	-4(6)	-11(5)
N(2)	55(7)	26(5)	48(7)	7(4)	29(6)	15(5)
N(3)	47(7)	32(6)	71(8)	-11(5)	13(6)	-3(5)
N(4)	56(8)	36(6)	65(8)	0(5)	31(6)	-5(5)
C(1)	26(6)	35(7)	46(8)	24(6)	-1(6)	-5(6)
O(1)	169(13)	59(7)	126(11)	-15(7)	43(9)	-27(8)
C(2)	50(8)	17(6)	67(10)	8(6)	22(7)	-4(6)
C(3)	44(9)	31(7)	71(11)	3(7)	1(8)	5(6)
C(4)	39(8)	52(9)	41(9)	3(6)	1(7)	-5(7)
O(2)	142(11)	73(8)	127(12)	6(7)	27(9)	-29(8)
C(5)	89(13)	36(7)	44(10)	-4(6)	24(9)	-2(8)
C(6)	77(11)	35(7)	44(9)	9(6)	3(9)	12(7)
C(7)	65(10)	40(8)	37(8)	-8(6)	1(7)	-4(7)
C(8)	68(10)	39(8)	54(10)	7(7)	13(8)	-8(7)
C(9)	89(11)	15(6)	85(11)	-20(6)	39(9)	1(7)
C(10)	60(10)	19(6)	70(10)	-15(6)	8(8)	-7(6)
C(11)	76(12)	37(7)	44(10)	7(6)	12(9)	-9(8)
C(12)	87(11)	31(7)	45(10)	-4(7)	12(8)	18(7)
C(13)	47(9)	39(8)	75(11)	6(7)	18(8)	-5(7)
C(14)	39(8)	52(8)	39(8)	-8(6)	-14(7)	-14(7)
C(15)	52(9)	18(6)	83(11)	14(7)	3(8)	-6(6)
C(16)	80(11)	45(8)	56(10)	2(7)	33(8)	-11(8)
C(17)	92(11)	24(6)	44(9)	5(6)	15(8)	5(7)
C(18)	59(9)	40(8)	55(10)	-3(7)	-12(8)	8(7)
C(19)	72(10)	40(7)	39(8)	-4(6)	6(7)	-2(7)
C(20)	63(10)	53(8)	39(9)	21(7)	6(7)	-17(7)
C(21)	59(10)	31(7)	46(9)	-4(6)	-20(8)	-1(6)
C(22)	93(12)	22(7)	82(11)	-3(7)	42(9)	-17(7)
C(23)	75(10)	42(8)	49(10)	-3(7)	10(8)	-14(7)
C(24)	77(11)	58(9)	51(10)	16(7)	2(8)	-27(8)

C(25)	51(9)	31(7)	84(12)	8(7)	6(8)	13(7)
C(26)	67(10)	28(7)	104(13)	-6(7)	23(9)	5(7)
C(27)	81(11)	26(7)	61(10)	-12(6)	9(9)	3(7)
C(28)	50(9)	72(10)	56(10)	26(8)	0(7)	-20(8)
C(29)	63(10)	23(7)	71(10)	-12(6)	33(8)	12(6)
C(30)	73(11)	57(9)	72(12)	5(8)	21(9)	-15(8)
C(31)	70(10)	31(7)	70(11)	3(7)	23(8)	1(7)
C(32)	75(10)	25(7)	69(10)	2(6)	-12(9)	-6(7)
C(33)	81(12)	71(10)	52(11)	-2(8)	-8(10)	-5(9)
C(34)	102(12)	14(6)	63(10)	-1(6)	12(9)	-21(7)
C(35)	42(10)	46(8)	110(16)	-21(9)	3(10)	-6(7)
C(36)	90(13)	64(10)	61(11)	-4(8)	2(10)	-9(9)
C(37)	102(15)	27(7)	80(13)	6(7)	1(11)	-13(8)
C(38)	107(15)	72(11)	47(10)	-7(8)	18(10)	13(10)
C(39)	94(12)	33(8)	102(13)	-5(8)	1(10)	-21(8)
C(40)	64(11)	32(7)	109(15)	-3(8)	19(11)	0(7)
C(41)	80(13)	61(10)	95(14)	5(9)	-8(11)	14(9)
C(42)	91(13)	77(12)	119(16)	-36(11)	49(12)	-11(10)
C(43)	280(30)	70(12)	73(14)	-30(10)	94(16)	-81(15)
C(44)	148(17)	134(16)	38(10)	27(10)	40(10)	50(14)
C(45)	98(15)	157(19)	92(15)	-5(13)	38(12)	21(14)
C(46)	111(14)	58(10)	116(16)	-2(10)	-40(13)	-1(10)
C(47)	330(40)	86(14)	140(20)	-88(14)	180(20)	-105(19)
C(48)	127(17)	79(13)	128(17)	-33(12)	11(13)	17(12)
C(49)	99(16)	155(19)	91(15)	4(13)	20(12)	52(14)
C(50)	152(19)	84(14)	140(20)	-38(13)	32(15)	33(13)
C(51)	157(19)	91(13)	90(15)	12(11)	-27(13)	-61(13)
C(52)	76(14)	41(9)	300(30)	-61(14)	11(16)	3(9)
C(53)	310(30)	32(8)	55(11)	-11(7)	28(15)	-50(13)
C(54)	320(30)	44(10)	106(17)	-10(10)	42(19)	-69(15)
C(55)	440(40)	68(12)	85(16)	-28(11)	70(20)	-150(20)
C(56)	159(19)	46(10)	113(17)	2(10)	-17(14)	-11(11)
C(57)	430(40)	33(9)	116(18)	-4(10)	-150(20)	-49(17)
C(58)	145(18)	62(11)	113(16)	-33(11)	-38(14)	-6(12)
C(59)	101(14)	140(18)	98(15)	10(13)	26(12)	46(13)
C(60)	360(40)	49(10)	41(11)	28(8)	-5(16)	-91(15)

X-Ray analysis of 3-36

Crystal data and structure refinement

Identification code: **3-36**

Empirical formula: C61 H60 Cl2 N4 O2

Formula weight: 952.03

Temperature: 150(2) K

Crystal system, space group: Triclinic, P-1

Unit cell dimensions:

a = 9.7862(5) Å, a= 105.279(4)°

b = 16.3610(8) Å, b= 101.693(4)°

c = 16.5988(8) Å, g = 97.299(4)°

Volume: 2464.3(2) $Å^3$

Z, calculated density:2, 1.283 g/cm^3

F(000): 1008

Crystal size: 0.134 x 0.106 x 0.080 mm^3

θ range for data collection: 2.963 to 29.730°

Refl. collected: 22481

Independent refl.: 11663 [R(int) = 0.0340]

Completeness to θ = 25.242, 99.8 %

Refinement method: full-matrix least-squares on F^2

Data/restraints/parameters: 11663/84/664

Goodness-of-fit on F^2: 1.033

R indices [I>2σ(I)]: R1 = 0.0688, wR2 = 0.1693

R indices (all data): R1 = 0.1016, wR2 = 0.1933

Largest diff. peak and hole: 0.569 and -0.751 $Å^{-3}$

Table 1 Atomic coordinates (× 10^4) and equivalent isotropic displacement parameters ($Å^2$ × 10^3) for **3-36**. U(eq) is defined as one third of the trace of the orthogonalized U^{ij} tensor.

Atom	x	y	z	U(eq)	Atom	x	y	z	U(eq)
Cl(1)	1882(1)	104(1)	-848(1)	55(1)	C(27)	2533(3)	1440(2)	3183(2)	23(1)
Cl(2)	4804(1)	651(1)	-833(1)	90(1)	C(28)	1657(3)	400(2)	1502(2)	23(1)
O(1)	1561(2)	1585(1)	986(1)	26(1)	C(29)	2385(3)	555(2)	2995(2)	25(1)
O(2)	5500(2)	8233(1)	4769(1)	25(1)	C(30)	1924(3)	9(2)	2149(2)	22(1)
N(1)	3810(2)	5619(1)	2006(1)	17(1)	C(31)	2018(3)	3203(2)	4249(2)	23(1)
N(2)	4057(2)	5971(1)	3824(1)	18(1)	C(32)	2679(3)	6576(2)	7538(2)	22(1)
N(3)	2843(2)	4233(1)	3713(1)	18(1)	C(33)	509(3)	4025(2)	-627(2)	24(1)
N(4)	2663(2)	3879(1)	1914(1)	18(1)	C(34)	-53(3)	3819(2)	-1508(2)	24(1)
C(1)	4708(2)	6741(1)	3792(2)	18(1)	C(35)	5978(3)	8463(2)	4118(2)	22(1)
C(2)	4398(3)	6476(1)	2226(2)	17(1)	C(36)	1791(3)	6688(2)	6828(2)	27(1)
C(3)	2948(3)	5834(1)	5849(2)	18(1)	C(37)	2837(3)	4265(2)	-834(2)	27(1)
C(4)	2746(3)	4638(2)	4529(2)	19(1)	C(38)	195(3)	3602(2)	-3051(2)	20(1)
C(5)	4988(2)	6993(1)	3090(2)	18(1)	C(39)	1697(3)	-975(2)	1962(2)	24(1)
C(6)	2530(3)	4450(2)	675(2)	18(1)	C(40)	1925(3)	6331(2)	5998(2)	26(1)
C(7)	4120(3)	6720(2)	1455(2)	19(1)	C(41)	7109(3)	9043(2)	2948(2)	24(1)
C(8)	3844(3)	6133(1)	4647(2)	18(1)	C(42)	2268(3)	4050(2)	-1715(2)	27(1)
C(9)	2356(3)	3777(2)	1043(2)	18(1)	C(43)	6626(3)	9322(2)	4330(2)	28(1)
C(10)	3179(3)	5519(2)	4961(2)	19(1)	C(44)	3782(3)	5676(2)	6549(2)	25(1)
C(11)	5797(3)	7874(1)	3303(2)	19(1)	C(45)	3665(3)	6049(2)	7383(2)	28(1)
C(12)	3193(3)	5300(2)	1132(2)	18(1)	C(46)	7177(3)	9635(2)	3740(2)	28(1)
C(13)	1960(3)	4244(1)	-276(2)	19(1)	C(47)	2547(3)	7001(2)	8455(2)	29(1)
C(14)	813(3)	3814(1)	-2076(1)	18(1)	C(48)	-1305(3)	3067(2)	-3331(2)	30(1)
C(15)	2224(3)	1846(2)	2541(2)	19(1)	C(49)	1107(3)	3076(2)	-3551(2)	28(1)
C(16)	3380(3)	6009(2)	797(2)	20(1)	C(50)	153(3)	4450(2)	-3274(2)	30(1)
C(17)	4926(3)	7390(2)	4615(2)	20(1)	C(51)	1507(4)	-1440(2)	1003(2)	35(1)
C(18)	2434(3)	3355(2)	3520(2)	19(1)	C(52)	344(3)	-1274(2)	2221(2)	36(1)

C(19)	2395(3)	3071(1)	1981(2)	18(1)	C(53)	2963(3)	-1222(2)	2482(2)	34(1)
C(20)	2190(3)	3981(2)	4851(2)	23(1)	C(54)	1344(3)	6444(2)	8647(2)	40(1)
C(21)	4385(3)	7024(2)	5147(2)	21(1)	C(55)	7798(4)	10595(2)	3928(2)	46(1)
C(22)	2378(3)	2785(1)	2704(2)	19(1)	C(56)	3923(4)	7064(3)	9126(2)	51(1)
C(23)	1821(3)	1288(2)	1694(2)	22(1)	C(57)	2205(6)	7900(2)	8540(2)	73(2)
C(24)	1874(3)	2882(2)	539(2)	22(1)	C(58)	3481(4)	797(3)	-284(3)	70(1)
C(25)	1930(3)	2449(2)	1128(2)	21(1)	C(59)	7826(6)	11133(2)	4826(3)	53(1)
C(26)	6447(3)	8194(2)	2737(2)	22(1)	C(60)	9167(5)	10735(3)	3697(4)	66(2)
C(61A)	6950(16)	11204(10)	4314(11)	59(4)	C(61)	6678(5)	10945(3)	3305(3)	56(1)
C(59A)	9245(13)	10703(10)	4647(9)	69(5)	C(60A)	8326(19)	10809(10)	3185(8)	56(4)

Table 2 Bond lengths (Å) of **3-36**.

Bond	Å	Bond	Å	Bond	Å
Cl(1)-C(58)	1.735(4)	C(19)-C(22)	1.401(3)	C(48)-H(48B)	0.98
Cl(2)-C(58)	1.734(4)	C(19)-C(25)	1.452(3)	C(48)-H(48C)	0.98
O(1)-C(25)	1.358(3)	C(20)-C(31)	1.361(3)	C(49)-H(49A)	0.98
O(1)-C(23)	1.378(3)	C(20)-H(20)	0.95	C(49)-H(49B)	0.98
O(2)-C(17)	1.357(3)	C(21)-H(21)	0.95	C(49)-H(49C)	0.98
O(2)-C(35)	1.379(3)	C(23)-C(28)	1.384(3)	C(50)-H(50A)	0.98
N(1)-C(2)	1.368(3)	C(24)-C(25)	1.347(3)	C(50)-H(50B)	0.98
N(1)-C(12)	1.381(3)	C(24)-H(24)	0.95	C(50)-H(50C)	0.98
N(1)-H(1)	0.89(3)	C(26)-C(41)	1.377(3)	C(51)-H(51A)	0.98
N(2)-C(1)	1.357(3)	C(26)-H(26)	0.95	C(51)-H(51B)	0.98
N(2)-C(8)	1.385(3)	C(27)-C(29)	1.380(3)	C(51)-H(51C)	0.98
N(3)-C(4)	1.372(3)	C(27)-H(27)	0.95	C(52)-H(52A)	0.98
N(3)-C(18)	1.372(3)	C(28)-C(30)	1.387(4)	C(52)-H(52B)	0.98
N(3)-H(2)	0.89(3)	C(28)-H(28)	0.95	C(52)-H(52C)	0.98
N(4)-C(19)	1.352(3)	C(29)-C(30)	1.397(3)	C(53)-H(53A)	0.98
N(4)-C(9)	1.375(3)	C(29)-H(29)	0.95	C(53)-H(53B)	0.98
C(1)-C(5)	1.400(3)	C(30)-C(39)	1.534(3)	C(53)-H(53C)	0.98
C(1)-C(17)	1.449(3)	C(31)-H(31)	0.95	C(54)-H(54A)	0.98
C(2)-C(5)	1.416(3)	C(32)-C(36)	1.384(4)	C(54)-H(54B)	0.98
C(2)-C(7)	1.424(3)	C(32)-C(45)	1.392(4)	C(54)-H(54C)	0.98
C(3)-C(44)	1.382(3)	C(32)-C(47)	1.537(3)	C(55)-C(60)	1.474(5)
C(3)-C(40)	1.388(3)	C(33)-C(34)	1.386(3)	C(55)-C(61A)	1.477(8)
C(3)-C(10)	1.503(3)	C(33)-H(33)	0.95	C(55)-C(59)	1.510(4)
C(4)-C(10)	1.396(3)	C(34)-H(34)	0.95	C(55)-C(60A)	1.533(8)
C(4)-C(20)	1.418(3)	C(35)-C(43)	1.387(3)	C(55)-C(59A)	1.613(8)
C(5)-C(11)	1.469(3)	C(36)-C(40)	1.388(3)	C(55)-C(61)	1.616(5)
C(6)-C(12)	1.396(3)	C(36)-H(36)	0.95	C(56)-H(56A)	0.98
C(6)-C(9)	1.402(3)	C(37)-C(42)	1.387(3)	C(56)-H(56B)	0.98
C(6)-C(13)	1.494(3)	C(37)-H(37)	0.95	C(56)-H(56C)	0.98
C(7)-C(16)	1.366(3)	C(38)-C(48)	1.523(3)	C(57)-H(57A)	0.98
C(7)-H(7)	0.95	C(38)-C(50)	1.531(4)	C(57)-H(57B)	0.98
C(8)-C(10)	1.396(3)	C(38)-C(49)	1.532(3)	C(57)-H(57C)	0.98
C(8)-C(21)	1.444(3)	C(39)-C(53)	1.524(4)	C(58)-H(58A)	0.99

C(9)-C(24)	1.444(3)	C(39)-C(51)	1.534(4)	C(58)-H(58B)	0.99
C(11)-C(35)	1.402(3)	C(39)-C(52)	1.535(4)	C(59)-H(59A)	0.98
C(11)-C(26)	1.405(3)	C(40)-H(40)	0.95	C(59)-H(59B)	0.98
C(12)-C(16)	1.419(3)	C(41)-C(46)	1.397(4)	C(59)-H(59C)	0.98
C(13)-C(33)	1.382(3)	C(41)-H(41)	0.95	C(60)-H(60A)	0.98
C(13)-C(37)	1.387(4)	C(42)-H(42)	0.95	C(60)-H(60B)	0.98
C(14)-C(42)	1.388(3)	C(43)-C(46)	1.385(4)	C(60)-H(60C)	0.98
C(14)-C(34)	1.389(3)	C(43)-H(43)	0.95	C(61)-H(61A)	0.98
C(14)-C(38)	1.536(3)	C(44)-C(45)	1.393(3)	C(61)-H(61B)	0.98
C(15)-C(27)	1.401(3)	C(44)-H(44)	0.95	C(61)-H(61C)	0.98
C(15)-C(23)	1.404(3)	C(45)-H(45)	0.95	C(60A)-H(60D)	0.98
C(15)-C(22)	1.470(3)	C(46)-C(55)	1.534(4)	C(60A)-H(60E)	0.98
C(16)-H(16)	0.95	C(47)-C(57)	1.528(4)	C(60A)-H(60F)	0.98
C(17)-C(21)	1.344(3)	C(47)-C(54)	1.533(4)	C(61A)-H(61D)	0.98
C(18)-C(22)	1.414(3)	C(47)-C(56)	1.537(5)	C(61A)-H(61E)	0.98
C(18)-C(31)	1.424(3)	C(48)-H(48A)	0.98	C(61A)-H(61F)	0.98
C(59A)-H(59E)	0.98	C(59A)-H(59F)	0.98	C(59A)-H(59D)	0.98

Table 3 Angles (◦) of **3-36**.

Angle	◦	Angle	◦	Angle	◦
C(25)-O(1)-C(23)	116.98(18)	C(11)-C(26)-H(26)	118.9	H(50A)-C(50)-H(50B)	109.5
C(17)-O(2)-C(35)	117.50(18)	C(29)-C(27)-C(15)	122.2(2)	C(38)-C(50)-H(50C)	109.5
C(2)-N(1)-C(12)	110.5(2)	C(29)-C(27)-H(27)	118.9	H(50A)-C(50)-H(50C)	109.5
C(2)-N(1)-H(1)	127.5(19)	C(15)-C(27)-H(27)	118.9	H(50B)-C(50)-H(50C)	109.5
C(12)-N(1)-H(1)	121.6(19)	C(23)-C(28)-C(30)	121.0(2)	C(39)-C(51)-H(51A)	109.5
C(1)-N(2)-C(8)	105.03(18)	C(23)-C(28)-H(28)	119.5	C(39)-C(51)-H(51B)	109.5
C(4)-N(3)-C(18)	110.5(2)	C(30)-C(28)-H(28)	119.5	H(51A)-C(51)-H(51B)	109.5
C(4)-N(3)-H(2)	124.0(18)	C(27)-C(29)-C(30)	121.9(2)	C(39)-C(51)-H(51C)	109.5
C(18)-N(3)-H(2)	125.4(18)	C(27)-C(29)-H(29)	119	H(51A)-C(51)-H(51C)	109.5
C(19)-N(4)-C(9)	105.15(18)	C(30)-C(29)-H(29)	119	H(51B)-C(51)-H(51C)	109.5
N(2)-C(1)-C(5)	130.2(2)	C(28)-C(30)-C(29)	116.7(2)	C(39)-C(52)-H(52A)	109.5
N(2)-C(1)-C(17)	109.9(2)	C(28)-C(30)-C(39)	122.4(2)	C(39)-C(52)-H(52B)	109.5
C(5)-C(1)-C(17)	119.3(2)	C(29)-C(30)-C(39)	120.8(2)	H(52A)-C(52)-H(52B)	109.5
N(1)-C(2)-C(5)	123.0(2)	C(20)-C(31)-C(18)	107.9(2)	C(39)-C(52)-H(52C)	109.5
N(1)-C(2)-C(7)	106.7(2)	C(20)-C(31)-H(31)	126	H(52A)-C(52)-H(52C)	109.5
C(5)-C(2)-C(7)	129.8(2)	C(18)-C(31)-H(31)	126	H(52B)-C(52)-H(52C)	109.5
C(44)-C(3)-C(40)	117.9(2)	C(36)-C(32)-C(45)	117.2(2)	C(39)-C(53)-H(53A)	109.5
C(44)-C(3)-C(10)	121.5(2)	C(36)-C(32)-C(47)	121.0(2)	C(39)-C(53)-H(53B)	109.5
C(40)-C(3)-C(10)	120.5(2)	C(45)-C(32)-C(47)	121.7(2)	H(53A)-C(53)-H(53B)	109.5
N(3)-C(4)-C(10)	126.0(2)	C(13)-C(33)-C(34)	121.2(2)	C(39)-C(53)-H(53C)	109.5
N(3)-C(4)-C(20)	106.3(2)	C(13)-C(33)-H(33)	119.4	H(53A)-C(53)-H(53C)	109.5
C(10)-C(4)-C(20)	127.6(2)	C(34)-C(33)-H(33)	119.4	H(53B)-C(53)-H(53C)	109.5
C(1)-C(5)-C(2)	122.5(2)	C(33)-C(34)-C(14)	121.6(2)	C(47)-C(54)-H(54A)	109.5
C(1)-C(5)-C(11)	115.3(2)	C(33)-C(34)-H(34)	119.2	C(47)-C(54)-H(54B)	109.5

C(2)-C(5)-C(11)	121.8(2)	C(14)-C(34)-H(34)	119.2	H(54A)-C(54)-H(54B)	109.5
C(12)-C(6)-C(9)	124.8(2)	O(2)-C(35)-C(43)	114.8(2)	C(47)-C(54)-H(54C)	109.5
C(12)-C(6)-C(13)	117.5(2)	O(2)-C(35)-C(11)	122.3(2)	H(54A)-C(54)-H(54C)	109.5
C(9)-C(6)-C(13)	117.7(2)	C(43)-C(35)-C(11)	122.9(2)	H(54B)-C(54)-H(54C)	109.5
C(16)-C(7)-C(2)	108.0(2)	C(32)-C(36)-C(40)	121.7(2)	C(60)-C(55)-C(59)	113.5(3)
C(16)-C(7)-H(7)	126	C(32)-C(36)-H(36)	119.2	C(61A)-C(55)-C(60A)	113.6(7)
C(2)-C(7)-H(7)	126	C(40)-C(36)-H(36)	119.2	C(60)-C(55)-C(46)	112.7(3)
N(2)-C(8)-C(10)	124.8(2)	C(42)-C(37)-C(13)	120.7(2)	C(61A)-C(55)-C(46)	115.5(7)
N(2)-C(8)-C(21)	111.6(2)	C(42)-C(37)-H(37)	119.6	C(59)-C(55)-C(46)	113.3(3)
C(10)-C(8)-C(21)	123.6(2)	C(13)-C(37)-H(37)	119.6	C(60A)-C(55)-C(46)	113.8(6)
N(4)-C(9)-C(6)	124.8(2)	C(48)-C(38)-C(50)	108.9(2)	C(61A)-C(55)-C(59A)	107.7(7)
N(4)-C(9)-C(24)	112.1(2)	C(48)-C(38)-C(49)	107.3(2)	C(60A)-C(55)-C(59A)	103.5(6)
C(6)-C(9)-C(24)	123.1(2)	C(50)-C(38)-C(49)	110.0(2)	C(46)-C(55)-C(59A)	100.9(6)
C(4)-C(10)-C(8)	125.7(2)	C(48)-C(38)-C(14)	111.6(2)	C(60)-C(55)-C(61)	106.8(4)
C(4)-C(10)-C(3)	117.4(2)	C(50)-C(38)-C(14)	108.53(19)	C(59)-C(55)-C(61)	104.1(3)
C(8)-C(10)-C(3)	116.9(2)	C(49)-C(38)-C(14)	110.5(2)	C(46)-C(55)-C(61)	105.5(3)
C(35)-C(11)-C(26)	114.9(2)	C(53)-C(39)-C(51)	108.8(2)	C(47)-C(56)-H(56A)	109.5
C(35)-C(11)-C(5)	120.5(2)	C(53)-C(39)-C(30)	109.9(2)	C(47)-C(56)-H(56B)	109.5
C(26)-C(11)-C(5)	124.5(2)	C(51)-C(39)-C(30)	111.9(2)	H(56A)-C(56)-H(56B)	109.5
N(1)-C(12)-C(6)	126.6(2)	C(53)-C(39)-C(52)	109.5(2)	C(47)-C(56)-H(56C)	109.5
N(1)-C(12)-C(16)	106.2(2)	C(51)-C(39)-C(52)	108.3(2)	H(56A)-C(56)-H(56C)	109.5
C(6)-C(12)-C(16)	127.2(2)	C(30)-C(39)-C(52)	108.4(2)	H(56B)-C(56)-H(56C)	109.5
C(33)-C(13)-C(37)	117.8(2)	C(36)-C(40)-C(3)	120.8(2)	C(47)-C(57)-H(57A)	109.5
C(33)-C(13)-C(6)	119.8(2)	C(36)-C(40)-H(40)	119.6	C(47)-C(57)-H(57B)	109.5
C(37)-C(13)-C(6)	122.5(2)	C(3)-C(40)-H(40)	119.6	H(57A)-C(57)-H(57B)	109.5
C(42)-C(14)-C(34)	116.7(2)	C(26)-C(41)-C(46)	121.7(2)	C(47)-C(57)-H(57C)	109.5
C(42)-C(14)-C(38)	121.4(2)	C(26)-C(41)-H(41)	119.2	H(57A)-C(57)-H(57C)	109.5
C(34)-C(14)-C(38)	121.8(2)	C(46)-C(41)-H(41)	119.2	H(57B)-C(57)-H(57C)	109.5
C(27)-C(15)-C(23)	114.8(2)	C(37)-C(42)-C(14)	122.0(2)	Cl(2)-C(58)-Cl(1)	112.2(2)
C(27)-C(15)-C(22)	124.5(2)	C(37)-C(42)-H(42)	119	Cl(2)-C(58)-H(58A)	109.2
C(23)-C(15)-C(22)	120.6(2)	C(14)-C(42)-H(42)	119	Cl(1)-C(58)-H(58A)	109.2
C(7)-C(16)-C(12)	108.6(2)	C(46)-C(43)-C(35)	120.8(2)	Cl(2)-C(58)-H(58B)	109.2
C(7)-C(16)-H(16)	125.7	C(46)-C(43)-H(43)	119.6	Cl(1)-C(58)-H(58B)	109.2
C(12)-C(16)-H(16)	125.7	C(35)-C(43)-H(43)	119.6	H(58A)-C(58)-H(58B)	107.9
C(21)-C(17)-O(2)	127.8(2)	C(3)-C(44)-C(45)	121.1(2)	C(55)-C(59)-H(59A)	109.5
C(21)-C(17)-C(1)	108.6(2)	C(3)-C(44)-H(44)	119.4	C(55)-C(59)-H(59B)	109.5
O(2)-C(17)-C(1)	123.5(2)	C(45)-C(44)-H(44)	119.4	H(59A)-C(59)-H(59B)	109.5
N(3)-C(18)-C(22)	122.2(2)	C(32)-C(45)-C(44)	121.1(2)	C(55)-C(59)-H(59C)	109.5
N(3)-C(18)-C(31)	106.5(2)	C(32)-C(45)-H(45)	119.5	H(59A)-C(59)-H(59C)	109.5
C(22)-C(18)-C(31)	131.1(2)	C(44)-C(45)-H(45)	119.5	H(59B)-C(59)-H(59C)	109.5
N(4)-C(19)-C(22)	130.6(2)	C(43)-C(46)-C(41)	117.1(2)	C(55)-C(60)-H(60A)	109.5
N(4)-C(19)-C(25)	109.9(2)	C(43)-C(46)-C(55)	122.1(2)	C(55)-C(60)-H(60B)	109.5
C(22)-C(19)-C(25)	119.2(2)	C(41)-C(46)-C(55)	120.7(2)	H(60A)-C(60)-H(60B)	109.5
C(31)-C(20)-C(4)	108.7(2)	C(57)-C(47)-C(54)	108.8(3)	C(55)-C(60)-H(60C)	109.5
C(31)-C(20)-H(20)	125.6	C(57)-C(47)-C(32)	110.5(2)	H(60A)-C(60)-H(60C)	109.5
C(4)-C(20)-H(20)	125.6	C(54)-C(47)-C(32)	109.2(2)	H(60B)-C(60)-H(60C)	109.5

C(17)-C(21)-C(8)	104.8(2)	C(57)-C(47)-C(56)	109.6(3)	C(55)-C(61)-H(61A)	109.5
C(17)-C(21)-H(21)	127.6	C(54)-C(47)-C(56)	107.7(3)	C(55)-C(61)-H(61B)	109.5
C(8)-C(21)-H(21)	127.6	C(32)-C(47)-C(56)	110.9(2)	H(61A)-C(61)-H(61B)	109.5
C(19)-C(22)-C(18)	122.2(2)	C(38)-C(48)-H(48A)	109.5	C(55)-C(61)-H(61C)	109.5
C(19)-C(22)-C(15)	115.1(2)	C(38)-C(48)-H(48B)	109.5	H(61A)-C(61)-H(61C)	109.5
C(18)-C(22)-C(15)	122.7(2)	H(48A)-C(48)-H(48B)	109.5	H(61B)-C(61)-H(61C)	109.5
O(1)-C(23)-C(28)	114.5(2)	C(38)-C(48)-H(48C)	109.5	C(55)-C(60A)-H(60D)	109.5
O(1)-C(23)-C(15)	122.3(2)	H(48A)-C(48)-H(48C)	109.5	C(55)-C(60A)-H(60E)	109.5
C(28)-C(23)-C(15)	123.1(2)	H(48B)-C(48)-H(48C)	109.5	H(60D)-C(60A)-H(60E)	109.5
C(25)-C(24)-C(9)	104.4(2)	C(38)-C(49)-H(49A)	109.5	C(55)-C(60A)-H(60F)	109.5
C(25)-C(24)-H(24)	127.8	C(38)-C(49)-H(49B)	109.5	H(60D)-C(60A)-H(60F)	109.5
C(9)-C(24)-H(24)	127.8	H(49A)-C(49)-H(49B)	109.5	H(60E)-C(60A)-H(60F)	109.5
C(24)-C(25)-O(1)	127.9(2)	C(38)-C(49)-H(49C)	109.5	C(55)-C(61A)-H(61D)	109.5
C(24)-C(25)-C(19)	108.5(2)	H(49A)-C(49)-H(49C)	109.5	C(55)-C(61A)-H(61E)	109.5
O(1)-C(25)-C(19)	123.6(2)	H(49B)-C(49)-H(49C)	109.5	H(61D)-C(61A)-H(61E)	109.5
C(41)-C(26)-C(11)	122.2(2)	C(38)-C(50)-H(50A)	109.5	C(55)-C(61A)-H(61F)	109.5
C(41)-C(26)-H(26)	118.9	C(38)-C(50)-H(50B)	109.5	H(61D)-C(61A)-H(61F)	109.5
C(55)-C(59A)-H(59F)	109.5	C(55)-C(59A)-H(59E)	109.5	H(61E)-C(61A)-H(61F)	109.5
H(59D)-C(59A)-H(59F)	109.5	H(59D)-C(59A)-H(59E)	109.5	C(55)-C(59A)-H(59D)	109.5
H(59E)-C(59A)-H(59F)	109.5				

Table 4 Anisotropic displacement parameters (A^2 × 10^2) for **3-36**. The anisotropic displacement factor exponent takes the form: –2 pi2 [h^2a*^2 U11 + ... + 2 h k a* b*U12]

Atom	U11	U22	U33	U23	U13	U12
Cl(1)	53(1)	52(1)	51(1)	6(1)	11(1)	5(1)
Cl(2)	59(1)	138(1)	63(1)	14(1)	24(1)	1(1)
O(1)	44(1)	15(1)	15(1)	4(1)	2(1)	1(1)
O(2)	36(1)	17(1)	16(1)	2(1)	7(1)	-2(1)
N(1)	23(1)	16(1)	12(1)	4(1)	3(1)	2(1)
N(2)	23(1)	17(1)	15(1)	5(1)	6(1)	5(1)
N(3)	24(1)	17(1)	14(1)	5(1)	7(1)	3(1)
N(4)	22(1)	16(1)	14(1)	4(1)	3(1)	2(1)
C(1)	16(1)	18(1)	18(1)	4(1)	4(1)	4(1)
C(2)	20(1)	16(1)	17(1)	5(1)	8(1)	4(1)
C(3)	22(1)	17(1)	16(1)	5(1)	7(1)	3(1)
C(4)	23(1)	21(1)	15(1)	6(1)	6(1)	7(1)
C(5)	18(1)	17(1)	17(1)	4(1)	5(1)	4(1)
C(6)	20(1)	20(1)	14(1)	3(1)	4(1)	5(1)
C(7)	23(1)	19(1)	19(1)	8(1)	7(1)	5(1)
C(8)	21(1)	19(1)	16(1)	5(1)	5(1)	7(1)
C(9)	21(1)	19(1)	14(1)	4(1)	4(1)	4(1)
C(10)	22(1)	21(1)	14(1)	5(1)	4(1)	8(1)
C(11)	19(1)	17(1)	19(1)	4(1)	5(1)	4(1)

C(12)	20(1)	20(1)	14(1)	6(1)	5(1)	5(1)
C(13)	24(1)	18(1)	15(1)	5(1)	4(1)	5(1)
C(14)	23(1)	17(1)	13(1)	6(1)	3(1)	4(1)
C(15)	22(1)	18(1)	18(1)	6(1)	4(1)	3(1)
C(16)	25(1)	21(1)	14(1)	6(1)	6(1)	5(1)
C(17)	23(1)	18(1)	15(1)	1(1)	2(1)	3(1)
C(18)	22(1)	18(1)	17(1)	6(1)	4(1)	3(1)
C(19)	20(1)	16(1)	15(1)	2(1)	2(1)	3(1)
C(20)	28(1)	23(1)	18(1)	7(1)	10(1)	3(1)
C(21)	25(1)	18(1)	16(1)	1(1)	3(1)	3(1)
C(22)	22(1)	17(1)	17(1)	5(1)	2(1)	2(1)
C(23)	27(1)	19(1)	17(1)	7(1)	4(1)	2(1)
C(24)	29(1)	20(1)	14(1)	3(1)	2(1)	3(1)
C(25)	26(1)	17(1)	16(1)	2(1)	3(1)	3(1)
C(26)	23(1)	20(1)	21(1)	3(1)	5(1)	4(1)
C(27)	30(1)	19(1)	18(1)	4(1)	4(1)	2(1)
C(28)	29(1)	19(1)	18(1)	3(1)	5(1)	2(1)
C(29)	30(1)	23(1)	23(1)	11(1)	5(1)	4(1)
C(30)	25(1)	17(1)	25(1)	7(1)	9(1)	5(1)
C(31)	28(1)	22(1)	22(1)	8(1)	9(1)	3(1)
C(32)	29(1)	21(1)	15(1)	3(1)	8(1)	1(1)
C(33)	23(1)	31(1)	18(1)	7(1)	9(1)	3(1)
C(34)	19(1)	33(1)	18(1)	6(1)	3(1)	4(1)
C(35)	25(1)	22(1)	17(1)	5(1)	5(1)	1(1)
C(36)	35(2)	29(1)	20(1)	4(1)	9(1)	15(1)
C(37)	19(1)	42(2)	17(1)	4(1)	2(1)	3(1)
C(38)	23(1)	23(1)	13(1)	5(1)	2(1)	4(1)
C(39)	29(1)	18(1)	28(1)	9(1)	10(1)	5(1)
C(40)	30(1)	32(1)	16(1)	7(1)	5(1)	13(1)
C(41)	25(1)	22(1)	29(1)	8(1)	12(1)	3(1)
C(42)	19(1)	43(2)	17(1)	6(1)	7(1)	4(1)
C(43)	36(2)	19(1)	23(1)	-2(1)	7(1)	0(1)
C(44)	26(1)	33(1)	18(1)	8(1)	7(1)	12(1)
C(45)	32(2)	37(2)	18(1)	11(1)	5(1)	10(1)
C(46)	32(2)	20(1)	29(1)	4(1)	9(1)	-1(1)
C(47)	45(2)	27(1)	15(1)	3(1)	10(1)	5(1)
C(48)	26(1)	39(2)	19(1)	7(1)	-1(1)	-3(1)
C(49)	32(2)	36(2)	16(1)	6(1)	6(1)	12(1)
C(50)	39(2)	27(1)	20(1)	9(1)	-1(1)	6(1)
C(51)	52(2)	18(1)	32(2)	4(1)	10(1)	5(1)
C(52)	39(2)	25(1)	52(2)	18(1)	20(2)	8(1)
C(53)	39(2)	23(1)	43(2)	11(1)	9(1)	11(1)
C(54)	42(2)	53(2)	25(2)	6(1)	17(1)	7(1)
C(55)	66(2)	18(1)	47(2)	-2(1)	30(2)	-11(1)
C(56)	44(2)	78(3)	16(1)	0(2)	5(1)	-9(2)
C(57)	162(5)	34(2)	29(2)	4(1)	37(2)	34(2)

C(58)	51(2)	87(3)	56(2)	-1(2)	13(2)	0(2)
C(59)	73(3)	19(2)	58(3)	-7(2)	29(3)	-8(2)
C(60)	59(3)	27(2)	102(4)	-8(2)	49(3)	-15(2)
C(61)	81(3)	26(2)	61(3)	14(2)	19(3)	7(2)
C(60A)	70(9)	26(7)	65(9)	5(7)	21(8)	-8(7)
C(61A)	81(9)	36(7)	58(9)	12(7)	27(8)	-3(7)
C(59A)	86(9)	26(7)	78(9)	5(7)	16(8)	-24(7)

AICD calculations

AICD plots of neutral and dication species of O-annulated porphyrins. Aromatic clockwise current density – blue arrow, antiaromatic counter clockwise current density – red arrow.

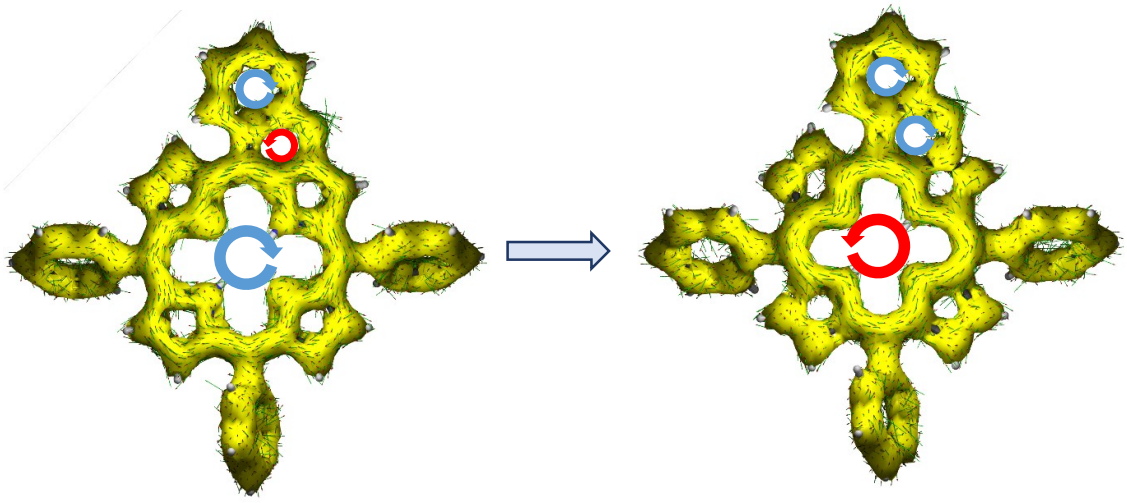

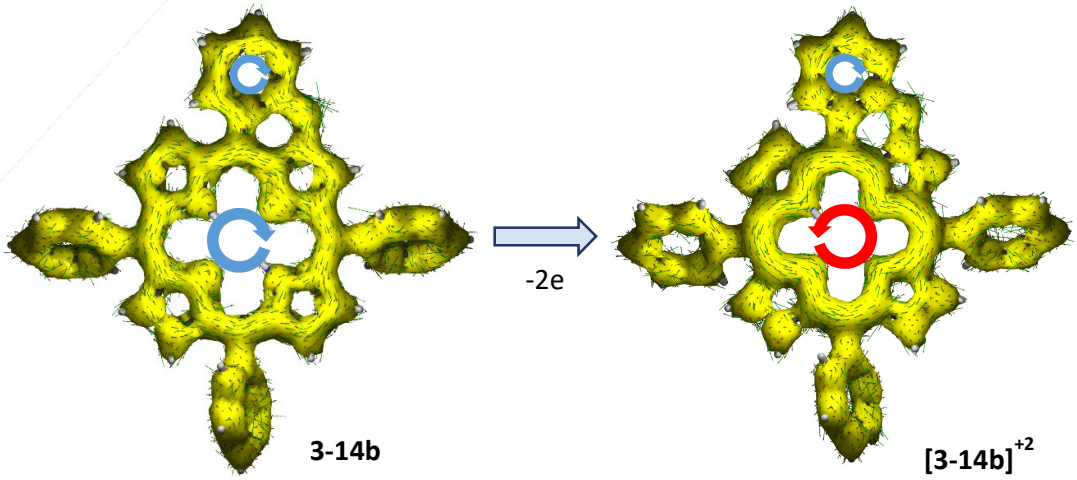

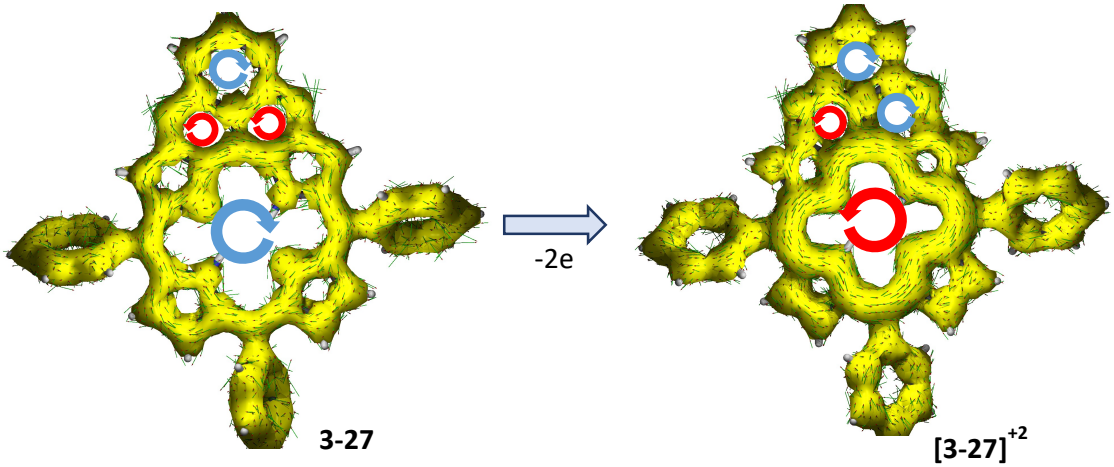

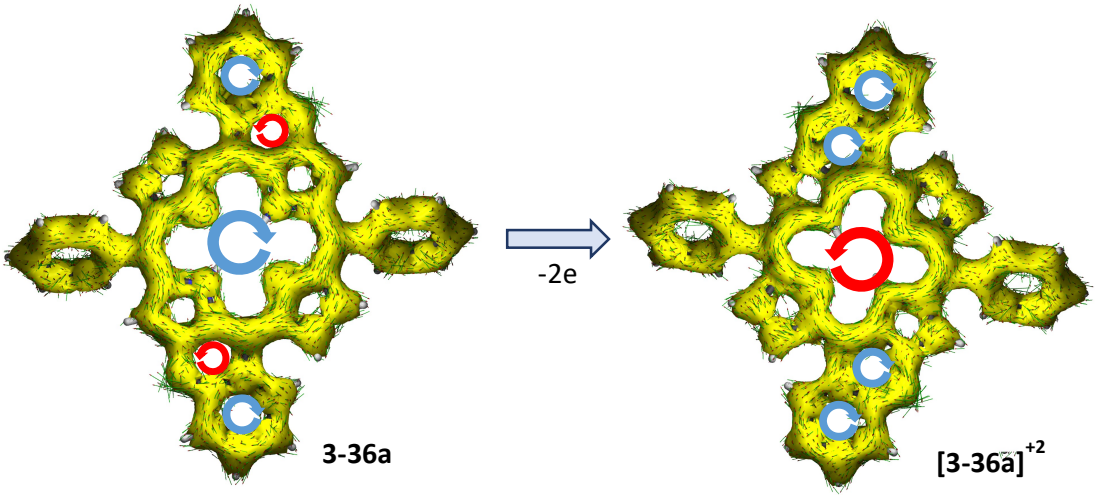
-2e
3-36a
[3-36a]+2

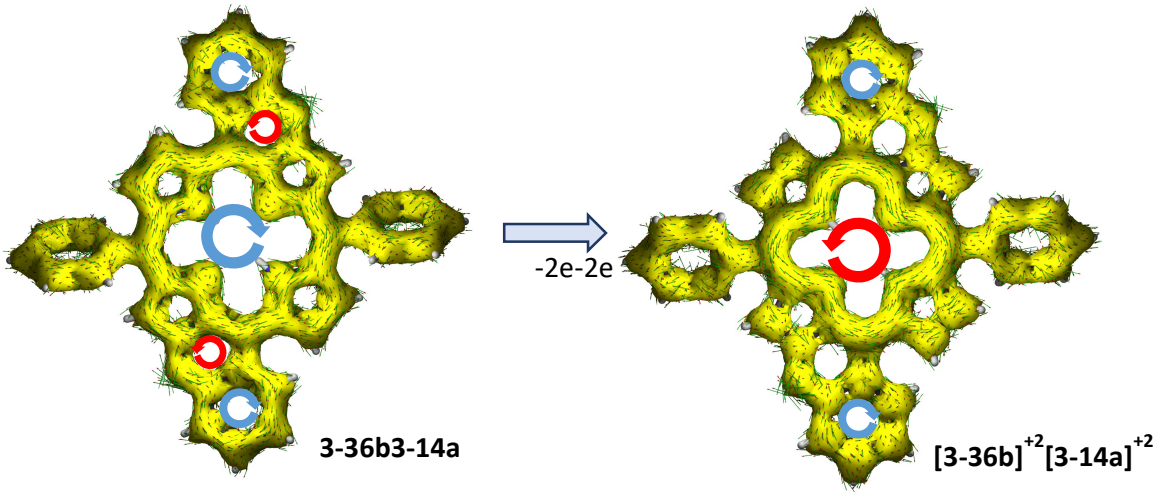
-2e-2e
3-36b3-14a
[3-36b]+2[3-14a]+2

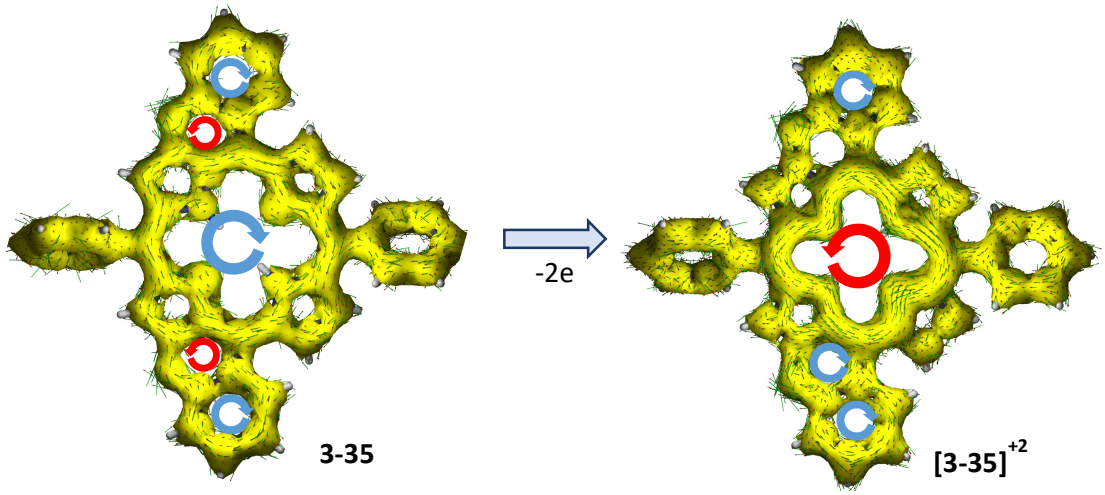
-2e
3-35
[3-35]+2

Bibliography

[1] Y. Karzazi, *J. Mater. Environ. Sci.* **2014**, *5*, 1–12.

[2] H. Sasabe, J. Kido, *Chem. Mater.* **2011**, *23*, 621–630.

[3] C. Zhong, C. Duan, F. Huang, H. Wu, Y. Cao, *Chem. Mater.* **2011**, *23*, 326–340.

[4] C. R. Newman, C. D. Frisbie, D. A. da Silva Filho, J.-L. Brédas, P. C. Ewbank, K. R. Mann, *Chem. Mater.* **2004**, *16*, 4436–4451.

[5] O. Ostroverkhova, *Chem. Rev.* **2016**, *116*, 13279–13412.

[6] A. Facchetti, *Chem. Mater.* **2011**, *23*, 733–758.

[7] C. Wang, H. Dong, W. Hu, Y. Liu, D. Zhu, *Chem. Rev.* **2012**, *112*, 2208–2267.

[8] Y. Kobuke, K. Ogawa, *Bull. Chem. Soc. Jpn.* **2003**, *76*, 689–708.

[9] T. S. Balaban, *Acc. Chem. Res.* **2005**, *38*, 612–623.

[10] D. Gust, T. A. Moore, A. L. Moore, *Acc. Chem. Res.* **2001**, *34*, 40–48.

[11] L. J. Hoard, K. M. Smith, *Porphyrins and Metalloporphyrins*, Elsevier, Amsterdam, **1975**.

[12] T. L. Poulos, *Chem. Rev.* **2014**, *114*, 3919–3962.

[13] D. Dolphin, *The Porphyrins V7: Biochemistry*, Elsevier Science, **2012**.

[14] E. M. Beems, T. M. A. R. Dubbelman, J. Lugtenburg, J. A. van Best, M. F. M. A. Smeets, J. P. J. Boegheim, *Photochem. Photobiol.* **1987**, *46*, 639–643.

[15] K. Sauer, *Annu. Rev. Phys. Chem.* **1979**, *30*, 155–178.

[16] L. R. Milgrom, M. J. Warren, *The Colours of Life: An Introduction to the Chemistry of Porphyrins and Related Compounds*, Oxford University Press New York, **1997**.

[17] G. Färber, W. Keller, C. Kratky, B. Jaun, A. Pfaltz, C. Spinner, A. Kobelt, A. Eschenmoser, *Helv. Chim. Acta* **1991**, *74*, 697–716.

[18] E. C. Duin, M. L. McKee, *J. Phys. Chem. B* **2008**, *112*, 2466–2482.

[19] E. Vogel, *J. Heterocycl. Chem.* **1996**, *33*, 1461–1487.

[20] E. Vogel, W. Pretzer, W. A. Böll, *Tetrahedron Lett.* **1965**, *6*, 3613–3617.

[21] F. Sondheimer, R. Wolovsky, Y. Amiel, *J. Am. Chem. Soc.* **1962**, *84*, 274–284.

[22] T. D. Lash, *J. Porphyr. Phthalocyanines* **2011**, *15*, 1093–1115.

[23] H. Fischer, H. Orth, *Die Chemie Des Pyrrols, Vol. II/2*, Akadem. Verlagsgesellschaft, Leipzig, **1940**.

[24] G. P. Moss, *Pure Appl. Chem.* **1987**, *59*, 779–832.

[25] P. Rothbmund, *J. Am. Chem. Soc.* **1935**, *57*, 2010–2011.

[26] P. Rothemund, *J. Am. Chem. Soc.* **1939**, *61*, 2912–2915.

[27] P. Rothemund, A. R. Menotti, *J. Am. Chem. Soc.* **1941**, *63*, 267–270.

[28] A. D. Adler, F. R. Longo, W. Shergalis, *J. Am. Chem. Soc.* **1964**, *86*, 3145–3149.

[29] A. D. Adler, F. R. Longo, J. D. Finarelli, J. Goldmacher, J. Assour, L. Korsakoff, *J. Org. Chem.* **1967**, *32*, 476–476.

[30] D. Dolphin, *J. Heterocycl. Chem.* **1970**, *7*, 275–283.

[31] J. S. Lindsey, H. C. Hsu, I. C. Schreiman, *Tetrahedron Lett.* **1986**, *27*, 4969–4970.

[32] J. S. Lindsey, I. C. Schreiman, H. C. Hsu, P. C. Kearney, A. M. Marguerettaz, *J. Org. Chem.* **1987**, *52*, 827–836.

[33] J. S. Lindsey, *Acc. Chem. Res.* **2010**, *43*, 300–311.

[34] G. P. Arsenault, E. Bullock, S. F. MacDonald, *J. Am. Chem. Soc.* **1960**, *82*, 4384–4389.

[35] J. L. Sessler, M. R. Johnson, V. Lynch, *J. Org. Chem.* **1987**, *52*, 4394–4397.

[36] N. Kobayashi, *J. Porphyr. Phthalocyanines* **2000**, *04*, 377–379.

[37] Y. Rio, M. Salomé Rodríguez-Morgade, T. Torres, *Org. Biomol. Chem.* **2008**, *6*, 1877.

[38] T. Hashimoto, Y. Choe, H. Nakano, K. Hirao, *J. Phys. Chem. A* **1999**, *103*, 1894–1904.

[39] C. Weiss, H. Kobayashi, M. Gouterman, *J. Mol. Spectrosc.* **1965**, *16*, 415–450.

[40] L. Bajema, M. Gouterman, B. Meyer, *J. Mol. Spectrosc.* **1968**, *27*, 225–235.

[41] K. B. Fields, J. V Ruppel, N. L. Snyder, X. P. Zhang, in *Handbook of Porphyrin Science*, World Scientific Publishing Company, **2010**, pp. 367–427.

[42] T. Akasaka, A. Osuka, S. Fukuzumi, H. Kandori, Y. Aso, *Chemical Science of π-Electron Systems*, Springer Japan, **2015**.

[43] S. Hiroto, Y. Miyake, H. Shinokubo, *Chem. Rev.* **2017**, *117*, 2910–3043.

[44] V. I. V. Serra, S. M. G. Pires, C. M. A. Alonso, M. G. P. M. S. Neves, A. C. Tomé, J. A. S. Cavaleiro, in *Top. Heterocycl. Chem.*, **2013**, pp. 35–78.

[45] Q. Chen, Y.-Z. Zhu, Q.-J. Fan, S.-C. Zhang, J.-Y. Zheng, *Org. Lett.* **2014**, *16*, 1590–1593.

[46] Y. Zhu, R. B. Silverman, *J. Org. Chem.* **2007**, *72*, 233–239.

[47] D. Shimizu, J. Oh, K. Furukawa, D. Kim, A. Osuka, *J. Am. Chem. Soc.* **2015**, *137*, 15584–15594.

[48] D. Shimizu, A. Osuka, *Chem. Sci.* **2018**, *9*, 1408–1423.

[49] T. Higashino, H. Imahori, *Dalton Trans.* **2015**, *44*, 448–463.

[50] H. Song, Q. Liu, Y. Xie, *Chem. Commun.* **2018**, *54*, 1811–1824.

[51] Y. Matano, K. Matsumoto, Y. Nakao, H. Uno, S. Sakaki, H. Imahori, *J. Am. Chem. Soc.* **2008**, *130*, 4588–4589.

[52] Y. Matano, K. Matsumoto, Y. Terasaka, H. Hotta, Y. Araki, O. Ito, M. Shiro, T. Sasamori, N. Tokitoh, H. Imahori, *Chem. Eur. J.* **2007**, *13*, 891–901.

[53] Y. Matano, K. Matsumoto, T. Shibano, H. Imahori, *J. Porphyr. Phthalocyanines* **2011**, *15*, 1172–1182.

[54] Y. Matano, K. Matsumoto, H. Hayashi, Y. Nakao, T. Kumpulainen, V. Chukharev, N. V Tkachenko, H. Lemmetyinen, S. Shimizu, N. Kobayashi, et al., *J. Am. Chem. Soc.* **2012**, *134*, 1825–1839.

[55] Y. Matano, T. Shinokura, K. Matsumoto, H. Imahori, H. Nakano, *Chem. – An Asian J.* **2007**, *2*, 1417–1429.

[56] K. Fujimoto, T. Yoneda, H. Yorimitsu, A. Osuka, *Angew. Chem. Int. Ed.* **2014**, *53*, 1127–1130.

[57] W. M. Campbell, K. W. Jolley, P. Wagner, K. Wagner, P. J. Walsh, K. C. Gordon, L. Schmidt-Mende, M. K. Nazeeruddin, Q. Wang, M. Grätzel, et al., *J. Phys. Chem. C* **2007**, *111*, 11760–11762.

[58] W. M. Campbell, A. K. Burrell, D. L. Officer, K. W. Jolley, *Coord. Chem. Rev.* **2004**, *248*, 1363–1379.

[59] G. C. Ferreira, *Handbook Of Porphyrin Science: With Applications To Chemistry, Physics, Materials Science, Engineering, Biology And Medicine*, World Scientific Publishing Company, **2013**.

[60] C.-W. Lee, H.-P. Lu, C.-M. Lan, Y.-L. Huang, Y.-R. Liang, W.-N. Yen, Y.-C. Liu, Y.-S. Lin, E. W.-G. Diau, C.-Y. Yeh, *Chem. Eur. J.* **2009**, *15*, 1403–1412.

[61] H.-P. Lu, C.-Y. Tsai, W.-N. Yen, C.-P. Hsieh, C.-W. Lee, C.-Y. Yeh, E. W.-G. Diau, *J. Phys. Chem. C* **2009**, *113*, 20990–20997.

[62] T. Bessho, S. M. Zakeeruddin, C.-Y. Yeh, E. W.-G. Diau, M. Grätzel, *Angew. Chem. Int. Ed.* **2010**, *49*, 6646–6649.

[63] L. Han, A. Islam, H. Chen, C. Malapaka, B. Chiranjeevi, S. Zhang, X. Yang, M. Yanagida, *Energy Environ. Sci.* **2012**, *5*, 6057.

[64] C.-Y. Chen, M. Wang, J.-Y. Li, N. Pootrakulchote, L. Alibabaei, C. Ngoc-le, J.-D. Decoppet, J.-H. Tsai, C. Grätzel, C.-G. Wu, et al., *ACS Nano* **2009**, *3*, 3103–3109.

[65] M. Grzybowski, K. Skonieczny, H. Butenschön, D. T. Gryko, *Angew. Chem. Int. Ed.* **2013**, *52*, 9900–9930.

[66] J. P. Lewtak, D. T. Gryko, *Chem. Commun.* **2012**, *48*, 10069.

[67] S. Fox, R. W. Boyle, *Tetrahedron* **2006**, *62*, 10039–10054.

[68] A. M. V. M. Pereira, S. Richeter, C. Jeandon, J.-P. Gisselbrecht, J. Wytko, R. Ruppert, *J. Porphyr. Phthalocyanines* **2012**, *16*, 464–478.

[69] T. Tanaka, A. Osuka, *Chem. Soc. Rev.* **2015**, *44*, 943–969.

[70] H. Mori, T. Tanaka, A. Osuka, *J. Mater. Chem. C* **2013**, *1*, 2500–2519.

[71] T. Okujima, J. Mack, J. Nakamura, G. Kubheka, T. Nyokong, H. Zhu, N. Komobuchi, N. Ono, H. Yamada, H. Uno, et al., *Chem. Eur. J.* **2016**, *22*, 14730–14738.

[72] N. Ono, H. Yamada, T. Okujima, in *Handbook of Porphyrin Science*, World Scientific Publishing Company, **2010**, pp. 1–102.

[73] L. Edwards, M. Gouterman, C. B. Rose, *J. Am. Chem. Soc.* **1976**, *98*, 7638–7641.

[74] T. D. Lash, J. J. Catarello, *Tetrahedron* **1993**, *49*, 4159–4172.

[75] T. D. Lash, P. Chandrasekar, *J. Am. Chem. Soc.* **1996**, *118*, 8767–8768.

[76] N. Ono, H. Hironaga, K. Ono, S. Kaneko, T. Murashima, T. Ueda, C. Tsukamura, T. Ogawa, *J. Chem. Soc. Perkin Trans. 1* **1996**, 417.

[77] T. Murashima, K. Fujita, K. Ono, T. Ogawa, H. Uno, N. Ono, *J. Chem. Soc. Perkin Trans. 1* **1996**, 1403.

[78] D. H. R. Barton, S. Z. Zard, *J. Chem. Soc. Chem. Commun.* **1985**, 1098.

[79] D. H.R. Barton, J. Kervagoret, S. Z. Zard, *Tetrahedron* **1990**, *46*, 7587–7598.

[80] J. D. Spence, T. D. Lash, *J. Org. Chem.* **2000**, *65*, 1530–1539.

[81] O. S. Finikova, A. V Cheprakov, I. P. Beletskaya, P. J. Carroll, S. A. Vinogradov, *J. Org. Chem.* **2004**, *69*, 522–535.

[82] O. Finikova, A. Cheprakov, I. Beletskaya, S. Vinogradov, *Chem. Commun.* **2001**, *26*, 261–262.

[83] O. S. Finikova, A. V Cheprakov, P. J. Carroll, S. A. Vinogradov, *J. Org. Chem.* **2003**, *68*, 7517–7520.

[84] O. S. Finikova, S. E. Aleshchenkov, R. P. Briñas, A. V Cheprakov, P. J. Carroll, S. A. Vinogradov, *J. Org. Chem.* **2005**, *70*, 4617–4628.

[85] V. Yakutkin, S. Aleshchenkov, S. Chernov, T. Miteva, G. Nelles, A. Cheprakov, S. Baluschev, *Chem. Eur. J.* **2008**, *14*, 9846–9850.

[86] A. V. Cheprakov, M. A. Filatov, *J. Porphyr. Phthalocyanines* **2009**, *13*, 291–303.

[87] O. S. Finikova, A. V. Cheprakov, S. A. Vinogradov, *J. Org. Chem.* **2005**, *70*, 9562–9572.

[88] S. Kotha, S. Banerjee, *RSC Adv.* **2013**, *3*, 7642.

[89] S. Ito, T. Murashima, N. Ono, H. Uno, *Chem. Commun.* **1998**, 1661–1662.

[90] S. Ito, N. Ochi, T. Murashima, N. Ono, H. Uno, *Chem. Commun.* **2000**, 893–894.

[91] H. Yamada, D. Kuzuhara, T. Takahashi, Y. Shimizu, K. Uota, T. Okujima, H. Uno, N. Ono, *Org. Lett.* **2008**, *10*, 2947–2950.

[92] T. D. Lush, in *The Porphyrin Handbook Vol. 2*, Academic Press, New York, **2000**, p. 152.

[93] H. S. Gill, M. Harmjanz, J. Santamaría, I. Finger, M. J. Scott, *Angew. Chem. Int. Ed.* **2004**, *43*, 485–490.

[94] C. Jiao, L. Zhu, J. Wu, *Chem. Eur. J.* **2011**, *17*, 6610–6614.

[95] K. Kurotobi, K. S. Kim, S. B. Noh, D. Kim, A. Osuka, *Angew. Chem. Int. Ed.* **2006**, *45*, 3944–3947.

[96] N. K. S. Davis, A. L. Thompson, H. L. Anderson, *Org. Lett.* **2010**, *12*, 2124–2127.

[97] N. K. S. Davis, A. L. Thompson, H. L. Anderson, *J. Am. Chem. Soc.* **2011**, *133*, 30–31.

[98] N. K. S. Davis, M. Pawlicki, H. L. Anderson, *Org. Lett.* **2008**, *10*, 3945–3947.

[99] K. Sugiura, T. Matsumoto, S. Ohkouchi, Y. Naitoh, T. Kawai, Y. Takai, K. Ushiroda, Y. Sakata, *Chem. Commun.* **1999**, 1957–1958.

[100] A. Tsuda, H. Furuta, A. Osuka, *Angew. Chem. Int. Ed.* **2000**, *39*, 2549–2552.

[101] A. Tsuda, *Science* **2001**, *293*, 79–82.

[102] T. Tanaka, B. S. Lee, N. Aratani, M.-C. Yoon, D. Kim, A. Osuka, *Chem. Eur. J.* **2011**, *17*, 14400–14412.

[103] D. Kim, A. Osuka, *Acc. Chem. Res.* **2004**, *37*, 735–745.

[104] N. Aratani, A. Osuka, *Bull. Chem. Soc. Jpn.* **2001**, *74*, 1361–1379.

[105] T. Ikeda, N. Aratani, A. Osuka, *Chem. Asian J.* **2009**, *4*, 1248–1256.

[106] O. Fenwick, J. K. Sprafke, J. Binas, D. V. Kondratuk, F. Di Stasio, H. L. Anderson, F. Cacialli, *Nano Lett.* **2011**, *11*, 2451–2456.

[107] M. P. Balanay, D. H. Kim, *Curr. Appl. Phys.* **2011**, *11*, 109–116.

[108] S. Fox, R. W. Boyle, *Chem. Commun.* **2004**, *44*, 1322.

[109] D.-M. Shen, C. Liu, Q.-Y. Chen, *J. Org. Chem.* **2006**, *71*, 6508–11.

[110] D.-M. Shen, C. Liu, Q.-Y. Chen, *Chem. Commun.* **2005**, 4982.

[111] Y. Mitsushige, S. Yamaguchi, B. S. Lee, Y. M. Sung, S. Kuhri, C. A. Schierl, D. M. Guldi, D. Kim, Y. Matsuo, *J. Am. Chem. Soc.* **2012**, *134*, 16540–16543.

[112] R. G. Bergman, *Acc. Chem. Res.* **1973**, *6*, 25–31.

[113] H. Aihara, L. Jaquinod, D. J. Nurco, K. M. Smith, *Angew. Chem. Int. Ed.* **2001**, *40*, 3439–3441.

[114] M. Nath, J. C. Huffman, J. M. Zaleski, *Chem. Commun.* **2003**, 858–859.

[115] M. Nath, J. C. Huffman, J. M. Zaleski, *J. Am. Chem. Soc.* **2003**, *125*, 11484–11485.

[116] M. Nath, M. Pink, J. M. Zaleski, *J. Am. Chem. Soc.* **2005**, *127*, 478–479.

[117] A. Osuka, N. Fukui, K. Fujimoto, H. Yorimitsu, *Dalton Trans.* **2017**, DOI 10.1039/C7DT02815F.

[118] K. Jayaraj, A. Gold, L. M. Ball, P. S. White, *Inorg. Chem.* **2000**, *39*, 3652–3664.

[119] N. Fukui, W.-Y. Cha, S. Lee, S. Tokuji, D. Kim, H. Yorimitsu, A. Osuka, *Angew. Chem. Int. Ed.* **2013**, *52*, 9728–9732.

[120] A. Nowak-Król, D. T. Gryko, *Org. Lett.* **2013**, *15*, 5618–5621.

[121] M. Pawlicki, K. Hurej, K. Kwiecińska, L. Szterenberg, L. Latos-Grażyński, *Chem. Commun.* **2015**, *51*, 11362–11365.

[122] N. Fukui, H. Yorimitsu, A. Osuka, *Angew. Chem. Int. Ed.* **2015**, *54*, 6311–6314.

[123] N. Fukui, W. Cha, D. Shimizu, J. Oh, K. Furukawa, H. Yorimitsu, D. Kim, A. Osuka, *Chem. Sci.* **2017**, *8*, 189–199.

[124] K. Fujimoto, A. Osuka, *Chem. Sci.* **2017**, *8*, 8231–8239.

[125] K. Fujimoto, Y. Kasuga, N. Fukui, A. Osuka, *Chem. Eur. J.* **2017**, *23*, 6741–6745.

[126] K. Kato, J. O. Kim, H. Yorimitsu, D. Kim, A. Osuka, *Chem. Asian J.* **2016**, *11*, 1738–1746.

[127] C. Dou, S. Saito, K. Matsuo, I. Hisaki, S. Yamaguchi, *Angew. Chem. Int. Ed.* **2012**, *51*, 12206–12210.

[128] S. Saito, K. Matsuo, S. Yamaguchi, *J. Am. Chem. Soc.* **2012**, *134*, 9130–9133.

[129] Z. Zhou, A. Wakamiya, T. Kushida, S. Yamaguchi, *J. Am. Chem. Soc.* **2012**, *134*, 4529–4532.

[130] K. Fujimoto, J. Oh, H. Yorimitsu, D. Kim, A. Osuka, *Angew. Chem. Int. Ed.* **2016**, *55*, 3196–3199.

[131] S. Richeter, C. Jeandon, J.-P. Gisselbrecht, R. Graff, R. Ruppert, H. J. Callot, *Inorg. Chem.* **2004**, *43*, 251–263.

[132] D.-M. Shen, C. Liu, Q.-Y. Chen, *Eur. J. Org. Chem.* **2007**, *2007*, 1419–1422.

[133] A. M. V. M. Pereira, C. M. A. Alonso, M. G. P. M. S. Neves, A. C. Tomé, A. M. S. Silva, F. A. A. Paz, J. A. S. Cavaleiro, *J. Org. Chem.* **2008**, *73*, 7353–7356.

[134] A. M. V. M. Pereira, M. G. P. M. . Neves, J. A. S. Cavaleiro, J.-P. Gisselbrecht, C. Jeandon, R. Ruppert, *J. Porphyr. Phthalocyanines* **2011**, *15*, 575–582.

[135] M. Chevrier, S. Richeter, O. Coulembier, M. Surin, A. Mehdi, R. Lazzaroni, R. C. Evans, P. Dubois, S. Clément, *Chem. Commun.* **2016**, *52*, 171–174.

[136] A. J. Jimenez, N. S. Mesa, A. M. V. M. Pereira, M. Jean, B. Vincent, C. Jeandon, J.-P. Gisselbrecht, R. Ruppert, *Asian J. Org. Chem.* **2015**, *4*, 1294–1300.

[137] A. J. Jimenez, C. Jeandon, J.-P. Gisselbrecht, R. Ruppert, *Eur. J. Org. Chem.* **2009**, 5725–5730.

[138] C. Jeandon, R. Ruppert, *Eur. J. Org. Chem.* **2011**, *2011*, 4098–4102.

[139] J. Akhigbe, M. Zeller, C. Brückner, *Org. Lett.* **2011**, *13*, 1322–1325.

[140] J. Akhigbe, M. Luciano, M. Zeller, C. Brückner, *J. Org. Chem.* **2015**, *80*, 499–511.

[141] Y. Cao, A. F. Gill, D. W. Dixon, *Tetrahedron Lett.* **2009**, *50*, 4358–4360.

[142] S. Tokuji, J.-Y. Shin, K. S. Kim, J. M. Lim, K. Youfu, S. Saito, D. Kim, A. Osuka, *J. Am. Chem. Soc.* **2009**, *131*, 7240–7241.

[143] M. A. Hyland, M. D. Morton, C. Brückner, *J. Org. Chem.* **2012**, *77*, 3038–3048.

[144] M. A. Hyland, N. Hewage, K. Panther, A. Nimthong-Roldán, M. Zeller, M. Samaraweera, J. A. Gascon, C. Brückner, *J. Org. Chem.* **2016**, *81*, 3603–3618.

[145] N. Hewage, M. Zeller, C. Brückner, *Org. Biomol. Chem.* **2017**, *15*, 396–407.

[146] M. J. Crossley, P. L. Burn, *J. Chem. Soc. Chem. Commun.* **1987**, 39.

[147] M. J. Crossley, P. L. Burn, *J. Chem. Soc. Chem. Commun.* **1991**, *8*, 1569.

[148] M. J. Crossley, L. J. Govenlock, J. K. Prashar, *J. Chem. Soc. Chem. Commun.* **1995**, *39*, 2379.

[149] K. M. Kadish, K. M. Smith, R. Guilard, *The Porphyrin Handbook: Applications: Past, Present, and Future*, Academic Press, **1999**.

[150] K. E. Torraca, X. Huang, C. A. Parrish, S. L. Buchwald, *J. Am. Chem. Soc.* **2001**, *123*, 10770–10771.

[151] G. Chen, A. S. C. Chan, F. Y. Kwong, *Tetrahedron Lett.* **2007**, *48*, 473–476.

[152] A. B. Naidu, O. R. Raghunath, D. J. C. Prasad, G. Sekar, *Tetrahedron Lett.* **2008**, *49*, 1057–1061.

[153] E. Buck, Z. J. Song, D. Tschaen, P. G. Dormer, R. P. Volante, P. J. Reider, *Org. Lett.* **2002**, *4*, 1623–1626.

[154] R. Frlan, D. Kikelj, *Synthesis (Stuttg).* **2006**, *2006*, 2271–2285.

[155] B. Liu, B.-F. Shi, *Tetrahedron Lett.* **2015**, *56*, 15–22.

[156] R. Pummerer, E. Prell, A. Rieche, *Berichte der Dtsch. Chem. Gesellschaft (A B Ser.* **1926**, *59*, 2159–2161.

[157] D. Stassen, N. Demitri, D. Bonifazi, *Angew. Chem. Int. Ed.* **2016**, *55*, 5947–5951.

[158] A. Faldt, F. C. Krebs, N. Thorup, *J. Chem. Soc. Perkin Trans. 2* **1997**, 2219–2228.

[159] M. Iwata, S. Emoto, *Bull. Chem. Soc. Jpn.* **1974**, *47*, 1687–1692.

[160] J. Zhao, Y. Wang, Y. He, L. Liu, Q. Zhu, *Org. Lett.* **2012**, *14*, 1078–1081.

[161] J. Zhao, Q. Zhang, L. Liu, Y. He, J. Li, J. Li, Q. Zhu, *Org. Lett.* **2012**, *14*, 5362–5365.

[162] B. Bollweg, L. Zeh, E. Kramer, *Patent No. 545212*, **1932**.

[163] B. J. Brennan, M. J. Kenney, P. Liddell, B. R. Cherry, J. Li, A. L. Moore, T. Moore, D. Gust, *Chem. Commun.* **2011**, *47*, 10034.

[164] M. O. Senge, W. W. Kalisch, I. Bischoff, *Chem. Eur. J.* **2000**, *6*, 2721–2738.

[165] D. Dolphin, *The Porphyrins V3 Physical Chemistry, Part A*, **1978**.

[166] K. M. Kadish, K. M. Smith, R. Guilard, *The Porphyrin Handbook: Electron Transfer*, Academic Press, **2000**.

[167] K. M. Kadish, E. Van Caemelbecke, in *Encycl. Electrochem.*, Wiley-VCH Verlag GmbH & Co. KGaA, Weinheim, Germany, **2007**.

[168] K. M. Kadish, M. Lin, E. Van Caemelbecke, G. De Stefano, C. J. Medforth, D. J. Nurco, N. Y. Nelson, B. Krattinger, C. M. Muzzi, L. Jaquinod, et al., *Inorg. Chem.* **2002**, *41*, 6673–6687.

[169] G. R. Seely, D. Gust, T. A. Moore, A. L. Moore, *J. Phys. Chem.* **1994**, *98*, 10659–10664.

[170] L. A. Truxillo, D. G. Davis, *Anal. Chem.* **1975**, *47*, 2260–2267.

[171] A. D. Becke, *J. Chem. Phys.* **1993**, *98*, 5648–5652.

[172] J. Aihara, Y. Nakagami, R. Sekine, M. Makino, *J. Phys. Chem. A* **2012**, *116*, 11718–11730.

[173] M. K. Cyrañski, T. M. Krygowski, M. Wisiorowski, N. J. R. Eikema Hommes, P. R. Schleyer, *Angew. Chem. Int. Ed.* **1998**, *37*, 177–180.

[174] J. I. Wu, I. Fernández, P. R. Schleyer, *J. Am. Chem. Soc.* **2013**, *135*, 315–321.

[175] P. R. Schleyer, C. Maerker, A. Dransfeld, H. Jiao, N. J. R. Eikema Hommes, *J. Am. Chem. Soc.* **1996**, *118*, 6317–6318.

[176] Z. Chen, C. S. Wannere, C. Corminboeuf, R. Puchta, P. R. Schleyer, *Chem. Rev.* **2005**, *105*, 3842–3888.

[177] A. Stanger, *J. Org. Chem.* **2006**, *71*, 883–893.

[178] D. Geuenich, K. Hess, F. Köhler, R. Herges, *Chem. Rev.* **2005**, *105*, 3758–3772.

[179] R. Herges, D. Geuenich, *J. Phys. Chem. A* **2001**, *105*, 3214–3220.

[180] W. R. Scheidt, K. E. Brancato-Buentello, H. Song, K. V. Reddy, B. Cheng, *Inorg. Chem.* **1996**, *35*, 7500–7507.

[181] R. Sakamoto, M. Nishikawa, T. Yamamura, S. Kume, H. Nishihara, *Chem. Commun.* **2010**, *46*, 2028.

[182] K. M. Kadish, D. Sazou, Y. M. Liu, A. Saoiabi, M. Ferhat, R. Guilard, *Inorg. Chem.* **1988**, *27*, 686–690.

[183] A. Giraudeau, A. Louati, M. Gross, J. J. Andre, J. Simon, C. H. Su, K. M. Kadish, *J. Am. Chem. Soc.* **1983**, *105*, 2917–2919.

[184] H.-G. Jeong, M.-S. Choi, *Isr. J. Chem.* **2016**, *56*, 110–118.

[185] A. A. Ghogare, A. Greer, *Chem. Rev.* **2016**, *116*, 9994–10034.

[186] M. DeRosa, *Coord. Chem. Rev.* **2002**, *233–234*, 351–371.

[187] P. R. Ogilby, *Chem. Soc. Rev.* **2010**, *39*, 3181.

[188] A. A. Frimer, *Chem. Rev.* **1979**, *79*, 359–387.

[189] J. E. Anthony, J. S. Brooks, D. L. Eaton, S. R. Parkin, *J. Am. Chem. Soc.* **2001**, *123*, 9482–9483.

[190] M. A. Wolak, B.-B. Jang, L. C. Palilis, Z. H. Kafafi, *J. Phys. Chem. B* **2004**, *108*, 5492–5499.

[191] W. Ried, *Angew. Chem.* **1964**, *76*, 973–981.

[192] J. L. Marshall, D. Lehnherr, B. D. Lindner, R. R. Tykwinski, *ChemPlusChem* **2017**, *82*, 967–1001.

[193] D. R. Maulding, B. G. Roberts, *J. Org. Chem.* **1969**, *34*, 1734–1736.

[194] D. Lehnherr, R. McDonald, M. J. Ferguson, R. R. Tykwinski, *Tetrahedron* **2008**, *64*, 11449–11461.

[195] C. O. Clark, C. P. Poole, H. A. Farach, *J. Phys. C Solid State Phys.* **1978**, *11*, 769–774.